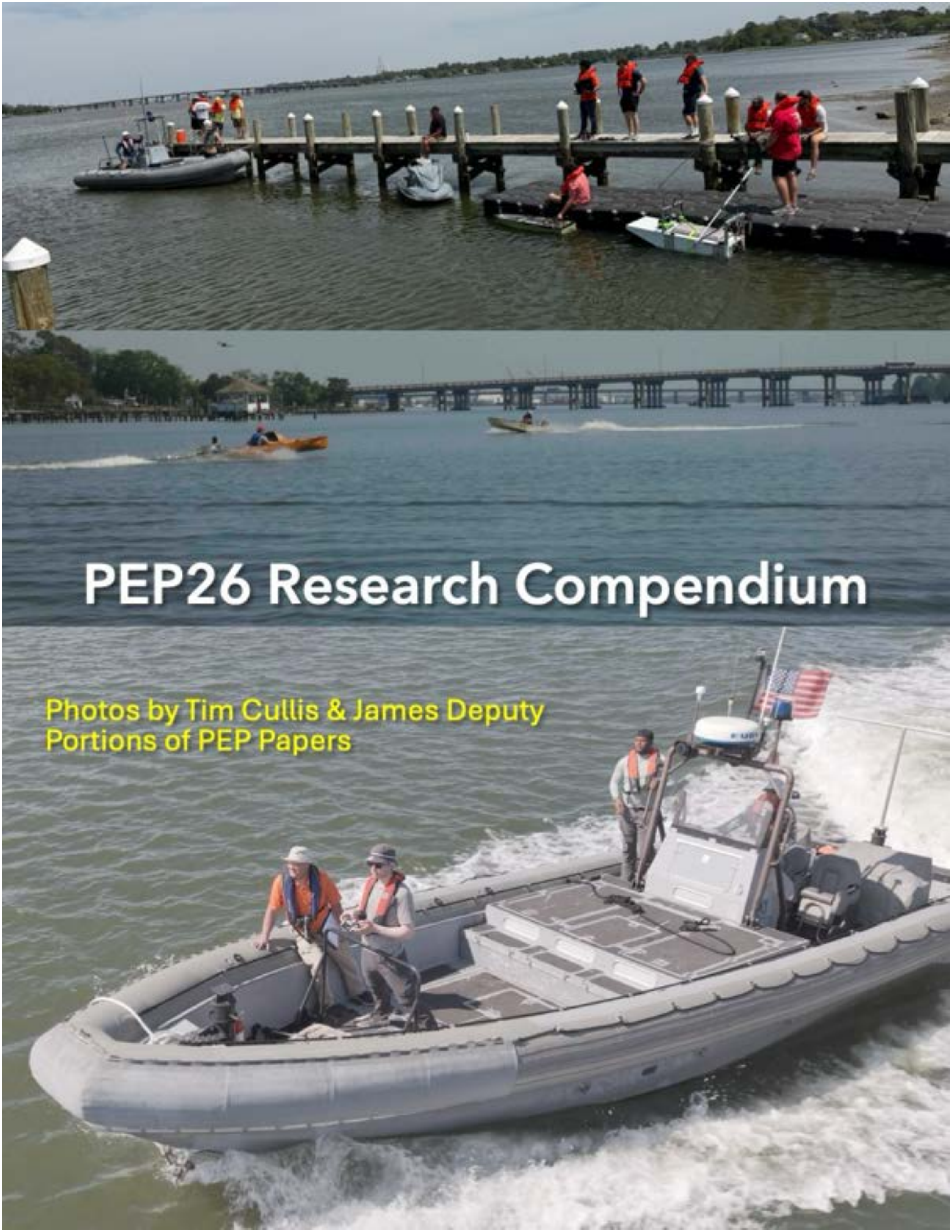

PEP26 Research Compendium

Photos by Tim Cullis & James Deputy
Portions of PEP Papers

Table of Contents

Forward

People always ask what's the secret to PEP. For new competitors, the secret is to build often and test for many months. For growing teams, the secret is to make sure every teammate has meaningful work and knows their contributions matter. For faculty, we emphasize how teams will be in the lab earlier than expected and are supported by a community excited to support the future engineers that will be leading our country. But, the real secret to PEP is the comradery within and between the teams.

The challenge is hard; the water sneaks into where it should never go, the slamming effects beat up electronics, and the salt is slowly wearing out components. The PEP community needs each other to be successful. This reflects how the American engineering community meets together regularly to work maritime problems.

PEP has grown into a national workforce-development program that puts college engineering students directly into real-world naval engineering challenges. PEP26 brought more than 350 collegiate engineers from 43 universities to Portsmouth City

Park, where teams designed, built, tested, and raced electric-powered craft across six divisions, including autonomous, over-the-horizon, budget, open unmanned, planing, and displacement competitions.

PEP is about much more than racing. We encourage students to work through the complete engineering process—hull design, propulsion, batteries, controls, autonomy, electronics, testing, documentation, and troubleshooting—while developing the systems-thinking and hands-on skills needed by the modern naval engineering workforce. PEP26 also connected students directly with employers through a job fair supported by Campus757 and the Hampton Roads Workforce Council, as well as industry mentors and professionals who engaged with teams throughout the year.

The result is a national recruiting network built around hands-on engineering. Students from large research universities and smaller colleges compete side by side, giving industry an opportunity to discover talent based not only on a résumé, but on what students can actually design, build, test, and accomplish. PEP gives companies a year-round connection to hundreds of emerging engineers while giving students a direct window into careers in naval architecture, maritime systems, electric propulsion, autonomy, manufacturing, and the broader naval engineering community.

Proper Preparation for PEP

Amber arcs of awakening water adhere to Arkansas Tech afts,
Alabama audaciously advances aggressively across the aqueous arena,
Auburn's agile artisans of acceleration answer with awe,
Brisk and buoyant, Buffalo's bright boats buck the breaking breeze,
Calm, courageous Cedarville cuts cleanly through curling channels,
Carefully carved Central Connecticut's craft crests confidently over currents,
Futuristic Central Florida's fast fleet flashes forward in foaming flight,
Daring and determined, Dayton drives its dynamic design downstream,
Delaware's disciplined designers deftly dance through dashing wakes,
Eager and enduring, East Carolina's engineers engage the estuary,
While lithe and lively, Elon's electric launch leaps along the liquid lane.
Golden Georgia glides grandly creating a gleaming gulf of gathering spray,
Buff-and-blue George Washington's gallant craft surveys with grace and grit,
Howard's proud blue-and-white hull hums ahead through hissing harbor haze,
Illinois' orange-and-blue innovators ignite an intense, insistent inland surge,
Johns Hopkins' blue-clad crew joins the jaunty journey while jetting autonomously,
Kentucky's cobalt current-cutters keenly keep their course through curling chop,
Longwood's lively launch lifts lightly along the lengthy lane lapping automatically,
Madison College's masterpiece masters the murmuring midriver momentum,
Mass Maritime's birddogging mariners move mightily through mist and motion,
Michigan's maize-and-blue machine marches mightily across the mirrored water,
Norfolk State's noble navigator knifes neatly through these neighboring narrows,
North Carolina State's red-and-white racers roar resolutely along the river's reach,
Northeastern's naval knowledge & accomplishments necessitates national acknowledgment,
Pitt's poised blue-and-gold professional prow presses past pulsing patches of spray,
Princeton's proud orange-&-black pioneers push purposefully around Portsmouth,
Quinnipiac's quick blue-and-gold craft quietly quickens across quivering currents,
Rutgers' resolute red riders rush relentlessly along the rigorous racecourse,
Rhode Island's royal-blue runners remotely ride rising ripples with rhythmic resolve,
Stevens's scarlet-striped sailors slice steadily through shimmering shallows,
Stony Brook's strong red seaworthy shells surge through swirling streams,
Tennessee's tenacious orange-&-white team tears through tumbling tides,
Texas A&M's tireless maroon team thunders through the turning troughs,
Toledo's tough blue-and-gold trailblazers totally master the trembling track,
UCONN's courageous blue current-cutters charge confidently and courageously,
Virginia's vivid orange-and-navy vessel vaults vigorously through veering vortices,
VCU's vigilant black-and-gold voyagers venture boldly into the vibrating wake,

Virginia Tech's valiant vessel autonomously veers victoriously through vast water,
Wake Forest's black-&-gold wave-riders wonderfully weave with watchful will,
Washington College's watchful mariners work the widening waterway with wisdom,
William & Mary's wise watercraft winds winningly through the whispering waves.

Alabama: Saban's Sailors Z-Drive

Joshua Mathews, Merrell McCormick, Michael DiLascia, Andrew Gordon, Harrison Wilson, Nant Prachuabmoh

www.navalengineers.org/Alabama

Per the 2025 Alabama Tide Chasers reporting, the boat had experienced major issues with the props lifting out of the water. The team found 3 main options for the driveshaft to help mitigate this. The first was a single straight flex shaft with a packing tube. The pros of this would be simplicity and waterproofing, while also allowing the driveshaft to remain submerged at most speeds. However, this design option was seen as not optimal, due to the motor system being designed for two motors. Using only one of our motors would likely not be strong enough to effectively propel the boat.

The second design option was two angled driveshafts. This design would allow the driveshaft to be submerged, while simultaneously being completely straight from input to output. This design's primary strength is its simplicity; it would be the easiest to fabricate with our given materials. The primary weakness of this design is that it would not only destroy our hull permanently, meaning future teams could not build their own unique propulsion designs on the hull, but also be less effective, moving some of the propelling force in the z-direction.

The final and chosen design is an external z-shaped gearbox similar to that of an outboard boat motor. The advantages of this design would be that it allows the output shaft to be lower than that of the other two designs. The main disadvantages would be vibration and waterproofing. The gearbox requires significant design considerations to minimize the components vibrating within the housing, as well as designing an effective way to waterproof the output shaft tube. The team turned this basic concept

into a fully original design using 3-D CAD models of existing parts from McMaster-Carr combined with wholly original housing and mounting components.

New Design

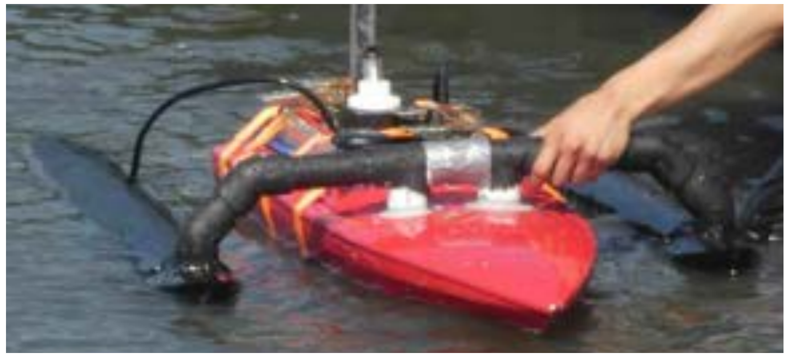

To develop the z-drive, a basic concept, similar to that of an outboard motor on a full-size boat, was created. The first stage of the design was to decide on the components that would be implemented into the internal system. Knowing that the team's primary objective was to lower the elevation of the propellers without making use of an angled shaft, like the Tide Chasers', the use of bevel gears was the most appropriate. This decision was made based on their nearly unique ability to transmit rotary motion vertically, while also maintaining around 97% efficiency.

The highest safe RPM available from the motors was desired. From data recorded by the Tide Chaser's testing, the safe range for the system would be between 10,000 and 20,000 RPM. The z-drive internal components were selected to support these RPM ratings. At that speed, to ensure that the gears and shafts do not overheat, ample amounts of grease and gear lubricant are needed within the housing. Flanged ball bearings were chosen to radially support the shafts within the housing, with shaft collars to prevent displacement of the shafts from excessive axial forces. The axial load on the shafts was determined from the necessary propulsion required to overcome the drag calculated from the hull fluid simulations. The ball bearings were selected accordingly to support such axial forces. Theoretically, the ideal bearing type for the design would be a tapered roller bearing; however, ball bearings were selected due to cost effectiveness and availability of the parts while still being able to support the calculated axial loads.

The modeling began with the assembly of the z-drive components. Using the specific component files, as provided by McMaster-Carr, a working 3D-model of the internal components of the z-drive was created in SolidWorks to be used as a reference and proof-of-concept. Once the internal system of the z-drive was designed and modeled, the housing for the system was designed. The housing design had to first prioritize the fit and form of the internals: ensuring the bearings were properly supported and secured while allowing the rest of the

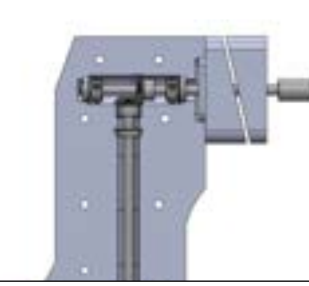

Figure 2. Full Z-Drive 3D-Model (Open)

components to rotate freely. Once the internal surface of the housing was designed, the external surface was created to maintain a hydrodynamic profile while allowing for ample surface area to fasten the hardware required to hold the z-drive together. The model also had to include a solution to the angled transom of the hull on which the z-drive is to be fastened to. Mounting plates were added to the design to allow the z-drive to remain horizontal while allowing for the adhesion to an angled surface.

For the competition, the team seeks to achieve a speed of approximately 12-15 miles per hour whilst maintaining a motor RPM range of 10,000 to 15,000. To ensure that these performance goals are met, and that the equipment is adequate to achieve this, a set of theoretical calculations are performed to estimate a baseline performance. Equations for the advance ratio (J), the thrust produced in Newtons (T), the torque generated in Newton-meters (Q), and drag force in poundsforce ($FDrag$) are utilised to obtain the resulting speed and the performance of the system. They are listed as follows:

$$J = \frac{V_{Desired}}{nD} \tag{1}$$

$$T = C_T \rho n^2 D^4 \tag{2}$$

$$Q = K_Q \rho n^2 D^5 \tag{3}$$

$$F_{Drag} = 0.0636V_{calculated}^2 - 0.2752V_{calcualted} + 4.6792 \tag{4}$$

Arkansas Tech: Gearing Up for Success

Logan Ashley, Kade Cartwright, Nathan Gibbons,
Michael McCarty, Caleb Soller
www.navalengineers.org/ArkansasTech

The gearbox subsystem was designed to efficiently transfer power from the electric motor to the propeller while maintaining reliability and compact integration at the stern of the hull. In small-scale marine propulsion systems, it is often necessary to redirect power from the motor to the propeller shaft with minimal mechanical losses. Accordingly, this gearbox design emphasizes efficient torque transmission, structural integrity, and preservation of the motor's operating speed while redirecting rotational motion to the propeller.

The propulsion system incorporates an electric motor mounted in a vertical, face-down orientation at the stern of the hull. Power is transmitted from the motor through a vertically oriented composite shaft, which is encased within a metal support rod. This metal enclosure enhances rigidity and protects the composite shaft, while still maintaining a lightweight drivetrain. At the base of the vertical shaft, a bevel gear is mounted to serve as the primary component responsible for redirecting rotational motion.

This bevel gear engages with a second bevel gear oriented at a 90-degree angle, forming a right-angle gearbox configuration. This arrangement redirects rotation from the vertical motor shaft to a horizontal shaft connected to the propeller. The gear pair operates with a 1:1 gear ratio, ensuring that the rotational speed of the output shaft matches that of the motor. Rather than altering speed, the gearbox primarily changes the direction of rotation, enabling a compact vertical motor configuration while effectively driving a horizontal propeller shaft.

The use of bevel gears in this application offers several advantages. Bevel gears enable efficient torque transmission between intersecting shafts while maintaining a compact mechanical layout. Additionally, this configuration reduces the number of drivetrain components, minimizing potential failure points and simplifying maintenance. The

1:1 gear ratio ensures that the motor operates within its optimal speed range while delivering torque directly to the propeller without unnecessary losses.

During the design process, torque transmission and structural loading were considered to ensure the gearbox could withstand expected operating conditions. Estimated motor torque values and standard mechanical design principles were used to evaluate gear and shaft performance within the system. CAD modeling supported visualization of component interactions and helped identify potential areas of concern related to alignment, load transfer, and structural integrity. These considerations informed decisions regarding material selection, shaft dimensions, and gear geometry, contributing to a design that is capable of reliable performance under anticipated loading conditions.

Overall, the gearbox design provides an effective and efficient solution for transferring power from the electric motor to the propeller. The right-angle bevel gear configuration enables a compact system layout at the stern while maintaining structural integrity and minimizing energy losses. This design supports consistent torque delivery to the propeller, contributing to improved acceleration, system stability, and overall performance during operation.

Arkansas Tech: Jetting to the Uncrewed Future

Tony Muniz, Justin Parker, Xavier Robinson, Brooklyn Smith

www.navalengineers.org/ArkansasTech

Another critical challenge faced when dealing with electric propulsion systems is thermal management. Electric motors operating under high loads generate significant amounts of heat due to electrical losses and inefficiencies. If not properly managed, excessive heat can degrade components, reduce motor efficiency, and lead to system failure. In conventional marine systems, active cooling solutions often add weight and complexity. Research in heat transfer demonstrates that the use of high-conductivity materials, such as copper, in combination with forced convection significantly enhances heat dissipation.[2]

Our team decided that to best address this challenge, we needed the design to repurpose the jet ski's existing jet pump system to provide continuous water flow for motor cooling. The integration of ¼" copper tubing around the motor utilizes the natural flow of water through the jet pump, which allows the system to achieve efficient heat removal without introducing additional mechanical complexity. This approach creates a dual-purpose system that simultaneously supports thermal regulation and propulsion.

Overall, the design is grounded in established principles of fluid dynamics, electric propulsion, and heat transfer. By leveraging these principles and adapting proven marine components in innovative ways, the system provides an efficient solution for a high-performance, unmanned, remote controlled electric watercraft.

Propulsion System Design-

The propulsion system consists of four major subsystems: Battery Energy Storage, Electric Motor, Electronic Speed Controller, and Jet Pump Assembly. These components work together to efficiently convert electrical energy into thrust while maintaining reliability in demanding open-water conditions.

Engineering Analysis-

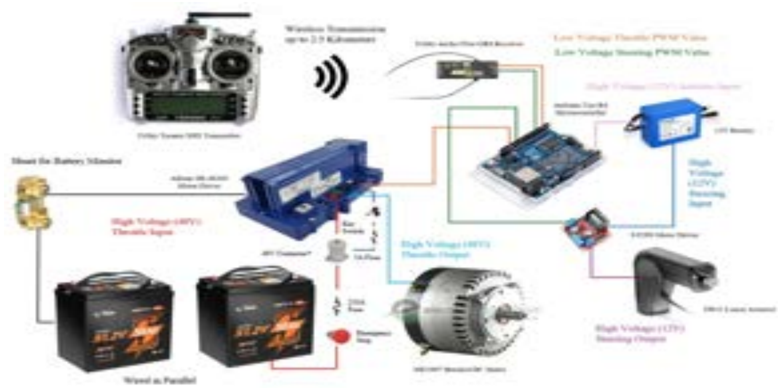

The performance of the watercraft is primarily governed by hydrodynamic drag and the ability of the propulsion system to overcome this resistance. The target velocity for this year's race is 15 mph. Drag was estimated using:

$$F_D = \frac{1}{2}(\rho)(C_D)(A)(v)^2$$

$\rho = 1000\ kg/m3$ (Density of water)

$CD = 0.15$ (Drag Coefficient)

A = 0.35 (Front area of our hull)

$$F_D = \frac{1}{2}(1000)(0.15)(0.35)(6.7)^2 = 1178N$$

This relationship shows that drag increases with the square of velocity, meaning higher speeds require significantly more power. The required propulsion power to achieve the target velocity was determined using:

$$P = F_D \times v$$

$$P = (1178)(6.7) = 7.89kW$$

These calculations were used to size the propulsion system to achieve a target speed of approximately 15 mph while maintaining a margin for real-world conditions such as waves and wind. The selected motor provides sufficient power and torque to meet these demands while maintaining efficiency under load.

Motor performance was further evaluated using:

$$P = T\omega$$

This ensured that the motor could deliver adequate torque to drive the jet pump while maintaining responsive control.

Battery capacity was selected based on total energy requirements:

$$E = v \times Ah$$

This ensures the system can complete the competition course without exceeding safe discharge limits. Two 48V batteries wired in parallel were chosen for the competition.

With the two 48V 30 Ah batteries wired in parallel with a discharge rate of 2.67C, 80 A for 20 minutes, we calculate the power provided within our system.

$$P = IV$$

$$P = (80A)\,(48V) = 3.84kW \text{ (Per Battery)}$$

Accounting for both batteries:

$$(3.84kW)\,(2) = 7.68kW \text{ of power produced}$$

Auburn Propeller Pioneers & Cool (Big) Cats

Owen Basso, Skylar Grobe, Bryce Jordan, Amber Mathis, Dalton Robinson

www.navalengineers.org/Auburn

Research identifies the toroidal propeller as the highest efficiency and hydrodynamic propeller for marine applications; however, previous evaluations at low gas-engine speeds (0-6000 RPM) prove these results are inapplicable to high-speed electric motors operating up to 45,000 RPM. Accordingly, further analysis was deemed necessary for competition conditions, resulting in both physical and virtual evaluation of a similarly sized toroidal propeller, shown in (Figure 7), and the 3-Blade propeller (Figure 8). The other propellers being evaluated during experimentation are the prior 3-Blade propeller and 4-Blade propeller shown in Figure 5 and 6.

Prior 3-Blade

Prior 4-Blade

Designed 3-Blade

Designed Toroidal

An ANSYS CFD simulation was conducted to evaluate the propellers' hydrodynamic behavior, following the methodology adapted from the *Journal of Marine Science and Engineering* for vortex structure of the toroidal propeller. While the reference study utilized 600 RPM, a higher rotational speed of 30,000 RPM was applied here, acknowledging the possibility of inflated results but would remain valid for comparison between propeller types. The computation domain included a rotational region and surrounding stationary region of water measured using the propeller diameter (D) shown in Figure 9 [4].

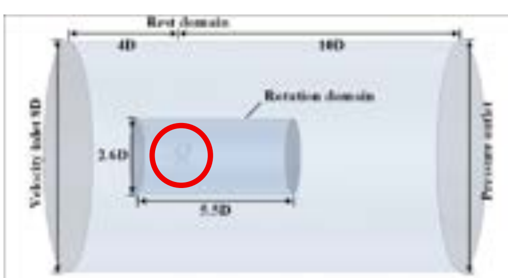

[4]

A fine mesh was utilized, with emphasis on the propeller walls, to ensure accuracy.

Boundary conditions include a velocity inlet, with a 11 $\frac{m}{s}$ estimated traversing speed, and a pressure outlet in the stationary fluid region. The simulation involved the Reynolds Stress 7 equation turbulent model due to effectiveness in high rotational flow, swirl, and strong streamline curvature, allowing the evaluation of surface pressure, thrust, torque, and fluid velocity [5].

Results were analyzed using streamlines for velocity and pressure contours for surface loading to identify high-stress regions for manufacturing. Marine Science and Engineering evaluated the thrust coefficient (K_T), torque coefficient (K_Q), and advance coefficient (J) in terms of Thrust (T), advance velocity (υ_A), rotational speed (n), fluid density (ρ), and torque supplied to the propeller (Q). Propeller efficiency (η) and supporting equations are in Equations (4-4), (4-5), (4-6), and (4-7) [4].

$$J = \frac{\upsilon_A}{nD} \tag{4-4}$$

$$K_T = \frac{Q}{\rho n^2 D^5} \tag{4-5}$$

$$K_Q = \frac{Q}{\rho n^2 D^5} \tag{4-6}$$

$$\eta = \frac{J}{2\pi}\frac{K_T}{K_Q} \tag{4-7}$$

The toroidal propeller results (Figure 11 and Figure 13) show a large trailing vortex in the rotational region, demonstrating significant rotational flow, and high-pressure regions concentrated along the leading edge of the blade and the blade-shaft connection. The resulting thrust and torque from the simulation was $4578.43\ N$ and $372.545\ Nm$, with using the previous Equations (4-5)-(4-7), provides an efficiency of 4.3029%. Under identical conditions (Figure 10 and Figure 12), the 3-Blade propeller exhibits higher trailing velocity regions than the toroidal, maintaining a coherent vortex, with pressure contours revealing localized high-pressure regions along the blade's leading edge. The thrust and torque results were $10562.6\ N$ and $419.341\ Nm$, providing an efficiency of 8.8203%, approximately twice that of the toroidal, with generated thrust nearly 2.5 times greater.

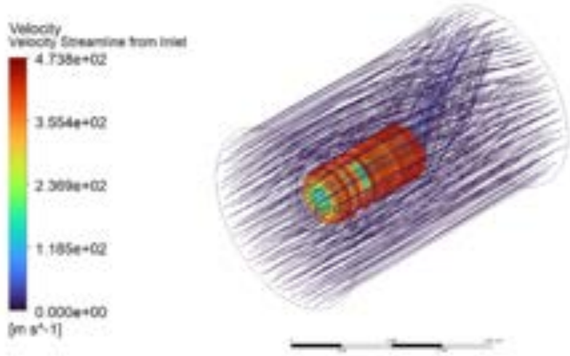

Figure 10: 3-Blade Propeller Velocity Flow Trajectory Simulation Results

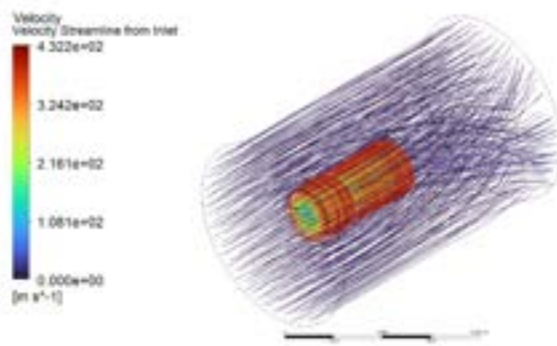

Figure 11: Toroidal Propeller Velocity Flow Trajectory Simulation Results

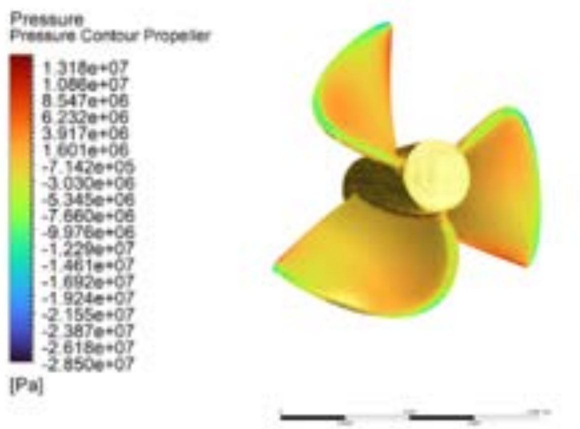

Figure 12: 3-Blade Propeller Surface Pressure Contour Results

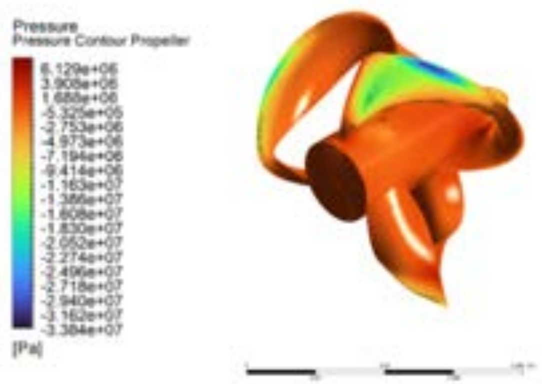

Figure 13: Toroidal Propeller Surface Pressure Contour Results

To complement computational results, experimental validation was conducted using propellers printed with Siraya Tech Sculpt-High Temperature Resistant Resin in a testing setup to compare the performance of the designed and previously used brass propellers. The testing setup was constructed from a previous hull, rope, and a mechanical force gauge, shown in Figure 14.

Four propellers, a prior 3-Blade brass propeller, a prior 4-Blade brass propeller, the designed toroidal propeller, and the designed 3-Blade propeller, were tested twice each for consistency, with results summarized in Table 1. The findings confirmed the simulation trends,

Figure 14: Propeller Testing Setup

showing the toroidal propeller produced significantly lower thrust than the 3-Blade, leading to the selection of the designed 3-Blade propeller for its superior performance in both simulation and experimental testing.

Table 1: Propeller Testing Results

Propeller Type	Test 1 (lbs)	Test 2 (lbs)	Average
Prior 4-Blade	14 lbs	16 lbs	15 lbs
Prior 3-Blade	17 lbs	15 lbs	16 lbs
Designed Toroidal	14 lbs	15 lbs	14.5 lbs
Designed 3-Blade	25 lbs	22 lbs	23.5 lbs

Next steps will include machining the selected 3-Blade propeller at the Montgomery Advanced Manufacturing Lab in Wiggins Hall after completing testing to avoid unnecessary cost and lead time. Chosen for its higher thrust, larger surface area, and simpler geometry, the 3-Blade propeller will require 5-axis machining on a HAAS - UMC 750 CNC mill for the curvature of the blades. With ordering 6061 aluminum bar stock, programming the toolpath in Fusion360 (Figure 15), and then running the program on the machine, the machined propellor will have uniform material properties to handle the anticipated stress and high load of competition conditions.

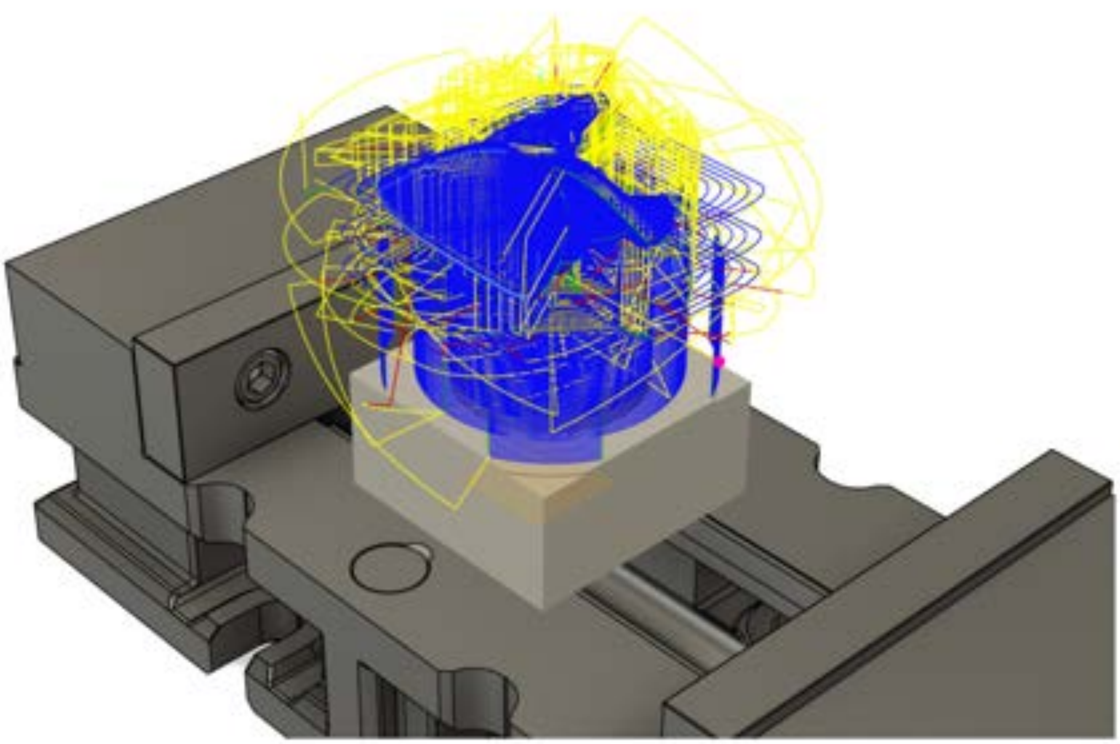

Figure 15: Generated Toolpath for Three Blade Propellor Simulated in Fusion360

An improved cooling system is necessary due to prior overheating, including replacing the ESC and integrating a water-based cooling system. Calculations were made with the following assumptions: energy is conserved, system energy is converted from purely electrical to purely thermal, pure water, maximum power from battery, and maximum water temperature. The mass flow rate is determined by using the simplified steady-flow thermal energy equation below in (48) and (4-9) [6].

If the heat (q) is approximated as the maximum battery power, it yields 17.64 kW. This value, with Equation (4-9), computes mass flow rate, then converted to volumetric flow rate with water density as 1000. An inlet temperature (T_{in}) of 290 K is assumed based on average water temperature conditions in Portsmouth, VA in April, with a corresponding specific heat (c_p) of 4.184 $\frac{kJ}{kg*K}$ from table A-6 [7][6]. The outlet temperature (T_{out}) is assumed in accordance with the manufacturer, at °C, or 358 K [2]. These assumptions intend to overestimate cooling requirements to mitigate overheating risk observed in prior designs.

$$q = \dot{m}c_p(T_{out} - T_{in}) \tag{4-8}$$

$$\dot{m} = \frac{q}{c_p(T_H - T_L)} \tag{4-9}$$

The required volumetric flow is determined from the preceding equations, with a conversion factor of one cubic meter per second $1\frac{m^3}{s}$ equal to 1.585×10^5 gallons per minute (GPM) [8]. The analysis yields a required flow of 0.9856 GPM. Figure 16 demonstrates the system flow path with the navy outlines as bodies of water, the orange outlines as the internal components, the blue arrows as cool water, and the red arrows as hot water.

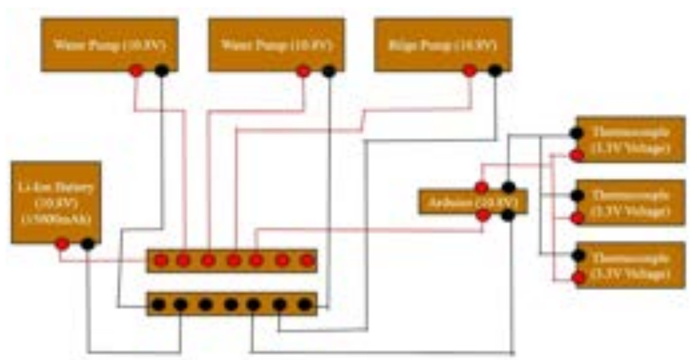

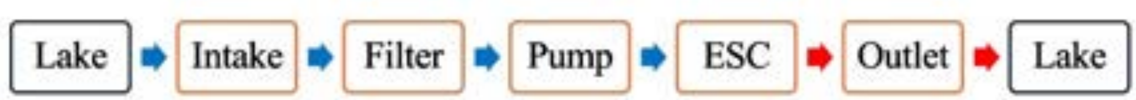

Figure 16: Cooling System Water Circulation Flow Chart

With these improvements, and the thermal monitoring system, the electronics should be closer to their ideal operating temperatures.

Buffalo Displacement Defense

Jason Barnes, Timothy Kraycar, Emma Liang, Jacob Newton, Julia O'Malley, Williams Prevet, Gabrielle Schinzel, Nicholas Schuck, Melanie Valladares

To ensure an accurate CFD simulation, the waterline of the pontoons would need to be calculated. This can be calculated via the Archimedes principle found in equation (7). This formulation would require an accurate weight of the boat being 760 lbs. or 344 kg. The effective height and width of the pontoon would also be required to accurately describe the displaced water. This can be calculated using the length effective (eq. 8). This can then be used in the approximate volume of the elliptical shape found in equation 9 to find the waterline of the pontoons.

$$V_{total} = \frac{m}{\rho} \tag{7}$$

$$L_{effective} = 0.75 \cdot L_{hull} \tag{8}$$

$$A = \frac{\pi}{4} Bd \tag{9}$$

When evaluated, the draft on the boat turns out to be 0.22 meters. With this number, the multiphase fluid interface can be created which will increase the accuracy of the results. To ensure that the simulation is as accurate as it can be while also saving on computation time a few key assumptions were made.

1) Power loss due to external waves is negligible.
2) Power loss due to pitching and yawing of the vessel is negligible.

Under assumption 1 losses due to oncoming external beach waves would not be accounted for; this is due to variability in the environment and predicting the weather for competition day is impossible till the week of. Under assumption 2 the boat is consistently going through the water in a fixed frame. This assumption works as the

pitching and yawing of the vessel in a 5-mile race would average over time causing power losses and gains due to this motion to average out to about zero. With these two assumptions a CFD simulation was conducted to model the performance.

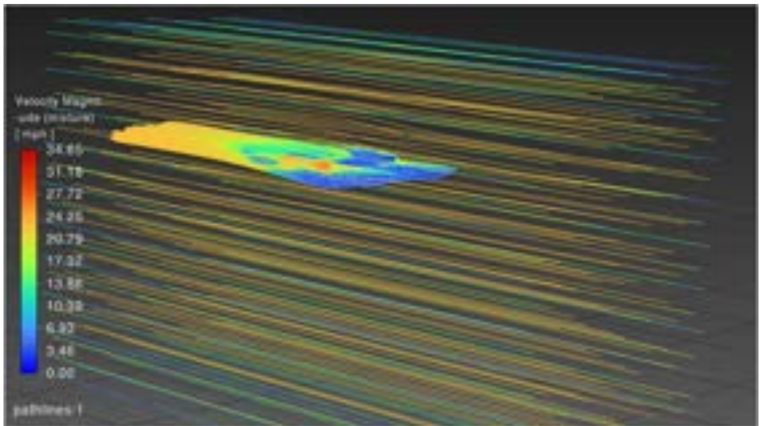

Figure 1. CFD Simulation Path Line Results

Figure 1 describes the path lines about a plane that sits through the boat which shows the fluid flow separation that occurs in the air as well as the wake created by the boat as it moves at a constant speed throughout the water.

This trend can be corroborated by experimental data of hull speed vs hull resistance done by Olivieri et. al. [1]. There are differences between the data and the data found in [1]. These are mostly since the experimental data uses lightweight models to gather the data which will react differently at high speeds.

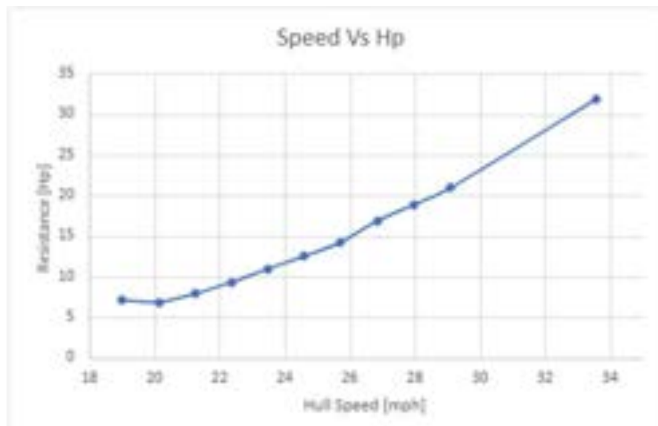

Figure 2. Horsepower Requirement as a Function of Hull Speed

To ensure that the catamaran hull is the most optimal design, a secondary design was incorporated into our CFD simulation. This was a jet ski hull, specifically a Tiger Shark jet ski that would hopefully allow for a speed above the 23-mph benchmark found in the catamaran design. Using Archimedes principle, a waterline of 0.21 m was found. Then plugging it in with the same parameters as the catamaran design, it was found that to go 23 mph it would require nearly five times the amount of power which is unrealistic for the limited budget the team was given as seen in Figure 4. This confirmed the catamaran design as the most optimal design for this competition.

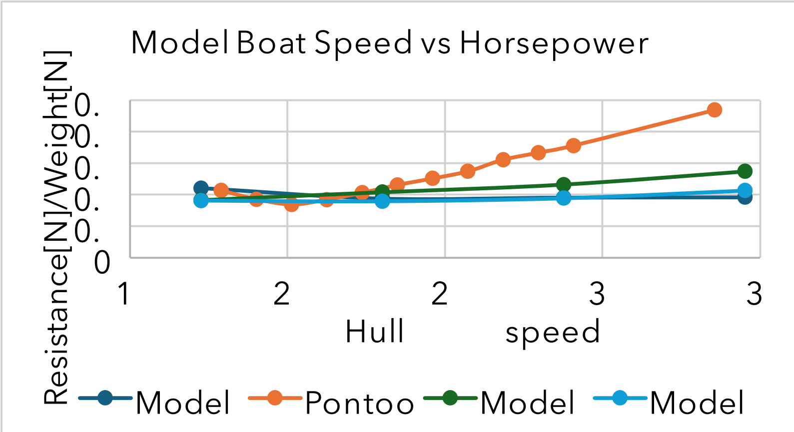

Figure 3. Experimental Power vs Velocity [4]

To establish the maximum possible boat speed given the operating parameters, the efficiency of the drive system and propeller must be known. It is assumed that the losses in the drive system are minimal compared to the losses due to propeller motion, so that is the primary focus of the analysis. A model was implemented in MATLAB that iteratively calculates the power required to hold the boat at a given speed for a certain propeller diameter. Force and speed data provided by the CFD simulation were used to support the calculation. The program then compared this maximum with the power output of the motor (noted on motor's specification sheet at 14 horsepower) to get a top speed vs. propeller diameter graph.

The theoretical efficiency of a boat propeller, η, is given by the equation,

$$\eta_I = \frac{2}{1 + \sqrt{1 + \frac{8T}{\rho \pi D^2 V_A^2}}} \tag{10}$$

Where T is the thrust force is required to propel the boat at a given boat advance speed, V , D is the diameter of the propeller, and ρ is the density of the fluid that the propeller is moving through, in this case water (Techet). For the actual

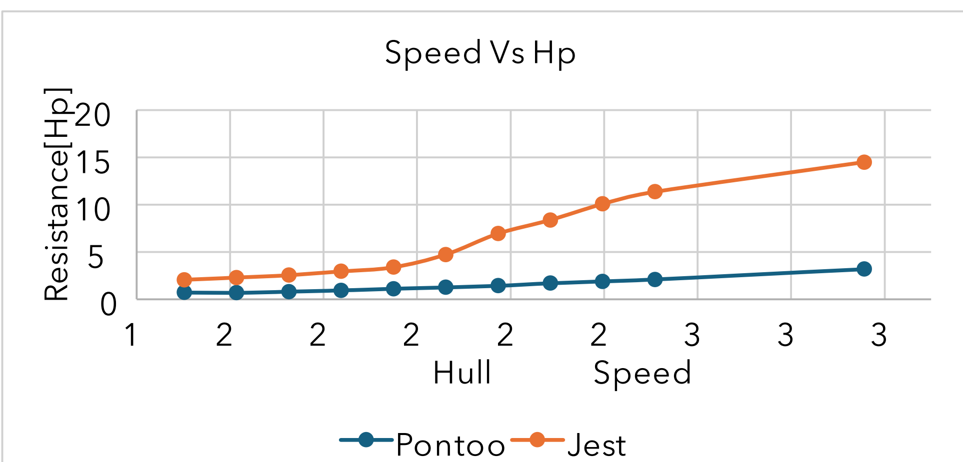

Figure 4. Resistance vs Horsepower Pontoon and jet ski

propeller, a 20% loss was assumed, accounting for drive system losses, turbulent flow, and cavitation effects on the propeller. Thus, the actual propeller efficiency, η, is given by,

$$\eta \qquad = 0.8 \cdot \eta \qquad (11)$$

This efficiency can be used to relate the power output of the motor, P, to the effective power produced, P.

Powertrain

Our motor and control system was selected based on the maximum amount of current we could purchase on a limited budget. We deduced that we could provide 300 amps of continuous current through our battery system which led us to the ME 1616 motor. The ME 1616 motor is rated for 250 amps continuous at 48V which is a near perfect match for our max continuous amperage from the battery pack. Using the Curtis 1236SE controller we can supply the max amperage of 250 amps at a capped RPM of 5000. Due to the limited budget a lower unit from a fifteen horsepower Evinrude outboard motor was obtained, providing a practical way to connect the motor and propeller together offering a 2.33:1 gear ratio. This ratio, however, is too extreme, requiring an additional gearbox to reach the ideal propeller speed of 2,600 rpm.

A new gearbox was created to sit on top of the lower unit and connect the motor using a chain and sprocket. The motor is mounted within the gearbox frame and includes an additional shaft extending from the lower unit to be parallel with the motor output shaft, ensuring proper chain alignment as shown in Figure 9. The frame was primarily constructed out of 1″ x 1″ x 0.12″ mild steel square tubing that was cut to size and welded together. To mount the frame to the lower unit an 8″ x 7.5″ x 0.25″ mild steel plate was cut on a CNC plasma table seen in Figure 10, ensuring hole accuracy with the preexisting holes on the lower unit. Similarly, the motor is mounted to the frame using a 15″ x 14″ x 0.25″ mild steel plate, cut with a CNC plasma table with slots allowing the motor to pivot to adjust chain tension.

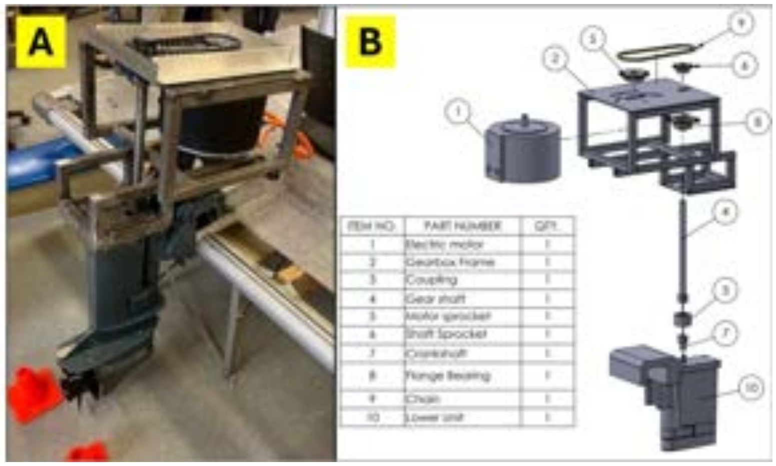

Figure 9. Produced (A) and CAD (B) model of motor mount and lower unit.

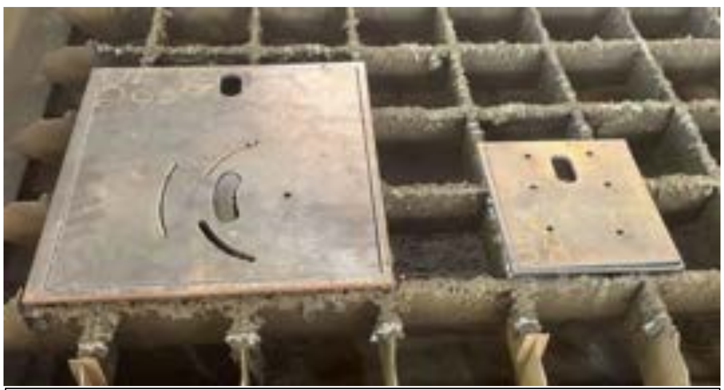

Figure 10. CNC Plasma Cut Plates for Gearbox

To connect the motor to the outboard unit an adapter was needed as the lower unit used a nonstandardized output shaft end. The crankshaft from the internal combustion engine originally connected to the lower unit was cut to length and then turned down to a cylindrical shape. To then connect the crankshaft to the motor, it was coupled to a shaft using a keyway. The coupling and shaft were both made of 4140 steel for its high fatigue strength. The 16″ shaft had an original diameter of 1 3/8″, and 14″ of the shaft was turned down to a diameter of 7/8″ leaving 2″ at 1.375″ to fit into the coupling. A four-bolt flange bearing was connected to the shaft keeping it parallel to the motor.

Buffalo Powerful Unmanned Craft

Lila Ruff, Madison Piechowski, Roland Orselli, Lauren Affronte, Isabella Martin, Lily Zaborows

www.navalengineers.org/Buffalo

The power storage system is made up of a configuration of eight 14.8 Volt, 4s 5200 mAh lithium polymer batteries. The power is stored in these eight batteries and connected to a kill switch that controls the flow of power from the batteries to its associated electrical components. The batteries power the motor, the telemetry sensor, two electronic speed controllers, the bilge pump, the servo and receiver. The full system uses 34V of power, well below the 55V max. This is accomplished by connecting the batteries in both series and parallel, as shown in the diagram, Figure 8, below. The electronics are soldered together with an 8-gauge wire and then waterproofed by being wrapped in electrical tape. The telemetry sensor and the electronic speed controller (ESC) are remotely controlled by the Futaba 4PM Plus RC Controller and Receiver. The remote controller has an effective operating range of about 230 feet (70 meters) under optimal conditions. The power flows out of the batteries and into these components, while the remote controller uses the servo to steer the vessel and the motors to control the amount of power/speed being translated from the motors, down the drive shafts, to the propellers that is thrusting the vessel forward.

The power storage system is unique due to the configuration of the batteries in parallel and series. The batteries are configured as seen in Figure 8 because it allows the batteries, which have a higher voltage capability, to perform within the competition requirements. Configuring the batteries to preform within the competition requirements was done through both research and testing. By using a multimeter set to DC Voltage and connecting the positive probe to the positive terminal, and the negative probe to the negative terminal, the voltage was observed on the display screen of the multimeter. Additionally, it was observed that while the configuration

maintains a system output of 34V while the batteries are held at 4.2V per cell, the system decreases to 31V when the batteries are held at 3.8V per cell.

The powertrain system was mostly replaced and improved upon this year from the previous year's boat. The driveshafts, drive dogs, propellers and bullet collars were all improved upon. The propeller is additively manufactured from CRES 316L Stainless Steel through MOOG from SolidWorks designs made by the team. The propeller is different in both material and configuration. While the previous propellers had two blades, the new propellers have three blades and a larger diameter, which provides more surface area for displacing the water and propelling the boat forward. The propellers operate by rotating with the drive shaft, powered by the motor it is connected to. The propellers are secured in between the drive dog and bullet collar. There are two propellers alongside each other, each rotating opposite directions. They rotate towards each other to balance out torque and cancel out side-force, which can also be referred to as "prop-walk". This allows the vessel to travel straight without excessive steering correction. If the propellers rotated in the same direction, the vessel would travel in a circle without steering correction, and steering correction would be very difficult.

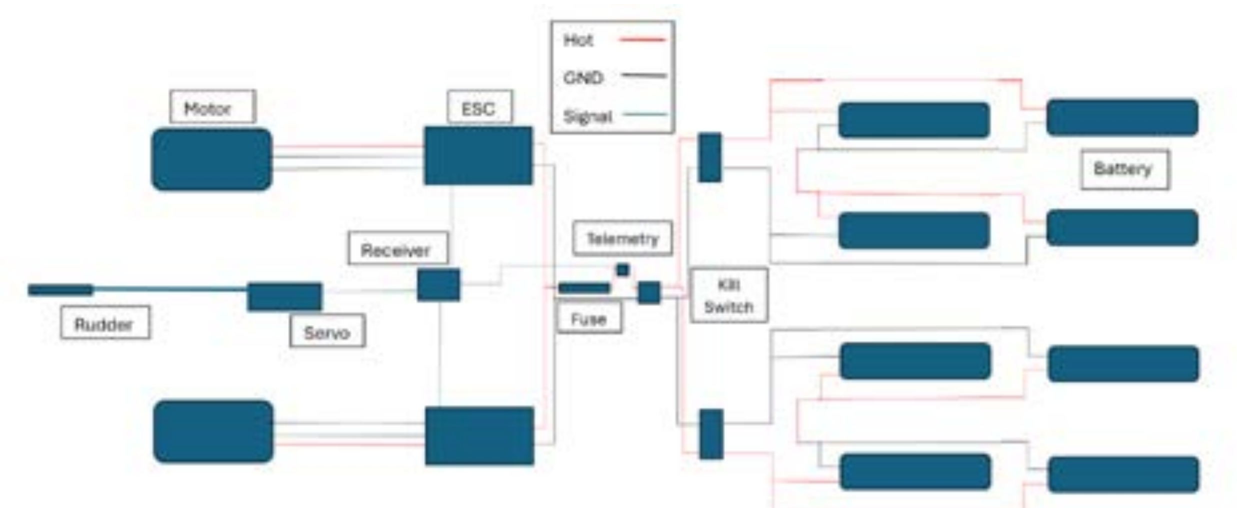

Figure 8: Propulsion and Telemetry System Electronics Diagram

The propeller is kept on the shaft by being placed in between a drive dog and a bullet collar. The drive dog acts as a base against the thrust washer. The drive dog has pawls which fit into the notches on the propeller as an interlocking method. Then the thrust washer, drive dog, and propeller are kept on the shaft by the bullet collar at the end of the shaft. The bullet collar is placed on at the end of the configuration and has a set screw which holds it on the shaft. The bullet collar then keeps the other components on and is tapered to a tip, similar to the shape of a bullet, for hydrodynamic purposes.

The propellers were designed to fit on the stock shaft, in between the thrust washer, drive dog, and bullet collar. It was important to ensure the dimensions of the custom designed propeller could fit properly with the rest of the stock components. If the dimensions for the length of the propeller or the inner and outer diameter were incorrect, it could result in manufacturing a propeller which does not fit with the rest of the system. This would be a very bad situation that could result in a failed project. With the propeller's dimensions correct, it is designed to interact and function cohesively within the system.

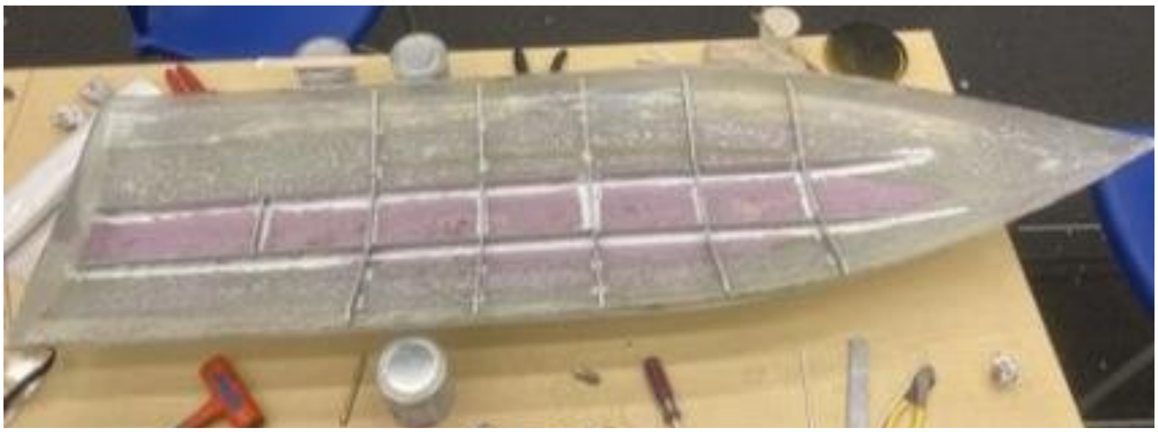

Figure 4: Bottom section of the hull showing alignment of aluminum stringers

From the drive shaft, where the propeller, drive dog, thrust washer, and bullet collar are secured, the drive shaft is then connected into the motors. The motors convert the electrical energy from the batteries into the driveshafts which spin and translates the power into the propellers which give the boat thrust, which is called propulsion. The motors themselves convert the electrical power into mechanical rotational energy, which is controlled by the remote controller, an electronic speed controller (ESC) which manages speed and torque, as well as direction. The direction is controlled through the same remote control, but it is connected to a servo motor that controls the rudder.

Cedarville: Iterative Testing & Design

Kolson Kytta, Dawson Propes, David Roer, Timothy Wenger, Josh Martus, Elijah Otto, Grant Luman, Danny DeHimer, Hazen Swenson, Jarod Savard, Blake Doss, Ben Hubbard, Matias Cavajani, Johann Honegger, Jeremy Gonzalas Conteras, Ryan Strellman, Sam Madison, Joram Ramirez, Logan Montgomery, Kieran Dempsey, Matthew Shepherd

www.navalengineers.org/Cedarville

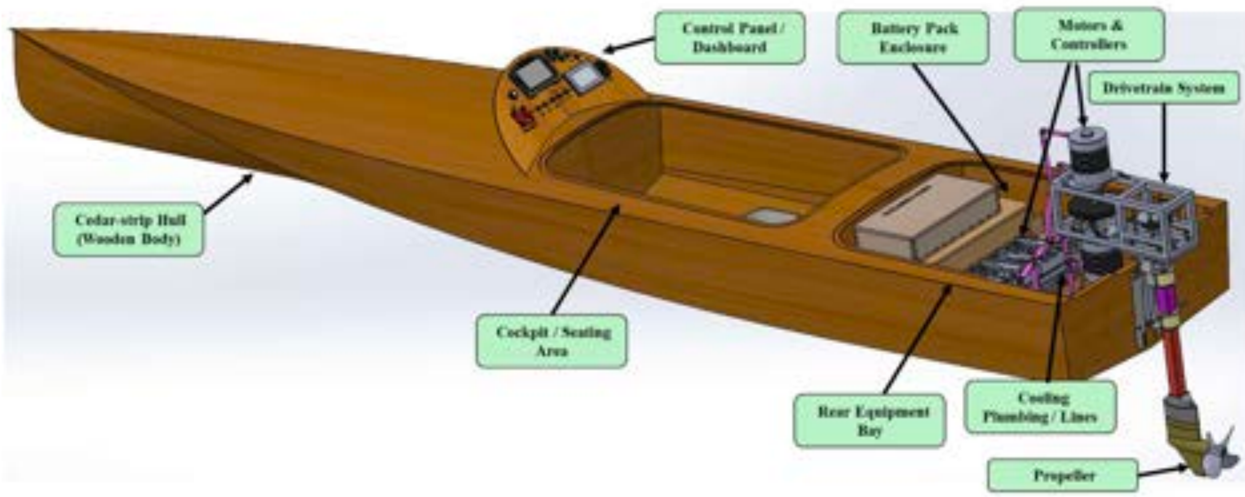

Figure 1. Complete CAD Assembly of "Marvelous Grace" with important components and systems labeled.

The starting point for all our design and testing procedures is the power budget. This is a critical thread that runs through each of our design and fabrication decisions. The power budget tracks how power from the battery is distributed and consumed by each system, accounting for losses, to determine how much usable power remains for propulsion. Energy in the boat is stored in the batteries. Before it is transmitted to the water it must be converted several times. Every time power is converted in our boat, a percentage of it is lost. It is first converted from DC power in the batteries to AC power by passing through the motor controllers, where a percentage of power is lost. The power then goes to the motors, through the drivetrain, and to the propeller, from which it is transferred to the water. At each of these steps a percentage of the power is lost. We are limited by the cooling capacity of the batteries which limits how much current and power can be drawn from them. This limited battery power, along with the

efficiency of each step, determines our propulsive power. Below in Figure 2 is our power budget for the planing race.

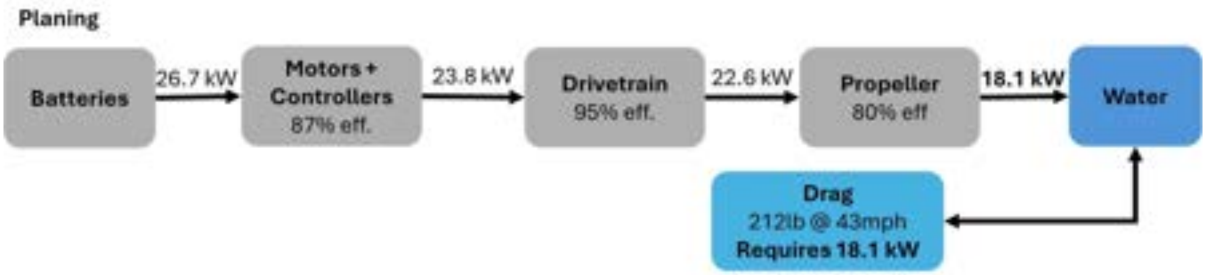

Figure 2. Calculated Power Budget for the Planing Division

We used a cedar-strip hull developed by previous Cedarville teams that is capable of both displacement and planing operation. The hull transitions from a V-shaped bow to a flatter aft section with slight deadrise, allowing it to efficiently displace water at low speeds and generate hydrodynamic lift at higher speeds. As the boat accelerates, the wetted surface area decreases, reducing drag and enabling efficient planing. We evaluated hull performance through drag testing to determine the relationship between speed and required propulsion power.

Drag testing was performed by towing the hull at controlled speeds while measuring force with a load cell and velocity with GPS (Figure 3). To process the data, we developed a computer vision-based pipeline that extracts synchronized force measurements from recorded video. Steady-state data were isolated and filtered to remove outliers.

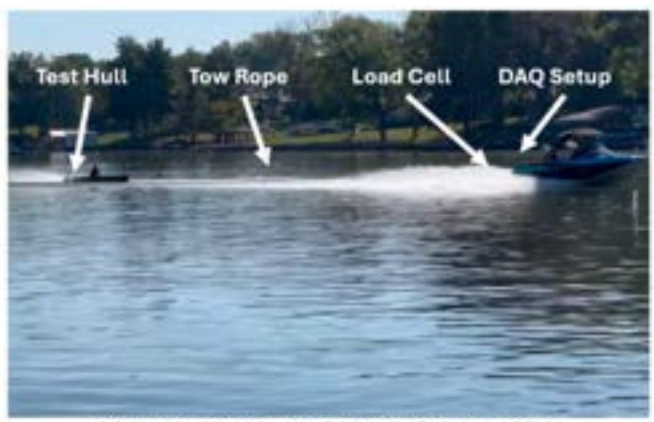

Figure 3. Experimental Setup of Drag Testing

Drag force was converted to propulsion power using Eq. 1:

$$P = D \cdot V \qquad (1)$$

where D is the measured drag force and V is the hull velocity and P is the propulsion power. The resulting power-speed relationship is shown in Figure 4. Results indicate that a hull with equivalent mass and trim characteristics requires approximately 18.1 kW to achieve 43 mph in planing mode and approximately 8.76 kW to achieve ~24 mph in displacement mode. These values were used directly in the system power budget and propulsion design to ensure proper matching between available power and hull resistance.

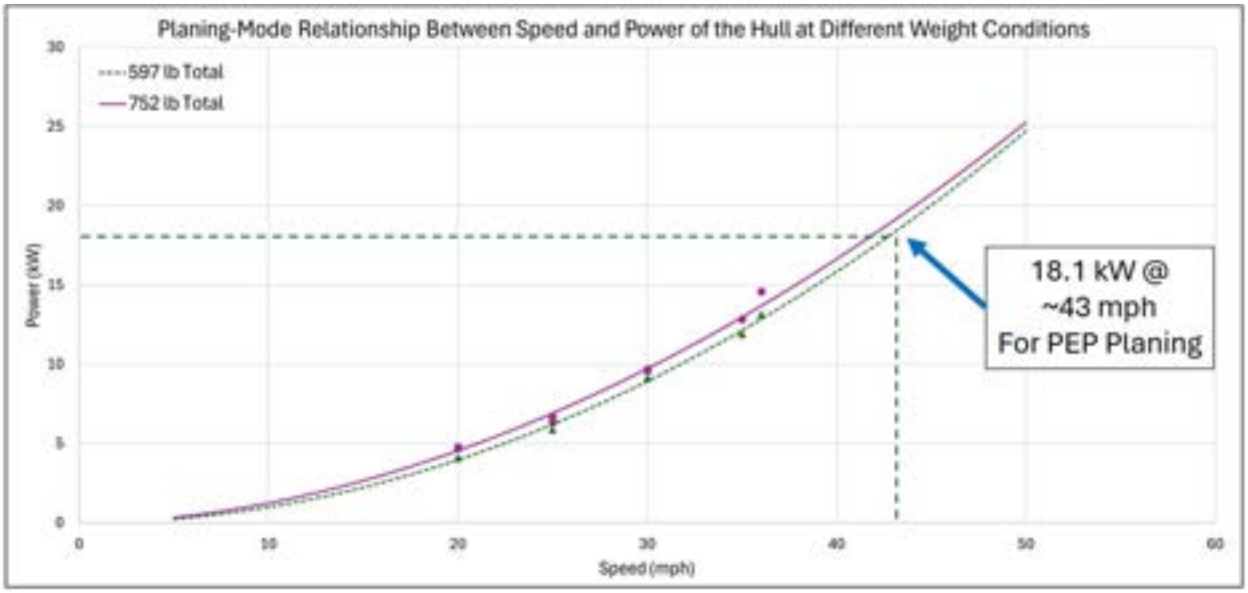

Figure 4. Power vs. Speed Relationship of Planing Hull at Different Weight Conditions

Fabrication and Testing: The cedar-strip hull was originally constructed using a strip-built method, where cedar planks are formed over station molds, bonded, and reinforced with fiberglass and epoxy to create a smooth, rigid structure. The deck is built similarly and bonded to the hull, with internal bulkheads providing structural support and compartmentalization.

Although the hull was not newly fabricated, we reused and integrated it into our design. We modeled the hull and deck in CAD using physical measurements, enabling accurate placement of all subsystems and ensuring proper packaging within the hull.

Powertrain Testing

To test our P40 motors and InMotion controllers, we used a Land & Sea Dynamometer test setup to see how our motor and controllers would perform under race conditions. Using a Yokogawa Scopecorder, an oscilloscope with data calculation and recording abilities, we were able to measure the speed, torque, and power output of the motor as well as the voltage, current, and power input to the controllers. With these measured and calculated values, we were able to determine the efficiency of the motor at different operating points. Figure 7 shows a diagram of our motor test setup.

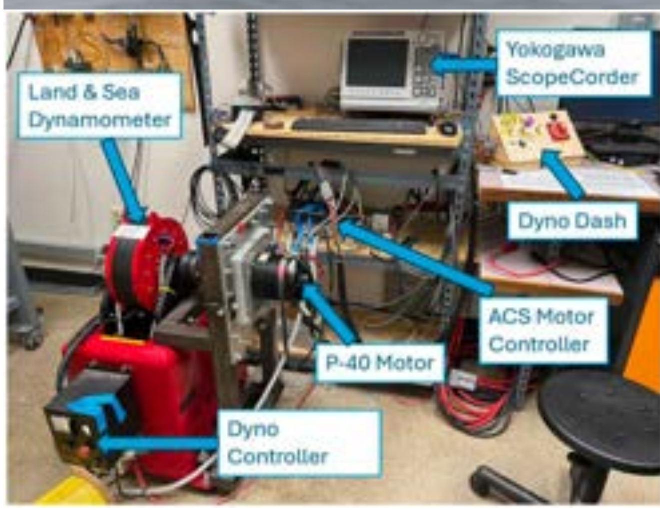

From the data of several tests involving changes in speed and applied torque, we found that our best operating point for the planing competition was to operate at 3500 RPM and 30 Nm of torque. This provides our team with a combined motor and controller efficiency of 89.17%. Figure 8 shows a motor efficiency plot for all the tested regions.

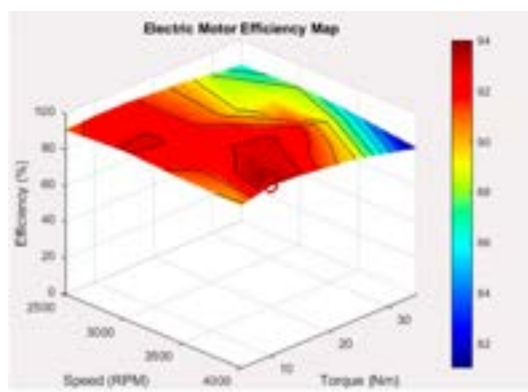

The operating point that we selected keeps the motors below our current operating limit of 300 amps, while still providing a sizeable power output of 11.02 kW. Using this data, we designed our propeller around this operating point, to maximize overall propulsion efficiency.

Central Connecticut: Gorgeous Fabrication; Practical Design

Skylre Hine, Dephtany Ayala, Dinh Doan, Max Prunier, Micheal Fritz, Samuel Iselin

www.navalengineers.org/CCSU

Planing vessels rely on hydrodynamic pressure generated at high speeds to support the hull. They ride smoothly in calm water, but when traveling through waves, planing boats experience rough motion that places significant stress on the vessel's structure. At low speeds, a planing craft behaves like a displacement vessel and is supported primarily by hydrostatic forces. Based on the hull type and geometry of a planing vessel, the boat selected for this project is the FS14 from BoatBuilderCentral, which was designed for competition use. The FS14 is a planing hull without a rocker. Planing boats must withstand higher impact loads on the bottom, and the transom must be capable of transmitting engine thrust efficiently into the hull. For these reasons, planing hulls are typically stronger and heavier than displacement hulls. Because of these structural and operational demands, this project adopts a modified mechanical outboard design inspired by traditional Southeast Asian mud motors. Conventional outboard motors often cannot operate in very shallow or debris-filled waters without risk of damage. In contrast, mud motor propulsion systems can operate in just inches of water, offering better capability of cutting through weeds and providing rugged durability. These characteristics allow successful operation in environments where standard outboards would fail.

Propulsion System Requirements

The vessel has an overall length of 14 ft 4 in, a maximum beam of 65 in, and a hull weight of approximately 185 lb. The designed displacement is 585 lb at a draft of 5 in, with a passenger and capacity rating of 950 lb (five persons) according to USCG standards. FS14 is rated for outboard motors between 6 and 15 horsepower, with a maximum of 25 horsepower permitted by USCG regulations. At a displacement of approximately 600 lb, the expected maximum speed at wide-open throttle is about 18 mph with a 6 HP motor, 23 mph with a 10 HP motor, and 28 mph with a 15 HP motor.

The hull was fabricated using marine plywood with fiberglass overlay; this method was selected for its strength and manufacturability. Marine-grade plywood was chosen as

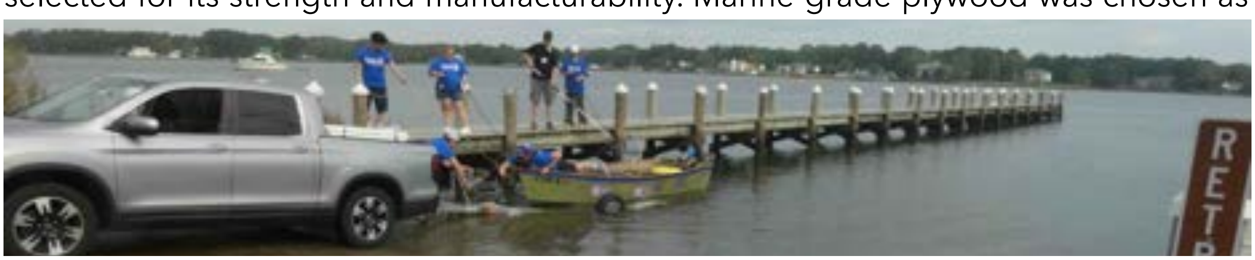

the main structural material because of its resistance to moisture, dimensional stability, and compatibility with epoxy bonding.

Purchased hull plans were converted into MasterCam Files, which ensured dimensional accuracy and allowed the hull components to be cut using a CNC wood cutting machine. Due to machine size limitations, full-length hull panels could not be cut in a single piece. Instead, the panels were cut into seven-foot segments, and puzzle joints were used to put them together. The puzzle joints not only ensured alignment but also created higher strength at these connections. The mating surfaces were bonded using marine-grade epoxy, and each joint was clamped and set aside to cure for twenty-four hours to ensure complete bonding. After curing, the joints were sanded flush to create a smooth surface and to prevent stress concentrations.

A strongback was constructed to serve as the primary assembly fixture. This feature ensures correct hull geometry, symmetry, and alignment throughout the fabrication process. Once the hull structure was fully assembled, fiberglass and epoxy were applied to all exposed wood surfaces to protect against moisture and create a durable product.

Fiberglass cloth was laid over the hull surfaces and saturated with marine-grade epoxy resin, creating a composite skin that improved strength and reduced the risk of moisture infiltrating the boat. Fiberglass was applied to the inside and outside hull to create a durable vessel capable of carrying the weight of a passenger and the motor equipment. Following fiberglassing, a fairing compound was applied across the entire outside surface of the hull. This was used to fill surface irregularities and any imperfections that occurred during assembly. The fairing compound was then sanded to achieve a smooth,

Figure 3: Fiberglass Laying on Outside of Vessel


hydrodynamic surface. This process reduced surface roughness and drag, improving the overall performance of the vessel.

The deck structure was installed using the same fiberglass technique. However, prior to installation, spray foam was placed under the deck in accordance with competition safety requirements to prevent sinking if capsizing were to occur. Once the foam was installed, the decking panels were bonded into place along with the bulkheads. To mount the motor onto the vessel, the transom was shortened to 10 inches in height.

The propulsion system was mounted to a modified transom, which was shortened to match the mud-motor geometry. The bolt pattern on the outboard was modified to match the bolt pattern on the D&D motor. Electrical integration included wiring the battery, controller, solenoid, kill switch, and throttle into a unified system with proper fusing and disconnects.

Delaware Dynamos

Alec Klarmann, Jaxon Vaughan, Andrew Colonello, David Kennedy

www.navalengineers.org/Delaware

Our 2025 entry utilized donated catamaran hulls from the College of Earth, Ocean, and Environment. Notably, those structures presented significant limitations in buoyancy, reserve capacity, and waterproofing, ultimately leading to water ingress that compromised internal components during the race. For this year's competition, the University of Delaware team shifted from repurposing material to a comprehensive engineering build from scratch. The 2026 platform is a custom 6-foot Deep-V monohull designed entirely in Rhino3D, Orca3D, and Fusion 360. While debating the construction of a tunnel planning hull, we ultimately opted for a shape with enhanced wave-piercing ability and stability, taking into account the rough water conditions from the previous year. To manufacture this complex curvature, we looked towards the University's Center for Composite Materials to produce a lightweight, advanced composite vessel. Due to the significantly different naval architecture and scale of the new hull, the propulsion system, steering, high-voltage power management, cooling system, and remote navigation have been redesigned to accommodate a high-performance 8800W powertrain. By moving to a custom build, we eliminated the geometric constraints of previous years, allowing for optimized component integration, a significantly higher power-to-weight ratio, and the structural integrity required to survive high-speed open-water conditions.

Hull Form Selection & Stability

Following a technical session with Professor Michael DeLorme from the Stevens Institute of Technology, the team selected a Deep-V monohull configuration. This choice was driven by the need for high-speed stability and the ability to mitigate slamming impacts at racing velocities.

At low speeds, a Deep-V hull sits deep in the water, which can induce roll instability due to the elevated center of gravity created by heavy battery placement. However, as the craft accelerates and transitions into a planing state, the hydrodynamic lift shifts the craft onto the aft section of the hull. The sharp 29-degree dead rise acts as a cutting edge, slicing through waves rather than bouncing over the surface. This reduces the peak vertical acceleration (G-loading) during wave impacts, protecting internal electronics from severe vibrational shock while minimizing wetted surface area to reduce drag.

Hydrodynamic Simulation & Drag Calculation

To validate the hull form and dimensions of our propulsion system, we performed a full static and hydrodynamic drag analysis in Orca3D. Utilizing the parametric functions within Orca3D, we iteratively manipulated key hull features—such as chine beam and deadrise—to observe their direct impact on hydrodynamic performance and stability. We conducted a comprehensive hydrostatic simulation with a 120 lb load to confirm the hull's sufficient load capacity and buoyancy for the 2026 payload (Figure 2). To accommodate this increased load while maintaining high-speed efficiency, the hull was designed with a greater-than-average height, which directly informed the selection of a sharp 29.12° deadrise. Using the standard drag equation, the force required to propel the vessel was calculated:

$$F_D = \frac{1}{2}\rho C_d A v^2$$

Where ρ is the density of seawater, C_d is the estimated drag coefficient of the hull, A is the frontal wetted area, and v is the target velocity of 12.86 m/s (25 knots).

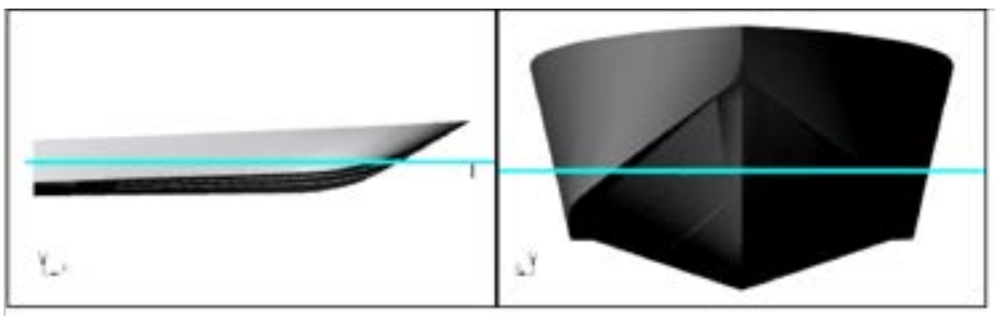

Figure 2: Hydrostatic simulation with 120 lb load placed on the back third of the hull.

Applying the Savitsky prediction method for a 54 kgf (119 lb) bare displacement, the simulation confirmed that the vessel achieves a stable planing state (Figure 3). At our target velocity of 25 knots, the analysis predicted a running trim angle of 3.28 degrees. Based on this drag data, we calculated the optimal propeller diameter and pitch to ensure our 8 kW motor, running at 53V, could deliver the required thrust.

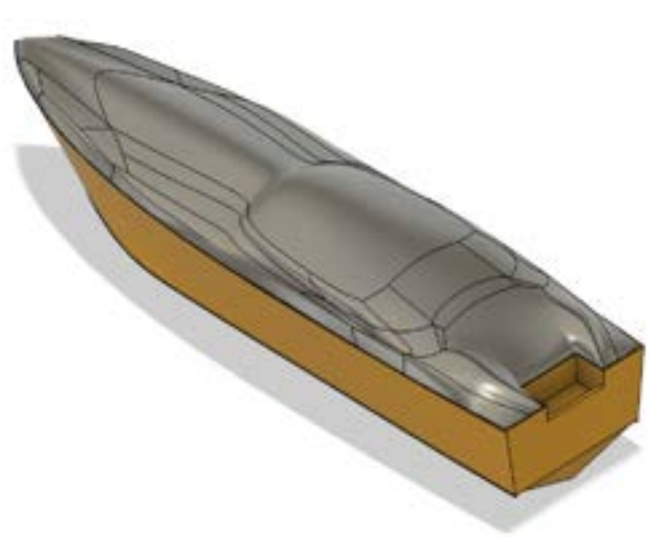

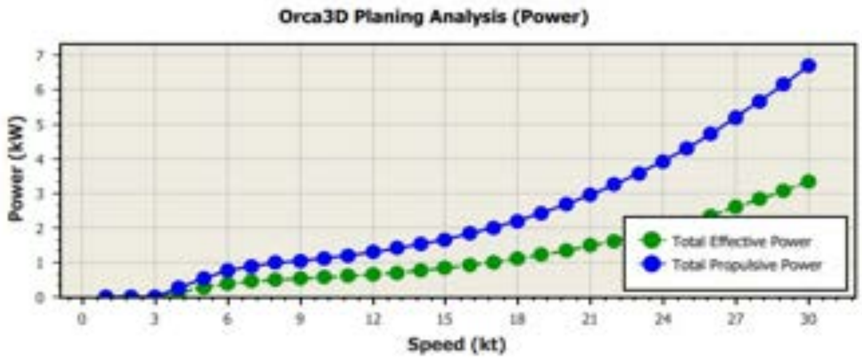

Figure 3: Speed vs Power, Speed vs Resistance graphs using Savitsky analysis

Hull CAD Design

The upper portion of the hull was developed within Fusion 360 with a focus on aerodynamic efficiency and component integration Figures 4 & 5. Given the high target velocity, the superstructure was designed to be as aerodynamically streamlined as possible to minimize wind drag at the bow and midsection. A specialized notch was integrated into the aft section of the hull to house the outboard motor and its custom swivel-type retractable mount. This design choice mimics the engine well or transom notch found in full-scale high-performance vessels, which serves to anchor the propulsion subsystem deeper into the primary structure of the hull. By recessing the mount into this notch, we achieve a more rigid mechanical connection that effectively handles the extreme torque generated by the brushless motor while simultaneously lowering the center of gravity. Furthermore, this configuration ensures the entire propulsion unit remains a stable, modular subsystem that is easy to access for maintenance or mechanical adjustments.

To further optimize the vessel's performance during the transition from displacement to planing, a reverse chine was integrated into the bottom hull to serve two critical functions. By redirecting the flow of water downward at the edges of the hull, the reverse chine generates additional hydrodynamic lift, which allows the 120 lb vessel to reach a stable planing state more efficiently. Additionally, the chine provides effective spray control by deflecting water away from the hull, reducing the wetted surface area and preventing water from interfering with the streamlined profile of the upper hull.

Elon University: High-Quality Metal Design & Fabrication

Gracyn Speter, Alex Strassberg, Maggie Dion, Cassidy Parrish, Will Larkin

www.navalengineers.org/Elon

Following our research, we delved into the more specific points of the design process. This process required constant communication between subsystems as each minute change had ramifications for the entire system. With the change to a V-hull we had to create a section for the placement of the motor mount. To do this, we created a small step to a flat section near the back of the boat to allow for the placement of the motor mount. This step was then further utilized as the starting height for the internal floor of the boat. With the floor now at a set level, we designed specific cutouts beneath it for the ballast that needs to be added for both our testing and competition. Finally, with the increase in total battery size, we had to increase the length of the hull to over nine feet.

After initial testing of the boat hull, the next task was to integrate the batteries into the system in a safe and controlled manner. Unlike the previous year, the batteries take up too much space to be put in a box. Our plan instead was to have a good margin from the waterline to the lip of the hull to minimize water intake. Our early tests vindicate this as safe enough connection and when we modeled the batteries' heat through a SOLIDWORKS thermal simulation, we did not see evidence that the batteries would overheat to the point of breaking down or experiencing a noticeable decrease in power. However, if this does not prove sufficient for water safety as we progress through our testing, our other option is a light foam top to seal onto the hull, creating a watertight seal. This would increase the risk of the batteries overheating but should completely prevent water from contacting the batteries. For both situations the batteries are secured onto the wooden floor of the boat using high strength Velcro.

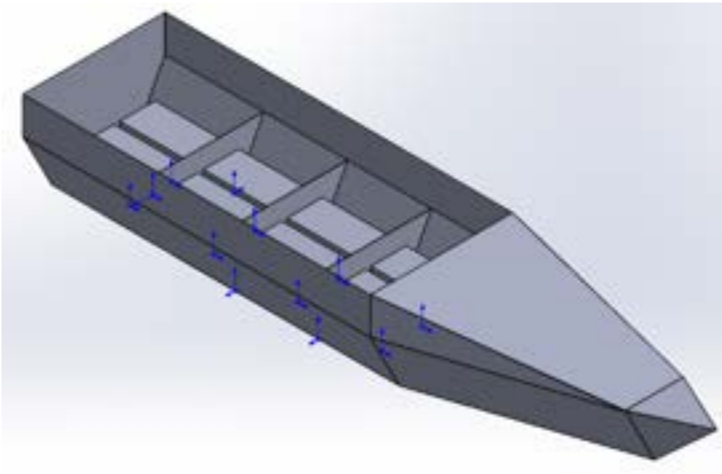

As previously mentioned, we sized up the motor from 3kWs to 9kWs. With this change comes an increase in weight and therefore a change to the motor mount. Our new design provides more reinforcement for the connection to the boat while allowing for a faster setup. The mount is made of 6061 aluminum to provide the strength to deal with the extra motor weight while not adding excess weight itself. It only requires six total bolts (four M4 and two 1/4-20) for total assembly through utilizing the mounting features present on the motor itself. The geometry of the motor aligns itself with the primary plate, allowing the nuts to be tightened easily. With this design the motor is stable and the assembly time of the mount is decreased to below 1 minute.

The final rudder design is an outboard rudder completely independent of the propulsion subsystem. It operates with a push/pull connection to the servo and is designed with the least number of linkages possible, minimizing potential failure points. The design was also made to be easy to redesign, repair, and replace, making it the optimal option for testing.

Because this design uses a 550kg-cm RC servo, two LifePO4 12V 25Ah batteries are needed to power it. These batteries were put in series and connected directly to the servo. The servo is then connected directly to the Flysky receiver, which is connected to the VESC for the motor controller. This wiring allows convenient testing of the servo without the VESC.

ECU: Electronics & Telemetry

James Miller, Trent Byrum, Preston Andres, Patrick Sprague Front row (left to right): Molly Lasure, Ty Parks, Max Martinez, Blake Isla

www.navalengineers.org/ECU

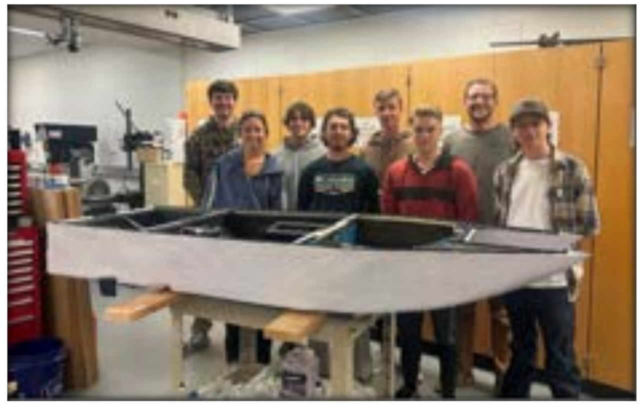

When formulating the hull design, the team prioritized speed, stability, and maneuverability, while also considering the vessel's ability to house the required propulsion components. The design that fulfilled all requirements was the catamaran style, specifically modeled from Mystic Powerboats' Miss GEICO. This style offers many advantages to the specific competition course having long straight runs with minimal turns. The narrow twin hulls minimize the wetted surface, allowing for fast acceleration, while the low-profile design reduces air resistance, and, therefore, drag. The bridge of the hull provides an open gap in the hull that contributes to higher efficiency at top speeds.

The length to width ratio of the vessel was determined to be 3.2:1. The goal was to keep the vessel's width as small as possible to maximize speed, while also considering the conditions of the competition by making sure the vessel was large enough to withstand significant wake if necessary. Additionally, the team decided to add steps to the underside of the boat to introduce airflow under the boat, which reduces drag. The dimensions of the vessel are shown in the model displayed in Figure 1. The most important characteristics for material selection in this specific application were strength and weight. High strength is necessary because the vessel must withstand repeated stress during testing, and it must remain intact if involved in a collision. The weight of the vessel is a main factor in efficiency and speed, as a lighter boat requires less force to move.

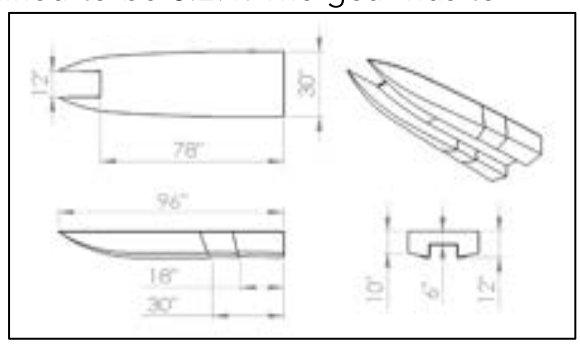

To maximize the power to weight ratio, it is typically more cost effective to reduce weight in comparison to adding more power. To achieve this, the team considered many different materials to make the hull. One study from the University of Kingston investigated the benefits and drawbacks of several composite/natural materials frequently used in ship building. It showed that carbon fiber absorbed the least amount of water, had the highest tensile strength, and had the highest flexural strength when compared to other materials such as glass fiber, flax fiber, hemp fiber, and a few combinations of each [2]. Carbon fiber is not only strong, but lightweight. The same study measured carbon fiber mat to be the second lightest material per volume [2]. Because of the high strength to weight ratio and the capability to add layers that increase strength, carbon fiber was selected as the hull material. For similar reasons, epoxy was the favored resin material when compared to polyester and vinyl ester resin. Additionally, the vacuum bagging technique was used to achieve the ideal resin to composite ratio, while also holding the laminate layers together during the curing process.

A 3D model of the hull was developed in SolidWorks (Figure 2). SolidWorks also listed its volume, surface area, and mass properties (Table 1). This SolidWorks model was used to perform the buoyancy and draft calculations.

The model of the hull used the composite density of the carbon fiber and epoxy [3]. Using Archimedes' Principle, the required displacement volume was calculated to be 2.08 cubic feet, as shown in Equation 1. The displacement requirement calculation included an estimated weight of the empty hull, the propulsion system, batteries, electronics, and payload, which was assumed to be 130 pounds. This information was used to determine an estimated waterline in SolidWorks, which was calculated to be 3.03 inches.

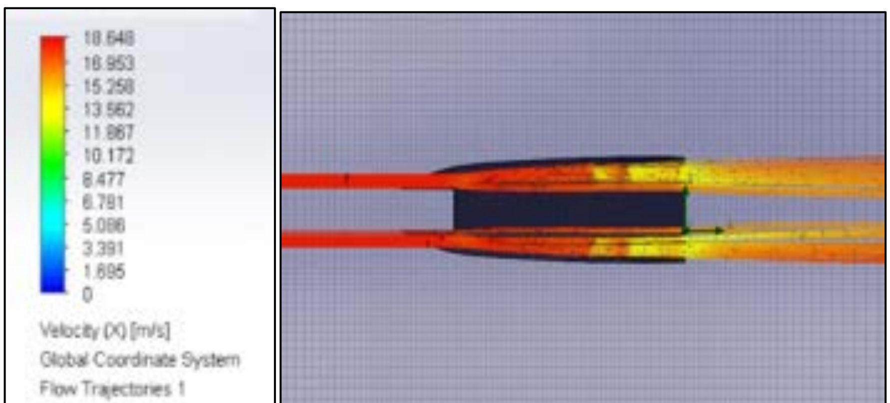

Figure 3. SolidWorks Flow Simulations.

The SolidWorks flow simulation (Figure 3) was used to estimate the hydrodynamic behavior of the vessel at a calculated operating speed of 40 mph (18 m/s). The results showed relatively low hydrodynamic resistance and low cavitation along the bottom of the hull at operating speeds. The result of the simulation supported the feasibility of the hull design.

Table 1. Hull Properties.

Parameters	Data
Density	0.034 lb/in^3
Weight	20.08 lb
Volume	580.69 in^3
Surface area	12314.5 in^2

Propulsion

The twin-motor electric catamaran presented in this paper integrates a high-reliability control system, high-RPM electric propulsion, water-cooled motor controllers, a multi-battery power system, and a wire steering mechanism. The design emphasizes controllability, safety, and operational durability within competition constraints and the possibility for future performance improvements.

The safety system centers around high-current battery disconnect switches and fuses. This system provides independent on/off control for the propulsion and control battery banks, enabling immediate shutdown of propulsion power while keeping the control system active for steering and remote sensing. Redundant kill switches ensure propulsion can be disabled even if one system fails. The propulsion circuit routes the 48V battery through the fuses and disconnect switches before reaching the electric speed controllers (ESCs), while the control circuit routes the 12V battery through another disconnect switch and universal battery eliminator circuit (UBEC) to the receiver, servo, and pump. This system meets competition safety requirements and maintains steering capabilities during emergency propulsion shutdown.

The system is organized into five major subsystems: The control system provides throttle and steering commands; The propulsion system converts electrical energy into thrust; The motor control system regulates motor speed and protects against overload; The power system distributes high-current and low-voltage energy to all integrated electronics; The steering and cooling systems maintain directional power and thermal stability. These subsystems operate as an integrated whole, ensuring that the catamaran can deliver consistent performance under varying load and environmental conditions. A high-level overview of subsystem interactions is shown in Figure 4.

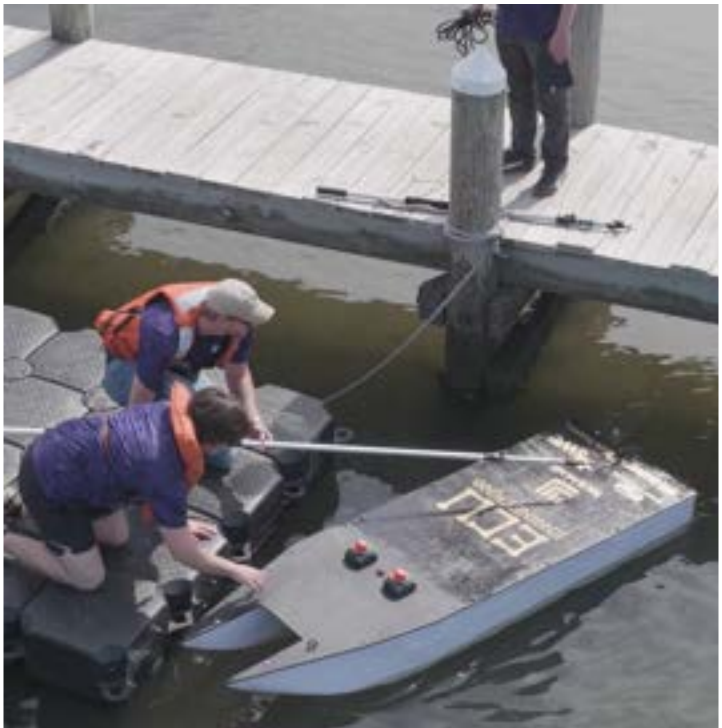

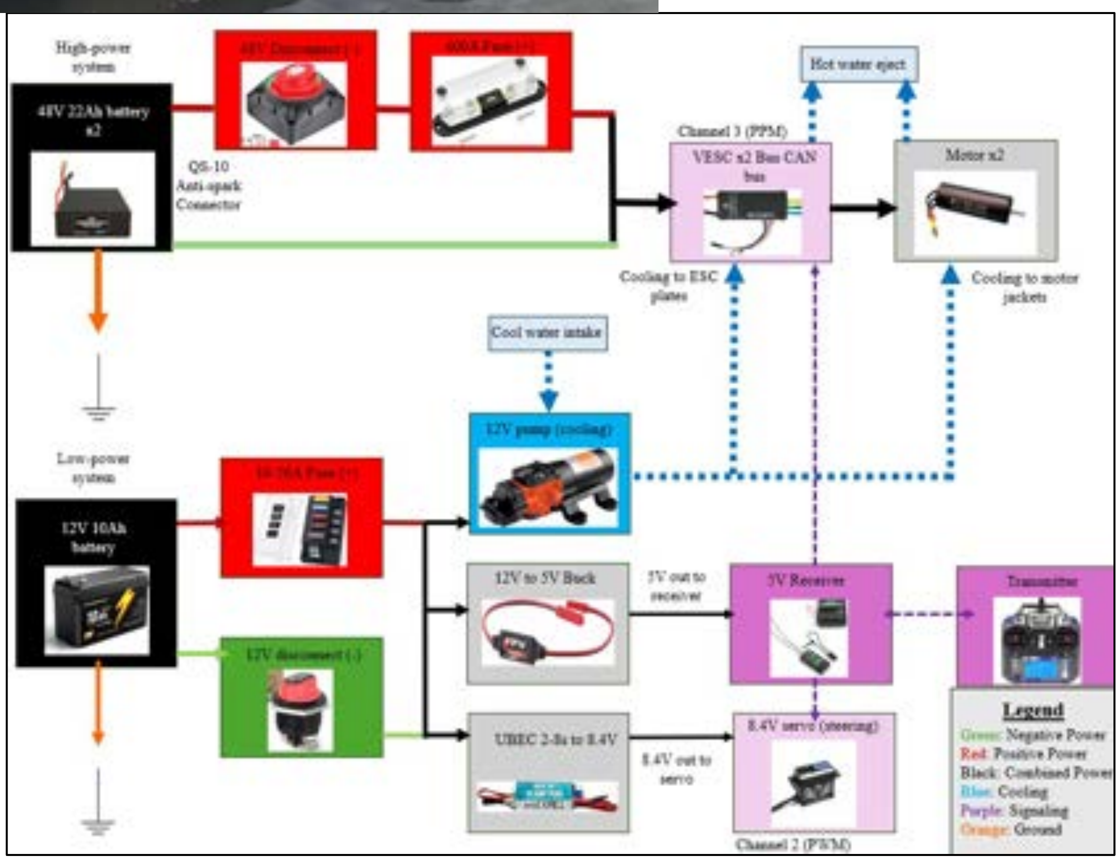

Figure 4. Propulsion system block diagram [4-15].

Georgia: Upgrading a Strong Platform

Nicholas Goodstone, Audrey Pearce, Seth Brand

www.navalengineers.org/UGA

The electrical system design proposed for this year's vessel has been fully implemented, and it's a big step forward in terms of reliability and overall performance. All of the planned upgrades, including the larger battery system, new wiring layout, and added circuit protection, have been completed. Because of delays with the hull redesign, we haven't been able to fully test the system in the water yet. That said, all of the electrical components have been tested out of the water and are working as expected.

The battery system was upgraded from six to eight 22.2V LiPo batteries in parallel, which increases the total capacity and gives us a much better safety margin for runtime. This was an easy decision, since the previous team wasn't able to complete the race distance. Even though the requirement is now only 2 miles, we wanted to make sure we had more than enough capacity to avoid running into the same issue.

We also completely redesigned the wiring system. The old setup used a lot of EC5 Y-splitters, which made things cluttered and introduced multiple points of failure. In the new design, all connections are routed through positive and negative bus bars. This makes the system much cleaner, easier to work on, and reduces the chances of something overheating or failing at a connection point.

Another major improvement was adding a 150A circuit breaker to the positive bus bar. The previous system didn't have a real power cutoff and was always live, which led to sparking when connecting batteries. Now, we can safely connect everything first and then turn the system on using the breaker. This makes the system a lot safer and easier to handle.

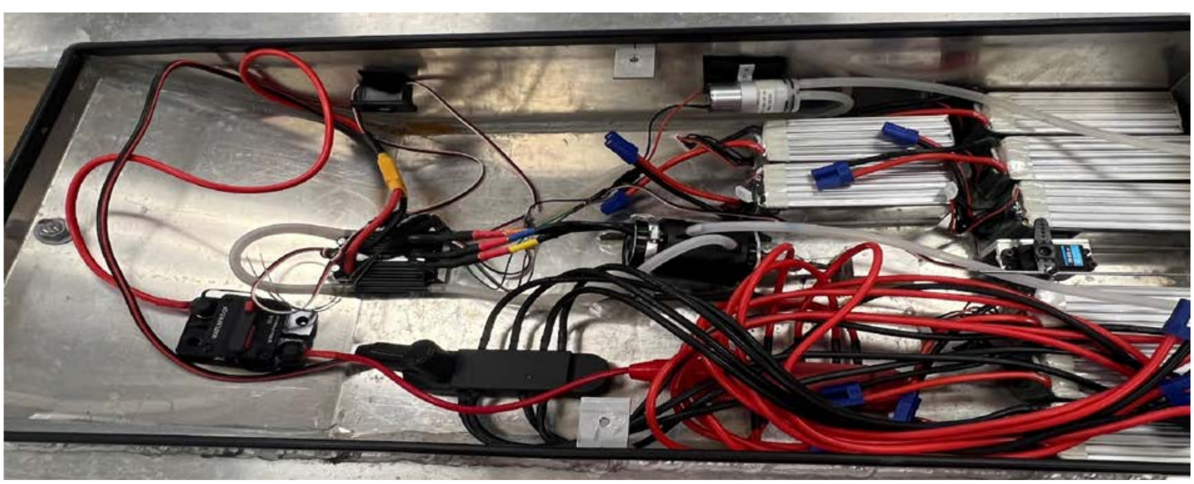

GW: Powering A Class D Hydrofoil

Adam Newman, Claire Caltabiano, William Barry, Ronan Mas, Richard Wagner, Zain Mohsin, Ilyas Jenson, Yumemi Malm-Akiyama, Robert Welles, Nnamdi Felix-Ugorji, Katherine Cruz, Aidan Flores, Patrick McCannm, Brian Martinez, Amanuel Wendimu, Stella Iyengar, Brasen Agungm, Jack Ploshnick, Cole Schwab, Zach Canning, Tim Harrington

www.navalengineers.org/GW

A 14' long plywood APBA Class D hydroplane hull was selected. Hydroplanes operate on a cushion of air, reducing wetted surface, thus allowing for reduced hydrodynamic drag. Since APBA racing only turns left, the hull was asymmetrical with a turning fin on the port sponson and the cockpit offset to port by a few inches. US-0 was acquired through a secondhand market, sourced in Long Island, NY, for a purchase price of $500. Since the hull was purchased in and spends most of its time in NY, stored at Mr. Alper-Nocera's residence, it qualifies for the criteria to avoid NY registration, as a vessel does not need to be registered if it is racing in a competition.

In standard racing, a hydroplane would have one vertical turning fin on the port sponson to help it dig into the water. Simply adding another vertical fin on the starboard side could cause the boat to flip laterally on the outside of the turn. As the inside fin grips the water and pulls the vessel into the turn, the outside fin has an opposite reaction force.

Adjusting the camber and adding a second turning fin improves stability at higher speeds and faster bidirectional turns. By angling two fins inward, the hydrodynamic force vector now has a vertical component. This means the outside sponson is pushed down, counteracting the rolling moment that would otherwise flip the boat. The vessel allows for adjustment between 10 and 25 degrees of camber, depending on the water conditions. A smaller degree of inward camber has a better turning bite, while a greater degree increases rolling stability at the expense of drag.

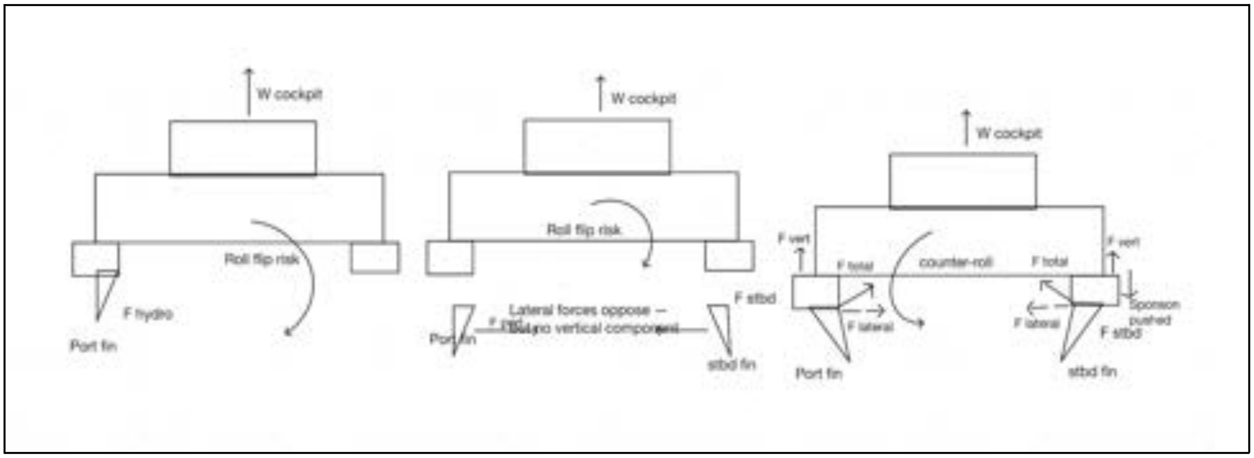

Figure 1. Free body diagrams: One fin on the left side going straight down (left), two fins each on either side going straight down (middle), and two fins angled inward between 10-25 degrees (right).

Motor

The ME1616 motor from Motenergy was selected for its excellent performance-to-price ratio. Weighing 55 lbs, the ME1616 is a compact alternative to internal combustion equivalents weighing around 115 lbs while also delivering up to 55 kW peak power. This motor provides an exceptional power-to-weight ratio that significantly improves overall system performance compared to heavier engines or lower-output motors. Its high efficiency (around 92%) minimizes energy losses and heat generation, resulting in longer run times and reduced battery demand. The onboard water-cooling infrastructure allows power to be delivered continuously up to 96 V and 250 A, with a peak current of 600 A for 1 minute. In addition, the brushless PMAC design ensures low maintenance, high reliability, and smooth torque delivery, which is critical for applications requiring responsive and stable performance. The ME1616 motor is a frequently used choice for DIY go-karts due to its high torque at low speeds, allowing for quick acceleration without the need for complex gearing. Combined with its durable construction and relatively affordable cost compared to similarly capable motors, the ME1616 stands out as a well-balanced, high-performance option that delivers superior efficiency and practicality over competing motors.

Howard: Control & Autonomy

Nicole Miller, Matthew Cofer, Arinola Mordi, Asiya Sadeq

www.navalengineers.org/Howard

The propulsion system was redirected from a traditional propeller-shaft configuration to a thruster-based setup due to procurement constraints. This shift allowed the team to move forward with a configuration that could be reliably sourced, integrated, and tested into the system.

The current setup uses two 24V Blue Robotics thrusters at the rear as the primary propulsion units, and two 12V Blue Robotics thrusters at the front for directional control and turning assistance.

This configuration allows the rear thrusters to provide forward propulsion while enabling steering through differential thrust. The front thruster supports turning, particularly at low speeds, where precise maneuvering is required.

Each thruster is driven by a dedicated Blue Robotics Basic ESC (Electronic Speed Controller), which regulates power delivery and allows for smooth, controlled actuation based on input signals.

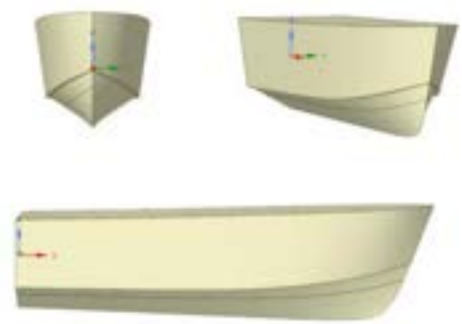

Control System Architecture

The control system is structured to support manual operation, allowing the boat to be tested safely. A radio transmitter and receiver system is used for manual control. The receiver acts as the interface between user input and the onboard system, sending throttle and directional signals to the ESCs.

The ESCs receive these signals and regulate power delivery to each thruster. Proper ESC calibration ensures that both rear thrusters respond consistently, which is important for stable differential steering.

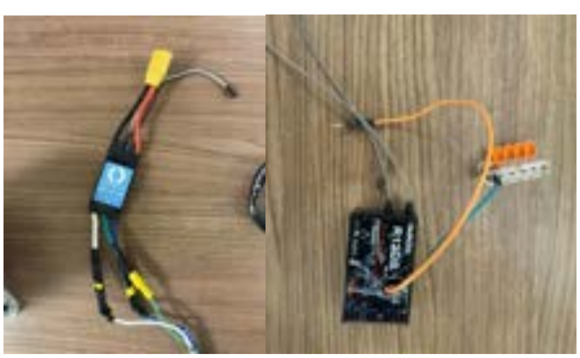

Electrical and Power System

An electrical performance analysis was conducted to validate the selection of the power distribution system and ensure safe, efficient operation of the propulsion subsystem. Key performance metrics evaluated include voltage drop across power cabling, thermal losses in wiring, overcurrent protection requirements, and estimated battery runtime under continuous load.

Category	Parameter	24V Subsystem (2 Thrusters)	12V Subsystem (2 Thrusters)
Current Draw	Per thruster	15 A	15 A
	Total current	30 A	30 A
Voltage Drop	Per line	0.24 V	0.24 V
	% Voltage Drop	~1.0%	~2.0%
Thermal Losses	Per thruster line	3.6 W	3.6 W
	Subsystem total	7.2 W	7.2 W
	Total system	-	-
Overcurrent Protection	Per ESC fuse	20–25 A	20–25 A
	Main battery fuse	40 A	40 A
Battery Runtime	Example capacity	20 Ah	20 Ah
	Ideal runtime	~40 min	~40 min
	Realistic runtime	~30 min	~30 min
Cooling System	Fan current draw	-	~1 A (total)
	Power source	12V	Independent 12V battery
	Runtime	Several hours	Several hours

DelftShip Modeling and Hydrostatic Analysis

DelftShip Pro was used to generate a more accurate hull representation and evaluate hydrostatic behavior, including draft, displacement, and buoyancy distribution.

Earlier estimates using a block coefficient predicted a draft of about 3.7 inches, but this underestimated the true submerged volume. Using DelftShip's hydrostatic calculations, the correct displacement (~0.070 m^3) corresponded to a draft of approximately 7.5 inches, which better reflects the actual vessel weight and geometry.

This corrected draft was critical for ensuring realistic CFD setup and proper hull positioning relative to the free surface.

Illinois: Control & Autonomy

Dominick Braico, Patrick Moore, Venkata Krishna Teja Kolla, Keshat Mehra, Mason Norris, Dylan Pruemer, Josh Anderson, Daniel Damasco, JT First, Roberts Fulss, Riku Kanzaki

www.navalengineers.org/Illinois

Autonomous surface vehicles depend heavily on sensing and onboard electronics because of the noisy, dynamic nature of marine environments. Unlike ground robots, boats cannot rely on lane markings, stable terrain, or predictable traction. Wind, surface reflections, vibration, and drift all interfere with perception and localization, so the electronics architecture of an autonomous boat must be based on sensing redundancy rather than on a single sensor. Research in autonomous marine navigation [4] therefore emphasizes the importance of selecting sensors according to the operating environment and the mission objective, rather than simply maximizing sensor count or complexity.

For a race in which the vehicle must follow a course marked by buoys over open water, the most useful sensor classes are those that provide complementary information such as a global reference for position, and inertial information for short-term motion estimation. That is why GPS and IMU appear repeatedly in autonomous surface vehicle research and in small-boat autonomy practice. Therefore, it is common practice to use GPS and IMU sensors in autonomous surface vehicles. More complex sensing systems such as LiDAR or stereo depth cameras can be valuable in mapping-heavy applications, but they impose greater cost, integration burden, and power demand, and their added value is limited when the task is surface navigation rather than dense 3D reconstruction. For this reason, the technical baseline for a competition boat favors a practical multi-sensor architecture built around robust, lightweight, and computationally manageable electronics [5].

A second electronics consideration is that small electric boats must integrate sensing with propulsion hardware under strict weight, waterproofing, and power constraints. The electronics are therefore part of the broader challenge of packaging reliable autonomy into a compact marine platform. Weight distribution limits the number of batteries we can have in the boat. The rating of our ESCs and the connectors we used were determined by our power constraints and power draw. Waterproofing helped us determine the distribution of our electronics through the boat.

Controls

The controls system was shaped by background research in maritime autonomy, especially research showing that marine navigation is highly sensitive to disturbances such as wind, drift, changing visual conditions, and high-speed maneuvering. Our background research shows that LiDAR-only SLAM becomes less reliable in marine environments with limited features and at higher speeds, while sensor fusion using GPS and IMU data through a Kalman filter [7] significantly improves path-following accuracy for autonomous surface vehicles. This directly supports the team's decision to avoid a single-sensor strategy and instead use a multi-sensor autonomous navigation architecture.

Cooling

Thermal management is a fundamental background issue in electrically propelled marine vehicles because electric propulsion systems convert only part of stored electrical energy into useful thrust; the rest appears as heat in motors, ESCs, wiring, and batteries. In small high-power craft, this heat can build rapidly because the hull interior offers limited airflow and little room for oversized thermal hardware. As a result, cooling is not merely a detail of implementation but a central reliability concern in electric boat engineering.

This becomes even more important in autonomous boats, where overheated components can directly result in mission failure. A crewed boat can sometimes be throttled back or corrected immediately by an operator. An uncrewed boat, by contrast, must sustain safe component temperatures while continuing to navigate on its own. Background work in electric propulsion therefore points toward cooling strategies that use the operating environment efficiently. Because the craft is already moving through water, marine vehicles can exploit that surrounding water as a heat sink far more effectively than they could rely on passive air cooling alone.

For small racing craft, water-based cooling is attractive because it removes heat without requiring large fans or bulky heat exchangers, both of which would consume space, mass, and power. In order to reduce power consumption, we decided to use a rudder capable of picking up water naturally, eliminating the need for a water pump.

Autonomous Controls System

The autonomous control system is built around the CubePilot Cube Orange+ flight controller, which serves as the central processing unit for navigation, motor control, and steering. The Cube Orange+ runs ArduPilot in Rover mode configured for a motorboat, which supports matched-throttle twin motor output combined with a dedicated servo steering output.

Navigation data is handled by a Here3+ GPS module, which provides positional data to the flight controller over CAN bus. Heading is derived from the Cube Orange+'s internal IMUs. Waypoint missions are planned and uploaded to the flight controller using Mission Planner ground control software, which communicates with the Cube Orange+ via a pair of RFD 900x radio modems. The RFD 900x link provides the connection between the ground station laptop and the craft, allowing the operator to monitor vehicle state, upload or modify waypoint missions, and issue commands in real time from shore after the boat has been placed into the water.

During autonomous operation, the Cube Orange+ executes the uploaded waypoint sequence, fusing GPS and IMU data through an extended Kalman filter to estimate the state of the boat and adjust the steering angle.

If the GPS signal is lost or the position fix is corrupted, the FS_GPS_ENABLE parameter configured in the Mission Planner software triggers an immediate mission hold, commanding the craft to stop and maintain position until a valid GPS fix is restored. This behavior is preferable to continuing a waypoint mission on degraded position data, which could result in the craft deviating significantly off course. GPS degradation is a realistic concern in the operating environment and testing will be conducted to verify the functionality of this failsafe method.

Iowa: Design & Fiberglass

Mathew Boemmel, Aayush Mistry, Nathan Premo, Ryan West, Adam Schilz, Jacob Plesek, Peter Kotchick

www.navalengineers.org/Iowa

Using the same CAD for the hull that we had last year, which was the Southampton 3b, we began by deciding on an appropriate scale factor for the hulls dependent on the max payload they would be carrying. Adding up our estimated weight for one hull, we ended up at an estimated carry weight of 27 kg for each hull.

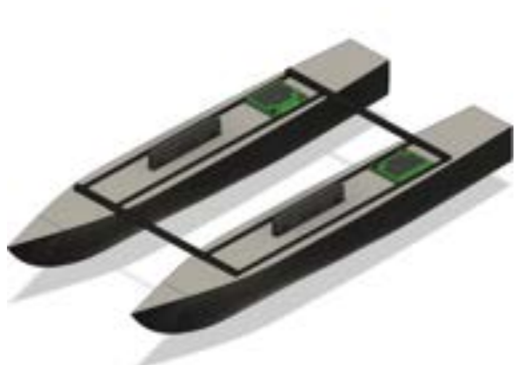

To determine the appropriate scaling for the hulls, we cut the model at the desired waterline. Then we calculated the appropriate volume of water given 27 kg of weight, which ended up at 0.978612 cubic feet. Then we scaled the cut the model until its volume aligned with volume of the displaced water. Our boat ended up needing to be scaled by a factor of 1.28.

To reinforce the structure of the boat and prevent the hulls from collapsing, we created a rigid 8020 sub-structure that is inserted into the top of the hulls and gets epoxied into place. The purpose of this substructure is to avoid the buckling forces we noticed on our older hull, simulated through Fusion's analysis software. We noticed that certain forces along the top of the hull caused a concavity in the shape of the hull, which could lead to potential cracks in the hull.

The new frame was configured to be more rigid across the length of each hull, preventing any concave forces, as well as distributing the payload weight more evenly across the surface of each hull. The dual bars on each hull also prevent torsional forces from acting across them and causing twists that may shear the boat in half. The hulls were built using blanks of polystyrene insulation foam glued together using special contact cement intended for use on the foam blocks. The foam blocks were then milled on a CNC by IIHR, by first milling the top surface and grooves into the material, and then flipping the blanks over and cutting the curved hull shape. The hulls are then covered in a fiberglass wrapping to reduce the porosity of the foam surface and create a smooth, gliding surface along the faces.

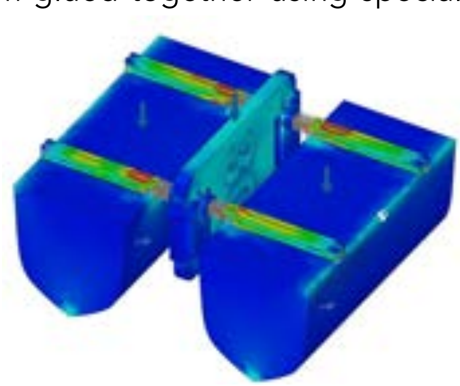

Johns Hopkins: Mastering Autonomy

Aryan Unnikrishnan, Daniel Collum, Elmer Alexis Mendoza, Matthew Dao

www.navalengineers.org/JHU

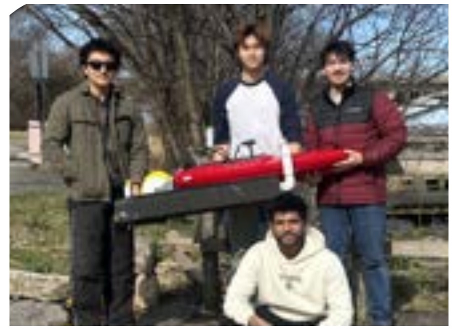

After conducting research into autopilot software commonly used by professionals and hobbyists, three autopilot software options were evaluated: ArduPilot,

PX4, and a homemade Python-based navigation algorithm. The Python algorithm option was quickly eliminated due to the significant time required to build navigation, control, and failsafe functions from scratch. The trade study therefore focused on ArduPilot and PX4, both of which are fully developed, open-source, no-cost systems supported by our selected hardware. While each offers sufficient autonomy features and hardware compatibility, ArduPilot provides a larger documentation base and community support network, reducing integration risk and easing development. This comes at the cost of PX4 having higher customizability and popularity in commercial markets; however, these were both deemed insignificant factors in our case. For these reasons, ArduPilot was selected as the primary navigation

Table 1.1: Software Trade Study

Category	ArduPilot	PX4	Python Algorithm
Cost	Free	Free	Free, high time cost
Documentation	Extensive, large community	Good, smaller but professional community	None; minimal hobbyist community
Hardware Support	Wide board support	Wide board support	Must build drivers
Features	Hobby-grade, extensive failsafes, many modes	Commercial-grade, extensive failsafes	Must build all navigation & control
Integration Ease	Easier, many tutorials	Moderate, more technical	Hardest, all custom
Customization	Open source & Lua scripting	Highly modular uses C++	Fully custom
Industry Use	Broad hobby UAV/UGV/ROV use	Strong in research labs	Rare
Decision	Chosen: best docs & support	Backup option	Rejected: too time-intensive
Switching Risk	N/A	Low: same hardware	High: complete rewrite

software. However, because the hardware fully supports both platforms, switching to PX4 was a low-effort fallback option if the project needed a change.

The control hardware was selected based on recommendations from Johns Hopkins professors conducting research in the marine robotics sector, Baltimore-based maritime companies, ArduPilot documentation, and community forums. The flight controller was the most critical component, as the rest of the control system was designed around it. We selected the Pixhawk 6C due to its low cost, compatibility with a variety of navigation software, high processing speed, and modular design. To ensure seamless integration, we also purchased a power module from the same vendor to ensure safe power delivery to the Pixhawk.

For positioning, we selected an M10 GPS and a DroneCAN F9P module, both recommended by the Pixhawk documentation and known to provide high GPS accuracy when used together. We reused an existing TF8B controller from previous years and purchased a compatible RC receiver to avoid the cost of a new transmitter. Finally, we added a telemetry radio rated for up to 3 km range to enable reliable communication with the ground station. After testing, the GNC system is capable of centimeter-level accuracy and 0.75-mile communication range, which is well above what we expect to encounter during the range.

Figure 1.1: Pixhawk 6C Flight Controller

Additionally, all our electronics were temperature tested before being secured onto the vessel. We identified the points of our circuit most vulnerable to high temperature to be our XT-60 connectors as they're rated for 60 Amps continuous and 180 Amps peak. This is usually with 12 AWG wires, however, and we are using 10 AWG

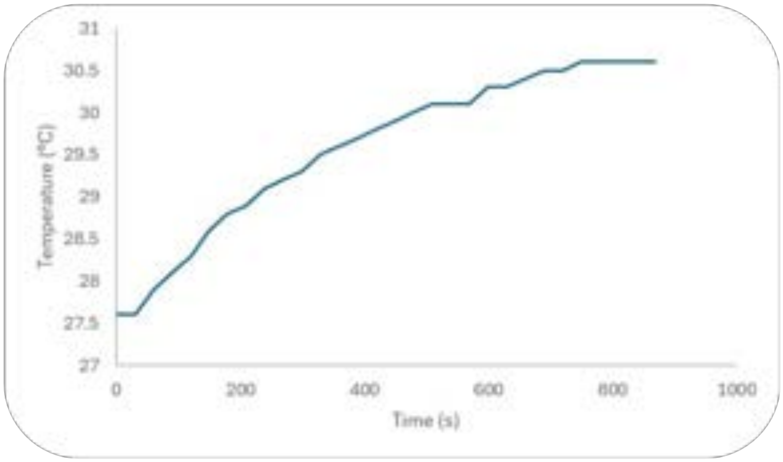

Figure 3.4 Results of temperature test

throughout our circuit, raising our maximum current. To ensure our safety against high current, we ran 65 A throughout our circuit, in an enclosed environment all while regularly measuring the temperature of the connectors. The figure below shows that our connectors are more than capable of handling their expected load.

Table 1.3: Hardware Trade Study

Component	Chosen Hardware	Reason for Selection
Flight Controller	Pixhawk 6C	Strong ArduPilot compatibility, well-documented, reliable foundation for control system
Power Components	Vendor-matched PDB + Power Module	Proven compatibility with Pixhawk; reduces integration risk
Primary GPS	M10 GPS	Recommended by Pixhawk documentation; reliable baseline GNSS performance
High-Accuracy Positioning	DroneCAN F9P RTK Module	Provides high GPS accuracy; proven compatibility with Pixhawk and ArduPilot
RC Control	Existing TF8B + compatible receiver	Cost-effective; maintains required control capability; acceptable range
Telemetry	3 km telemetry radio	Ensures stable long-range communication with ground station

Kentucky: Aquanamous Preparation

Jake Allen, Callie Feltner, Spencer Goode-Kulchar, Nadia Turner

www.navalengineers.org/Kentucky

The Autonomy prototype is contained in an IP67 rated waterproof junction box that is 8.7″ x 6.7″ x 4.3″ inches shown in Figure 5. The system sinks a maximum of 12V 3A from the 12V bus that goes through a 12V to 5V buck converter and powers the Raspberry Pi 4B via USB-C. The power cables are hidden on the bottom level of the housing. The Raspberry Pi supplies power to the PixHawk 2.4.8 flight controller and communicates across the micro-USB connection using MAVLink protocol to receive the throttle and steering values. The Pi computer then communicates these values to the Controller Electronics system via a 2-wire cable on the UART interface.

The PixHawk receives data from the GPS/compass module for positional data and communicates via the 915 MHz radio with the base station laptop. This connection communicates using MAVLink protocol and issues a constant real time data stream of the boat's telemetry to the base station. The base station also issues missions to the flight controller with the same interface. The PixHawk also has connected a physical safety switch that toggles the outputting to motors and servos and the throttle and steering data. This is for testing purposes and during the competition it will be removed so that the motor does not get turned off accidentally.

The controller electronics prototype was built upon work from previous teams and is housed in an IP67-rated waterproof junction box. This system was developed to manage throttle and steering by integrating inputs from the automation subsystem for autonomous operation. It functions by receiving automation packets and using control logic to determine whether they represent valid commands, then sending appropriate control signals to the motor controller and steering system for real-time operation. The system is powered by a 12V battery, with a 12-5V DC-DC buck converter used to supply the required voltage to the microcontroller.

We're using a LiDAR-based setup to support collision avoidance by detecting and analyzing nearby objects in real time. The current prototype operates as a standalone system, with the sensor powered by an external battery and connected to a laptop via Ethernet for live monitoring and data collection. This simple configuration allows us to test detection performance and validate reliable data communication before integrating the LiDAR into the full collision avoidance system.

The existing subsystems provide the structural, mechanical, and electrical foundation required for the autonomous vessel platform. The BRIS inflatable hull offers sufficient buoyancy and structural capacity to support the propulsion system, battery storage, and electronics while remaining within the manufacturer's motor and load ratings. The D&D electric propulsion motor, paired with the 1268 SepEx controller, provides high torque and controllable power delivery suitable for marine propulsion while maintaining compatibility with the 48 V power system. The linear actuator steering mechanism enables precise control of the propulsion thrust angle, allowing the vessel to maneuver effectively and respond to navigation commands. The power subsystem architecture separates propulsion power from electronics power to improve system stability and prevent electrical noise from affecting control systems. The 48 V $LiFePO_4$ propulsion battery bank provides approximately 4.8 kWh of energy capacity, exceeding the 55-minute competition endurance requirement, while the lighter battery chemistry reduces overall system weight compared to lead-acid alternatives, improving efficiency and vessel performance.

Controller Electronics

The final prototype of the Controller Electronics subsystem consists of a competition-ready custom printed circuit board (PCB) integrated with the Heltec AB02S microcontroller implementing multi-layered logic control to ensure safe maritime operation. This subsystem contains the core control logic for both throttle and steering, with its primary role being the integration of data from the Collision Avoidance and Autonomous Navigation subsystems. These subsystems communicate with the Controller Electronics through direct wired connections, allowing the Heltec microcontroller to process incoming control packets and make real-time decisions. The subsystem is responsible for autonomously controlling throttle and steering while simultaneously responding to obstacle avoidance commands. In addition to propulsion control, the Controller Electronics subsystem manages the on-board electronics power distribution, as illustrated in Figure 6. The schematic shown in Figure 6 presents the overall power flow of the current electronics architecture and highlights the major inputs and outputs associated with the Controller Electronics subsystem.

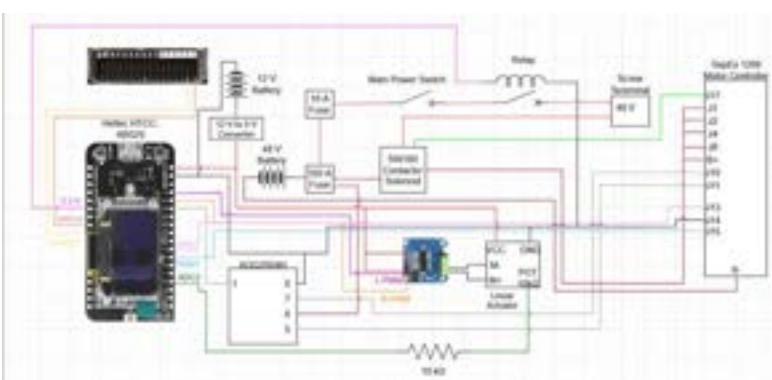

Figure 6: Boat Electronics Schematic

As shown in Figure 6, the subsystem utilizes two independent battery systems for operation. The primary system for on-board electronics is a 12 V battery system, which supplies power to the linear actuator and the microcontroller. The microcontroller voltage is stepped down from 12 V to 5 V using a DC-DC buck converter to ensure stable operation. The second battery system is a 48 V propulsion system composed of four 12 V batteries in series, providing a total energy capacity of approximately 4.8 kWh. This 48 V system supplies power to the motor controller and motor. The motor power path incorporates multiple layers of safety logic to ensure reliable and compliant operation under all conditions. The system was tested by simulating the automation packets and testing a range of scenarios as well as invalid data points ensuring the proper safety measures are taken to ensure safe operation.

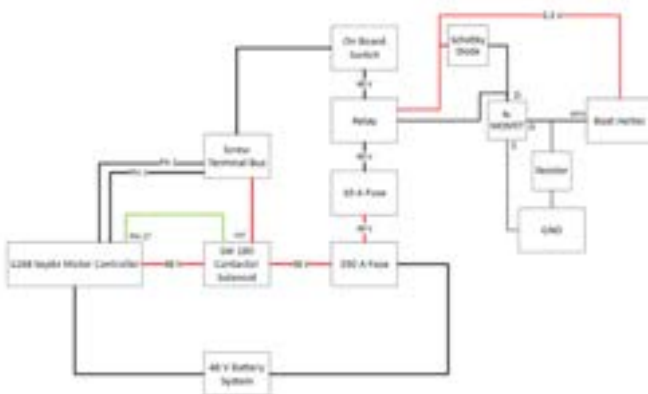

Figure 7: Kill Switch Schematic

The motor safety logic consists of three independent layers. The first layer is the SW180 contactor solenoid, which serves as the primary means of disconnecting the 48 V supply from the motor controller. A 350 A fuse is placed in series with the 48 V line to protect downstream components in the event of a short circuit or high inrush transient. The second layer of ries with a manual control switch. This configuration allows the operator to manually enable or disable the system while also permitting electronic control via the third logic layer. The third layer consists of an NMOS relay control circuit that connects or disconnects the relay coil to ground depending on the gate voltage state. The gate signal is controlled by the Heltec microcontroller. If the Heltec does not receive valid automation packets, the NMOS state changes, causing the relay to open and disconnect propulsion power in accordance with competition safety regulations. The primary components used in this control stage include a 1 kΩ 0805 resistor, an SSM3K324RLFCT-ND NMOSFET, a TSS83L45 Schottky diode for flyback protection, and a G6C-1114P-US DC3 relay.

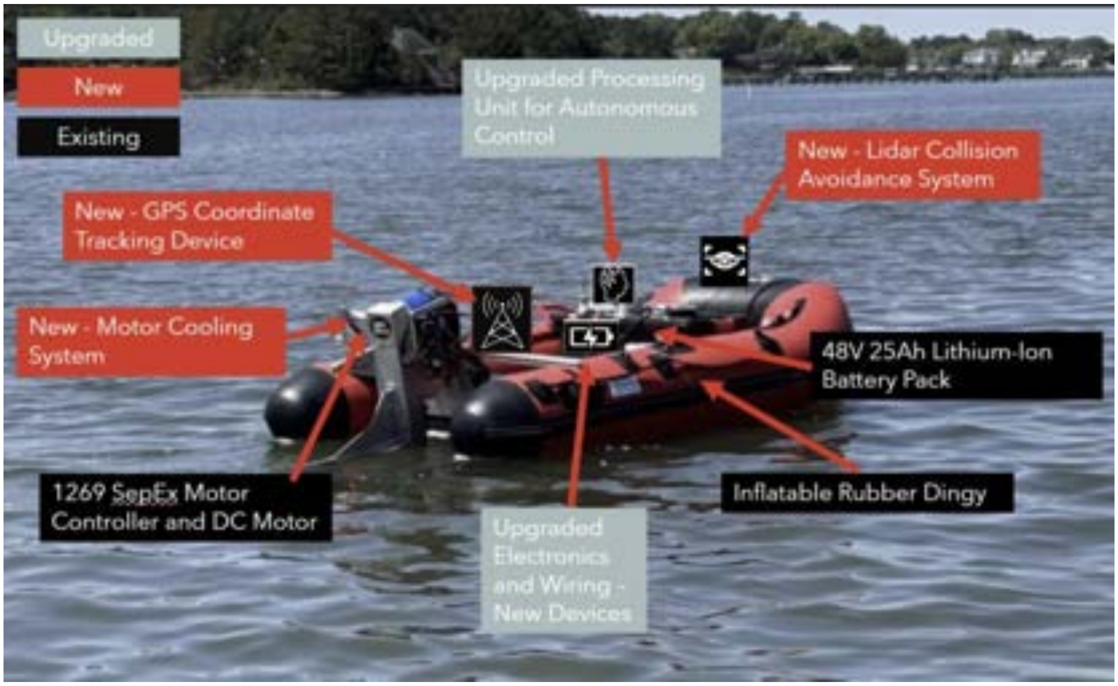
Upgraded
New
Existing
Upgraded Processing Unit for Autonomous Control
New - Lidar Collision Avoidance System
New - GPS Coordinate Tracking Device
New - Motor Cooling System
48V 25Ah Lithium-Ion Battery Pack
1269 SepEx Motor Controller and DC Motor
Inflatable Rubber Dingy
Upgraded Electronics and Wiring - New Devices

Kentucky: Ripples Runs to a Championship

Mikey Sims, Preston Keith, Ethan Staten, Lawson King

www.navalengineers.org/Kentucky

For the remote controller, all source code, diagrams, and documentation are stored in the team GitHub repository and shared project directory, with the link at Project-Ripple-Remote-Controller/README.md at main st8n2004/Project-Ripple-Remote-Controller. The source code includes how to read analog inputs from the potentiometers, converts them into digital values, packages them into LoRa communication packets, and transmits them to the onboard microcontroller at a fixed interval. The diagrams include the pinout for the LoRa microcontroller as well as its wiring. Additional tables in the read me show what connections are needed for all components and pins.

The code utilized for the microcontroller can be found in the following github link: pkeith67/Microcontroller__prototype_code_1. The code initializes serial communication, the board hardware, and the LoRa radio, then centers the steering servo at 90 degrees and performs an ESC arming sequence by sending minimum throttle pulses for several seconds to ensure safe motor initialization. After this process, the receiver enters continuous listening mode and begins monitoring incoming packets while maintaining a failsafe timer. When a LoRa packet is received, the payload is copied into a buffer and parsed using a formatted scan to extract the joystick values. These values are then passed into a control function that translates them into steering angles and throttle pulse widths. Steering is controlled using discrete zones mapped across the 0–4095 input range, where lower X values correspond to sharper left turns, higher values correspond to sharper right turns, and a small dead zone around the center maintains straight steering. This stepped mapping creates predictable, incremental steering responses rather than smooth proportional movement. The throttle system operates similarly, dividing the Y input range into multiple zones that correspond to hard reverse, soft reverse, medium reverse, neutral, medium forward, soft forward, and full forward. The selected throttle level is converted into a pulse width between 1000 and 2000 microseconds, which is stored in a global variable and continuously sent to the ESC. Instead of using hardware PWM, the program generates the ESC control signal through a manual bit-banging method that produces a 50 Hz waveform with a 20 millisecond period. Each cycle sends a high pulse for the desired throttle duration followed by a low signal for the remainder of the period, ensuring consistent motor control regardless of packet timing. The main loop continuously sends these pulses, processes LoRa interrupts, and checks the failsafe condition. If no signal is detected for more than three seconds, the system automatically resets the throttle to neutral and re-centers the steering servo.

The propulsion system utilizes a 160A rated ESC throttle controller that converts DC source in three phase power for our motor. The motor is Surpass Hobby 56102 600 KV brushless in runner motor rated up to 50V, 129A peak, and 6300W. Attached to this motor is a 3/16'' drive shaft that runs through a 4.76mm stinger and drive dog that then turns the 72 x 1.4 x 4.76 mm propeller. The steering system is utilizing a servo motor linked to a control arm that actuates the boat's rudder, powered by the ESC's BEC.

Remote

The remote controller serves as the primary human-to-boat interface for Project Ripple, allowing for long-range control from over a mile away by the user. The controller is built around the MakerFocus ESP32 LoRa V3 Development Board operating on 3.7V. This was selected due to the integrated LoRa transceiver, GPIO availability, and compatibility with the Arduino IDE. The ESP32 is continuously sampling from the two 10K potentiometer sliders that represent the throttle and steering. This is done based on the 12-bit analog-to-digital converter. The potentiometers are connected via GPIO pins and operate on a 3.3V logic and output a proportional voltage based on the slider position. These positions are converted into digital command values that are packaged into packets and transmitted to the microcontroller onboard the vessel. Long-range communication is achieved through LoRa through the 915MHz and 3dBi omnidirectional antenna connected through a SMA interface, which allows for out of sight communication past one mile away.

The remote controller will be tested to verify proper operation of the dual inputs, wireless communication, and safety. Testing will be conducted in lab and field settings. The first test was verifying control inputs. The potentiometer sliders will be moved through the full range of motion and the analog values will be monitored to see the accuracy of input. The next test is the short-range communication test where the controller will transmit command packets to the onboard receiver at a distance of less than 10 ft. The microcontroller will be monitored to make sure that the packets are received and the propulsion and steering responds accurately to the controller inputs. The next test is the long-range communication test where the vessel will be positioned progressively farther while maintaining command inputs from the controller. In addition, the emergency shutdown will be tested by having the motor running on the vessel and then activating the switch and seeing if the output stops when communication is interrupted. Lastly, the FCC compliance of the remote control was evaluated where the manufacturer documentation was confirmed to operate within the allowable limits. This included verifying transmit power settings and antenna gain.

Testing of the remote controller subsystem was conducted to evaluate control input, wireless communication, and safety. Results from the tests will be evaluated and described as to what engineering requirements are satisfied. The first test was the control input results, where the throttle and steering potentiometers were moved across their full range of motion. The serial monitor confirmed that the values changed proportionally to the slider movement and were transmitted into LoRa packets. The next test was the short-range test where the remote control and onboard microcontroller were tested at a distance of roughly 10ft. Command packets were received and decoded properly, and the propulsion and steering responded in real time. The next test was the long-range communication test where it had the same parameters as the short-range test, but the distance was up to a mile away. No packet loss occurred, and the steering and throttle reacted to remote control inputs. The emergency shutdown was tested where the boat would be receiving command inputs that suddenly stop sending and seeing if the boat stops all onboard power which it successfully completed. Lastly, the FCC compliance was tested and the LoRa transceiver and antenna were confirmed to operate within the FCC Part 15 limits.

Microcontroller/GPS

The Microcontroller is designed around a MakerFocus heltec ESP32 LoRa board. This board is attached to a 6dBi cable extended antenna. When the microcontroller receives the LoRa packet from the remote controller, it breaks down the X and Y values sent through the LoRa channel and turns them into control outputs. This is done using two GPIO pins that connect to our servo used for steering and our ESC throttle controller. The microcontroller system is powered from the battery eliminator circuit (BEC) from the ESC. This produces a 6V secondary which runs the smaller electronics. This 6V feeds a BUCK converter which produces a secondary of 3.7V which is what the microcontroller can handle. This whole system is housed in a 5.9 x 5.9 x 3.5 inch waterproof control box. This is mounted in front of the boat.

The GPS system is designed around the LandAirSea 54 GPS tracker. This is a satellite and cellular-based GPS system. The tracker is waterproof as well as a very strong magnetic bottom. This GPS is mounted in the front of the boat and will be sending signals to a phone through satellite and cellular. These signals will include GPS position on a map, relative direction of travel, speed, history of the GPS, and will also have geofences set that help us navigate the course. The system is powered by a rechargeable individual 1500mAh battery so as to not take away capacity from the motor.

The microcontroller and GPS system testing procedures were tested to confirm proper functionality and controllably. The microcontroller's first test was confirming the GPIO pin worked correctly by doing a LED blink test on them. The next test was confirming that the GPIO pins sending the PWM signals to the servo were working, then testing the bit banging approach of the ESC throttle controller to make sure that the throttle responded to this unique approach for throttle control. The main communication test was once our LoRa channel was set up between the remote and microcontroller. We began sending hello through the channel at short distances and making sure the microcontroller was showing received. Once this was confirmed, we upgraded the antennas to a 3 dBi setup and tested a range of 1 mile. Once this was confirmed successfully, the remote control began sending X and Y values through the LoRa channel which the microcontroller was tested to see if the code could break down these X and Y LoRa packets to control signals. This was confirmed by seeing the movement of the throttle and servo as the remote controls were moved. Once this was tested the next test was confirming the kill switch loss of communication feature in our code worked once connection was lost. This was tested by killing the remote power. The GPS testing involved first charging the GPS and making sure it could turn on and off and nothing was broken. The next test involves seeing if satellite connection or cellular connection could be established. Next was connecting the GPS to the smart phone to see real data movement. The final test was checking if speed readings, location, and range were accurate. The last test of the GPS was if geo fencing features could be utilized for navigational purposes of the boat.

Longwood: Control & Autonomy

Ben Gettier, Mackenzie Jerabek, Sean Harrigan, Ryan Urban, Bryce Gabriel Benito, Edward Corobana

www.navalengineers.org/Longwood

The hull was scratch-built using marine-grade plywood bulkheads, laid up with stick planks, and reinforced with fiberglass to achieve a balance of strength, buoyancy, and low drag. Internal ribs and bulkheads were added for structural rigidity, and all seams were sealed with epoxy or marine adhesive to ensure watertight integrity. The layout was customized to accommodate electrical components, including a reinforced motor mount and dedicated platforms for propulsion and power systems. Custom components for electrical mounting and internal structure were created using 3D printing with TPU, Nylon Polyamide, ASA, PLA, and PET-GF filaments. This fully original construction process demonstrates that no pre-manufactured hull kit was used.

The propulsion system was assembled entirely from individual components, including brushless DC thrusters, electronic speed controller, and marine-grade wiring. All components were independently sourced, aligned, soldered, and integrated without the use of any pre-built kit. Power is supplied by 2 securely mounted batteries housed in non-conductive enclosures designed to prevent movement during operation. The system complies with competition requirements, operating at or below 55.5V and within the 500 Ah capacity limit, with added protections such as insulated terminals and an inline fuse for safety.

Testing & Validation

The Autonomous Electric Surface Vessel (AESV) underwent rigorous testing to validate operational performance, subsystem reliability, and competition compliance. Component validation began with comprehensive waterproofing trials, where marine-grade enclosures and circuit board conformal coatings were subjected to controlled spray and immersion tests to ensure high ingress protection. Structural integrity and hydrodynamic stability were verified through "swamp tests," confirming that the internal foam and air-trap design provide positive buoyancy even if the craft is completely filled with water.

Competition safety protocols were validated through a series of functional checks. The emergency kill switch was tested under two critical conditions: manual engagement via the external deck button and automated software-based disconnection triggered by the loss or corruption of GPS navigation data. In both scenarios, the high-current contactor successfully isolated the battery from the motor controller, halting propulsion immediately. Additionally, the vessel demonstrated its capacity to carry the required 30-pound removable payload while maintaining optimal trim and waterline. Final open-water trials documented a consistent 200-meter run under autonomous control, proving the system is race-ready and compliant with all PEP 2026 regulations.

Norfolk State: Electronics & Telemetry

Wisdom Elikplim Korkortsi, Samuel Kafui Kwawukume, Daniel Goddard Brookman, Yaw Amankrah Sam-Okyere, Emmanuel Osei-Kwame, Emmanuel Wiafe

www.navalengineers.org/NorfolkState

The energy storage system consists of two lithium iron phosphate (LiFePO4) battery packs, one per hull. Each pack is a 4S10P configuration, yielding:

- Nominal voltage: 14.4 V
- Fully charged voltage: 16.6 V
- Capacity: 50 Ah
- Energy: approximately 249 Wh per pack
- Weight: approximately 2.886 kg (6.36 lb) per pack

Each pack is secured to the hull structure with cut-out wood on each side. A buckle is added to retain the battery in a capsize event (PEP Rule 8).

A main power disconnect switch (PEP Rule 7) is mounted on the upper surface of each hull, accessible without tools, through which all current to the propulsion system in that hull must travel. Moving either switch to OFF immediately ceases all high-voltage electrical activity in the respective hull. The location of each disconnect is marked with a bright orange label visible from above and from the waterline and is documented in our safety checklist for race-day inspection.

For the 24–55 V operating range, each hull includes a 60A ANL-type fuse in-line between the battery and the ESC (PEP Rule 9), sized to protect the 10 AWG silicone-jacketed wiring that constitutes the high-voltage bus. The fuse is housed in a waterproof fuse holder accessible through a deck hatch.

Controls and Communication

The "brain" of our craft is a Pixhawk flight controller running ArduRover. We integrated two Cytron MD30A motor drivers to translate the Pixhawk's logic-level commands into high-current power. We utilized a modern ExpressLRS (ELRS) 2.4GHz system to route both ultra-low-latency manual control and high-speed MAVLink telemetry through a single RF link.

The control architecture of the *Spartan Electric* is organized into three layers:

1. **Operator layer.** A 2.4 GHz frequency-hopping spread-spectrum (FHSS) RC transmitter provides the primary control link. The transmitter has been range-tested to over 1.5 km line-of-sight, well beyond the maximum distance from the shore to any point on the two-mile oval course. The transmitter outputs throttle and steering commands, which are mixed into individual motor speed commands by the receiver's built-in mixing function.
2. **Vehicle layer.** The RC receiver passes PWM signals either directly to the two ESCs (manual mode) or via the Pixhawk autopilot (assisted/autonomous mode). A two-position switch on the transmitter selects the mode. In manual mode, the operator has direct low-latency control of the motors. In autonomous mode (not yet activated for PEP26 but architecturally supported), the Pixhawk follows a pre-programmed waypoint mission.
3. **Telemetry layer.** The Pixhawk transmits telemetry data - GPS coordinates, speed over ground, heading, roll, pitch, battery voltage, battery current, and remaining capacity estimate - over a dedicated 915 MHz SiK radio link to a laptop running Mission Planner ground station software. Pixhawk also logs all sensor data to an onboard microSD card at 25 Hz for post-race analysis.

Build and Integration

Fabricating the control system required strict attention to power segregation and precise signal formatting to protect the embedded logic from the extreme electrical loads of the propulsion system.

1. **Power Segregation and Logic Isolation**: Electric brushed motors inherently create massive voltage spikes and severe voltage sag under heavy acceleration. To prevent these fluctuations from browning out or resetting the flight controller, the control electronics are completely isolated from the main propulsion power rail. The Cytron MD30A drivers are fed directly from the raw 12V battery array. In contrast, the Pixhawk and the ELRS receiver are powered entirely via a dedicated 5V Battery Eliminator Circuit (BEC). This buck converter acts as an electrical firewall, delivering a perfectly regulated 5V stream regardless of the voltage sag on the 12V rail.
2. **Actuation Wiring and Skid-Steer Mixing**: For actuation, the Pixhawk’s servo output rails were wired directly to the Cytron PWM (Pulse Width Modulation) and DIR (Direction) input terminals. Rather than utilizing external hardware mixers, ArduRover’s internal skid-steering parameters were configured to natively mix throttle and yaw inputs, translating a single joystick vector into independent, variable-voltage left and right motor commands.
3. **The Telemetry Pipeline**: A RadioMaster TX16S transmitter equipped with an internal ELRS module serves as the primary ground controller. The onboard ELRS

receiver was integrated via its TX/RX serial pads directly into the Pixhawk's TELEM2 port, establishing the physical bridge for wireless data transmission to the Mission Planner ground control station.

The kill-switch functionality is implemented as follows. The ArduRover firmware is configured with strict, automated fail-safes. The Pixhawk actively monitors the RC heartbeat. If the signal is lost for more than 2.0 seconds, the flight controller automatically overrides the current mission and transitions into "Hold" mode, instantly commanding a 1500µs neutral PWM signal to the Cytron drivers, stopping the vessel dead in the water until the RF link is reacquired.

A Battery Failsafe was configured within the ArduRover logic. The Pixhawk utilizes an analog-to-digital converter (ADC) via the power module to monitor real-time main battery voltage.

The BATT_LOW_VOLT parameter is programmed to a conservative threshold. If crossed, it triggers an audible and visual alarm on the Mission Planner ground station HUD, alerting the operator to reduce throttle thereby saving enough power for the rest of the mission

A dedicated channel on the RC transmitter is assigned to a spring-loaded switch. When this switch is activated, the Pixhawk commands both ESCs to zero throttle and asserts a relay that opens the main-power contactor, disconnecting the batteries from the high-voltage bus. The same relay is wired to the Pixhawk's GPS-fail-safe output: if GPS fix is lost for more than five seconds, the relay opens automatically, satisfying PEP Rule 21 for teams pursuing autonomy credits.

Michigan (UMEB): Impressive Design for Big Aspirations

Nick Robbins, Dillon Yoo, Phoenix Do, Charlie McIlvaine, Casseia Watson, Patrick Wydeven, Matthew Devine, Zhengcheng Zhu, Peter Zhao, Edward Vazquez-Hernandez, Logan Stoll, Andrew Dailey, Thomas McTigue, Xuzetong (Bob) Wu, Thomas Caulfield, Luke Aldrich, Teagan Fynan, Christopher Stein, Parisa Dong, Thomas Taylor, Charly Meyer, Benjamin Fuller, Andreas Petre, Andrew Line, Ben Bishop, Chase Davenport, Ryder Potts, Carter Grove, Kevin Yuan, Dylan Oltersdorf, Rylan Dephoure, William Dinkeloo, Allena Smiley, Jack Humphries, Thomas Brown, Henry Hanrahan, Imtihan Chowdhury, Spencer White, Dane Jarvis, Jishnu Borra, Raymond Yuan, Elaina Alig, Bridget Dorman, Aristo Wong, Charles Kindelt, Lucas Allen, Zachary Salloum, Arend Vyn

www.navalengineers.org/Michigan
https://umeb.engin.umich.edu/

A D-Stock hydroplane was determined to be the best hull option. Hydroplanes are very efficient hullforms at high speed, generating a substantial portion of lift from the aerodynamic effects of the tunnel, along with traditional hydrodynamic lift. At higher speeds, only the sponson edges and the propeller remain in contact with the water. Competition combustion D-Stocks run over 80mph with around 50 prop shaft hp and have a minimum weight of 500 lbs (including driver). Even with the voltage constraints, close to 50 continuous motor hp can be achieved and the total weight of the boat with an electric setup is estimated to be around 600 lbs (20% heavier than a combustion D-Stock), so we felt the D-Stock was the best hull choice for the PEP manned planing division.

The custom cowling encloses the motors, inverters, and electrical wiring on the outboard assembly, protecting these components from water ingress to an IP66 rating (protection against high pressure jets of water).

Design

The cowling is a vacuum infused carbon fiber composite part, with 1 ply of 6oz 2x2 carbon fiber on the inner skin, a 6 mm flexible Soric core, and 1 ply of 6 oz 2x2 carbon fiber on the outer skin. The design consists of a bottom shell and a removable top shell sealed together at a flange. Since the motors require air cooling, the cowling has a spray resistant air intake and outlet.

Propeller

Due to using a high performance racing hull and lower unit, the propeller is a surface-piercing, super-cavitating, cleaver propeller. This type of propeller is the most efficient to balance forward thrust and propeller slip percentage. It is half in and half out of the water at racing speeds, freeing up the propeller to spin in the air half of the time for efficiency while having sharp blade tips to grip the water upon re-entry for adequate forward thrust. Traditional, non-surface-piercing propellers typically have a slip percentage of 15-20+ percent, while surface-piercing propellers typically have a lower slip percentage of 5-10+ percent, which makes surface-piercing propellers more efficient. This higher efficiency, along with the fact that the surface piercing cleaver propeller creates extra lift at the rear of the boat to help the hydroplane "three-point" (as described above in the "Hull" section) for peak aerodynamic and hydrodynamic efficiency, led us to choose the surface-piercing cleaver propeller for this application.

Each motor has its own respective controller and ABI encoder, and they are geared to a single output shaft. Water cooling is routed to the motors and through custom plates mounted to the heatsink on the VESCs. The controllers are on the same isolated CAN network as the BMS and can either be controlled through CAN or from a direct analog signal from the throttle if need be. The controllers are run with current/torque control to ensure the motors don't fight each other and to prevent strange behavior if the gears ever don't make full contact. Power from the battery is routed to busbars in the cowling and then to each controller (each having three power leads).

Manufacturing/Testing Plan

To test the motor and control system, a 48V 20Ah test battery is used as a separate power source to provide isolation and mitigate risk of damaging components. Furthermore, to prevent potential damage to our gears we used a 3D printed model of the gearbox and gears rather than the final assembly for initial testing. First, a single motor was spun off of a simple throttle command done through the VESC tool, the controller's software. A potentiometer was then used to spin the motors with an analog throttle signal. Finally, we spun the motor with an isolated CAN signal, which is the communication protocol we are using on the boat. We then moved to testing the full system with all three motors. The magnetic ABI encoders were placed into the encoder plate with their respective magnets secured to the top of the motors. Each encoder was calibrated using the VESC tool through the shared CAN network and tested for accuracy by individually spinning each motor-controller pair. While calibrating, we removed the center gear to prevent any motors from fighting should they spin different directions, and a similar process will be followed when first throttling with an analog signal and then when moving to CAN. For testing more realistic load conditions, the motors will be spun using a load disk in water.

As for testing the other major components of our boat, we first measured the charger's output with a multimeter to ensure accurate voltage and will complete a full charge/discharge test with the battery while monitoring voltage, current, and temperature through the BMS. The step down converter will be connected to the battery and the voltage output will be measured with a multimeter, then we will test it (fused) on a 12V auxiliary system to verify it operates properly. We decided on a minimum 40 hp continuous output to be comparable to a typical combustion D-Stock, corresponding to 30 kW continuous. We originally designed our system around 48V nominal, which would require at least 625A at the motor(s). The selected motors had to be at least splashproof due to the marine environment, and the entire powertrain system (motors, controllers, etc.) in the outboard would ideally be under 50 lbs. A trade study was conducted to compare different motor options, but there were no single motors available that stayed under the weight limit at our required power. Therefore, we moved to gearing multiple motors together to meet power requirements, and settled on using three LMT 7065 motors. Each motor can sustain 11.2 kW (15 hp) continuously (>200A per motor), and the motor curves provided by LMT show that they've been tested to upwards of 500A at 54V with minimal (~5%) losses. Together, the three LMT 7065 motors exceed our continuous horsepower requirement at 45 hp total.

North Carolina State: Autonomous Tuffy

Hayden Flo, Sean Ferris, Aritra Gomes, Emma Bradley

www.navalengineers.org/NCstate

The command and control subsystem consists of all digital and radio electronics directly responsible for autonomous planning, position estimation, relaying remote user commands to the craft, relaying of telemetry data to the user, and propulsion & steering regulation. From the very start, we've been very conscious of the potential dangers that the S.S. Tuffy may pose due to both its large lithium-ion battery pack and its high target speeds. These two factors mean large amounts of electro-chemical and mechanical energy are present, energy which could cause grave harm if mismanaged. While designing the S.S. Tuffy's command and control subsystem, our core design philosophy has been to maximize reliability and safety.

With that, we decided to bias our design decisions towards using industry-standard parts and software. This is because these technologies have already been proven to be safe and reliable by the industry at large, reducing the risk of dangerous malfunctions. This influenced design decisions to use a CubePilot CubeOrange as our flight controller, a HolyBro F9P as our water-resistant GPS/compass, ArduRover as our OS, and MissionPlanner as our ground controller station software. Due to budget limitations, we weren't able to replace the SIYI MK15 Transmitter/Receiver system with a more industry-standard option, but that is a suggestion we have for next year's team.

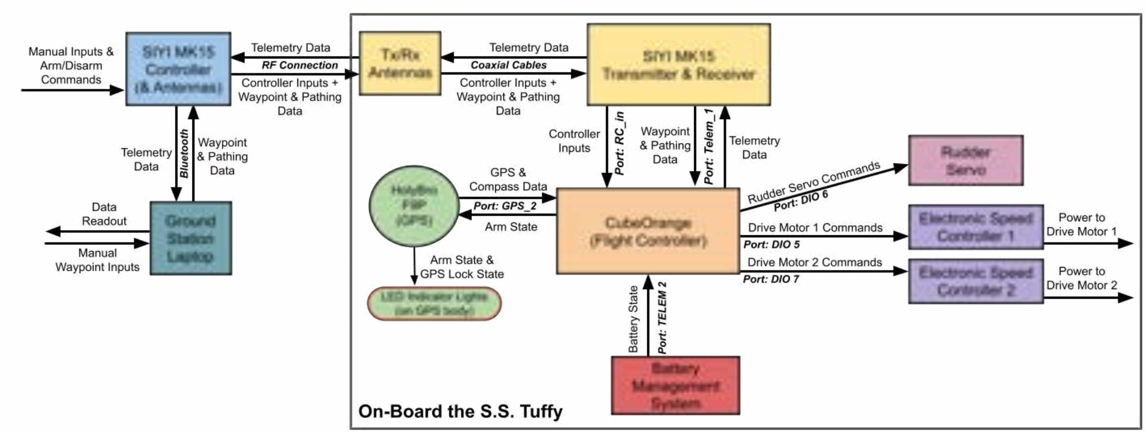

Figure 7: Command and Control Functional Block Diagram

As seen above, we have designed the command and control subsystem's overall structure to resemble that of a traditional RC car, but with a GPS/compass included and an additional bluetooth connection between the controller and the ground control station laptop. The CubeOrange flight controller receives commands from the receiver, whether they be autonomous waypoints or manual inputs. It then uses the parameters we configured to determine how to translate these inputs into commands to the motors' electronic speed controllers and to the rudder servo.

The bluetooth link from the controller to the ground control station laptop allows us to set the S.S. Tuffy's autonomous path and view telemetry without any physical connection to the boat. It also enables a designated team member to focus solely on monitoring the boat's telemetry data via the ground control station laptop, ensuring that they can quickly identify problems should they occur.

The GPS/compass module is key to the S.S. Tuffy's autonomous operation. Our flight controller, with ArduRover installed, uses the GPS and compass data provided by the module to determine where it is and what direction it is facing. This estimate is also further refined over time, as ArduRover's EK3 position estimation algorithm receives more samples from the GPS/compass module in conjunction with accelerometer data from the flight controller. While in autonomous mode, ArduRover uses this position and heading information to determine the forward velocity and heading changes required for the craft to reach the next target waypoint. The exact amount of throttle and steering applied depends on our configuration of ArduPilot's controller gains.

Command & Control Power System Testing:

Power Supply Set Voltage (V):	Power Supply Current (A):	Conv. Output Voltage (V):	Conv. Output Current (A):	Conv. Input Power (W):	Conv. Output Power (W):	Conv. Loss (W):	Conv. Effeciency (%):
30	0.22	24.12	0.22	6.6	5.3064	1.2936	80.4
35	0.197	24.12	0.22	6.895	5.3064	1.5886	76.96011603
40	0.185	24.12	0.23	7.4	5.5476	1.8524	74.96756757
45	0.176	24.12	0.22	7.92	5.3064	2.6136	67
50	0.167	24.12	0.23	8.35	5.5476	2.8024	66.43832335
52.5	0.162	24.12	0.23	8.505	5.5476	2.9574	65.22751323
55	0.16	24.12	0.23	8.8	5.5476	3.2524	63.04090909
57.5	0.156	24.12	0.23	8.97	5.5476	3.4224	61.84615385
60	0.153	24.13	0.22	9.18	5.3086	3.8714	57.82788671

To validate the performance of the electrical and control systems, testing was conducted to evaluate current draw and system stability across the expected operating voltage range. The command and control system was tested using a variable power supply from 30 V to 55 V to simulate real operating conditions. The measured current draw remained consistent at approximately 0.25–0.26 A across all voltages, indicating stable and efficient operation of components such as the flight controller, receiver, and sensors. This low current draw confirms that the control system places minimal load on the overall power system. Additional testing was performed on the DC-DC converter used to step down the voltage for low-power components. The converter was evaluated across an input range of 30 V to 60 V and showed an output current of approximately 2.4 μA under no-load conditions. This demonstrates very low standby power consumption and high efficiency when the system is idle.

Overall, the results confirm that the low-power system is stable, efficient, and well-integrated with the overall power system. The consistent performance across voltage ranges ensures reliable operation without significantly impacting battery usage.

Battery Pack

Analysis was conducted using a 6s1p battery pack with the cells that will be implemented in the new power system. The test was conducted in order to verify datasheet values and therefore our pack's capabilities. First, the pack was attached to a simulated load and discharged 20A. The pack experienced a 1.4V drop (0.233V for each cell) after 5 minutes of use. Assuming a conservative discharge depth of 0.5V per cell we can deduce that the run time of each cell is approximately,

$$\frac{5\,min}{0.233V} \cdot 0.5V = 10.87\,min \; = \; 0.1811hr$$

giving us a capacity of,

$$Capacity = 20A \cdot 0.1811hr = 3.62Ah$$

According to the datasheet, our cells should have a capacity of 4.05Ah at 20A. This is more than we measured while testing; however, this could be due to a larger assumed discharge depth. To predict how our pack would behave at 40A, which is what each of our parallel segments would output, we used a ratio of the predicted capacity according to the datasheet:

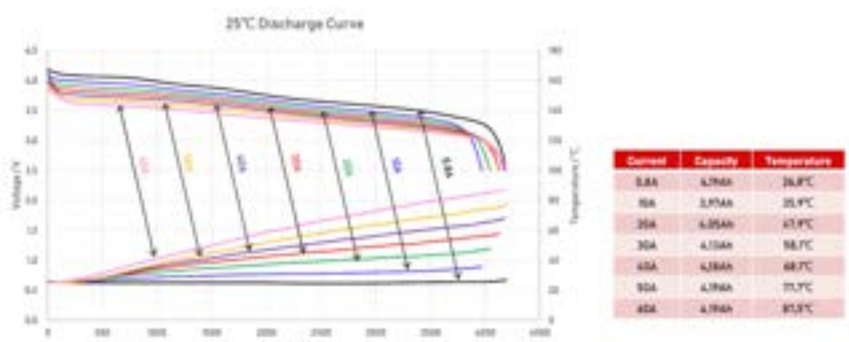

Figure 12: JP40 21700 Discharge Curve

$$\frac{4.18Ah}{4.05Ah} \cdot 3.62Ah = 3.74Ah \text{ for 40A}$$

$$\approx 5.6\,minutes\ at\ full\ speed$$

While the boat's maximum speed is not currently measured, we can predict a maximum speed of about 40mph. This would allow for the boat to travel 3.73 miles before it would need to be recharged. This would give us a cushion of almost two miles of extra battery capacity.

North Carolina State: Inaugural Long-Distance RC Champions

Luke Noble, Joshua Moyers, Calvin Clarke, Jose Perez, Andrew Aycock

www.navalengineers.org/NCstate

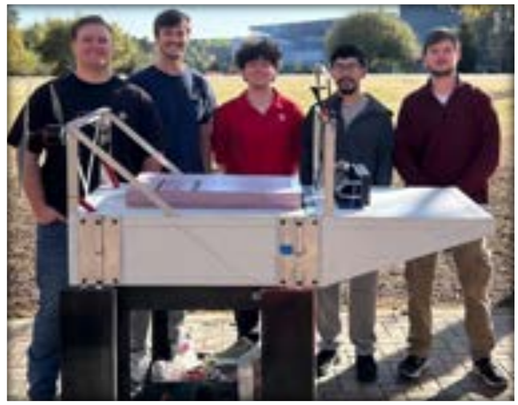

The power system was designed by first separating the load into three main subsystems: propulsion, low-voltage electronics (navigation and stabilization), and communication/interface components. The propulsion system dominates the power budget, with two brushless motors each drawing up to 125 A at 44.4 V, resulting in a total propulsion power of approximately 11.1 kW. This high demand dictated the selection of a high-voltage LiPo battery configuration (44.4 V nominal, 12S) and high-current components such as 300 A ESCs and appropriately rated wiring and connectors.

Lower-power subsystems were grouped into regulated 5 V rails supplied through a step-down converter from the main battery. The navigation and stabilization components (Arduino, sensors, servos, GPS) and communication hardware (Cube Orange+, receiver) together consume a relatively small portion of total power (~27 W combined), but require stable and noise-free voltage for reliable operation. A battery management system (BMS) was incorporated for protection and monitoring, and overall distribution was structured to isolate high-current propulsion paths from sensitive electronics. This design ensures efficient power delivery while maintaining system stability and safety across all operating conditions.

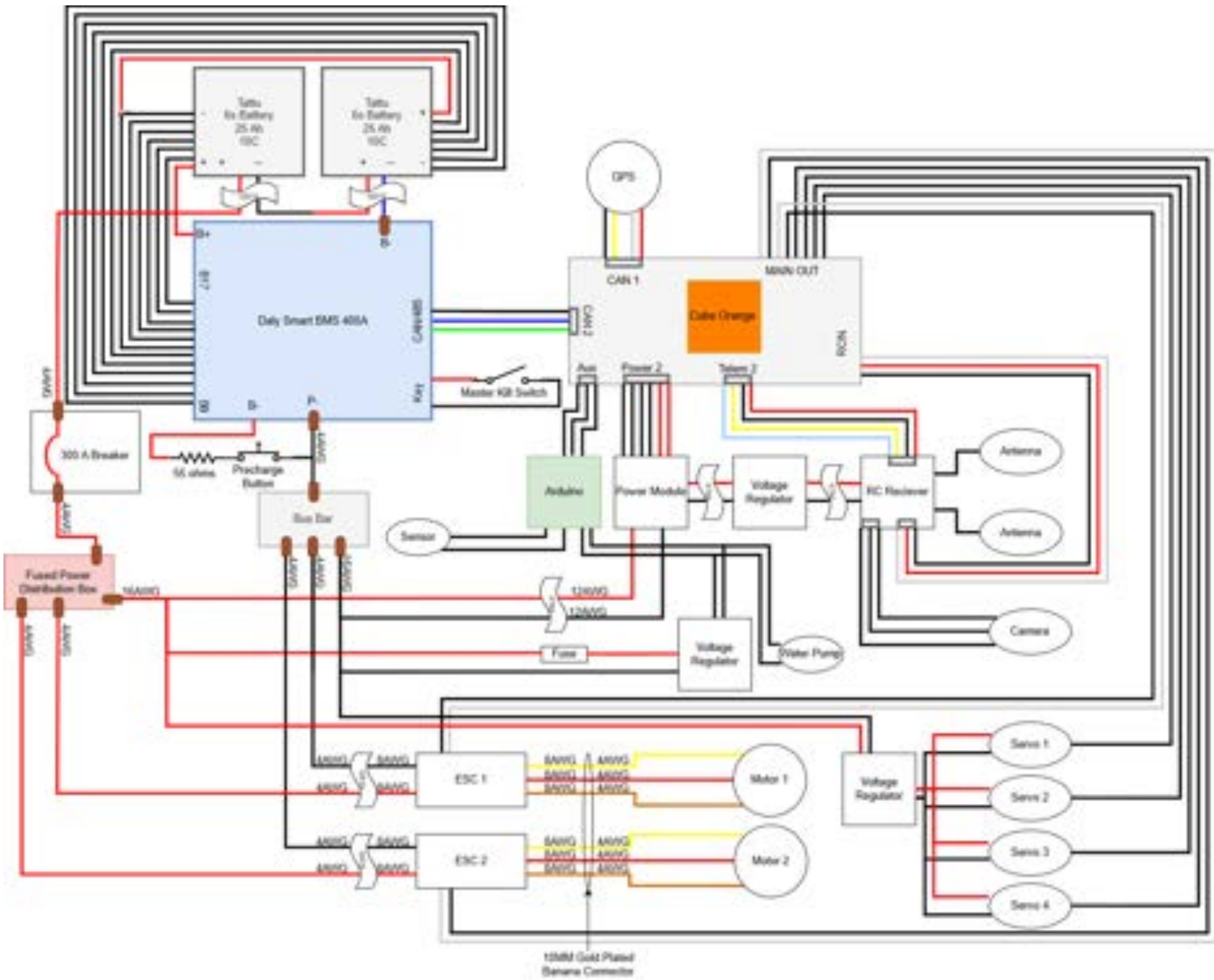

Arduino

The system uses an ultrasonic rangefinder (A02YYUW Waterproof Ultrasonic Sensor) to measure the vertical distance between the hull and the water surface. This measurement is critical for determining the ride height of the hydrofoil craft.

Due to incompatibility between the sensor's UART communication protocol and the Cube Orange+ flight controller, an intermediate microcontroller (Arduino) is used to process the sensor data. The Arduino reads the distance measurement from the ultrasonic sensor and converts it into a corresponding PWM signal.

The output signal represents a normalized distance range from 0 to 1 meter, which is the operational range of the control system. By converting the sensor data into PWM, the signal becomes compatible with the flight controller's input requirements.

Mission Planner

The processed PWM signal is sent to the Cube Orange+ flight controller, which runs ArduPlane firmware and is configured through Mission Planner. The flight controller serves as the central processing unit of the control system.

Within ArduPlane, the incoming height data is combined with onboard inertial measurement unit (IMU) data, including gyroscopic feedback. This allows the system to account for both vertical displacement and angular motion of the craft.

Custom Lua scripting is used to further process this data and implement a control algorithm that adjusts the elevon outputs. The control logic determines the necessary corrections required to maintain a stable ride height and overall craft stability.

For each servo motor, the script takes the ultrasonic sensor data and adds an offset based on the range data:

```
local out1 = clamp(elevon_r + offset,PWM_MIN,PWM_MAX)
local out2 = clamp(elevon_l + offset,PWM_MIN,PWM_MAX)
local out3 = clamp(elevon_l + offset,PWM_MIN,PWM_MAX)
local out4 = clamp(elevon_r + offset,PWM_MIN,PWM_MAX)
```

Receiver

The receiver on board, the SIYI MK32 Air Unit, handles all of our long-distance communication for the boat's end. This air unit also includes a 4S to 18S power module, which works to stabilize the voltage received from the power source. The air unit communicates with its sister ground unit that shares the SIYI MK32 name. By using a ground unit and an air unit that were particularly made for each other, we can guarantee compatibility for all functionality. These two units combine to handle the remote control, telemetry, and video streaming signals. The RF link, which carries these signals, is digitally transmitted using SIYI's proprietary wireless HD image transmission system. The RC control packets travel from the ground unit to the air unit, while the video stream packets and telemetry packets travel in the opposite direction. The RF link, which carries all of this information, is transmitted using two standard SIYI omnidirectional antennas with a gain of 5 dBi on both the boat and the ground unit. The user manual for this system claims that with these antennas, we have an operating range of up to eight kilometers. We plan on running a range test once our system is capable, where we will simply run our boat until we lose connection and record this range. This can be done safely as our ESCs are programmed to cut power to our motors in the event of a signal loss. More in-depth explanations of the testing process for the different functions are included in their respective subcategories.

RC Controls

The ground unit is made up of sixteen different physical channels, which are then combined into sixteen different communication channels and digitized into data carried within the RC control packets. Once these packets are received by the air unit, it converts them into a serial bus output, which is sent to the Cube Orange+, where

Ardupilot then reads the individual RC channel values and handles them as it has been programmed to do. The Cube Orange+ then sends any output signals to the different servos and electronic speed controllers as needed. To test this we powered the system with the air unit's S.Bus out port connected to the Cube Orange+'s RC IN pins. The Cube Orange+ was then connected to a laptop, which was running ArduPilot. Once the link between the air and ground units was secured, we viewed the RC channels in ArduPilot. We would then move the different physical channels on the ground unit and examine the outputs displayed in ArduPilot to confirm they were being properly received. After this was confirmed to be working, we connected a servo to one of the Main Out pins of the Cube Orange+. Then, in Ardupilot, we configured this servo to respond to one of the RC channels controlled by the left joystick of the ground unit. This allowed us to move the servo and prove we had achieved functionality that is ready to be integrated into the final overall design of our system.

Video Stream

The video stream used to allow for FPV functionality uses the SIYI IP67 Waterproof FPV Camera. The camera is connected to the air unit through an Ethernet port, so when searching for a camera, it is necessary to find one that utilizes ethernet protocol for video transmission. This camera was affordable, waterproof, and used the proper Ethernet protocol. It is once again within the SIYI ecosystem as well and comes with guaranteed compatibility with the rest of our communication system. The air unit breaks the encoded video stream into packets, which are then sent to the ground unit, where the packets are reconstructed into the video stream, which is then decoded and displayed. The testing for the video stream was very simple. Once the connection between the air unit and the camera was secured and powered, the ground unit was configured to use the waterproof camera. This was all that was required for the video stream to appear on the display of the controller. The range of our video system will also be tested alongside the range of the RC controls once we can carry out a range test. However, we would expect the range to be the same between the two, as they are sent over the same RF link between the ground and air units.

Telemetry

The telemetry utilizes the MAVLink protocol. The Cube Orange+ takes in all the information from its sensors as well as our Here3+ GPS. ArduPilot then processes this data and converts it into MAVLink messages, which are sent over UART to the air unit. The air unit then sends these messages to the ground unit as telemetry packets.

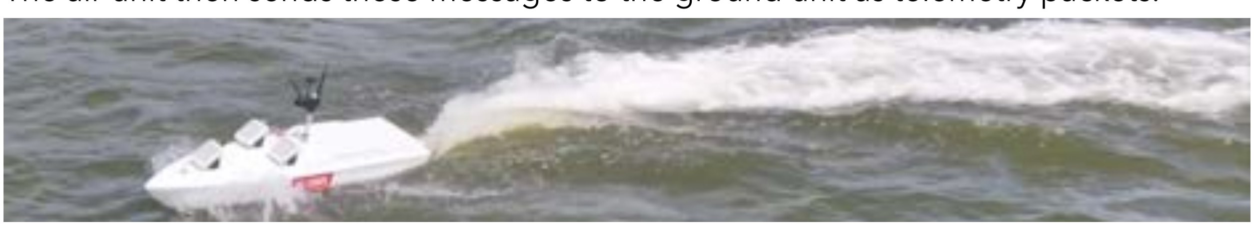

Northeastern: Hull Design for Stable Autonomy

Evan Lin, Lillian Miles, Nikolas Sanderson, Sam Elkerton, Libby Carney, Kiefer Read, Meera Patel, Elliot McQuaid, Juan-Mario Vuksan Mira Rieley, Neo Isak, Charlotte Stieve, Alejandro Downard

www.navalengineers.org/Northeastern

The team decided to pursue a trimaran hull for its advantages over other hull designs in the case of creating an autonomous vessel with maturing technology. Our design consists of a large center hull and 2 amas, each connected with 2 40mm x 40mm 80/20 aluminum extrusions on either side. These extrusions are typically made from 6105-T5 alloy, which have yielding stress of 150MPa, well above necessary tolerance this system will experience in its intended application. In this connection, the most likely point of failure is the connection between the hulls and extrusions. To address this issue, 10mm washers were added to the bolts connecting the 2 parts to spread the force over a larger area, thus reducing stress on that connection. A CAD model was first created, and it is depicted in figure 1 below.

Following established hull design practices, the average beam-to-length ratio of a trimaran's center hull is 1:6 or about 16% the length of the hull. The beam-to-length ratio on this vessel is 325mm/1750mm, which is about ~18.5% the length of the hull, which is fairly close to the 1:6 target. Additionally, the hull has a wave-piercing V-shaped bow profile that slowly transitions into a flat displacement hull towards the aft.

Since the displacement is spread across three hulls, calculations were done to determine the total available displacement. This was done back factoring in block coefficients, denoted by the symbol C, as hulls are not perfectly rectangular. Block coefficients account for the hull shape. $C_{b,c} = 0.50$ for the amas.

$$d = \frac{V_{disp}}{(C_{b,c})(L_c B_c) + (C_{b,a})(L_a B_a))} \qquad \text{(eq. 4)}$$

$$d = \frac{(0.042m^3)}{(0.45)(1.75m)(0.325m)(0.35m)+2(0.50)(1.35m)(0.15m)(0.19m)}$$

$$d = 121.7kg$$

This yields a buoyancy safety factor of:

$$n = \frac{d}{m_{tot}} = \frac{121.7}{42} = 2.9 \qquad \text{(eq. 5)}$$

Autonomous Control

The vessel can be configured for autonomous navigation using QGroundControl software. QGroundControl is used to create and set a planned path comprised of waypoints and to configure the radio connection between the RC controller and the flight controller, as well as the flight controller itself. Then, when the vessel is armed and set to the autonomous mode, it executes that plan autonomously. The flight controller monitors the data it receives from its sensors, namely the GPS and accelerometer, and uses S-curve path planning and an L1 controller that commands an underlying PID network to follow the path outlined by the waypoints, with Dijkstra's algorithm for object avoidance. The autonomous navigation does not require an active connection, radio or otherwise, to the flight controller during operation, only to arm the vessel and start the plan.

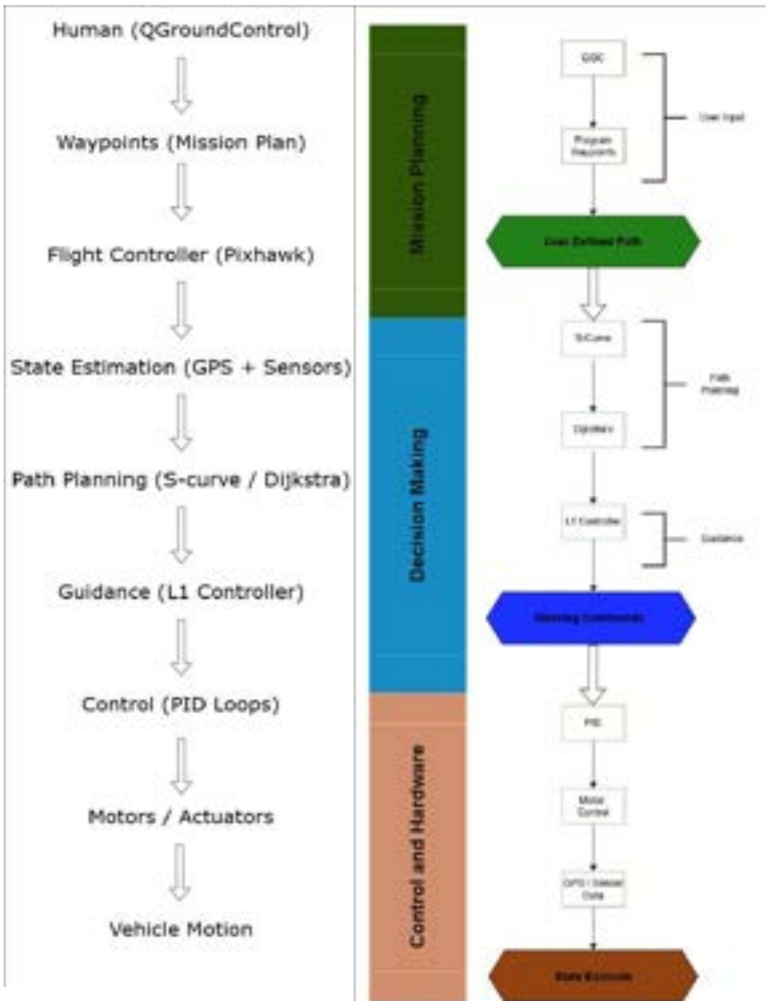

Figure 8: Autonomous Control Stack Diagrams

PITT: Planning for Planing Success

Varun Patel, Soumik Chakraborty, Rafayel Amirkhanyan, Chris Yeager, Jacob Sullivan, Emilia Stouffer, Benjamin Very, Justin Rickert, Trent Vacula, Zachary Kress, Jessica Silva, Matias Badino, Ben D'Ambrosia, Prashanth Kumaran, Alex Smith, Catherine Kirkwood, Evan Jennings, Evan Fletcher, Donovan Wood, Gautam Udupa, Jack Carfrey, Anthony Cardello, Ozzie Hassel

www.navalengineers.org/PITT

For the hull, we decided to go with a V-Hull Planing boat as it provides an ideal combination of straight-line speed and handling in rough water. Through referencing last year's crafts that competed in the ASNE PEP Unmanned category, we came up with a set of targets for our hull to fulfil to be considered a success. The main criterion for the hull was being able to reach a peak theoretical speed of 30 knots while also being stable in the rough waters. Using last year's craft as a guideline for our designs, we decided our boat's length would be in the range of 6 feet.

After that, we researched common deadrise angles for V-Hulls. The most common deadrise angles for handling rough water fall within the range of 20-24°, as the deeper angles provide more stability in rougher waters. However, with the higher deadrise angles, it would also become harder for the boat to reach a planing state. Eventually, we settled on running a deadrise angle of 22°, as that would provide stability while also not sacrificing speed.

For the bottom of the boat, we decided to add additional lifting strakes to make it easier for the boat to lift itself out of the water. The lifting strakes are an inch thick at their maximum point to maximize the potential surface area to generate lift but are also small enough to not have a sizeable effect on the overall hydrodynamic structure of the boat.

For the validation, we went with a two-step validation cycle during the design process. The initial designs were tested with Orca3D's hydrostatics and hydrodynamic analysis features, which helped us get good estimates on whether certain designs would be successful or not. Then, the final designs were validated with ANSYS Fluent with a multiphase simulation as a final validation.

For the hydrostatic and hydrodynamic analyses in Orca3D, we used fixed load cases to get accurate predictions of the center of gravity of the whole boat. These load cases mainly consisted of the heavier components of the boat including the motor, battery, motor controller, and so on, as those were the main contributors to the center of gravity which was then used in analyses. Overall, the total weight of everything in the boat was calculated to be 66 kgs, which was then used subsequently in the analyses.

The final design yielded the following static stability graph at free float conditions with Orca3D's hydrostatics report:

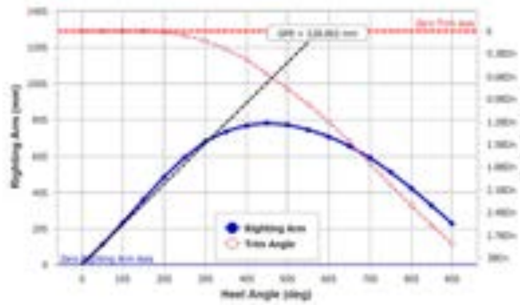

The maximum righting angle of the hull ended up being roughly 80 mm at a 45-degree heel angle, showing the correction ability of the craft when pushed to the higher heel angles. Additionally, the trim angle remains close to the zero-trim axis until a heel angle of roughly 20 degrees, after which the trim also starts to tilt, though not at a concerning rate. The trim angle does not change much with the heel angle, especially when the heel angle is under 45 degrees, which is the expected maximum heel angle that the craft should face.

After the hydrostatics validation that the hull will be able to survive the rough waters, we ran a hydrodynamics validation using Orca3D's Planing Analysis to ensure that our craft will be able to reach our desired velocity. With this analysis, we are mainly looking at whether our motor, which can supply 12 kW of continuous power, can power our boat to the necessary speed of 30 knots.

For the planing analysis, we took the resistive design margin to be 30% to account for the worst possible scenario in all aspects of manufacturing. Additionally, we used a propulsive efficiency of 80% as an additional buffer as this was our first time designing an outboard, and hence we were unsure about our overall propulsive efficiency with our powertrain.

After taking everything into account, the final design yielded the following power-speed graph using Orca3D's Planing Analysis:

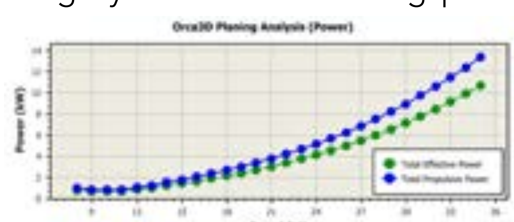

As our motor's maximum continuous power output is 12 kW, that translates to a maximum speed of just over 33 knots, which exceeds our initial expectations regarding the overall speed of the craft.

After this, we validated the final design with ANSYS Fluent Multiphase simulation to ensure that the boat matches the same trim angle as was given in the analysis. The simulation provided us with data that closely matched with the one provided by Orca3D's Planing Analysis, which confirmed our boat design and its stability.

The finalized hull design is as follows, with the overall dimensions being 72 in x 24 in x 14 in.

In regard to manufacturing the hull, we opted to make the hull out of carbon fiber due to its high strength to weight ratio. To manufacture carbon fiber, we used a positive mold manufactured using a combination of 3D printing and foam, which we then laid up with carbon fiber which was then vacuum bagged.

For the mold, we used a combination of ELFOAM P300 and 3D printing, as the foam was only able to create the mold for the first 10 inches of the hull's depth as that was all the foam we were able to procure. For the remaining 4 inches of the hull depth, we 3D printed the mold using PLA on our Prusa XL and Bambu P1S.

For the foam, we were able to glue the sheets of foam together using West System's 105 Epoxy Resin mixed with their 206 Slow Hardener. After gluing the sheets together, we were then able to route the foam at the CNC Lathe at our university machine shop. With the 3D prints, we glued them together using superglue and then used the epoxy resin to glue the foam to the prints.

After assembling the mold, we applied Bondo to fill in all of the gaps to make the surface smooth, after which we applied a layer of Fiberglast's Orange Tooling Gelcoat to seal the mold and make sure none of the foam or 3D prints seep into the carbon. Finally, we applied a layer of TR 104 Mold Release to allow us to properly remove the finished carbon fiber.

Once the mold was prepared, we laid up the carbon fiber using the epoxy resin and used vacuum bagging to ensure the epoxy was coated evenly over the entire surface.

We also used a similar process for manufacturing the lid, however for that we used a cut wooden board as our mold as it was a flat surface and did not require many intricacies.

Within the finished hull, we put custom ribs made from MDF to prevent buckling from sideways forces due to waves. The ribs also served another vital purpose, as it allowed us to mount an acrylic sheet to the ribs upon which all of the enclosures sat. Additionally, the lid screwed into the top of the ribs using threaded inserts that were inserted into the wood.

Princeton Electric Speedboating: New Autonomous Direction

Aidan Astudillo, Sean Lee, Dante Keil, Arun Iyer, Yahav Levy, John Atilano, Garrett Chong, Antoun Salib, Daniel Amoils, Mihika Tiwari, Calvin Nyugen, Fengyou Liu, Rihan Sajid, and Yash Iyer

www.navalengineers.org/Princeton

We manufactured the hull in house using a carbon fiber resin infusion process. We made molds by bolting together several 3D prints which were then sealed using bondo, primer, and epoxy paint. Mold release was then applied to prepare the mold for infusion. For the bottom of the boat we used three layers of 6 oz carbon fiber and two layers for the top. There is a very large hatch door which will allow easy access to most of the hull. There is also a 10 in by 10 in square deck door in the front to allow access to the front area. There will be a bulkhead which spans the full width of the boat halfway between the two access doors. The transom will be reinforced to make sure it can handle the torque of the rudder. Everything mounted in the boat will be epoxied down which will also add structure.

The driveline consists of everything between the motor and propeller. A shaft coupler is set screwed down to the motor shaft, and on the other side, the flex shaft is clamped down using a union nut. A load bearing is set into the motor mounting plate, and the coupler sits against it to allow the plate to partially relieve thrust loads from the internal motor bearings. A "stuffing tube" is a brass tube used to guide the flex shaft from the motor and into the stinger. The stuffing tube end is epoxied to the inside of the transom overhang wall and supported with two guide plates. A stinger is a shaft mounted to the transom overhang wall that guides the drive shaft and holds the propeller in place.

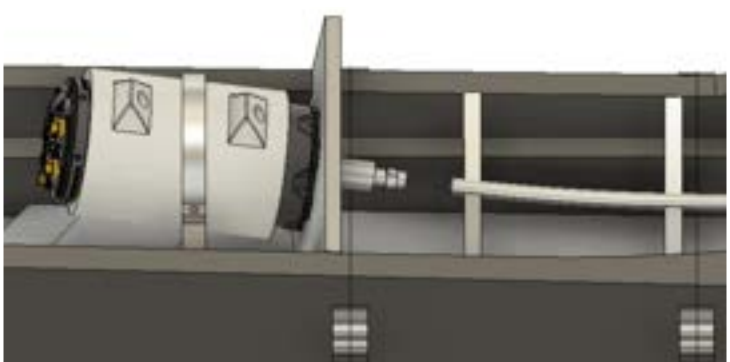

Figure 7: Driveline setup with four plates: middle motor support, front motor support, and two stuffing tube supports

There are different common driveshaft options: flex shaft, wire drive, and solid shaft. Flex shafts are most flexible because they are multistrand cables, which allows for misalignments, but also they lose power transfer efficiency due to their lower stiffness. Solid shafts are the opposite because they are made of solid steel, which provides the greatest efficiency but also requires much more precise alignment of the motor and stinger. Wire drive is the in-between, being a single solid spring steel wire that requires tensioning. Flex shaft was ultimately selected for its successful heritage, accessibility, and ability to absorb small misalignments that would likely exist, since it was the team's first time setting up a driveline like this.

Autonomy Design

The Cube Orange serves as the central processing unit of the autonomous system, running ArduRover firmware and coordinating all actuation, navigation, and fail-safe logic. It interfaces with every subsystem on the vessel, receiving positional data from the GPS module, sending PWM commands to the ESCs and rudder servo, and monitoring radio link status to trigger safety responses when needed.

Fig 12: Waypoint navigation mapping software

Waypoint navigation is managed natively through ArduRover's auto mode, with mission planning and upload handled via Mission Planner ground control software. The autopilot executes heading and speed control using tuned PID controllers that govern cross-track error correction and throttle response. To adapt to varying race day conditions, including wave height, wind drift, and payload variation, the team developed a set of LUA scripts that dynamically load pre-tuned PID profiles without requiring firmware modification. This provides operational flexibility between runs and allows the team to respond to changing water conditions without reflashing or recalibrating the autopilot.

RTK Positioning

Without RTK correction, the Here 3+ GNSS module provides approximately 5 meters of circular error possible. While sufficient for general navigation, this level of accuracy introduces meaningful deviation over a multi-waypoint racecourse. With the RTK4 base station providing differential corrections via radio link, positional

Figure 13: Here 3+ GNSS module

accuracy improves to under 5 centimeters. The base station acts as a fixed ground reference, continuously broadcasting carrier-phase corrections to the rover receiver on the vessel. This level of precision is critical for consistent waypoint tracking and repeatable course execution.

Radio System

Receiver and transmitter module

The Radiomaster ELRS True Diversity receiver is bound to the ELRS transmitter module, providing a reliable control link with a tested range exceeding 1.5 miles. A dedicated channel on the transmitter is mapped to the kill switch function, giving the safety operator an immediate manual disarm capability at all times. Fail-safe behavior, consisting of throttle cut and hold mode, is configured directly in the autopilot firmware and triggers automatically on signal loss. This means the vessel does not require operator intervention to reach a safe state if the radio link is interrupted.

Companion Computing

Figure 16: NVIDIA Jetson

An NVIDIA Jetson is integrated as a companion computer, communicating with the Cube Orange via MAVLink over serial. The Jetson handles computationally intensive tasks, including enhanced path planning and sensor fusion, offloading these from the autopilot and providing capacity for future capability expansion. Importantly, the Jetson is non-critical to the core autopilot function. If it fails or is disconnected, the Cube Orange continues operating fully autonomously with no degradation to basic waypoint navigation.

Software Development & LUA Scripting

LUA scripts were developed to interface with ArduRover's scripting API, enabling dynamic parameter updates at runtime. Scripts are loaded from the autopilot's SD card and executed on boot or triggered by channel input. This allows the team to switch between tuning profiles for different wave and speed environments without modifying firmware. The scripting approach keeps the core autopilot firmware untouched while giving the team full control over behavior customization, reducing the risk of introducing bugs into the flight stack itself.

Princeton Electric Speedboating: Over-The-Horizon Exploration

Aidan Astudillo, Sean Lee, Dante Keil, Arun Iyer, Yahav Levy, Andre Graves, Tom Wang, Mihika Tiwari, Calvin Nguyen, Fengyou Liu, Rihan Sajid, Yash Iyer

www.navalengineers.org/Princeton

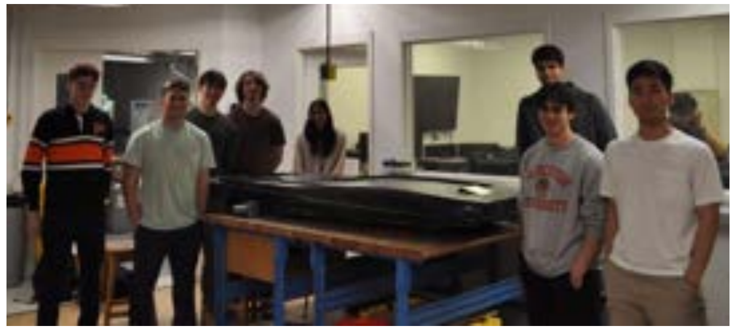

For the 2026 Over The Horizon division, the electrical system was redesigned as a fully remote-controlled and autonomous architecture. This redesign eliminates all manual control pathways and instead prioritizes communication reliability, modular integration, and system safety.

At the center of the system is the Cube Orange flight controller, which serves as the primary processing unit. Running the ArduPilot ecosystem, it coordinates all sensing, control, and communication across the platform. The system is structured as a centralized control architecture in which all inputs, state estimation, and actuation commands are processed through the flight controller.

Table 1: High-Level Electrical System Architecture

Subsystem	Function
Flight Controller (Cube Orange)	Central processing, sensor fusion, control logic, and PWM output generation
Communication System (Herelink)	Long-range RC input, telemetry transmission, and onboard Mission Planner interface
Vision System (Firefly Camera)	Real-time HD video streaming and recording for operator feedback and diagnostics
Actuation System (ODrive + BLDC Motor)	Closed-loop steering and throttle control with encoder feedback
Power Distribution Network	Regulated voltage supply to all subsystems with electrical isolation

Remote Control and Telemetry

A Cube Herelink transmission system was selected to unify remote control and telemetry into a single robust platform. This system integrates a ground controller running Mission Planner with an onboard air unit, eliminating the need for additional onboard computing hardware. Communication is handled using the MAVLink protocol, which provides structured, error-checked data transmission between the operator and the vehicle. The system supports long-range operation (up to 12.5 miles) while maintaining low latency and high reliability.

Table 2: Remote Control and Telemetry Architecture

Feature	Implementation
Control Input	SBUS link from Herelink to Cube Orange
Telemetry Protocol	MAVLink bidirectional communication
Ground Interface	Integrated Mission Planner on Herelink controller
Video Transmission	Micro-HDMI feed from Firefly camera to Herelink
Range	Up to 12.5 miles line-of-sight
Latency	Low-latency digital transmission optimized for real-time control

Flight Controller and Control Logic

The Cube Orange flight controller serves as the central node for all real-time decision making. It integrates onboard inertial and positional sensors to estimate vehicle state and execute control algorithms. The ArduPilot framework enables implementation of PID-based control loops for steering, throttle, and autonomous navigation behaviors.

Table 3: Flight Controller Sensing and Control Functions

Component	Role
Accelerometer & Gyroscope	Attitude estimation & dynamic response measurement
Compass	Heading estimation for navigation control
GPS Module	Global position and velocity tracking
Control Algorithms	PID loops for stable steering and throttle response
Autonomous Logic	Waypoint navigation and mission execution

Steering and Actuation System

Steering actuation is achieved using an ODrive S1 motor controller paired with an M8325 brushless DC motor. This system enables precise position control through encoder feedback and supports both manual remote input and autonomous command execution. The system uses a 10:1 gear reduction to deliver approximately 50 Nm of torque. A self-homing routine is implemented at startup, where the motor rotates until a limit switch is triggered. This establishes a consistent zero reference point and ensures repeatable steering calibration across all runs.

Table 4: Steering and Actuation Architecture

Element	Function
ODrive S1 Controller	Closed-loop motor control with encoder feedback
M8325 BLDC Motor	Mechanical actuation for steering system
Gear Reduction (10:1)	Torque amplification and improved control resolution
Encoder Feedback	High-precision position tracking
Limit Switch	Establishes zero reference during self-homing routine
PWM Interface	Command input from Cube Orange to motor controller

Princeton Electric Speedboating: Tiger's Championship

Stephen Burns, Evan Callas, Andrei Bazavan, Antoun Salib, Andre Graves, Tom Wang, Brandon Wilk, Calvin Nguyen, Graham Smith

www.navalengineers.org/Princeton

For the 2026 Promoting Electric Propulsion manned planing division, PES selected Tiger, a 12-foot D Stock hydroplane originally built in the early 2000s. We chose this hull because it offers an excellent combination of efficiency, controllability in rough water, flexibility for electric powertrain integration, and strong team familiarity. In its original gas outboard configuration, Tiger demonstrated exceptional efficiency for its class, and its hydroplane geometry is especially well suited for the 1-mile oval course, where maintaining speed through turns is critical. Compared with smaller hydroplanes, the D Stock platform also provides improved rough-water handling without a major weight penalty, which is important given the conditions encountered in past PEP events.

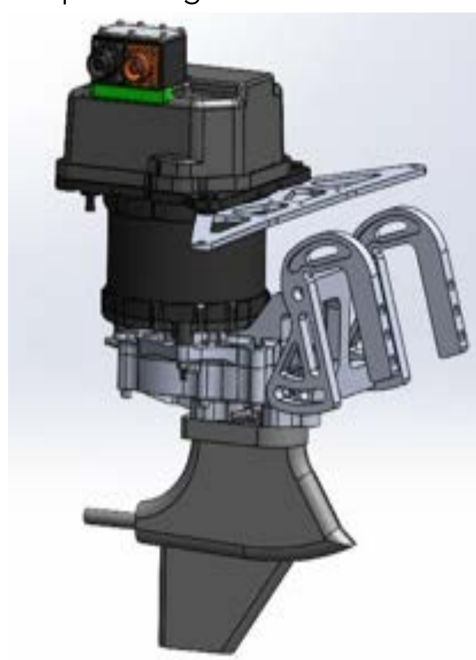

Figure 1: CAD model of the custom outboard assembly

The hull also gives us substantial freedom in powertrain development because the platform is naturally built around an outboard configuration. This allows us to develop our motor system and in-hull battery packaging while keeping installation simple at the transom. In addition, PES has several years of experience working with hydroplane hulls, giving us a strong understanding of setup, handling, and incremental performance optimization.

To adapt Tiger for this year's system, we made several targeted modifications. We coated the hull bottom with SpeedCoat49 to reduce drag, particularly in the corners where wetted area increases. Finally, we upgraded the left-side turnfin

by designing a billet aluminum mount that cants the fin 5 degrees inward for improved cornering stability, and we machined a new fin from 7075 aluminum to increase stiffness while slightly reducing thickness and drag.

Outboard Design

Last year, we built a dual-motor coupled outboard system with two separate motors and two inverters. We had issues with that design related to sharing a common shaft between motors, which resulted in stiffness issues outboard. This weakness was present in both the common shaft and the plate that the inverters and cooling system were sitting on. Additionally, we had inverter reliability issues that led to the end of our run at PEP last year. This year, we focused on minimizing some of the complexities that we dealt with last year while maximizing power output. Therefore, this year, we looked for an inverter-motor combination that is much more compact and efficient. We partnered with Zero Jet and got a 30 KW unit for this year. Using a combined motor and inverter system gave us the bandwidth to focus on other parts of the boat and create a more comprehensive outboard with minimal parts within the boat itself.

Electrical Systems – Low-Voltage

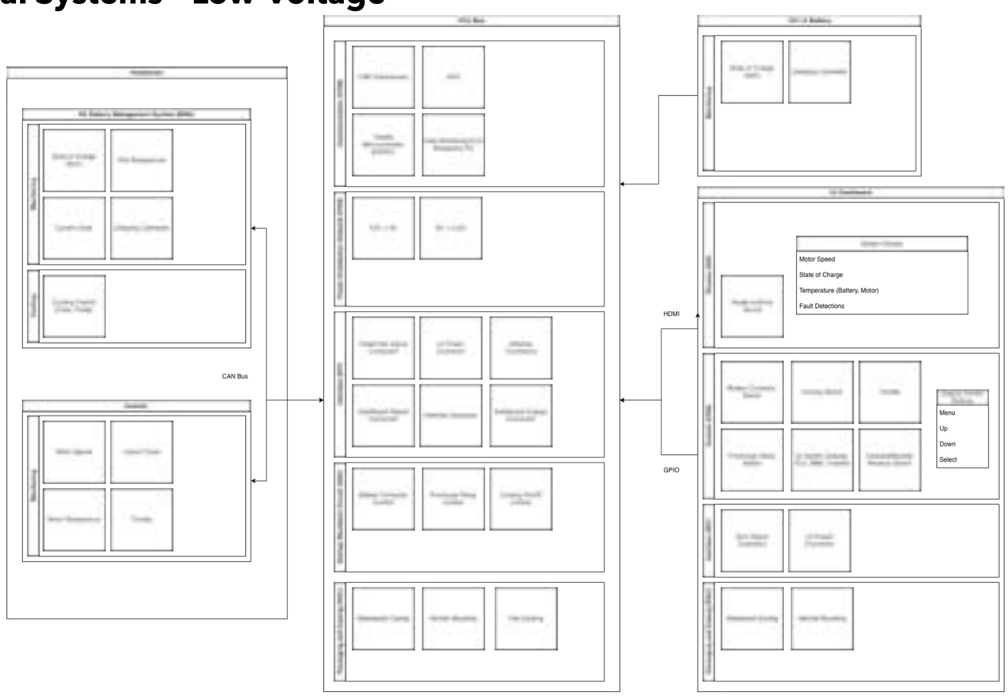

Figure 6: layout of entire proposed LV system

Previous System

To understand the goal of this year's system, we provide a brief overview of last year's system to show some of the shortcomings that influenced our design decisions this year. The system last year was able to complete the necessary functions of an LV system, but not much beyond that. The driver was able to activate parts of the system using a series of switches on the dashboard, which then fed into relays that managed power; throttle analog signal was sent through the wiring harness to the inverter. These two functions essentially encapsulate the main functionality of last year's LV system.

There were three main areas of concern:

1. Manually activated switches – if the wrong sequence of switches were to be flipped, it could cause damage to the system.
2. Lack of information for the driver – while the boat was running, the driver had no information about the motor RPM, battery temperature, motor temperature, and other crucial information about the system.
3. Difficulty debugging – when a fault occurred, it was difficult to pinpoint the point of failure given that there was no data log of any of the systems during a test run.

We planned out this year's LV system with those three concerns as main pillars.

This Year's System

We approached this year's LV system with three goals in mind: add robustness protection when starting the boat, provide the driver with crucial information about the boat, and log data so we can debug easier. In addition, we were also working with a new outboard this year from ZeroJet. To fulfill the three goals, and in the spirit of learning and pushing our engineering abilities, we designed a custom PCB – the low-voltage vehicle control unit (LV VCU) PCB – integrated with a dual-controller architecture consisting of an Autosport Labs ESP32 and a Raspberry Pi 4.

The LV VCU PCB handles power regulation, CAN communication, and relay control at the hardware level, while the ESP32 manages real-time driver inputs and the Raspberry Pi handles data aggregation, telemetry logging, and the driver display. As a redundant backup, a fuse block and relay combo unit provides an

alternative manual control path in case the primary PCB or controller experiences a fault, ensuring the boat can be safely operated or shut down under any failure condition.

Power Management

A two-stage power architecture consisting of a buck converter followed by an LDO regulator was selected to balance efficiency, thermal performance, and supply quality. The boat's 12 V LV battery is first stepped down to 5 V by the buck converter, then further regulated to 3.3 V by the LDO for the ESP32-S3 and logic-level devices. This approach avoids the excessive heat dissipation of a direct 12 V-to-3.3 V linear conversion while providing the clean, low-noise output required by sensitive digital electronics. Decoupling capacitors and inductors are used throughout to further suppress noise.

In addition to the PCB-based relay control, a fuse block and relay combo unit is integrated into the LV system as an alternative control path. This unit provides overcurrent protection for individual circuits via blade fuses and allows manual relay actuation independent of the PCB and ESP32. In the event of a PCB fault, controller failure, or communication loss, the operator can route power and control the high-voltage contactors directly through this unit without relying on any embedded logic. This hardware-level redundancy ensures that the boat can be safely powered down or operated in a degraded mode under any failure scenario, and it also simplifies bench testing by allowing subsystems to be individually energized without the full VCU stack running.

Princeton Electric Speedboating: Powering the Displacement Hull

Graham Smith, Stephen Burns, Brandon Wilk, Tom Wang, Andrei Bazavan, Raymond Wang, Isiahaz Whitaker, Samuel Finlayson, Sara Chen, Evan Callas, Calvin Nguyen, Saif Bernstein, Antoun Salib, Paige Baker

www.navalengineers.org/Princeton

We chose two LMT7065 because they are the highest power density motors that we could find at 55V. They fit within our RPM range of 6000-12000 revolutions per minute, which works with the gearboxes we have available. As we were working with these motors, we had to make some adjustments to our mechanical system, since these motors operate at the upper end of our RPM range, making it challenging to get peak performance. Another reason we chose these motors is that the power range is also compatible with our system. Our target is 20-25 kw continuous, and each motor is rated to do 10-15kw continuous, which we will be able to utilize.

Design and Analysis

This year, for the displacement boat, the same battery pack as last year was used, except that it was redesigned and optimized for higher current output. The pack consists of 405 3.6V lithium-ion cells arranged in a configuration with 15 in series and 27 in parallel to achieve a nominal voltage of 54V and motor current draw requirements. This configuration allows for a modular design such that groupings of 27 cells could be constructed independently and slid into a structural skeleton. Due to this modularization, structural components were 3D printed locally supporting rapid iteration and easing maintenance by being able to remove each rack of cells.

Figure: Modular INR-21700-P45B *Battery* Pack

Air cooling was chosen due to its lightweight, cost-effectiveness, and simplicity compared to liquid cooling. This design uses ventilation channels and strategically organized cell placement, building on thermal airflow research to optimize cooling efficiency. To facilitate active cooling, eight fans draw air through a closed airflow loop, optimized for their high static pressure and airflow characteristics during peak load conditions. Originally built for desktop computer cooling systems, these fans cycle air through a radiator (connected to an external water-cooling system), between the cells, and finally through a return duct along the outside of the pack. Thermal simulation models allowed us to design the pack so that temperature differences along the cooling path remained relatively constant, avoiding uneven thermal load on the cells.

Quinnipiac's Budget Warriors: Powering the Displacement Hull

Christopher Parisi, Marc Needleman, Conner Kass, Zachary Chapman, Cole McKirryher, Jonathan Thor, Neal Kapadia

www.navalengineers.org/Quinnipiac

Figure 1 – Deep-V hull CAD model showing the interior geometry and printed section layout

A monohull deep-V configuration was selected to match the speed and efficiency characteristics of high-performance powerboats. The deep-V geometry characterized by a pronounced V-shaped cross-section running the length of the hull allows the vessel to cut cleanly through chop and small waves rather than slamming over them. This reduces impact forces at speed, maintains directional stability, and keeps more of the propulsion energy directed into forward motion rather than wasted in vertical hull movement.

The deep-V configuration also offered practical advantages in terms of predictable handling and stability. Compared to tunnel hull or catamaran configurations that can offer higher peak speeds but demand more precise tuning, the deep-V provides a more forgiving balance of speed, stability, and ease of control.

Dimensions

Figure 2 – Side profile view of the hull design

The final hull measures 4 feet in length and 2 feet in width. These dimensions were determined by balancing three competing considerations: the build volume of the available 3D printers, the required payload capacity, and the target weight range. The chosen geometry allows the hull to be divided into eight equal 1 ft × 1 ft printed sections, which kept each section within the printer's build envelope while ensuring the assembled hull could comfortably carry the 30-pound payload and fall within the competition's 30–45 lb vessel weight range.

Material Selection

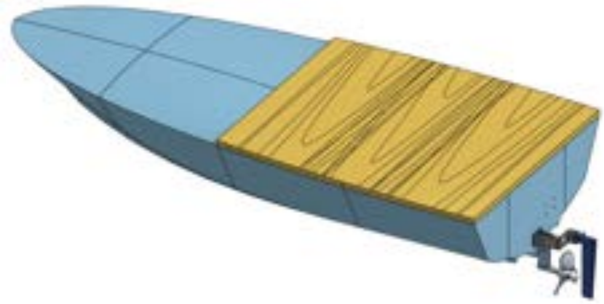
Figure 3. Full CAD render of assembled vessel with deck and propulsion unit

Acrylonitrile Styrene Acrylate (ASA) was selected as the primary hull material following a comparative evaluation of common 3D-printable thermoplastics. Since the hull will be exposed to sunlight, water, and variable outdoor temperatures throughout testing and competition, UV resistance and moisture stability were primary selection criteria.

Compared to PLA, which softens at elevated temperatures and is susceptible to moisture absorption, and ABS, which degrades under prolonged UV exposure and is prone to warping during printing, ASA offers superior long-term outdoor stability. It also provides excellent impact resistance, which is important for handling wave loads and the occasional contact with dock edges or debris during testing. Because the hull is reinforced with a fiberglass and epoxy composite outer shell, the printed ASA structure serves as a lightweight geometric core rather than the primary load-bearing layer, allowing the material's thermal and UV properties to take precedence over raw structural strength.

Fabrication

The hull was fabricated using FDM (Fused Deposition Modeling) 3D printing. Dividing the hull into nine sections addressed the build volume limitations of the available printers while also reducing the risk of print failures. Print orientation for each section was carefully selected to minimize weakness along layer boundaries and maximize strength in the directions most relevant to hydrodynamic loading.

After printing, sections were bonded using cyanoacrylate adhesive (Loctite Professional Super Glue) and 3M Marine adhesive sealant. The adjoining surfaces were sanded and cleaned before bonding to improve adhesion. The fully assembled hull was then reinforced with fiberglass cloth and epoxy resin, creating a composite outer shell that dramatically increased stiffness, impact resistance, and water resistance compared to the bare plastic.

Robotics Club of Central Florida: Powerfully Unmanned

James (Dylan) Kaney, Caicheng Li, Joshua Fernando, Matthew Barrs, Stephen Chapman, Brandon Zhang, Kamila Rodruiguez, Eduardo Calero, Quinten Ehrenberg, Lucas Mendicino, Nick Morrison, Cristiano Machado, Leam Mena, Laura Justavino, Hanah C

www.navalengineers.org/UCF

Building upon the previously developed "Rapid3D" unmanned electric platform, in this paper we explore current frontiers in fully additively manufactured maritime design for the Promoting Electrical Propulsion (PEP) national competition. Given that the old midsection incorporated a static air intake, a complete redesign and refabrication was necessary to correct the geometry. The new air intake would be modular, including a removable intake "lid" and six hardpoints that interface with M6 bolts, allowing future modifications to be easily attached and removed.

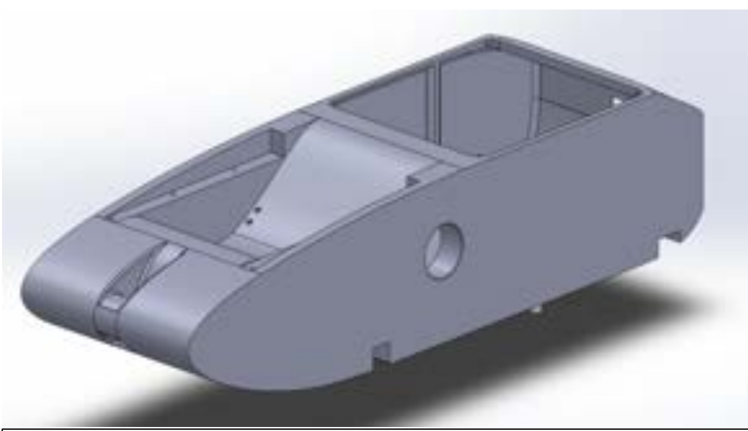

Figure 4 - Isometric view of the new (TideBreaker) midsection with the radiator chamber exposed

The new midsection, shown in Figure 4, places the intake chamber on the top of the bow of the midsection. This offers many advantages, the most important of which is that it is much less vulnerable to airflow obstruction due to a rising waterline. It also improves maintainability as the radiator chamber is more easily accessible given the removable lid. Three of six screw holes are also visible, the implementation of which are elaborated on in a later section.

The new midsection also includes geometry at the stern that accommodates the emergency stop switch and a new water-resistant high-current 3-pin connector, which is also elaborated on in a future section.

Propulsion Redesign

Rapid3D's outboard propulsion system was mounted on a lateral aluminum extrusion at the rear of the midsection, perpendicular to the direction of travel. This extrusion also acted to connect both pontoons; however, the propulsion system could not be adjusted forward nor backward to change the center of pressure, which is impactful for proper hydrodynamic performance. TideBreaker's propulsion system was designed to mount to a longitudinal aluminum extrusion to mitigate exactly this problem, with the motor positioned forward from the rudder.

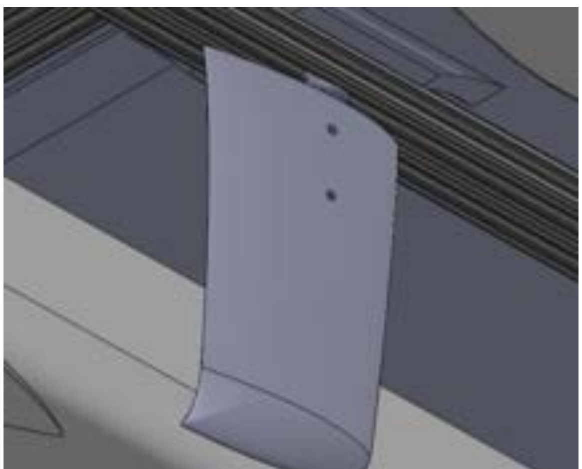

Fig. 8 - Position of rudder and longitudinal extrusion on the underside of TideBreaker's midsection.

The electrical system of TideBreaker closely follows that of the previous iteration. The system is divided into two subsystems, the High Voltage and steering system and the low voltage control and communications system, as with the previous design. The primary changes made to the system were through updating the enclosure, installing additional safety architecture and through incorporating a 3-pin high current connector for our outboard DC pod motor.

The low-voltage system is contained within the electronics box. It contains the 3S LiPo which is connected to the 12V water cooling system via a relay and to a 12V->5V buck converter. This buck converter provides regulated 5V power to the Cube flight controller and Raspberry Pi. The GPS, Arduino for stepper control, and RC receiver are powered by the flight controller. The PWM signal for the main motor and the stepper signals for the rudder control are connected from the flight controller and Arduino to the VESC and stepper driver respectively.

The high-voltage system is connected to a bus bar to allow for easy distribution. All power

from the batteries runs through the fuse and contactor before reaching the bus bar so that the batteries are completely cut off in the event of a power shutoff. The bus bar then provides power to the VESC and a 48V regulator to the stepper driver.

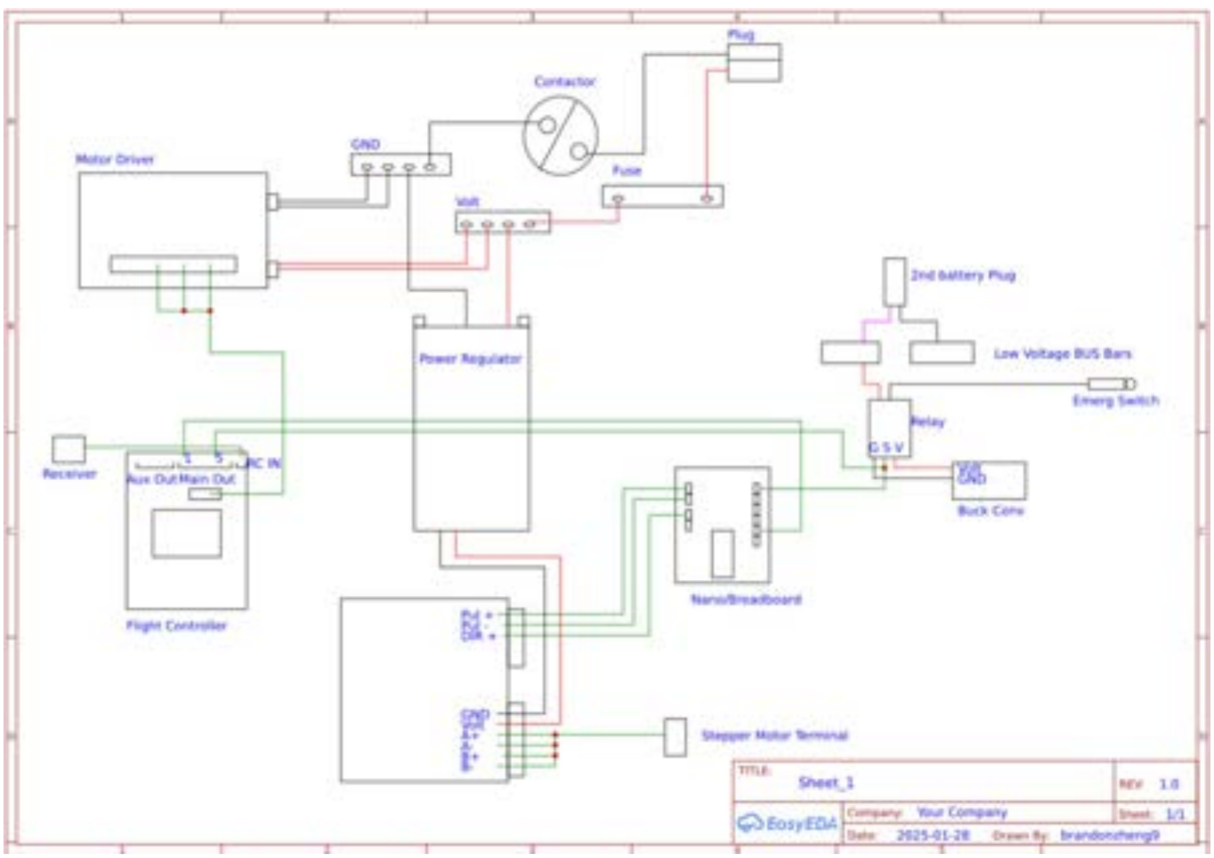

Figure 12. Updated low-voltage control system schematic diagram

Rutgers: Inflatable Racing

Benedetto Skirde, Kevin Arruda, Micah Shafer, Christopher Cafiero, Praneeth Damarla, Alexander Puhak, Matthew Mohammed, Shubham Sharma, Abhijit Nair, Jared Singer

www.navalengineers.org/Rutgers

Using an inflatable hull had a variety of benefits for the team's purpose. For one, it would be significantly lighter (only 71lbs) than an aluminum or wooden hull of equal size (10 feet in length), which would allow for increased acceleration. In addition, the craft is capable of holding 990lbs and can handle motor function up to 15 horsepower. Seeing as the hull was lightweight, strong, and able to handle a more powerful motor than last year's, this was a perfect choice.

The hull is made of PVC material, with joints that are made with quadruple overlap seams in order to ensure strength and reliability. For added durability, the bottom of the boat is lined with aluminum sheets, giving both stability to the operator and a place to mount materials inside the boat effectively. Other features include 3 separate air chambers to protect the operator in case of failure or puncture, four-person capacity, oars, and a repair kit.

This hull was also a great choice given REB's administrative struggles as an organization. With no formal storage area on campus, no lab space to work in, and no trailer or parking space to hold a hull long term, an inflatable boat meant an added flexibility that allowed the club to work much more effectively.

After choosing a hull that gave REB the freedom to upgrade our motor, research on motors within our price range that would fit our needs began. While AC motors are more efficient and perform better than DC motors in electric vehicles, finding an AC motor that fit the group's needs and a matching inverter would have been significantly more work and money than using a DC brushed motor, so it was decided to go forward with the latter. In future years, REB hopes to change the system to a 3-phase asynchronous motor, but for this year considering the available funding and manpower it made sense to go with the simpler option.

Last year, the team used a Motenergy ME0909/1906 DC brushed electric motor rated at 6.4 horsepower continuous. As a replacement, a Motenergy ME1602 DC brushed electric motor capable of 10.7 horsepower output (after efficiency losses) was obtained. The motor is rated for 200A continuous at any voltage between 48V and 72V. An image of the motor and its power curve is shown in the figures below.

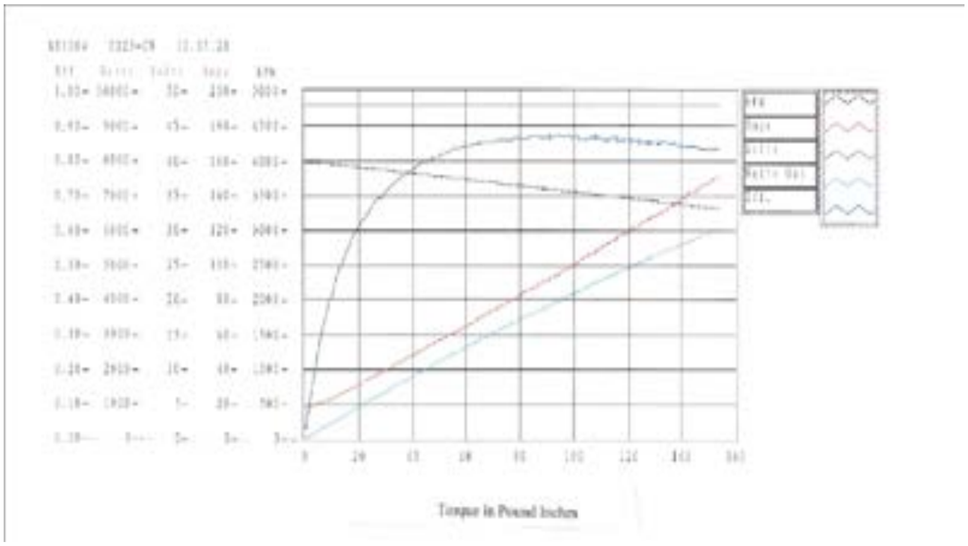

Figure 3: Motor power curve of ME1004, identical in power to ME1602.

From the power curve and the output current calculations (discussed later in the document), an output of 3100rpm and 24.6 Nm from the motor was determined. As evidenced, the power output from the motor will be much stronger than last year's setup. This will improve the acceleration of the boat, while maintaining a fully DC system and staying under the horsepower rating given by the hull manufacturer.

To power the motor, a new battery system, larger than the previous one, was required. This meant researching and designing an entire new battery pack to power our propulsion. Last year's system was powered using two Optima-branded BlueTop 12V 55Ah Lead Acid Marine Batteries, provided by ASNE. While AGM/lead acid batteries are durable, reliable, and cost-effective, they ultimately fall short in electric vehicle applications when compared to other battery chemistries like lithium-based batteries. For one, AGM batteries are far less energy dense and much heavier, meaning their power to weight ratio is much lower than that of other battery chemistries. In addition, AGM batteries perform worse under high current conditions, current spikes, and have a higher internal resistance and voltage sag. These issues, along with a variety of others, led the group to research other battery chemistries for our propulsion system.

Stevens Institute: Mechanical Design, Fabrication & Testing

Jack Ceriello, Ellie Yu, Gabriel Pust, Jeffrey Ober, Luke Saletta, Anthony Ventresca, Thiago Andrade, Liam Ruane, Matt Polvino, Alex Garcia, Brandon Huang, Ishaan Sayal, Lucas Moeller, Max Melaragno, Saajan Shah, Sebastian Guadalupe-Pena, Sebastian Spiechowski, Shivansh Kumar, Jack Meldrum, Christian Filsaime, Nelson VanMaaren

www.navalengineers.org/Stevens

An important aspect of integrating subsystems together is having a CAD assembly of the entire boat. The CAD assembly was modeled, iterated and integrated with the boat's hull model, updated dashboard, cooling system, and drivetrain. Other assembly components include the boat's battery box, fire extinguisher and seat. The CAD model of the manned boat was used as a visual reference to implement the boats' important subsystems. The boats CAD assembly was used as a great war to show the boat during presentations. Another use of the SolidWorks assembly was exporting the model so that users could view the manned boat directly from the website in a 3D viewer. The assembly ensured that everything fits together, there are no collisions with subassemblies and kept proper alignment with each part. Certain subassemblies such as cooling system and drivetrain required tolerance and clearance checks withing the subassembly. As each sub team works on their system, a full assembly of the manned boat allows the team to fully collaborate with each other.

Power transmission

It was selected to use a high torque spider coupling to connect the secondary motor, which will allow for 2 degrees of angular offset and 0.04 inches of parallel offset. The steel hubs are connected by a high density urethane spider allowing for these offsets and compensating for any disagreement in acceleration and alignment between motors. For the spider hubs to fit on the motor shaft, the shafts were extended by custom 1" to 1" shaft extenders.

AMEC ANSI 40 chain and sprockets were selected because at peak sprint speed, they will have a factor of safety of 6 based on the rated breaking load of 3530 lbs, and are a lighter alternative to timing belts and pulleys. Chain was selected instead of direct gearing to allow for the motors to be positioned inboard, avoiding them being involved in sea spray, and connect to a common shaft.

The custom vertical driveshaft was designed to interface between the drive sprockets, which require a 7/8” round shaft with a keyway at the top end, and the 12mm square shaft adapter at the opposing end. The material selected is 1045 carbon stainless steel with a maximum shear stress of 265mPa. The lower unit is connected by a 12 mm female to female set screw shaft adapter. The main diameter of the shaft was designed for a factor of safety of two at endurance speed. The point of failure in the system is the 12mm shaft coming out of the Konny lower unit. It’s factor of safety at expected race speed is 1.65, and we do not have enough power at sprint to meet the yield strength.

The square shaft stress was calculated with these equations:

τ =Qr/J J=(d^4)/6	τ =shear stress Q=torque r=1/2 diameter of square shaft J=polar moment of inertia of cross section d=diameter of square shaft

Inverters

Two ACS48L90-Y35T inverter motor controllers were selected for the 2026 drivetrain. These have a nominal voltage of 48V aligning with the electrical architecture of the vessel, and a rated continuous current of 450A. The current capacity allows our system to grow should we find we are able to cool the motors to up to 300+ amps each

in future seasons. The finned heat sinks were selected so that the controllers can be air cooled and to keep vessel weight low. The two controllers will be connected in synchronized torque control mode assuring that they will be distributing power evenly and rotating at the same rate. The controllers new placement will be directly over the vertical driveshaft, which is where the outboard rotates around. This ensures that the wiring harness going from the controllers to the fixed electronic systems in the vessel requires a minimum possible range of motion.

Cavitation plate and adapter

The length, width, and spacing to propeller tip of the anti-cavitation plate were determined by analyzing a broad dataset of commercial outboard plates in comparison to their corresponding propellers. It was found that the plate should be 50% as wide as the propeller diameter, and should extend 10% of the propeller's length past the tip. It was found that there should be a clearance of 20% of the propellers diameter between the propeller tip and the anti-cavitation plate to reduce air sucked in from the surface without introducing additional vortices.

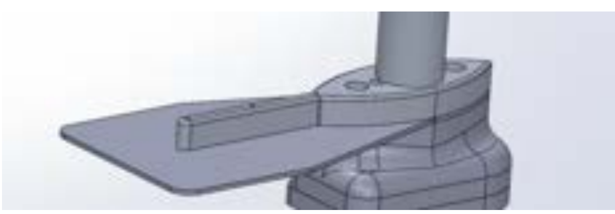

The cavitation plate mount and the lower unit have different bolt patterns. As a result, an adapter was manufactured out of aluminum to mate the pieces together, and to allow for propeller tip clearance.

It was found that our new maximum thrust would exert a stress on our stern with a factor of safety of 50, and so no new mounting system was necessary.

Propeller and gearing

The propeller selection was determined by comparing the maximum thrusts of a NewtonRadar series propeller at Blade Area Ratios of 0.48, 0.71, and 0.95 and the thrust produced by each of these

BARs was evaluated from a pitch of 10.5 to 20.6 inches. The experimental values provided by Newton-Radar were produced using an engine which operated at a higher RPM and torque than ours could produce, so our thrust values were evaluated based on available torque. The highest estimated thrust we could produce with a newton rader series propeller at 100nm is 289.98 lb coming from the A3/48/149. By this analysis our current A3/48/167 propeller will produce 288.25 lbs of thrust in the current drivetrain configuration. The 0.6% increase was too insignificant to warrant the cost of designing and machining the new propeller.

Tank Testing: Objectives & Testing Plan/Preparation

Preliminary design estimates suggested a likely increase in displacement related to drivetrain modifications to add power. In order to determine whether the added weight would "justify" itself and lead to a respectable speed increase, a model test was conducted using a 1/3rd scale model of the competition hull. The purpose of this model test was to verify that the increase in resistance at this new displacement will not prevent the increase in thrust provided from new machinery from actually resulting in a speed increase. Before testing, weights (previous displacement from 2024 competition and estimated 2026 displacement) were scaled down to model scale in freshwater.

Before towing the model, the necessary instrumentation was installed and calibrated. The details of the calibration are not within the scope of this paper, but the instruments installed are relevant. The model was outfitted with a drag balance to measure resistance, an inclinometer to measure steady trim angle, and a laser to measure heave.

The model was subsequently balanced-in-air to ensure that the LCG of the model was indeed at the pitch pivot. Due to the higher-than-required weight of the model and the weights required to balance it, an unloading spring was used to match the tested model displacements to the desired scaled down displacements. Since the model was going to experience steady dynamic trim and had a shaft angle, a thrust unload was required before each run, calculated by the following equation using the superposition of the estimated trim and shaft angles:

$$Wunload = Dest\ \sin(\tau est - \theta shaft)$$

Additionally, since the pivot axis in the model was not vertically aligned with the thrust axis of the boat, a pitch moment correction was applied before each run to account for the artificial moment produced by this vertical difference.

Data Collection

Once the model was prepared for testing, it was towed at the 2024 competition displacement at four speeds corresponding to full scale speeds between 17.5 and 25 knots. This established a baseline for comparison against the higher displacement. The

model was ballasted to the heavier 2026 estimated displacement and run at eight speeds corresponding to full scale speeds between 17.5 and 35 knots. This higher displacement condition was run with the same LCG as the 2024 competition craft.

Finally, the high load condition was run with an aft LCG shift at speeds corresponding to 20, 25, and 30 knots at full scale in order to establish a preliminary relationship between LCG and drag. It is worth noting that although this LCG shift did result in a drag decrease, it also created dynamic porpoising instability at speeds 25 knots and above.

Video was recorded for each of the fifteen runs, along with overwater and underwater photos to assist in post processing. The underwater and overwater photos for the 35-knot speed at the high load and original LCG condition are depicted below.

Expansion & Analysis

The expansion of the obtained model scale data to full scale will be reviewed at a high level. The minutiae of each calculation step are out of the scope of this paper but it is worth noting that it followed the conventional model data expansion process for a planing hull.

First, underwater photos were used to estimate wetted keel and chine lengths which were then used to geometrically calculate the wetted surface area at each speed. These wetted surface areas were used to non-dimensionalize the drag experienced at each speed as follows:

$$C_{tm} = \frac{D_m}{\frac{1}{2}\rho_m S_m {V_m}^2}$$

Subtracting viscous effects at model scale and adding them back in at the saltwater full scale (both using the ITTC 1957 skin friction equation), a total resistance coefficient for each speed was calculated.

$$ITTC\ 1957: C_f = \frac{0.075}{(\log_{10} Re - 2)^2}$$

These coefficients were then converted to drag values using the full-scale vessel and fluid parameters and the same equation as above, replacing each parameter with the full-scale value. Trim values were taken directly as they should be the same from model to full scale. The following plots were obtained after the data expansion to full scale:

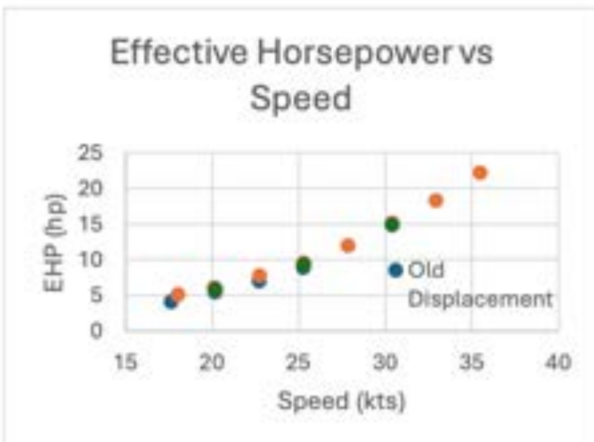

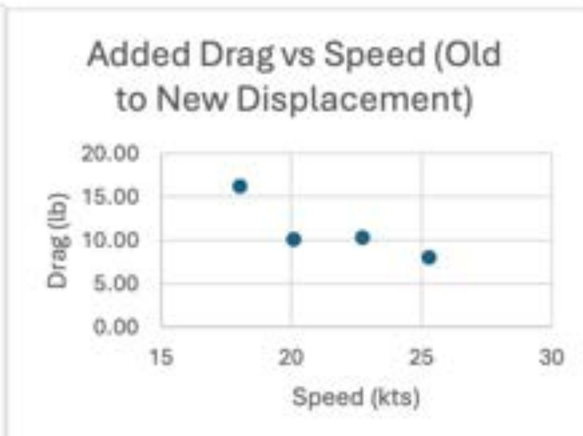

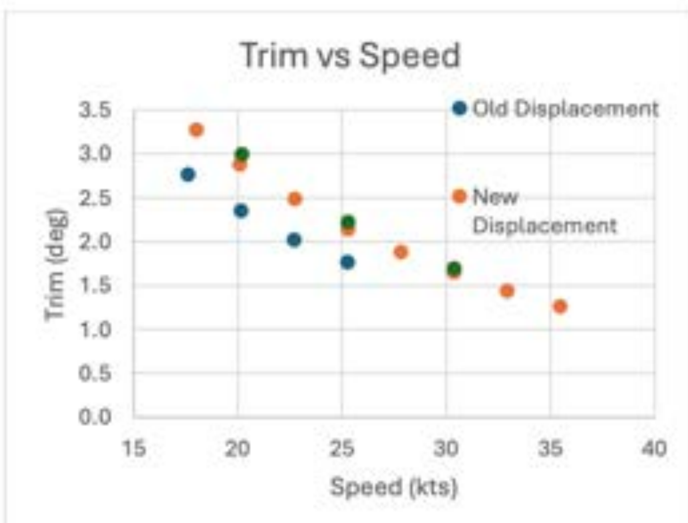

As the first plot displays, the effective power differences at each speed between the old and new displacements are extremely minimal. This suggests that modifying the drivetrain to produce more thrust is well worth the increase in weight that it precipitates.

Stevens Institute: Autonomous Beginnings

Oscar McMahan, Daniel Popov, Jack Ceriello, Jack Falen, Hanyue Shen, Gabriel Pust, Colin Leary, Ty Mazzga, Brianna Schaad, Emily Lossman, Aidan Berard, Max Melaragno, Sebastian Spiechowski

www.navalengineers.org/Stevens

In alignment for the team's goal of a high thrust, mechanically simplistic system, the propulsion options worth consideration were surface piercing propulsors (SPPs), underwater propulsors, and water jets. To assess the performance and efficiency of each method of propulsion, the following variables are defined:

P_E	Effective power output (W)
N	Number of propulsors
V	Nominal cruise speed (m/s)
ω	Wake fraction
t	Thrust deduction
η_R	Rotative efficiency (relative)
η_O	Open water efficiency
η_m	Mechanical efficiency

Figure 7: Definition of coefficients required to estimate propulsor efficiency.

The coefficients above give the net propulsion coefficient $\eta_\Sigma = \eta_H \eta_R \eta_O \eta_m$, where η_H is the hull efficiency coefficient given by $\eta_H = (1-t)/(1-\omega)$ [1, 2]. This provides the necessary coefficients to derive the nominal power required for each propulsor: $P_i = P_E/(N\eta_\Sigma)$.The respective coefficients for each type of drive are given in the table below:

Type	Surface	Water Jet	Submerged
ω	0	0.05	0.03
t	0	[-0.07, -0.02]	0
η_R	[0.97, 1.01]	0.99	[0.97, 1.01]
η_H	1.000	[1.074, 1.126]	1.031
η_O	[0.55, 0.62]	[0.62, 0.79]	[0.60, 0.68]
η_m	[0.95, 0.97]	[0.94, 0.97]	0.95
η_Σ	[0.51, 0.60]	[0.62, 0.84]	[0.59, 0.67]

Figure 8: Efficiency coefficients table for different types of propulsors.

Using the conservative end of each range, we find the net efficiency factor through the formula presented in the previous paragraph, and submerged drives yield the highest net efficiency coefficient at 0.62, while surface piercing drives have the lowest at 0.51. However, with information concerning operational range for the three types of propellers and their respective physical configurations, other factors are taken into consideration. These are depicted in Figure 9.

Drive	Output	Cost	Weight	Simplicity
Submerged	x			x
Surface Drives	x	x		
Water Jets		x	x	

Figure 9: Propulsor decision matrix based on available products.

Although surface drives yield comparatively low efficiency levels, they are considerably less costly than submerged propulsors with high thrust output. Additionally, due to them requiring less waterproof capability, SPPs are considerably less costly than fully submerged drives. Given that power is not a limiting factor, this justifies that in pursuit of higher speed, surface drives are the logical solution.

Propulsor Performance Estimation Algorithm

To select the optimal combination of motor and propeller, the team derived an algorithm to estimate the performance of the propulsion system under given conditions. The user inputs P/D ratio, operating speed, and input power. The algorithm outputs efficiency and requires RPM, thrust, and torque. The process is outlined in the following section.

The advance coefficient is derived from the given conditions. Assuming that the wake fraction can be set to 0 for SPPs as shown in the efficiency table, this gives the special case where the advance coefficient equals the advance fraction directly, given by:

$$J = \frac{V}{n \cdot D} \quad [10]$$

V is the velocity of the vessel, ***n*** the rotational speed of the propeller in rotations per second, and ***D*** the diameter of the blade. Then the immersed area is found using the following equation:

$$A_i = I_t \cdot \frac{\pi D^2}{4} \quad [11,6]$$

I_t is the standard immersion ratio, and in our case, it is given that 50% is a fair and typical value. Due to the unique ventilation of SPPs classical scaling fails [11] so empirical multipliers are used:

$$M_{KT} = 1 + 0.35 \cdot \log\left(\frac{D}{D_{ref}}\right);$$

$$M_{KQ} = 1 + 0.12 \cdot \log\left(\frac{D}{D_{ref}}\right).$$

These formulas are given by logarithmic interpolations for the given percentage increases when scaling up from a 150mm blade to a 300mm blade, giving changes of 46% for KT and 8.14% for KQ based on empirical results [11]. The coefficients for thrust and torque in relation to P/D and corrected J_ψ [6] are used to calculate K_T and K_Q values with ***n*** and ***J*** values inputs.

$K_T = -0.620J_\psi + 0.146(P/D) + 0.72956J_\psi(P/D) - 0.305{J_\psi}^2 - 0.125(P/D)^2 + 0.284$

$10K_Q = -0.185J_\psi - 1.21(P/D) + 0.695J_\psi(P/D) - 0.562{J_\psi}^2 + 0.805(P/D)^2 + 0.751$

From these the nominal thrust and torque can be calculated by reorganizing the formulations from Ferrando et al. [6]:

$$T = K_T \cdot M_{KT} \cdot \rho \cdot n^2 \cdot D^2 \cdot A_i;$$

$$Q = K_Q \cdot M_{KQ} \cdot \rho \cdot n^2 \cdot D^3 \cdot A_i.$$

From these equations and the one following, the power demand is calculated [10]:

$$P = 2\pi nQ\ .$$

And the overall efficiency is calculated using the following equation [6]:

$$\eta = \frac{K_T}{K_Q}\,\frac{J}{2\,\pi}$$

The algorithm finds an equilibrium that satisfies the given conditions, taking propeller selection, targeted speed and power input, and giving the performance and motor requirements. The figure below gives an exemplary batched run the solver generates.

Stony Brook: Powerful Unmanned Craft

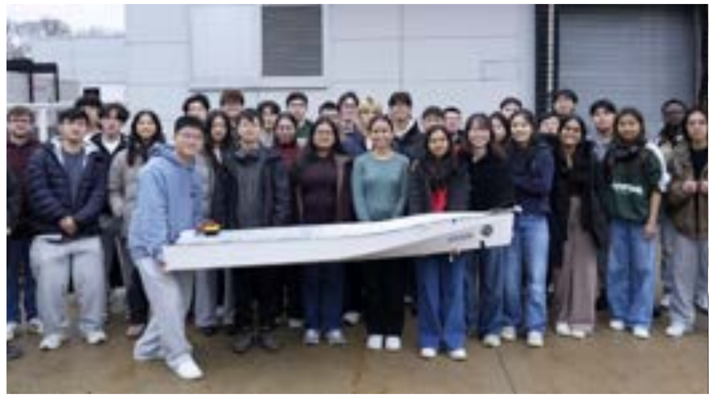

Steven Chen, Suhayla Yousuf, Maggie Tan, Chloe Jiang, Ryan Tang, Owen Chen, Daniel Lew, Nancy Zhu, Allen Li, Joseph Litjens, Brian Hui, Nick Zhang, Brandon Avena, Andy Ye, Ella Chen, Mirali Hajiyev, Yong Lin Wu, Adrian Borawski, Eric Chen, Rio Hessler, Brian Wong, Oscar Lin, Sean Lee, Emily Alex, Serra Demir, Safa Shikder, Spencer Lam, Vier Nguyen, Anton Yanaky, Peihuan Ma, and Austin Giordano

www.navalengineers.org/StonyBrook

When designing the body of our powertrain, the outboard, we referenced the NACA 0020 airfoil profile for its symmetrical geometry and low specific thickness-to-chord ratio. When scaled proportionally to the hull's dimensions, this profile provides the necessary internal volume to enclose the 1-inch diameter driveshaft without compromising hydrodynamic efficiency. Our reference, the NACA 0020 is characterized by a 20% thickness-to-chord ratio, with a larger leading-edge radius or a more blunt nose than other airfoils. Compared to thinner airfoils, the blunt edge due to the large nose radius allows a change in the angle of attack that wouldn't cause a sudden pressure spike, where a sharp turn will lead to flow separation and stalling. Its symmetrical section ensures even pressure distribution across the foil, facilitating efficient fluid splitting and minimizing the stagnation point at the leading edge, making it perfect for the applications of our outboard. With this in mind, we created the profile for the outboard using airfoil geometry with modifications to mount the Flipsky motor and propeller and simplify the rest of the outboard assembly.

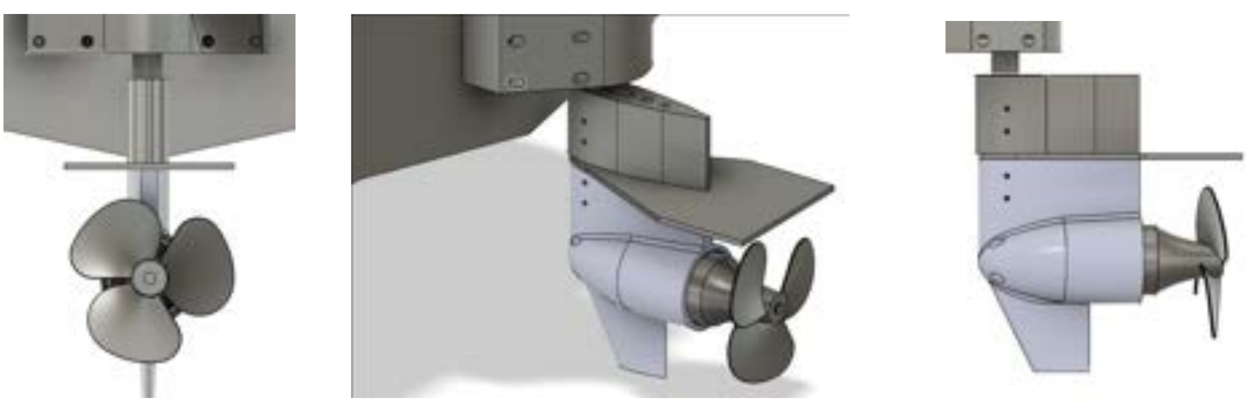

Fig. 2: Several angles of the designed outboard modeled in Autodesk Fusion

Our choice of motor for this year is the Flipsky Waterproof Brushless DC 6384 motor, selected based on its mechanical performance and compatibility with the overall design requirements. As a BLDC motor, it provides high efficiency, reduces mechanical wear, and outputs a consistent torque value, making it suitable for sustained propulsion. The motor's 63 mm stator diameter and 84 mm length create a large electromagnetic interaction volume, enabling a rated torque of approximately 3.8 N·m, which is sufficient to drive the selected Flipsky ABS 3-blade propeller under target conditions of 20–25 knots with a payload exceeding 60 lb. The propeller operates with an approximate ~~pitch~~ of $\eta_p = (\frac{\frac{v}{nD}}{\frac{Pitch}{D}}) \times (1 - (\frac{(Pitch*n) - v}{Pitch*n}))$ 0.12m, representing the theoretical forward distance traveled per revolution, which provides a balance between thrust generation and forward speed for this application. Accounting for the target speed to be 20 knots (10.29 m/s) and other parameters taken from the motor and propeller, we can calculate the propeller efficiency using the master equation shown below .

After substituting values in, the equation yields $\eta_p = 58.44\%$. Its 12-slot, 14-pole configuration also improves torque smoothness and efficiency, while the 10 mm shaft diameter ensures adequate structural strength for load transmission. Ceramic bearings reduce frictional losses and enhance durability at high rotational speeds, and the waterproof construction supports reliable operation in marine environments.

Controls (Steering)

Fig. 3: The left shows the positioning of the geartrain, the right shows the herringbone gear type that was chosen.

For the steering system of the unmanned vessel, we used a servo-actuated system, where a servo controls the precise steering through a simple geartrain linkage. The servo chosen for this task is the DS3230MG 30KG Digital Servo Motor. This servo motor was chosen because its stall torque is rated for 36 kg* cm, provided an input voltage of 5V. This would be compatible with the 24V system voltage and will also provide sufficient torque for the steering system to function properly at a targeted 14-knot speed. From the 36 kg*cm rating, it can be converted to 3.53 Nm of torque. The maximum speed at which the vessel is expected to turn (v) is estimated to be 14 knots, which can be converted to 7.20 m/s.

We can then calculate the total steering torque required through these equations:

$$F_{hydro} = 0.5\rho v^2 AC_L = 0.5 \times 1000\,kg/m^3 \times (7.2\,m/s)^2 \times 0.0223\,m^2 \times 0.5 = 289.008\,N$$

$$T_{hydro} = F_{hydro} \times L_{cp} = 289.008\,N \times 0.03m = 8.67\,Nm$$

$$T_{friction} = F_{hydro} \times \mu \times r = 289.008\,N \times 0.005 \times 0.0127m = 0.018\,Nm$$

After acquiring the steering torque, the minimum gear ratio between the servo torque and the steering torque is set to be approximately 2.46:1 to amplify the torque provided by the servo to match the required steering torque needed by the outboard motor. Therefore, a gear ratio of 3:1 would satisfy this minimum GR and have a 1.21 factor of safety to ensure smooth steering. We chose to use herringbone gears for steering rather than standard helical gears or spur gears, since the V-shaped design of its teeth will eliminate the axial load applied that would slide the gear off the aluminum shaft, and are generally regarded as the smoothest operating and strongest gear that can be 3D printed. We also conducted some fundamental gear calculations to ensure that the gears do not fail catastrophically. We can calculate the output torque for the shaft gear (larger gear) using:

$$T_{out} = 3.53\,Nm \times 3 = 10.59\,Nm.$$

We then set the module m, equal to 2, helix angle to 15 degrees, pressure angle to 20 degrees, and the number of teeth for the pinion and gear to be 18 teeth and 54 teeth, respectively. Using these values, the stress exerted on the gear teeth can be determined using the Lewis equation:

$$W_t = 10.59\,Nm\,/\,0.054m = 196.11\,N$$

$$W_r = W_t \times \left(\frac{tan(\alpha_n)}{tan(\beta)}\right) = 196.11\,N \times \left(\frac{tan(20)}{tan(15)}\right) = 73.9\,N$$

$$W_{total} = \sqrt{W_t^{\,2} + W_r^{\,2}} = \sqrt{196.11^2 + 73.9^2} = 209.58\,N$$

$$\sigma = \frac{W_{total}}{(b \times m \times Y)} = \frac{209.58}{(20mm \times 2 \times 0.308)} = 17.01MPa$$

The printing material PA6-GF nylon filament will yield a material strength of approximately 65 MPa. This would result in a Factor of Safety (FoS) to be 65 MPa/17.01 MPa, or the value of 3.82, which is clearly under the maximum for the material strength in the 3D printed material for the gears. There is an additional safety feature since we use a 15-degree helix angle so that this stress is spread between multiple teeth at any certain time. All these calculations together would allow the boat to achieve accurate and reliable steering capabilities while maintaining high speeds in the water.

Stony Brook: Manned Control & Power

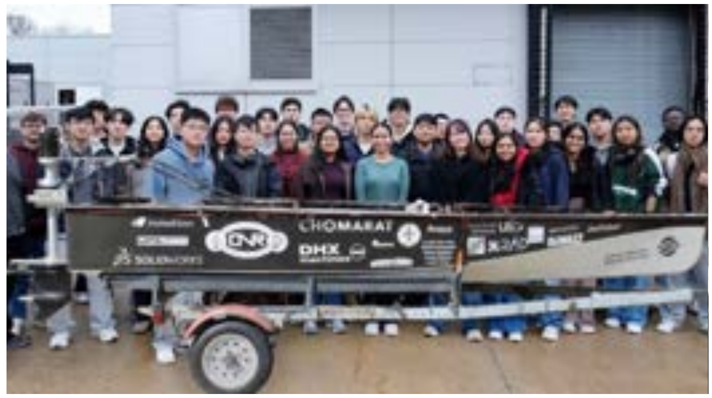

Steven Chen, Suhayla Yousuf, Maggie Tan, Chloe Jiang, Ryan Tang, Owen Chen, Daniel Lew, Nancy Zhu, Allen Li, Joseph Litjens, Brian Hui, Nick Zhang, Brandon Avena, Andy Ye, Ella Chen, Mirali Hajiyev, Yong Lin Wu, Adrian Borawski, Eric Chen, Rio Hessler, Brian Wong, and Austin Giordano

www.navalengineers.org/StonyBrook

The input and output gears chosen for the gearbox are the KHK SSG2-40 and MSGA2-25, which are module 2 steel spur gears with 40 teeth and 25 teeth, respectively. This size was chosen for its ability to withstand anticipated stresses while applying an acceptable radial load on the bearings and shafts. With the motor having a continuous torque rating of 50 Nm, the output torque is calculated to be 31.25 Nm. Accordingly, the input gear, with a bending strength rating of 98.3 Nm, has a safety factor of 1.97 against bending, and the output gear, having a bending strength rating of 157 Nm, has a safety factor of 5.02 against bending. Furthermore, the input and output gears, with surface durability ratings of 72.1 Nm and 110 Nm, respectively, have more than adequate resistance to surface pitting to last their expected service lives of no more than one hundred hours. The resultant normal load acting on the motor and driveshafts resulting from this torque transmission can be calculated as follows:

$$F_{res} = \frac{F_t}{cos(\alpha)} = \frac{T/r}{cos(\alpha)} = \frac{50\ Nm/0.04\ m}{cos(20^{o})} = 1330\ N.$$

As the motor is rated to support up to a 1500 N radial load, this gear configuration can be used without causing excessive wear to the motor bearings. Additionally, with this load supported by a 6200 ball bearing above the pinion and a Timken L21549/L21511 tapered roller bearing below the pinion, the ball bearing bears approximately 980 N and the tapered roller bearing bears approximately 350 N. Using the L_{10} life formulas and a speed of 5000 RPM, the ball and tapered roller bearings are expected to last approximately 560 and 590,000 hours, respectively, which are both far greater than the gearbox's anticipated service life. The power from the motor and gearbox is transferred to the lower unit via a ⅝" diameter 17-4PH stainless steel shaft adapted from a 50 HP gas outboard, providing a safety factor of approximately 11 for the anticipated torsional load of 31.25 Nm.

With gears and bearings operating at high rotational speeds, they must receive constant lubrication to limit wear and heat generation. While the typical approach for lubricating vertical shaft gearboxes is to partially submerge the gears in oil, for high-speed applications, this results in significant efficiency losses due to constant churning of the oil. To maximize efficiency, our gearbox utilizes an oil-slinging disk with low-viscosity automatic transmission fluid as the lubricant. As the disk is spun at 5000 RPM, it creates a fine oil mist that is carried around by windage from the gears, condenses on the gearbox walls and ceiling, and then flows down the sloped ceiling to drip directly into the gear mesh.

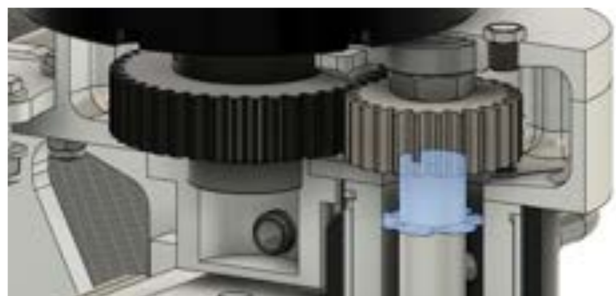

Fig. 7: Oil slinger attached to driveshaft.

Joining the gearbox and lower unit is a midsection constructed from a 2.5-inch outer diameter, 2.25-inch inner diameter 6061 aluminum tube overwrapped with a 0.04-inch layer of 200gsm 2x2 twill carbon fiber. The carbon fiber provides the bending resistance necessary to withstand anticipated thrust loads, while the aluminum tube comfortably handles the torsional loads. With highly overestimated assumptions of a thrust force of 1000 pounds and a torsional load of 35 lb-ft due to driveshaft and hydrodynamic forces, according to composite beam theory, the aluminum experiences a Von Mises stress of approximately 18 ksi while the carbon fiber experiences a bending stress of approximately 17.7 ksi, resulting in safety factors of 2.2 and 4.0, respectively.

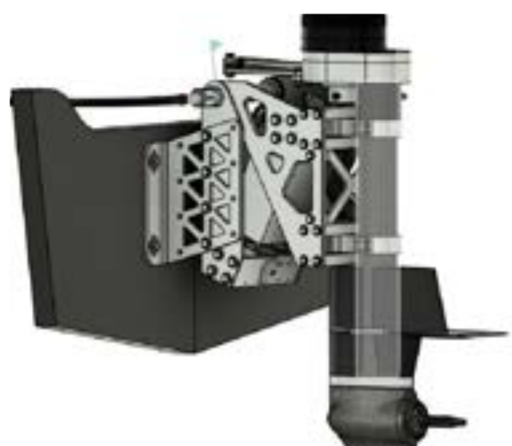

Fig. 8: Carbon fiber-overwrapped aluminum midsection.

A new lower unit has been integrated to reduce weight and drag and improve gearing compared to the previous design's lower unit. Sourced from a non-running Force 50 HP Outboard, the lower unit model was specifically chosen for its ability to support more than 30 HP, not having a through-hub exhaust design, and being built in two halves, with the lower portion housing the gears and prop shaft, and the upper portion housing the unnecessary water intake, water pump, and exhaust routing. As a result, only the lower portion is utilized to greatly reduce weight and complexity. Featuring a 1.62:1 gear ratio, the combined ratio from the new lower unit and gearbox is almost exactly 1:1, resulting in a propeller speed of 3100 RPM, which is in line with the speeds found in high-efficiency gas outboards.

Instead of the manually hinged system in the previous outboard design, the new design features an electric hydraulic actuator-operated hinge mechanism, enabling dynamic trim adjustment on the water. Via a rocker switch, the outboard can be trimmed down as much as -10 degrees to achieve faster acceleration or more stability while turning, and trimmed up while on plane to achieve higher speed. The mechanism also enables tilting up to 54 degrees for convenient launching and loading of the boat.

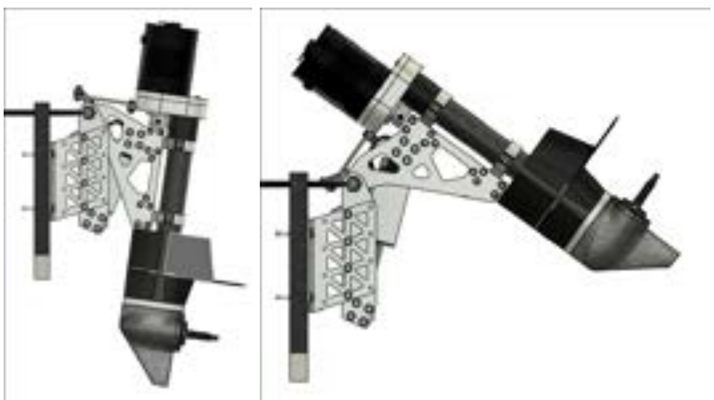

Fig. 9: Maximum trim and tilt range of the hinge mechanism.

With a grossly overestimated propeller thrust of 1000 pounds acting at a vertical distance of 21.1 inches from the hinge point and an estimated net weight of 70 pounds acting at a horizontal distance of 5.3 inches, the actuator operating at a perpendicular distance of 5 inches must exert 4294.2 pounds of thrust, which is well within its rating of 5000 pounds.

Finally, for mounting the drivetrain to the hull, a new bracket system has been developed with a hole pattern that enables adjustable outboard setback and depth. This adjustability enables precise control of the boat's dynamics, with greater setback providing improved planing ability and top speed, and less setback providing better stability and maneuverability. Relative to the mounting position of commercial 25 HP outboards, the brackets provide adjustable setback from 3 inches to 8 inches. Furthermore, following the general recommendation for planing hulls of raising the motor 1 inch for every 3 to 4 inches of setback, the anti-ventilation plate is maintained at the optimal level throughout varying setbacks by raising the position of the mounting holes by ⅝ of an inch for every 2 inches of setback. Further depth adjustment is enabled through multiple sets of mounting holes at the base of the brackets.

Fig. 11: Select manually machined steering and midsection components.

The combined midsection, hinge, and bracket assembly has been comprehensively evaluated using finite element analysis to ensure safety and reliability, with a minimum safety factor of 1.9 identified, given a thrust of 1000 pounds. With the most critical drivetrain components designed to handle such a thrust load, according to the general rule that a well-propped outboard is capable of 15 to 20 pounds of thrust per horsepower, it can be safely concluded that the drivetrain will be capable of supporting a 50 HP motor in the future.

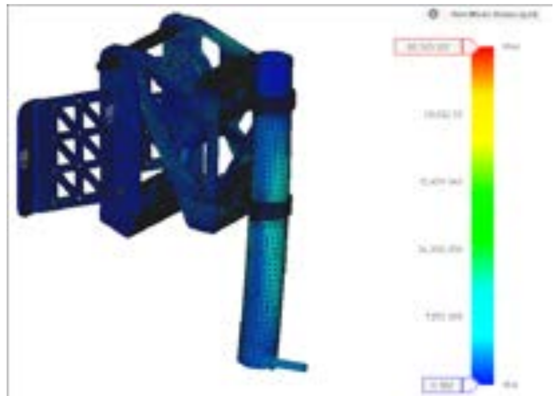

Fig. 10: FEA result showing the Von Mises stress of the midsection, hinge, and bracket assembly.

With the majority of the new drivetrain components requiring custom fabrication, efforts have been made to design components that can be fabricated as easily as possible to reduce costs and production time. As a result, most of them are able to be manually machined on milling machines and lathes or quickly laser cut and bent from sheet aluminum by SendCutSend. For more complicated components that require CNC machining, such as the gearbox, they have been outsourced to services including Xometry and local machine shops.

Fig. 12: Select laser-cut and CNC-machined components.

Controls

The steering system has been upgraded with a new commercially available lever-operated steering unit that utilizes one lever instead of two, like our custom design from last year. With less weight and complexity compared to the previous system, this design allows the driver to steer with their left hand and manage the throttle and trim with their right hand, allowing for precise throttle and trim control that mimics commercial throttle units. Mimicking commercial outboard assemblies, the end of the steering cable is mounted through the hinge mechanism's tilt tube and connected to a tiller arm using a linkage with ball joints. This configuration ensures the steering system does not interfere with the outboard's hinging motion and enables seamless integration with various commercial outboard steering solutions.

Texas A&M: Propeller Design & Electric Budget

Andrew Tucker, Allen Lawrence, Thomas Turner, Nevin McKay, Philemon Kim, Kai Marayag, An Nyugen, Sam Christian, Riley Bozone www.navalengineers.org/TAMU

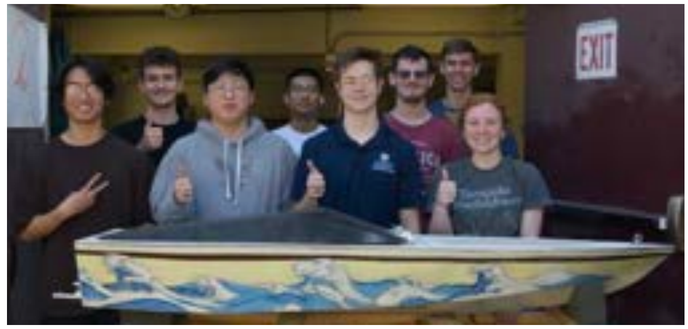

Through initial research, many inefficiencies were found with last year's propeller. Significant slip was experienced with the tri-blade cleaver propeller. From the geometric pitch of the blade at 4.64 inches, the slip experienced was 0.87 inches, for an effective pitch of 3.76 inches. Other coefficients were calculated, such as the blade-area-ratio (BAR), at 0.23. With ideal values of slip being near 0 inches and a BAR being in the 0.45 to 0.65 range, multiple types of cleaver props were looked into. However, there were no props that satisfied the criteria that were desired. This led to more research into how to design a tri-blade propeller from scratch.

The new propeller was made using Open Prop v3.3.4, a free software program coded in MATLAB m-files. Open Prop generates a prop (Figure 2) as well as related values seen in Table 2. Open prop does this by using given coefficients which were gathered from last year's boat such as the drag coefficient, and theoretical values we wanted to achieve such as top speed and motor RPMs, and attempts to solve for those values and output propeller geometry. By looking at the values it can be determined how efficient and optimal the propeller will be. Then the propeller geometry can be exported as slices of cross sections and exported to Solid Works as seen in (Figure 3), these cross sections were then lofted to make the CAD model of the propeller (Figure 4).

Having an EFFY or efficiency value as close to 0.8 was the aim of the iterative design process. When letting Open Prop dictate the geometry based off of the most efficient

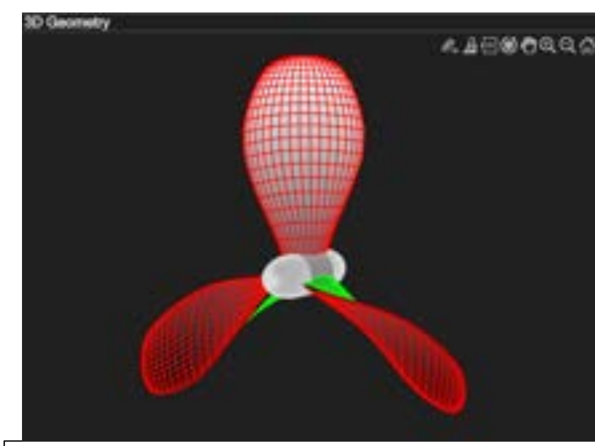

Figure 2: Open Prop Propeller Design

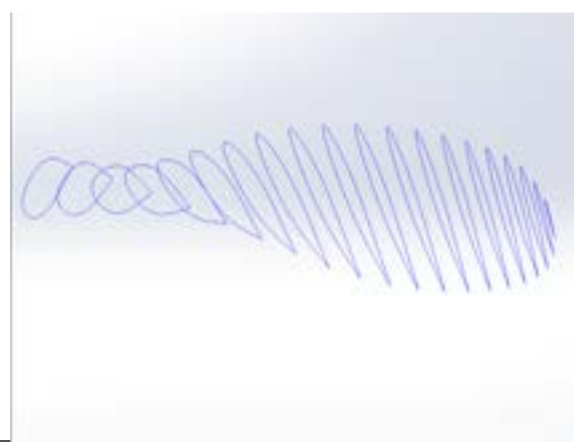

Figure 3: CAD Propeller Cross Sections

values, it created a propeller so thin the 3D printer was unable to complete the print. It was necessary to increase the thickness even if it meant decreasing the efficiency value. After multiple propeller attempts, the final propeller in Figure 5 had a much lower EFFY (Table 2), but its BAR and pitch was higher. When comparing this new propeller to last year's (Table 1)**,** t the Pitch and BAR increased but the BAR only increased a small amount. It is expected that the new propeller can perform better than the old one even with the lower EFFY than the initial propeller design from open prop. This propeller can be further improved by attempting to raise the EFFY while maintaining structural stability, which should improve the other values mentioned as well.

Table 1: New vs Old Prop

Design Parameters	New Prop Values	Old Prop Values
Diameter (in)	4.0	2.9
Pitch (in)	7.736	4.64
BAR	0.247	0.23

Table 2: New Prop Values

EFFY	J(Advance Coefficient)	CT (Thrust Coefficient)	L (Lift)	KT (Thrust)
0.42965	1.91197	0.00712	1.64312	0.01022

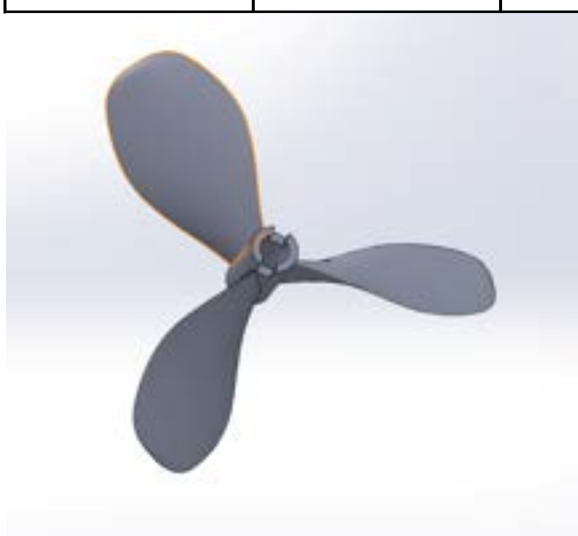

Figure 4: CAD Propeller Design with drive dog mating feature

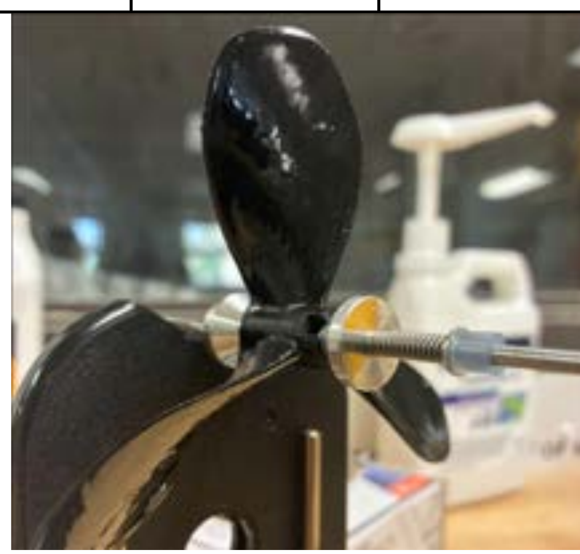

Figure 5: Printed Propeller on Balancer

Electrical and Propulsion Design

Multiple issues were found during the testing of last year's boat including melted wires, burnt out motors, and insufficient motor torque. All design decisions concerning part acquisition were completed with the previous year's lessons in mind.

Components:

- FrSky Taranis X9D Plus Transmitter
- FrSky X8R Receiver
- 2 Seal 300A OPTO ESCs
- 2 SSS 56123 V2 Brushless Motors, 700Kv, 9500W Continuous
- 2 Water Pumps
- 2 4.8V Batteries
- 4 Turnigy 6S 22.2V Li-Po Batteries
- 2 Blue Sea Systems 300A 32V Dual Circuit Switches

Maximizing the power output of the motors was the main design goal of the electronic propulsion system. This resulted in the purchase of new motors which had a lower kV of 700 compared to last year's motors which had 1250kV. A lower kV value allows for improved torque from the motors, which was a major issue of the design last year. The overall power output of the new motors is 9500W compared to the previous motors 4200W, almost half of the output of the new motors. Last year's motors burnt out due to their cheap quality and excessive current draw caused by limited motor torque. The burnt out motors prevented the team from completing the race last year, and led to the purchase of the new motors being a top priority for the electrical design of the current boat.

Using the new power from our new motors, the estimated velocity of the boat is 30 mph (**Table 3**). This value was found by assuming the same drag coefficient used last year of 0.012. The found velocity value does not account for mechanical friction within the driveshaft, or increased drag due to waves, wind, and other environmental factors.

Table 3. Power and Speed Calculations

Max Power output for 2 motors (W)	39000
Max Usable Power (W)	19500
Max Motor RPM (W)	35000
Max Prop Thrust (lb)	33.81
Max Thrust for 2 Props (lb)	67.62
Thrust Coefficient, CF	0.03
Prop Diameter (in)	2.90
Prop Efficiency (%)	50
Estimated Velocity (mph)	30

The overall connection between the electronics is very similar to last year with two batteries in series per motor, which connects to the kill switches and then fuses. After the fuses, the wire is then fed to the ESCs where it connects to both the receiver and motors (**Figure 6**). All 16 gauge wire was swapped for 8 gauge to prevent previous wire heating problems that were encountered last year. 4 new batteries were purchased this year to replace the 8 year old ones that were beginning to get puffy on the edges. These new batteries were the same brand and specifications as the old ones being 6 celled lipo batteries with 20000mAh. Each motor has two batteries wired in series to give a maximum voltage of 50.4V, and a max current draw of 188 amps. At 50% throttle it is estimated that the batteries will last around 13 minutes, which should give ample time to complete the course if the velocity is correct (**Table 4**). During the race, the boat will not be run at full throttle in order to prolong the life of the boat, and prevent any heat buildup issues that may occur.

Table 4. Run Time Calculations

Battery Capacity (mAh)	20000
Max Battery Voltage (V)	50.4
Max Current (A)	188
Constant Discharge rating	12
Constant Discharge rate	240
Percent Throttle	50
Number of motors	2
Number of batteries	2
Run Time (min)	12.73

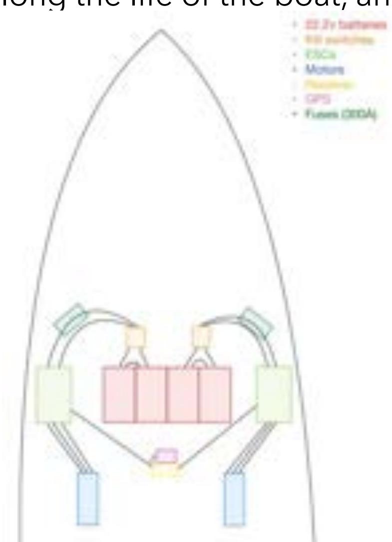

Figure 6: Design Drawing of Electronics Layout

University of Toledo PEP Team: Design with Rhino

Caroline Varner, Natasha Opaciuch, Tushar Sainju, Mohammed Mehaaz, Joshua Miller, Teo Perez, Kyle Aguilar, and Nathan Dolsen

www.navalengineers.org/Toledo

When choosing the design for our hull, we used a decision matrix to weigh the options seeing how almost everyone was new to boats and/or RC racing. We picked out the categories we felt were most important to the competition and did research on all the possible boat options.

	Importance	Inboard Monohull	Outboard Monohull	Inboard Catamaran	Outboard Catamaran
Simplicity of Design	10	8	8	7	6
Efficiency	8	7	9	9	8
Controls Complexity	8	5	5	7	5
Speed/drag	8	7	9	10	8
Mechanical Complexity	8	6	4	6	5
Waterproofing	8	7	9	8	9
Cost	6	8	4	8	4
Total		384	392	438	364

Once the Inboard Catamaran was chosen, we started researching how to make a racing catamaran optimized for the challenge given to us, the challenge being traveling 2 miles in semi-open water with 3 turns all while carrying a 60-pound payload. We felt as though prioritizing stability and efficiency would give us the best chance as first year competitors. We designed a deep pontoon on either side as our way of housing electrical components and the payload, as well as a flatter yet enclosed bridge deck area that would house the ESC and rudder.

Tapering the front of the boat higher up would generate more lift and get the catamaran on a higher riding plane. Paired with the dual sponson design where less water comes in contact with the boat, we are able to reduce lots of hydrodynamic drag.

We also wanted to take advantage of the strength that the dual sponson design has because we will be dealing with wakes and possibly small waves depending on weather. This design also allows forces and stress to be equally distributed across the boat without flipping or rolling.

By analyzing the challenges and requirements for the race and using a decision matrix we were able to choose the hull design and general layout of the components that we would later build off with 3D rendering.

Design and Analysis

The catamaran design was developed using Rhino CAD, with roughly eight design iterations leading to the final configuration. The final design measures 6 feet in length, 2.5 feet in width, and 1.5 feet in height. It features an inverted bow and dual chines on the outer edges of each hull 6 (see Figures 1 through 3). The inverted bow was selected for its ability to reduce resistance, enhance wave-piercing capability, and increase the hull's waterline length. All these factors contribute to better hydrodynamic performance. Our goal was to create a watercraft capable of planning efficiently, minimizing drag, and maximizing speed. To assist with this, the outer chines were added to provide flat surfaces that aid in pushing the craft onto plane. We used Orca3D CFD software to simulate the vessel's buoyancy and planning performance. These simulations were supported by feedback from a professional naval architect at Orca3D, who helped validate our assumptions and refine our model (see Figures 4 through 6). The CFD results indicated that with a total load of 150 pounds and at a target speed of 30 knots, the craft would require approximately 6,000 Watts of effective power delivered to the water. This data was instrumental in selecting appropriate motor and battery components capable of meeting performance goals.

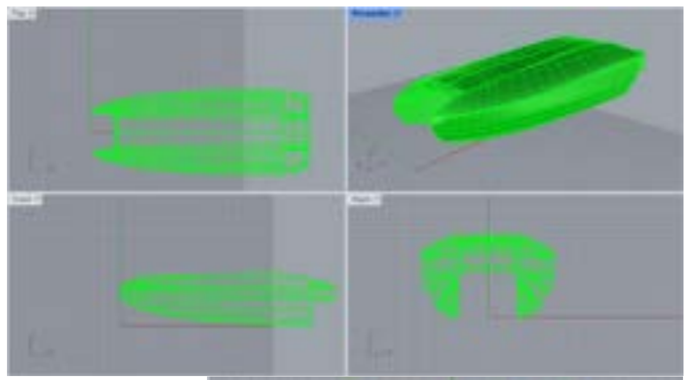

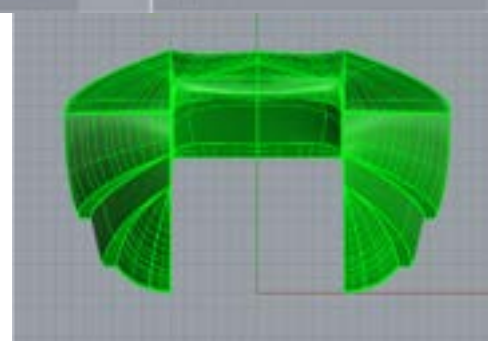

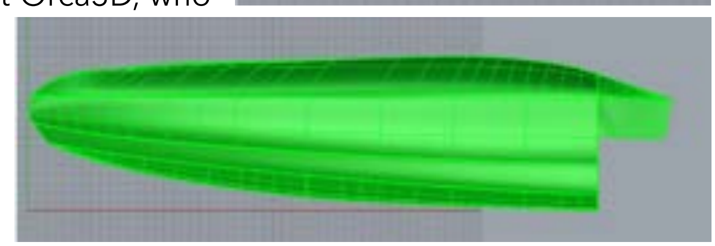

UCONN: Design & Calculation

Elizabeth Adams, Matthew Badorek, Michael Barbera, Gabriel Bartlett Thomas Cardinali, Samuel Carvalho, Andrew Marsigliano, Ziyan Mei, Cormac Nielsen

www.navalengineers.org/UCONN

CFD analysis is a very important part in design when making parts that have fluid flowing over them. Propellers can spin at very high RPMs, and it is necessary to have an idea how these parts will interact with the fluid they are meant to be used prior to manufacturing the part. CFD analysis can save time guessing what models will work and help jump straight to a viable product. In our case, we were deciding between what propeller we would use rather than designing one ourselves. We were graciously gifted a dozen 2 and 3 blade propellors last year, and feel it is in our best interests, time and money wise, to use one of these propellers. The 3-blade propeller was evaluated at an operating condition of 6000 RPM under identical simulation parameters as the 2blade configuration to enable a consistent comparison. The results indicate a total thrust generation of approximately 6031 N and a corresponding torque requirement of 297 N·m. The velocity streamline visualization, seen in Figure 1, demonstrates the formation of a strong and continuous slipstream downstream of the propeller, indicating effective momentum transfer to the fluid and a well-developed wake structure. The relatively uniform distribution of velocity

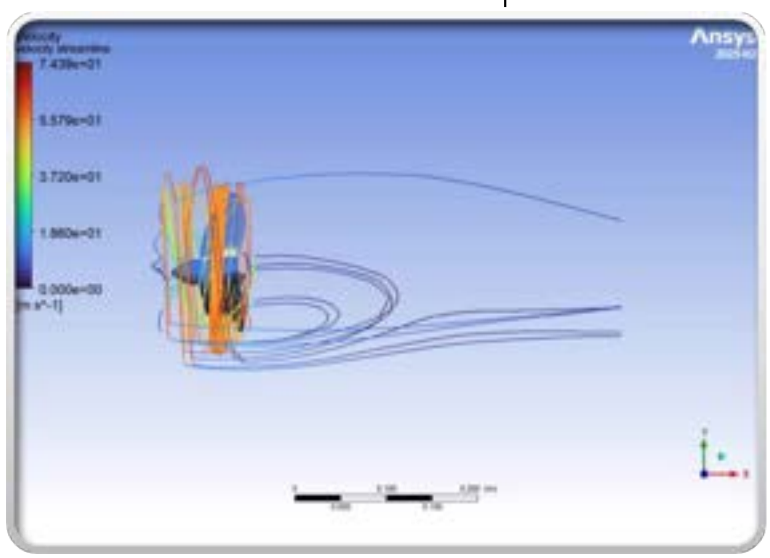

within the wake suggests consistent thrust production throughout the rotation cycle, which is desirable for stable propulsion performance.

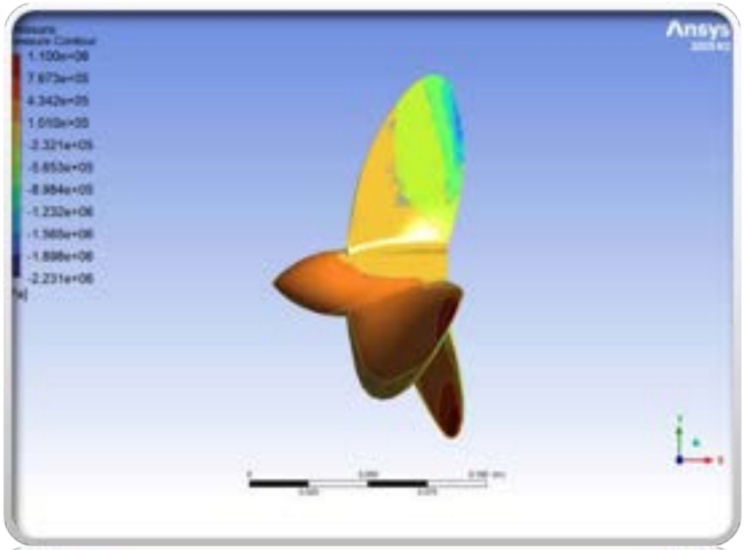

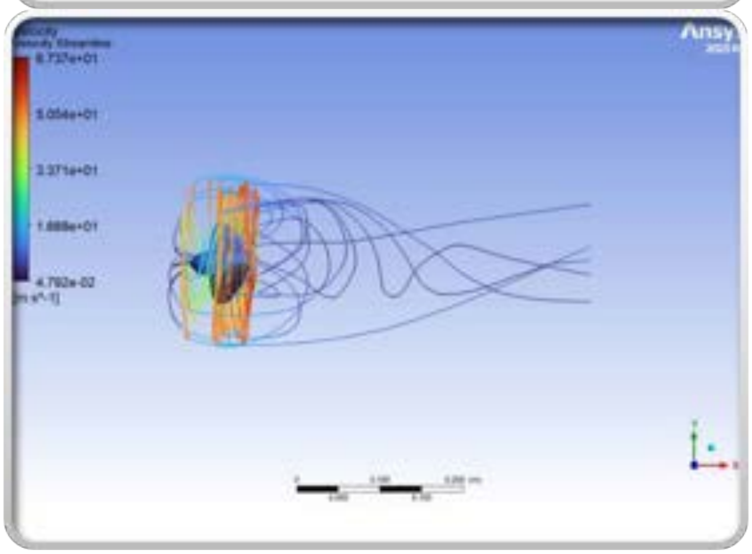

The pressure contour seen in Figure 2 further supports this behavior by showing a clear pressure differential across the blade surfaces, with higher pressure on the pressure side and lower pressure on the suction side. Due to the presence of three blades, the aerodynamic loading is distributed more evenly across the propeller disk, reducing the load carried by each individual blade. This more uniform load distribution contributes to smoother flow behavior and reduced fluctuations in thrust. Additionally, the more continuous wake structure suggests reduced spatial variation in the flow field, which can improve overall propulsion stability. However, the increased blade area interacting with the fluid results in a higher torque requirement, indicating greater power demand to achieve the same rotational speed.

The 2-blade propeller was analyzed under the same operating condition of 6000 RPM and identical simulation setup to provide a direct basis for comparison. The simulation results show a total thrust of approximately 4561 N and a torque requirement of 220 N·m. Compared to the 3blade configuration, the velocity streamline plot indicates a less uniform wake structure, with greater variation in velocity distribution, shown in Figure 3, downstream of the propeller. This suggests that the flow is influenced more strongly by individual blade passages, leading to a less continuous slipstream and increased variation in the wake.

The pressure distribution in Figure 4 reveals more concentrated aerodynamic loading on each blade, as the total force is carried by only two blades rather than being distributed across three. This results in stronger localized pressure differences, particularly in regions near the blade tips, where flow separation and vortex formation are more pronounced. While this configuration reduces the overall torque required to rotate the propeller due to the decreased wet surface area, it also leads to reduced thrust generation and less uniform flow characteristics. The more intermittent wake structure may contribute to increased unsteadiness in the flow field, which can negatively affect propulsion smoothness. Overall, the 2-blade propeller demonstrates lower power demand but reduced performance in terms of thrust output and wake uniformity.

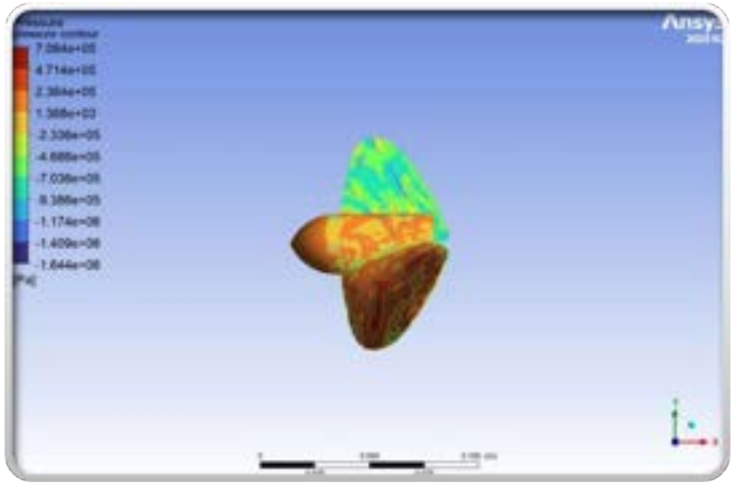

Center of Gravity and Center of Buoyancy Model Calculation

The next objective was to find the center of gravity and buoyancy of our boat. This was done by finding the center of gravity in one direction. This was the x-direction. The x direction was chosen because the model of the boat (figure 5) was symmetrical along the x-axis except for the indent of into one of the walls. The value that was found by hand was -0.0321inches from the center of the boat. This was compared to the value that was found using the SolidWorks center of gravity solution tool. If the values matched, which they did, the SolidWorks center of gravity tool was able to be used. The y and z directions were found using said tool. The local coordinates of the center of gravity, in reference to the center of the SolidWorks model, were (-0.0321, 29.8009, 45.3292) inches.

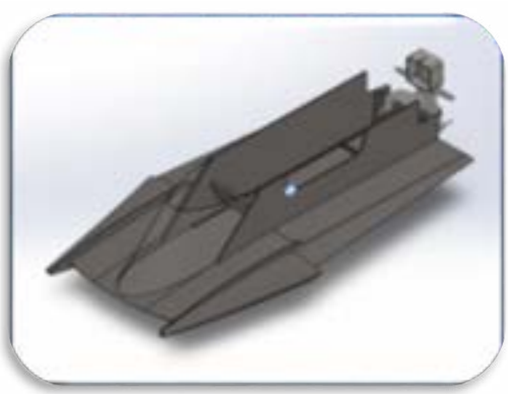

The center of buoyancy was then found by creating a new configuration of the boat model and converting the material from wood to water. When changing the material, this changed not only the density of the boat, but also the mass. A sensor was put into place to alert when the mass of the boat made of water equated to the mass of the boat made of wood. The configuration of water was then cut using the “extrude cut” command to shave the mass of the water down to when the masses equated. This can be seen in figure 6 below. Just as before, the center of gravity of this new volume was found by hand and verified to equal the value given by the SolidWorks center of gravity tool. Once the x-values equated, the tool was then used to find the y and z values. The local coordinates, in reference to the back-center of the model, for the center of buoyancy for our boat were (0.0000, 28.4170, 49.3282) inches.

New Hull and Motor Mount Design

This year, because of issues due to a cutout on one of the sides, the mechanical team decided to remove and patch the hole, creating a sleek aerodynamic design on both sides. The cutout initially was for the racer of the hydroplane to get in and out easily. Now that the hydroplane is being used for unmanned applications, there was no longer a need for the cutout. With the cutout filled, we now have a 42″x15″x12″ box in the middle of the boat where the battery and all other sensitive electronics will be stored. This box will be sealed with a custom-made plywood top that can easily be placed on top of the dry box and screwed into brackets for ease of access to the electronics. Having 3 separate sections of the inner hull allows us to move weight around easily. We plan on putting a 30lb payload in the front section of the boat, and a 30lb payload in the rear section near the motor. These spread weights, along with the battery, which weighs over 100lbs, in the middle, allow the boat to sit at the correct height and angle in the water while at rest and while underway. We also sanded the entire hull down to wood and epoxied all bare surfaces to ensure proper waterproofing on all surfaces.

Using a dual motor design with only one propellor means we needed to design a gearbox to direct the power into a central driveshaft. We are completing this using ¼" steel plates to form a rectangle that will house both motors, the drive shaft, and their corresponding gears. This gear/motor box will be screwed to the top of the outdrive, connecting the motors' power to the propellors. We are using a 2:1 gear ratio in the gearbox and a 1.5:1 gear ratio in the lower unit of the outdrive. This brings the total rpms of the motors down from the rated 20,000 to above 6,000 at the propellor, while increasing propellor torque in the process.

URI: Budget Warrior Champions!

Sam Miller, Julie DesAutels, Nicholas Lyons, Roman Taylor, Jacob Dickstein, Shubham Chomal, Leonard Tourgee

www.navalengineers.org/URI

The first iteration of Stingray is constructed as a 3 dimensional digital model, roughly modeled after the Bernico FTX27 [4]. As shown below in Figure 1, this model tapers on both the top and bottom to allow for early planing and aerodynamics above the waterline. The Bernico features a stepped hull, which is included in the 3D model, but omitted from our final design due to the complexity in constructing it. Our design features a unique full body strake and sponson hybrid design to promote stability, and help prevent excessive spray caused by our hull having a midlevel deadrise. Additionally, the strake creates a pocket of air under the waterline that helps to reduce the drag factor, thus increasing the maximum possible speed of the craft and assisting the craft in getting on plane [5]. In our design, this appears as a longitudinal step around the perimeter hull, tapered slightly upward towards the centerline.

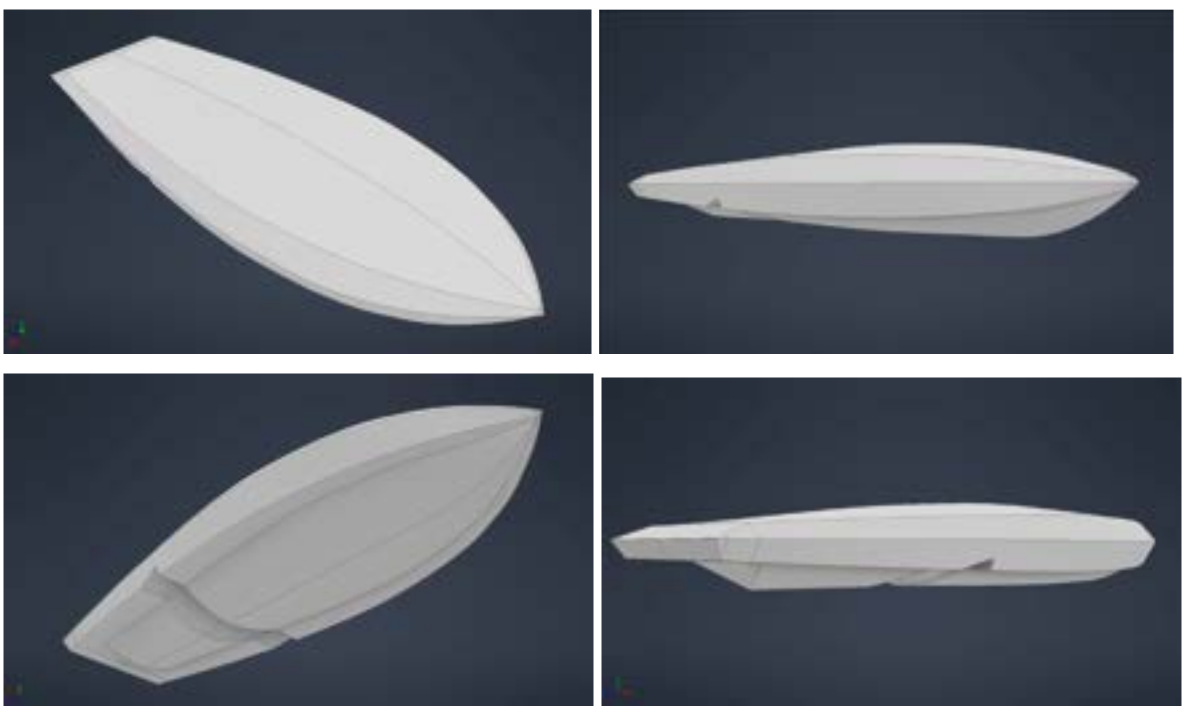

Figure 1: 3D digital rendering of Stingray

The hull is a 1:32 scale boat, analyzed through mass evaluations in solidworks to be able to carry up to 60 pounds of weight. We determined that this scale would properly

support our requirements as it left 30 pounds of weight available for the deadweight of the ship itself after the 30 pound payload is accounted for. This deadweight includes everything that makes up the structure and propulsion of the craft itself, including propulsion components, motors, batteries, and miscellaneous accessories.

Stingray is created with a wave piercing axe bow (Figure 2), which appears as a triangle cut out from the front of the boat. This design is adapted from our previous model, Naruto, to be implemented on a fully planing hull as opposed to a semi-planing hull. This adaptation allows the boat to maintain speed while underway, and disperses forces that would otherwise cause structural strain to the hull [3].

Our hull is constructed entirely by hand, made up of narrow popsicle sticks coated with epoxy and fiberglass for waterproofing and structure. The first step in construction is transferring the digital design accurately to a physically manipulatable state. This is

Figure 3: Frame sketches transferred from CAD model

accomplished by drawing a grid of points using the dimensions taken from a two-dimensional cutaway at different waterlines of the three-dimensional model (Figure 3).

The frame of the boat is then built up from this outline in pieces to ensure symmetry.

When applying the keel, one of the main concerns was maintaining a straight keel line longitudinally down the hull. To accomplish this, a structure of temporary supports is added to prevent shifting while the sides of the hull are added. The sidewalls of the upper hull, above the sponson-strake, and the lower hull, below the sponson-strake, are constructed separately as long walls that are cut to fit the framing. The construction of the hull itself took over 20 hours not including epoxy sealing.

To make the hull watertight and create a smooth finish, a two-part marine grade epoxy is used alongside fiberglass mat. The inside of the hull is coated first in epoxy with strategically placed fiberglass reinforcements, then set overnight to cure. During this time, the deck of the ship which contains two hatches to allow access to the internal components is constructed using a similar method to the hull, in a two-dimensional manner. After the interior is cured, the exterior is angle-ground with a flap disk to ensure smooth faces and transitions that can be effectively fiberglassed and epoxied. The top deck is then epoxied on its inside face and mounted onto the body. It is then subsequently angle-ground, fiberglassed, and epoxied as well. Photos of the build process in depth are shown in Figure 4. The total time spent to complete the hull including build, epoxy, sanding, and assembly came to over 40 hrs.

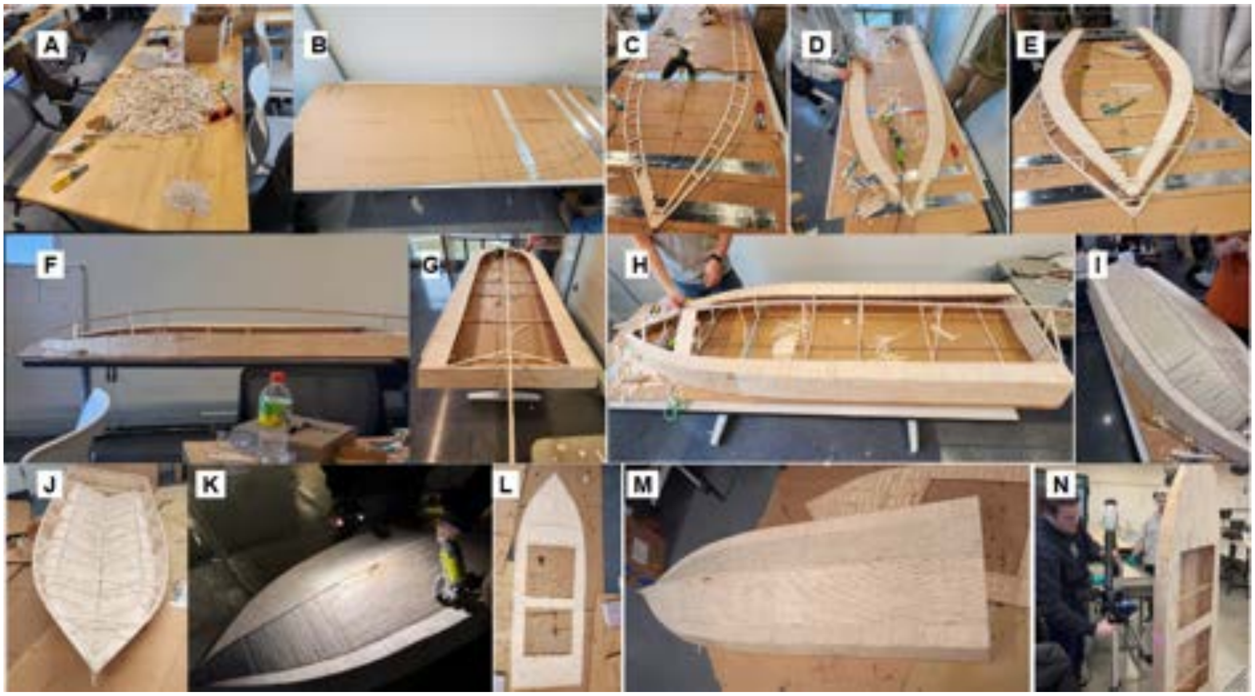

Figure 4: Photo documentation of hull build process

Build Process Breakdown: A) Cutting craft sticks to size: B) Creating frame dimensions: C) Building frame: D)Laying spray strake deck: E) Mounting spray strake to frame: F) Adding keel line: G) Adding keel line supports (with namesake keel): H) Building hull bow paneling: I) Adding side paneling: J) First epoxy and fiberglass coat: K) Hull angle grinding (in the dark): L) Building main deck: M) Epoxying main hull: N) Laser scan attempt

Propulsion System

Our propulsion system consists of a twin propeller system each connecting to separate motors by a 4mm drive shaft. The prop shaft selected is the same as previous years, however the propeller and motor differ slightly. In selecting the motor, we based our decision on the historical reliability listed in ratings. The two main conditions that the motor must meet are as follows: the ability to run on a 6s battery, and the cost given we are competing in the budget category. The propeller selected is a 40mm three blade propeller that is compatible with a 4mm shaft. We decided to order propellers separate from the prop shaft as previous experience proved the propellers included with the shaft to be inadequate. The motor selected is also optimal, as it advertises a waterproof sealing, eliminating the risk related to water reaching the motor. The motor is mounted on a wooden block modeled in Figure 5 such that the prop shaft is aligned concentrically with the motor shaft to alleviate angular deviation that has previously caused shaft coupling damage and failure. To lower costs the wood used for this was scrap material discarded from old furniture.

UVA Autonomous Watercraft Club: Navigating to the Future

Andrew Thepvongs, Jake Rivers, Jason Mensah-Homiah, Logan Tolbert, Marvin Stewart, Nathan Littreal, Abhinav Pappu, Nathan Vu

www.navalengineers.org/UVA

The diagram below illustrates the hardware topology of the autonomous navigation system. The Pixhawk flight controller serves as the central hub, interfacing directly with the port and starboard motors via electronic speed controllers, a radio receiver for manual override, the vessel power system, and the RTK GPS rover module. A Raspberry Pi 5 companion computer connects to the Pixhawk over a serial MAVLink link and also connects to an onboard LTE router, which tunnels all traffic over a VPN, enabling waypoint uploads, monitoring, and teleoperation, from any location with internet access.

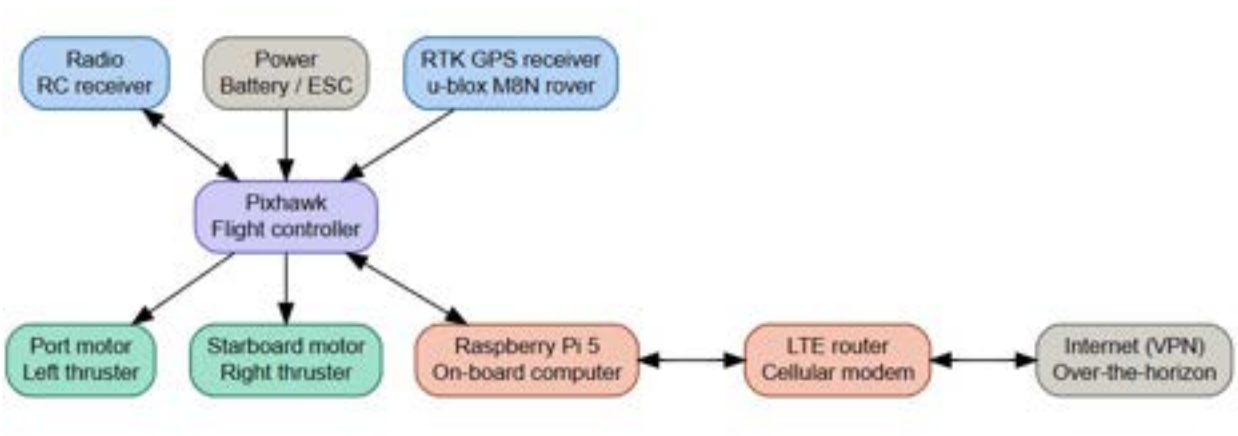

Components' description

Pixhawk: Autopilot flight controller. It runs the sensor fusion, navigation algorithms, and motor control loops. It reads from the GPS and IMU, executes the waypoint following logic, and outputs PWM signals to the motor Electronic Speed Controllers (ESC's)

Port and starboard motor: Twin electric thrusters. The Pixhawk drives them independently, via an Electronic Speed Controller (ESC) for each motor, enabling directional control through differential thrust rather than a rudder.

Radio receiver: Connects to the operator's RC transmitter for direct manual override, safety intervention, and arming and disarming.

Power system (batteries): Supplies regulated voltage to all onboard electronics.

RTK GPS (u-blox M8N): Provides the vessel's real-time position with centimeter-level accuracy when corrections from the shore-based base station are received.

Raspberry Pi 5: Acts as a companion computer. It communicates with the Pixhawk over MAVLink via a serial connection, and serves as the interface to the onboard router for over-the-horizon command and control.

LTE/5G router: Provides cellular internet connectivity to the Raspberry Pi. All traffic is routed through a VPN, enabling secure remote access from any internet-connected location.

Internet (VPN): Represents the over-the-horizon control path. An operator can connect to the vessel through the VPN tunnel to upload or modify waypoints, or to monitor telemetry, without requiring line-of-sight radio contact.

RTK GPS

The vessel uses two u-blox M8N GPS modules operating in an RTK (Real-Time Kinematic) configuration. One module is mounted on the vessel as the rover, and a second is placed at a fixed, known location on shore as the base station.

Standard GPS receivers determine position by measuring the time delay between a satellite signal's transmission and its reception, which is accurate to roughly two to five meters. RTK improves on this by additionally measuring the carrier phase of the satellite signals, which oscillate at a frequency of approximately 1.575GHz with a wavelength of about 19 centimeters. The base station, whose exact position is known, continuously computes the difference between where its satellite measurements suggest it is and where it actually is. These correction values are broadcast to the rover in real time over a radio link.

The rover receives both the raw satellite signals and the base station corrections. By combining its own carrier phase measurements with the corrections, the rover can resolve the integer number of full carrier wavelengths between itself and each satellite, a process called integer ambiguity resolution. Once this is solved, the rover can compute its position relative to the base station with an error of roughly one to two centimeters under open-sky conditions. This level of accuracy is what enables the vessel to follow planned waypoints precisely and return reliable path-following data during testing.

Waypoint Navigation Algorithm

Before departure, the operator loads a mission consisting of an ordered list of Global Positioning System (GPS) coordinates. Once active, the system continuously computes the desired bearing to the current target waypoint using the haversine formula, compares it against the Extended Kalman Filter

(EKF) fused heading estimate derived from GPS course-over-ground and Inertial Measurement Unit (IMU) gyroscope data, and feeds the resulting heading error into a PID controller whose output is mapped to a differential thrust command across the port and starboard motors. When the vessel falls within a configurable acceptance radius of the active waypoint, the system advances to the next coordinate, continuing until all waypoints are visited. The algorithm is outlined below:

Algorithm:	$RTK - GPSWaypointTracking$
Input:	$Currentstate(\phi_1, \lambda_1, \hat{\psi}), Target(\phi_2, \lambda_2)$
Constants:	$K_p, K_i, K_d, T_{base}, r_{accept}$
Output:	$Motorthrusts(T_{port}, T_{stbd})$
$1: ComputeBearing$	$\Delta\lambda = \lambda_2 - \lambda_1$ $\psi_d = atan2\big(\cos\phi_2 \sin\Delta\lambda, \cos\phi_1 \sin\phi_2 - \sin\phi_1 \cos\phi_2 \cos\Delta\lambda\big) \pmod{2\pi}$
$2: HeadingError$	$e_\psi = wrapToPi(\psi_d - \hat{\psi})$
$3: PIDControl$	$u(t) = K_p e_\psi(t) + K_i \int_0^t e_\psi(\tau)\, d\tau + K_d \frac{de_\psi}{dt}$
$4: Differential$	$T_{port} = T_{base} + u$ $T_{stbd} = T_{base} - u$

$5: Navigation$	**if** $dist(\phi_1, \lambda_1, \phi_2, \lambda_2) \leq r_{accept}$ **then**
	 $advancetonextwaypoint$
	 end if

Differential Thrust Steering

Our catamaran utilizes a Differential Thrust Steering (DTS) configuration, leveraging independent electric propulsion systems in each hull to manage directional control. This approach eliminates the need for traditional mechanical rudders, offering several distinct advantages for our current phase of development.

The steering is governed by the variance in Pulse Width Modulation (PWM) signals sent to the port and starboard motors. By creating a thrust imbalance, we generate a yaw moment proportional to the difference in signal. The width of our boat is sufficiently wide relative to our currently set maximum allowed throttle.

During initial trials and especially during our autonomous trajectory-following tests, we observed that DTS provides sufficient control authority at our current operating speeds. The decision to omit a rudder assembly was driven by two primary factors:

- Reduced Parasitic Drag: Removing underwater control surfaces minimizes the wetted surface area, improving overall hydrodynamics.
- Mechanical Simplification: Eliminating servo-actuated linkages reduces potential points of failure and streamlines the internal packaging of the hulls.

While DTS is effective for low-to-mid-range velocity and autonomous pathing, we recognize its limitations in high-speed regimes where the hull may require more aggressive control from a rudder. As we scale the boat's velocity through allowing more maximum throttle and incremental drivetrain improvements, the integration of a physical rudder remains a planned upgrade to enhance high-speed stability and precision.

Electrical Overview

Below is a breakdown of the architecture of the electrical system of the boat:

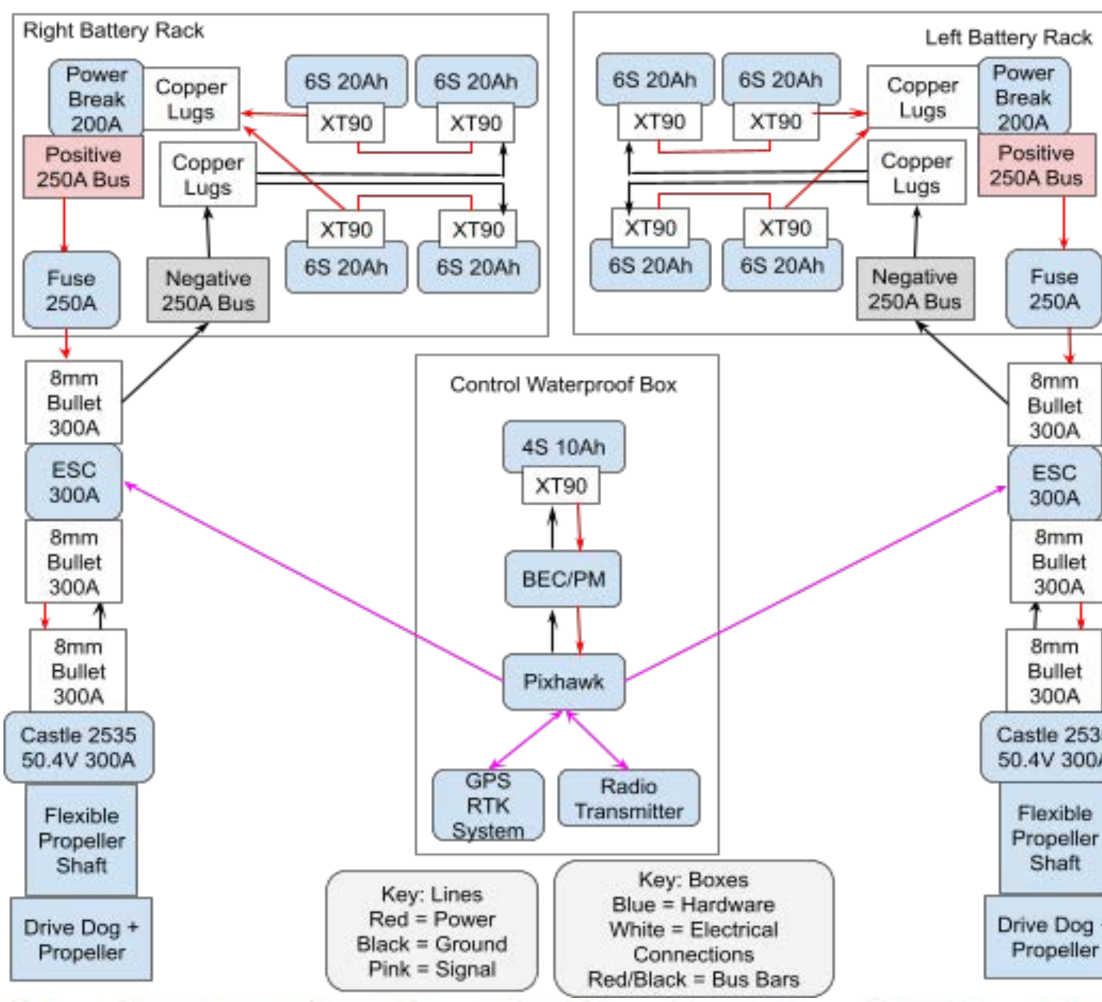

VT: Autoboat!

Barrett Wise, Christopher Nassif, Anne-Kinsey Wash, Elias Sharonov, Keith Owens (Kaceeowens@vt.edu), Sofyan Elshaer, Vladimir Leonov, Michael Hatami, Pragya Nidhi, Dimas Gonzalez-Ramos, Timothy Peace, Brandon Rhodes, Andrew Shear, Raymond Hong, Shane Pomajambo, Davis Chalmers

www.navalengineers.org/VT

This year, we have set a multitude of difficult objectives in electrical design and firmware alike. The primary objective was the implementation of a higher degree of firmware modularity through the use of C++. We have chosen to break away from our older implementation in C to implement an object-oriented programming paradigm. We have decided against switching over to the declarative programming paradigm as provided by the standard library due to our natural affinity for low-level algorithms that high-level abstractions would obscure rather than simplify. Electronically, we have taken a similar philosophy to break down our system into testable components that are easy to fix if broken.

For our firmware system, we utilize a cheap bare metal microcontroller by the name of RP2040, stationed on the Raspberry Pi Pico. It would interact with Jetson Orin Nano, our computer vision and autonomy board. They interact through a USB interface using the ROS2 middleware environment. Raspberry Pi Pico controls all of our low-level peripherals connected over I2C, SPI, and UART. This configuration ensures that our peripherals work independently of the current Jetson model that we use, as well as protects our more expensive electronics from miswiring and overvolting. If we accidentally overvolt our RP2040, it only costs $5 to replace, but if we overvolt the Jetson, then it would take a few hundred dollars out of our budget. Therefore, the only connection between the Jetson and the electrical system is an optically isolated USB cable in order to protect it.

Our PCBs were designed with the same idea in mind though for slightly different reasons. Last year, we ran into a problem where our power distribution system would break far more often than our low-level logic, but it would take the latter with it due to them being located on the same PCB. We would have to disassemble our entire system

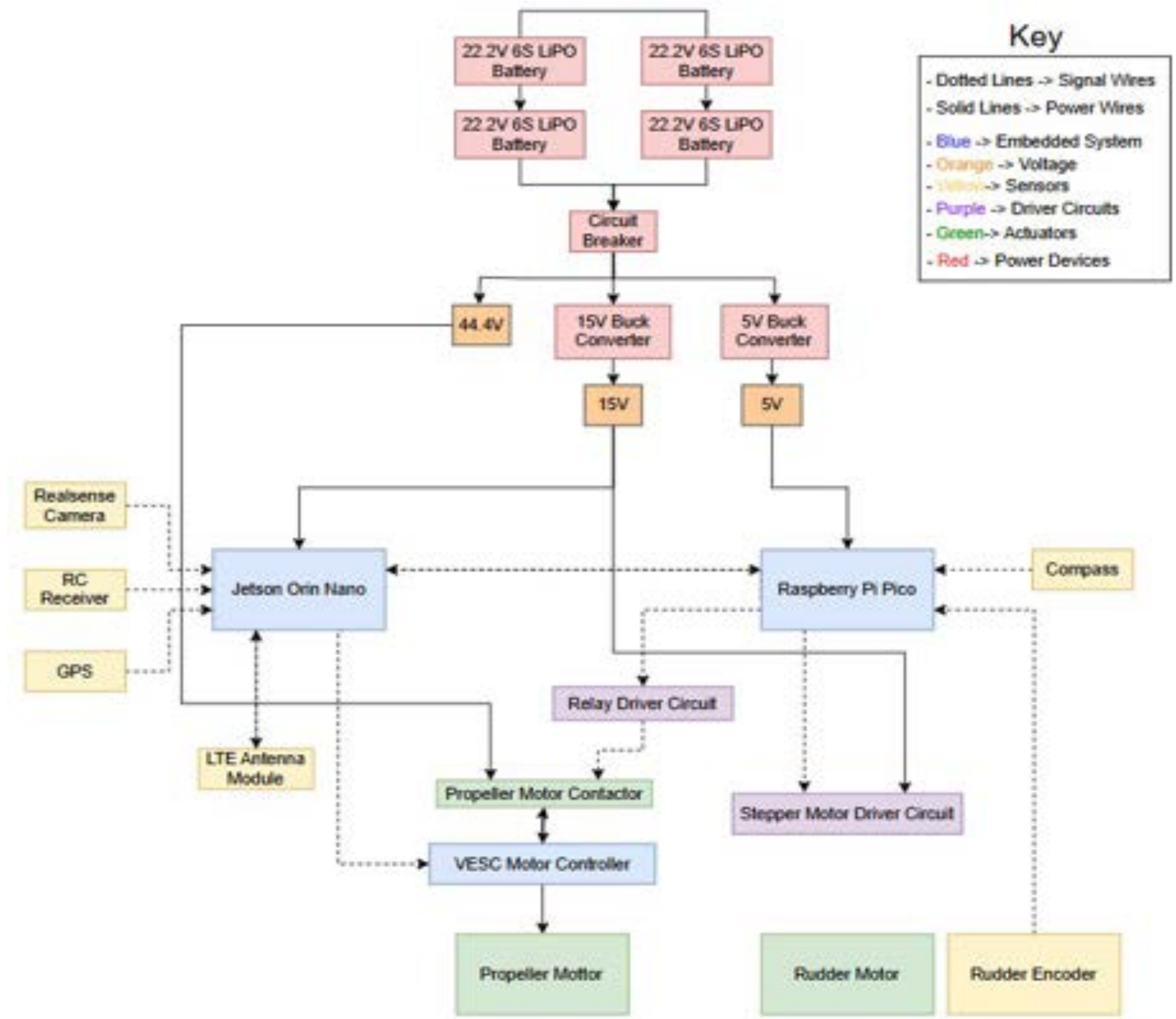

should we find ourselves in the need to debug an interface, solder a faulty component, or screw in a loose terminal. This is not a good practice and we now step away from it. We have split our old master PCB into the smaller digital portion and the larger analog portion. The analog portion is equipped with custom buck converter modules tailored to our larger system for efficiency. You can find the detailed discussion of both below.

Firmware and MicroROS

In order for the electrical systems to function properly, effective communication between components is vital. We utilized the MicroROS open source framework to create a communication network between our software system and sensor suite. MicroROS allows the microcontrollers to use the same framework as ROS2. Within the context of the Jetson and overall system, the MicroROS framework running on the Pi Pico can be considered as one node. One goal this year was for the MicroROS architecture to be applicable to multiple autonomous vehicles, so the node itself has to be well organized internally, as its role within the system and the sensors it manages change depending on the vehicle.

To accomplish this goal, we refactored our original MicroROS C Code into C++ to enhance readability and make the code more modular. On one side of the architecture is hardware communication. The peripherals are split into their communication protocols (I2C, SPI, UART). This standardizes the write/read byte functions between all embedded sensors, making the libraries much more modular and increasing the ease of adding future sensors for future years. Each device-specific class then inherits from the communication base class. The relevant functions that need to be exposed to the higher-level architecture are done so via the HAL namespace.

On the other side of the architecture is the MicroROS class. This specifically handles spinning up all the relevant topics and the related messages. Each peripheral is a node in the MicroROS structure and is represented with a struct to compartmentalize all relevant information. The System class then integrates the HAL and MicroROS classes and initializes and runs the entire application. By separating the hardware communication from the MicroROS, we are able to better identify and debug issues. A graphical representation is provided below.

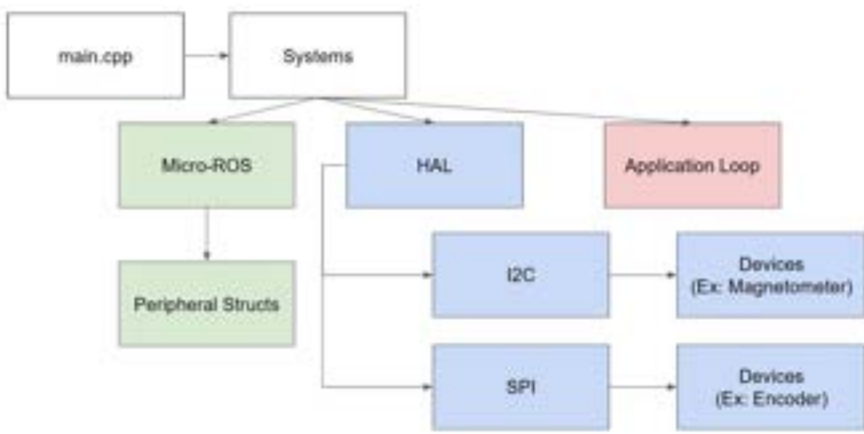

In addition, we are also working on an interrupt-based system for our embedded sensor suite and its publishing to its respective topics. Since waiting for protocols like I2C to complete can block the rest of the program, there's a risk that it can degrade the performance of the boat and create issues. To counteract this, we started designing a new framework that sends the transmitted data, continues the rest of the code, and triggers an interrupt that handles the received data at the moment it has finished arriving. Although the system has not been completed by this competition, it would help create a much more robust system and mitigate risk in the future.

Digital Communication PCB

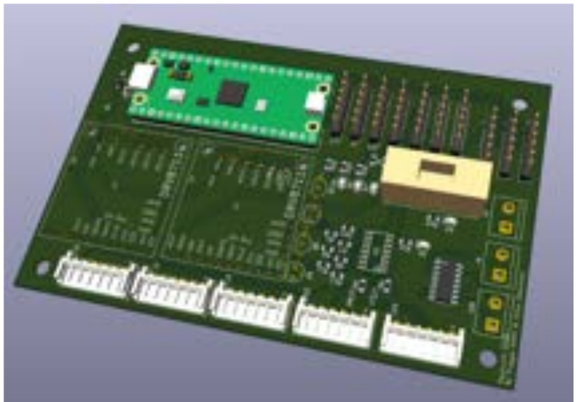

Figure 10. Render of Digital PCB

Our Digital Communication is handled by our PCB. It contains pins for a Raspberry Pi Pico, two DRV8711 motor controllers, a relay for our contactor, status LEDs for our signals, a chip select multiplexer, output pins to connect with sensors, and debug pins. We are using SPI (serial peripheral interface) for our encoders and our stepper motor drivers, and I2C (inter-integrated circuit) for our compass. After last year, we realized the number of chip select pins on the pico could be lessened by using a multiplexer, bringing the number of chip select pins on the pico from four to three. To power the board and the relay, we have terminal blocks that are fed 5 volts and 15 volts from the power distribution PCB.

Power Distribution PCB

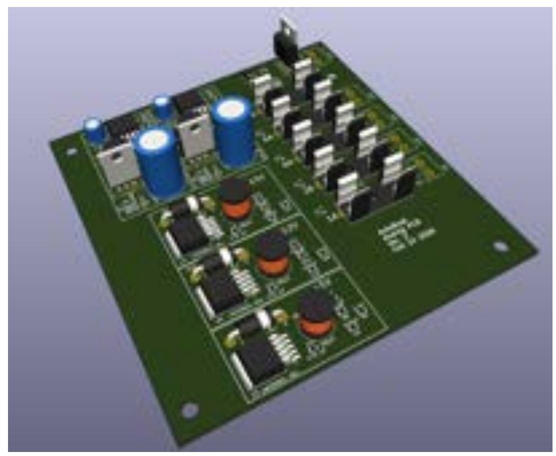

Figure 11. Render of Power Distribution PCB

The new power distribution PCB contains buck converters that are now integrated into the PCB instead of being on separate modules. By doing this, compared to last year's solutions of having 5 separate modules attached via connectors to the main board, this solution takes up less space and would also be more reliable. We are now using buck converters that are different for each needed voltage. We still have the same general layout of a pair of 50V to 25V buck converters that have an output that is fed to a connector, along with 3 more buck converters to create 15V, 12V, and 15V. Fuses are present for safety on each output, along with one on the input. We are also now using connectors that allow for easier attachment of cables, so that we can swap PCBs and the other components connected to it more easily, due to the cramped environment that it will be placed in inside the boat. Additionally, the use of components integrated into the PCB allows the overall size to be reduced compared to the versions from prior years. This PCB will be mounted in the main PCB box alongside the digital PCB. This PCB is always powered and does not communicate with the digital PCB. Compared to last year’s version, the outputs and fuses are also labeled so that testing can be done without needing to have documentation on hand to determine voltages on the outputs.

Wake Forest: Expert Mechanical Design

Olivia O'Connell, Katherine Sternberg, Chase Parker, Rhys Owens, Zachary Spencer, Gavin Bahner

www.navalengineers.org/WakeForest

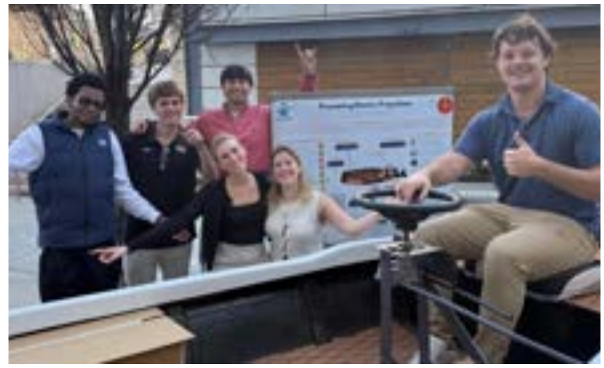

A three-blade, 14-inch pitch propeller was selected to balance thrust and top speed. A higher pitch allows the boat to travel farther per rotation for improved speed, while the three-blade design maintains consistent thrust and stability. This configuration provided the best overall performance based on analysis and simulation. A 3D scan of the chosen propeller is shown right.

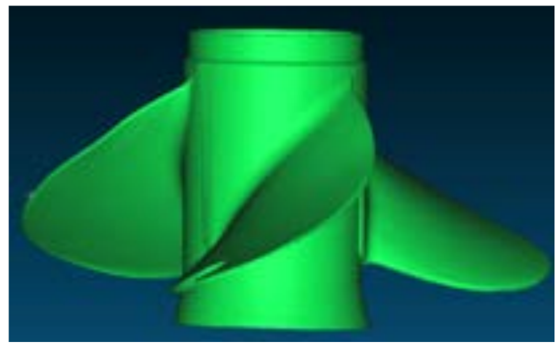

Hydrofoil

The hydrofoil was added to improve hydrodynamic performance by generating lift and reducing the wetted surface area of the hull. This decreases drag and allows the boat to achieve higher speeds with the same power input. It also helps reduce bow rise and improves overall stability during operation.

Hydrofoil Selection

Two Stingray hydrofoils, the Classic 2 Senior and Classic Pro, were evaluated using a weighted decision matrix based on lift, cost, ease of installation, and compatibility. Based on this decision matrix, the Classic 2 Senior offered a better balance of performance and feasibility, making it the final selection. This hydrofoil mounts directly to the anti-ventilation plate of the outboard using four bolts, making it a practical and reliable solution.

Simulation

To evaluate the performance of the selected hydrofoil, computational fluid dynamics (CFD) simulations were conducted using ANSYS Discovery. A 3D scan of the hydrofoil was imported into the software and processed using a shrinkwrap function to create a solid geometry suitable for analysis. An enclosure representing the surrounding water was created, and a velocity inlet corresponding to the target operating speed of approximately 20 mph (8.94 m/s) was applied.

The simulation allowed for visualization of velocity vectors and flow behavior around the hydrofoil. Results showed that the hydrofoil generates upward lift as water flows over its surface, confirming its ability to reduce the amount of hull submerged in the water. This supports the goal of decreasing drag and improving overall efficiency.

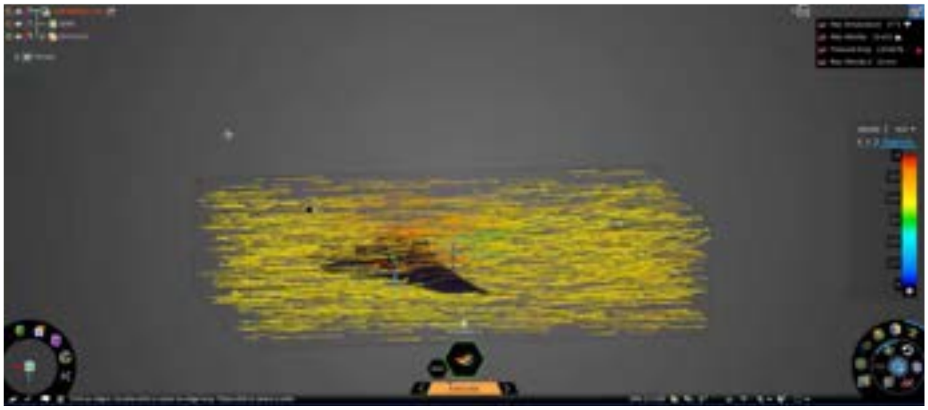

Figure 6. Ansys Simulation

Gear System: Design Concepts

As might be expected, in the design of the gearbox, choosing the type of the gearbox was a necessary first step. Doing this involved scoping out the many types of drive systems that are used in mechanical systems. The team took a step back to consider all gear system possibilities. Ultimately, the team felt that both designing gear systems and also purchasing fabricated gear components was the most realistic course of action. The team considered three types of gear systems and scope the feasibility and effectiveness of implementing each type. Of the many factors to consider, a major consideration was moment creation mandated by the spacing requirements of each gear system type. The electric motor weighs approximately 55 pounds. While comparable to the combustion power head that was removed from the outboard, in order to create a ratio, the center of mass of the motor will be offset from the original designed location of center of mass. In all gear systems, the electric motor drives along some axis parallel to the outboard drive axis. This means that depending on the gear system, a moment will be created that the outboard design did not account for. Moreover, the farther rearward that the motor is placed, a greater moment will act on the aft plate of the hull. Therefore, the overarching considerations in the gearbox were 1) achieving correct power, torque, RPM combination, 2) minimizing moment created by the electric motor and 3) reliability and ease of implementation. Consider Table 1 that depicts pros and cons of each type of gear system.

Sourcing of parts was a central part of deciding the best implementation of the gear system. Knowing that the gear ratio from motor to drive shaft should be close to 2:1, the limitations of belt drives were apparent and belt drives were dispelled as an option. Using part source websites like McMasterCarr and Grainger, the team considered the financial implications and ease of getting parts. While the financials of gear drive and chain drive seemed similar, the main deciding factor was the necessity of lubrication for the drive gear system. Many gear to gear systems–as seen in automotive applications–suspend the gear systems within oils in order to dissipate heat and limit the amount of metal degradation. The team believed that creating a sealed, leak-proof gear system would be unachievable considering budget and time constraints. Thus, the team considered enclosed, pre-fabricated gear systems (in other words, a gearbox). However, the cost and power limitations of these gear systems led to the choice of a chain drive gear system. Of the drive options, this should be the easiest to implement while maintaining efficiency and delivering the proper torque and RPM characteristics.

Table 1. Gear System Pros & Cons

Gear System Type	Specific Examples	Pros	Cons
Gear Drive	Spur Gear Planetary Gear Perp Bevel Gear	Close shaft proximity Many existing enclosed direct gear systems	Suspended/joint lubrication Cost of gear systems
Belt Drive	V-Belt Motorcycle (Toothed) Drive Belt	High efficiency No lubrication Handles misalignment Salvage Potential	Slipping Environmental susceptibility Reduces shaft speed (need for radius step up, decreasing prop RPMs)
Chain Drive	Roller Chain Leaf Chain Conveyor Chain	Less metal/metal contact Easier lubrication systems Larger tolerances	Potential need for chain tensioner

Final Design Selection

The decision to use a chain gear was a foundational part of the gearbox design. The design was built on top of this decision. Given that the team decided to purchase as opposed to manufacture the gear components, the next step was to decide the two gears and chain for the drive system. A standard ½ inch was chosen (Trade 40) for the gears. Logically, if both gears are trade 40, it implies that the tooth ratio is the same as the gear ratio. In order to optimize–while ensuring being able to handle chain torque, the team chose 24 teeth to 12 teeth gear combination. Other gear characteristics were dependent on the location of the gear. The electric motor has an extending shaft upon which torque is applied. By modeling the motor, it was determined that a gear attached to the shaft could horizontally align with the outboard drive shaft gear. Consider Figure 7 below for visualization. The shaft of the motor includes a keyhole. In order to minimize machining needs, the gear for the motor must be a keyed gear that fit the ⅞″ diameter of the electric motor shaft. The outboard drive shaft gear had different requirements. Because a splined adapter was machined for the drive shaft, the team desired a ½″

pitch, 12 tooth gear (2:1 gear ratio) with a machinable inside such that the gear could be machined, press fit, and keyed to move directly with the drive shaft.

However, a major concern within the design was the chain torque destabilizing the drive shaft. With the drive shaft rotating at 5000 RPM, a significant amount of torque is still applied to the drive shaft of the outboard. This could mean stress on the drive shaft. To ensure that the horizontal stress on the drive shaft was minimized, the team designed an upper/lower bearing configuration. By using a flange bearing on the lower plate and a press fit roller bearing in the top plate, the drive shaft would have two points of stabilization. While this was a concern for the motor side of the drive train, the team reviewed the technical specifications of the electric motor and found that it is designed with internal bearings that stabilize its shaft. So, with a properly mounted motor that only uses the standard motor extension piece, no bearings are required for the stabilization of the motor shaft.

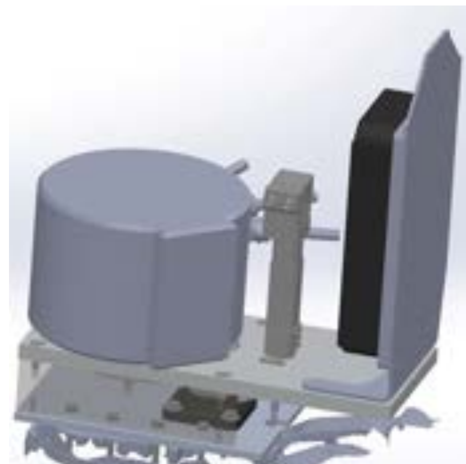

Figure 7. CAD of gear box

Using the CAD files of the gears and the roller chain, the team calculated an initial estimate of the possible center to center distances for the gears. Given the choice of half inch pitch and the decision to omit the gear tensioner, the best way to find the optimal center to center distance of the gears (close as possible without the gears touching) was to measure the perimeter of the path of the centerline of the chain system around the CAD files of the gears. The center to center distance of the gears was adjusted until the perimeter value of the chain pathlength was a multiple of ½” (meaning chain links could be removed to fit).

An important aspect of the gearbox is being able to disassemble the gear system. As such, the top plate needed to be removable. So, this meant that the top plate could be a different, non-weldable material than the stainless steel bottom and side plates of the gearbox. To make the top plate removable, the holes were designed to be socket hole screws. Moreover, the bottom plate was designed to include dowel pins that would locate the side plates. After locating the side plates, the side plates could be welded to the bottom plate. To ensure a good weld, the side plate was designed to sit on the bottom plate such that there was a small

lip of the bottom plate protruding. This creates a consistent weld line for the bottom and side plates. While the bottom and side plates were chosen to be steel (mainly for anti-corrosive, weldable, and accessibility properties), the top plate was chosen to be a comparatively less dense aluminum plate. This decrease in weight from the aluminum plate increases performance capability of the boat to plane and decreases the load on the gearbox walls.

Being from Wake Forest, sourcing these gearbox wall pieces from a local Winston manufacturer was important to our team. We chose to use Fischel Steel just outside of Winston Salem in Kernersville, NC. The option was convenient and priced in a range that the team could afford for the budget.

Manufacturing

The manufacturing of the gearbox was an involved process that served as a crash course in machine shop work. The plates, mounts, links, and gears were milled, CNC'd, and tapped. Many holes were also made using the drill press and bandsaw. Ultimately, depending on the part size, the team would have to consider manufacturing limitations while designing the parts. The CNC in the Wake Forest machine shop is meant for smaller parts which greatly hindered efficient progress when manufacturing the larger plates. However, one step was consistent for all parts being manufactured. Before manufacturing, the drawing for each part was checked and approved by our advisor, Gregory Mohler. These drawings were printed and used as reference for the entirety of the manufacturing process. For parts that needed the CNC, the g-code was programmed using Fusion360 CAM software. For pressing press fit parts together, the team used a ten ton hydraulic press. Lastly, the bottom plate and side plates were cleaned and welded together along the designed welding line on the bottom plate.

Center Console: Design Selection

The center console design was driven by functionality and integration with the hull. The initial console prototype revealed design flaws, requiring iterations to be made to better meet system requirements and user needs. For instance, the design did not fit perfectly with the steering system, and lengths and angles had to be altered to ensure that the console could be mounted firmly to the hull. The revised concept prioritizes a compact, lightweight structure that securely houses the steering system while maintaining accessibility for the operator. Special consideration was given to mounting location, with the console positioned to align with the boat's existing hull features, such as the built-in cooler, to simplify installation. This approach ensures the console contributes to overall system efficiency without adding unnecessary complexity or weight. The console also includes strategically placed locations to hold the throttle, ignition switch, speedometer, and voltmeter. It is important to note that the console will also include one extra mounting point for structural integrity.

Structural Design

From a structural standpoint, the center console must withstand a combination of mechanical loads during operation. These include forces generated by steering input, driver interaction, and vibrations transmitted through the hull while the boat is in motion. To address these demands, the design incorporates a rigid frame capable of resisting bending moments and shear forces, ensuring stability under dynamic conditions. Material selection plays a key role in this performance, with stainless steel identified as an optimal choice due to its high strength and corrosion resistance in marine environments. Structural validation was performed using SolidWorks analysis to evaluate stress distribution and confirm that the console can safely handle expected loading conditions.

Figure 8. CAD model of center console

Manufacturing

The manufacturing process for the center console emphasizes practicality, durability, and ease of integration with the rest of the boat. Fabrication involves welding for the steel plates, followed by secure mounting to the hull. This included fiberglassing a wood base into the floor of the hull, and drilling into the hull's cooler. The use of fiberglassing allows for a strong, permanent connection while conforming to the geometry of the hull. Additionally, as stated before, the design process incorporated iterative prototyping, beginning with simple cardboard models to identify design flaws before producing a final functional version. This stepwise approach reduces material waste and ensures that the final console meets both structural and operational requirements while remaining feasible within project constraints.

Washington College: Hardened Electronics

Douglas Hewes, Cole Davis, David Audette

www.navalengineers.org/WashingtonCollege

Reviewing our plans from last year, we have intended to continue with our current power system because it functions well with the boat and hull. Previously, as we mentioned in the section about our Battery Design and Considerations, our electric powertrain will pull 250A continuously during the race. After researching electric motors with a 55V nominal limit, we planned to purchase one of two motors from international manufacturers. However, both had extremely long lead times and no USA distributors, making the purchase difficult and risky given our competition deadline. These motors were intended to run on 48V nominal, and could produce as much as 50kW of power. Doing the rough math, that would require over 1041A in the case of a 50kW motor, which is a much greater electrical challenge to pull off than we have previously tackled.

Since we decided the safer bet was to use the motor we already had (for reasons of timing and availability), the power delivery challenge was simplified. We are using a Motenergy ME1616 radial air gap, permanent magnet synchronous motor (PMSM) with an internal permanent magnet rotor (IPM). This motor is rated to 250A continuously, about 11% of the current available from our battery pack, so our battery is somewhat future proof, capable of sustaining significantly more power than we plan to use this year.

The ME1616 produces 45Nm torque with an approximate KV rating of 75, meaning it will spin 3600RPM at 48V (48*75=3600). With our custom 15S 54V nominal battery, the unloaded motor will spin at 4050RPM. With a typical outboard lower unit using a 2:1 gear ratio, we knew our ME1616 motor would not be as ideal in an outboard conversion at this lower voltage. We therefore decided to modify the hull and run a straight shaft between the motor, through the hull, and directly to a propeller that would work well with real-world (loaded) RPMs around 3800-3900RPM.

We used all this data to help us select a propeller that would be most ideal for this application. One additional caveat is that we selected a cleaver-style racing propeller. Although this style prop is less efficient generally, on a hydroplane it is better equipped to handle the potential cavitation as the boat is skimming along the surface of the water. We found a used 10x15 three-blade cupped prop, which was ideal in every way, except it was designed for mounting on a 14-spline shaft of an outboard motor lower unit. To utilize the 1” stainless shaft we already found in a salvage yard, we had help from the college’s research boat captain, who TIG welded the 14-spline shaft onto the end of our 1” solid stainless shaft.

The full mechanical drivetrain consists of:

1. An ME1616 motor, held by a custom 13° steel motor mount we fabricated.
2. It’s connected with a ⅞ coupler with keyway to a 1” 316 Stainless Steel shaft (which has the end machined down to ⅞”).
3. The shaft passes through a thrust bearing that is coplanar with the face of the motor.
4. It then passes through a packing gland that is connected to the shaft log which is bolted to the hull.
5. A slot has been cut in the hull to allow the shaft to exit the bottom of the hull.
6. The shaft then passes to a matching 13° angled strut with two cutlass bearings.
7. Finally, the shaft transitions to the center-bored and TIG-welded 14-spline outboard shaft that allows the propeller to attach, retained by a 12mm x 1.5 nut and cotter pin.

The motor itself is controlled and fed AC power by a Curtis 1238SE-7971 motor controller. For throttle control, a wigwag style throttle uses two potentiometers (0-5k **Ω** in one direction, 5-10k **Ω** in the other). This is the first time we’ve used a Curtis controller, so we are also learning to use an OEM programmer to profile the motor and configure it for our purposes. A Curtis EnGauge II reads data from the CANBUS and provides the driver data including system voltage, motor RPM, motor temperature, and controller temperature. Our stand-alone BMS has its own small LCD display that provides cell data, voltages, as well as amperage, wattage, and battery State of Charge.




Since we are no longer using a modified outboard motor in our drivetrain, we needed to add a rudder and steering wheel to control thrust direction and steer the boat. We used a modified fiberglass rudder from a Nacra sailing catamaran, which is controlled by two braided stainless aircraft cables that run down either side of the hull. These cables are wrapped around a custom 3D printed steering hub with a small steering wheel mounted behind it. We decided to use this lower tech pull-pull cable driven steering mechanism instead of the push-pull cable driven method we previously used because it is more compact and lighter in weight.

William & Mary: Futuristic Autonomous Design

Michael Kelly Galdamez, Isaiah Lemmond, Ben Monforth, Keyra Ogura, Megan Blake, Alec Jaffe

www.navalengineers.org/WilliamMary

To improve stability during acceleration and planing, we designed and implemented an active aerodynamic control system using forward mounted canards. Unlike passive surfaces, this system allows real time adjustment of canard angle based on the boat's pitch, reducing excessive bow rise during the transition to plane.

Figure 2. Active Canard System Integration

Each canard is actuated by an independent 35 kg servo controlled through the Cube Orange flight controller using a Lua script. The system reads pitch data from onboard sensors and outputs corresponding PWM signals, allowing both canards to respond simultaneously. The use of 7.5V servos required the implementation of a dedicated 7.5V power bus within the electrical system to ensure consistent and reliable actuator performance.

A baseline linear relationship between pitch angle and canard position was established using CFD and refined through testing. This provides sufficient downforce at low speeds while minimizing drag at higher speeds. The goal of this implementation was to create a stable and responsive baseline system that can be further developed. To validate the control logic, we developed a small-scale prototype integrating the

telemetry system and canards. This enabled rapid testing and tuning before full scale implementation.

The mechanical system was developed iteratively using additive manufacturing, primarily PETG and PLA carbon fiber. A bearingless shaft design with greased tolerances was used to reduce complexity and improve reliability in a marine environment, while multiple housing iterations ensured proper servo placement and waterproofing.

The final system provides a reliable and adaptable method of controlling hull attitude while establishing a platform for future improvements in active aerodynamic control.

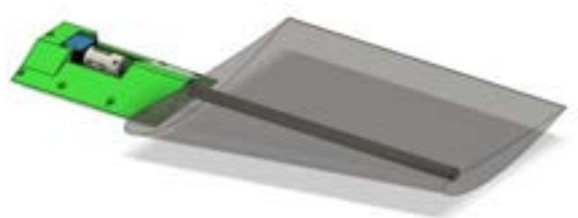

Figure 3. Canard Actuation Assembly

Drivetrain

When constructing our drive train, we wanted to choose a material that was light weight yet durable and strong. This led us to choosing aluminum as our internal drive train shaft. However, aluminum being a softer metal, started to deform and warp at 4000rpm. This led to the damaging of our internal driveshaft material along with the potential risk of damaging the boat. Using FEA tests we found that this was consistent with the resonant frequency of our shaft.

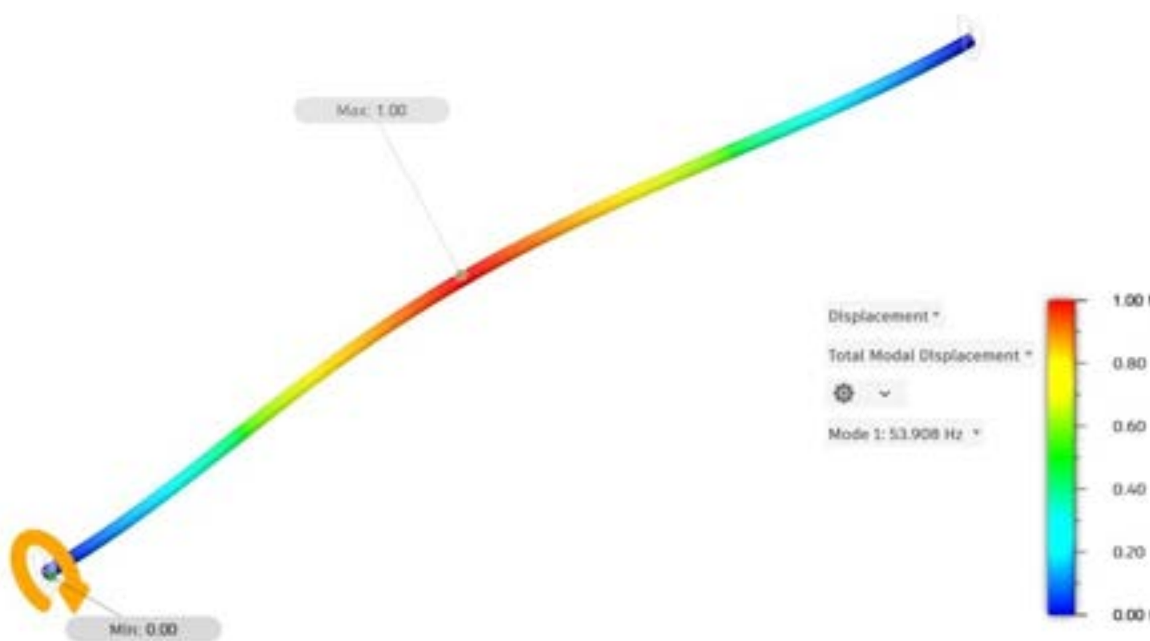

Figure 4. FEA test

After further research and FEA test we found that the best way to prevent this was to constrain the shaft. We designed and 3D printed a modular drive shaft stabilizer. The materials that were used were Nylon-6 with carbon fiber reinforcements, PETG with carbon fiber, along with a carbon fiber tube with radial ball bearings.

Figure 5. Drive Shaft Stabilizer

This stabilizer was attached to the USV using a high strength epoxy and has successfully prevented warping and damage to the aluminum drive shaft.

Propeller Design: Pitch, Rake, and Blade Profile Optimization

To improve thrust and overall propulsion efficiency, we designed and iterated on custom propellers with a focus on pitch, rake, and blade profile. Early development primarily explored increasing pitch to create more aggressive propellers; however, recent iterations have expanded to include rake as a key design variable. The current design utilizes a rake angle of 20°, which improves flow alignment and propeller loading under high speed conditions.

Blade geometry was also refined using hydrodynamic foil profiles with integrated cupping. This design reduces tangential thrust losses and redirects flow more effectively in the axial direction, improving overall thrust efficiency. The foil-based blade profile additionally reduces localized stresses and improves performance under high RPM operation.

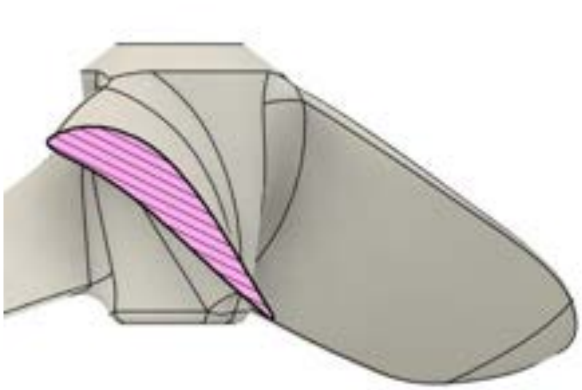

Figure 7. Foil Blade Profile with Cupping

All propellers were developed through iterative additive manufacturing, allowing rapid testing of multiple geometries. A range of materials were evaluated, including ABS, nylon, and carbon fiber reinforced filaments. Through testing, PETG was identified as a highly effective material, providing a balance of strength, print reliability, and surface quality. Despite initial expectations, PETG propellers demonstrated sufficient durability under operating conditions of approximately 4000 RPM and speeds near 25 mph.

Current designs prioritize a combination of increased rake, optimized pitch, and hydrodynamic blade shaping. While PETG remains the primary material, ongoing work includes investigating composite reinforcement methods such as carbon fiber layups and embedded mesh structures to further improve mechanical performance. This iterative approach has enabled the development of propellers tailored to the USV's operating conditions while establishing a foundation for continued performance improvements.

Rudder

With all the breakthroughs in other areas of the USV we found it easy to get on a plane. The one issue we observed was controlling the USV on a plane. Past teams have used skegs and skid steering to keep the boat stable on a plane. However, the skegs are known to cause more drag and cause the USV to use more power to get on a plane. To fix this issue we developed a rudder system using a servo, 3D printed and designed rudder mount and a kayak rudder. By using the rudder, we were able to maintain stability on a plane and higher speeds, all while using less power to get on a plane. The rudder reduces the turn radius of the USV allowing higher maneuverability.

PEP26 - Uncrewed Open

DAEDALUS

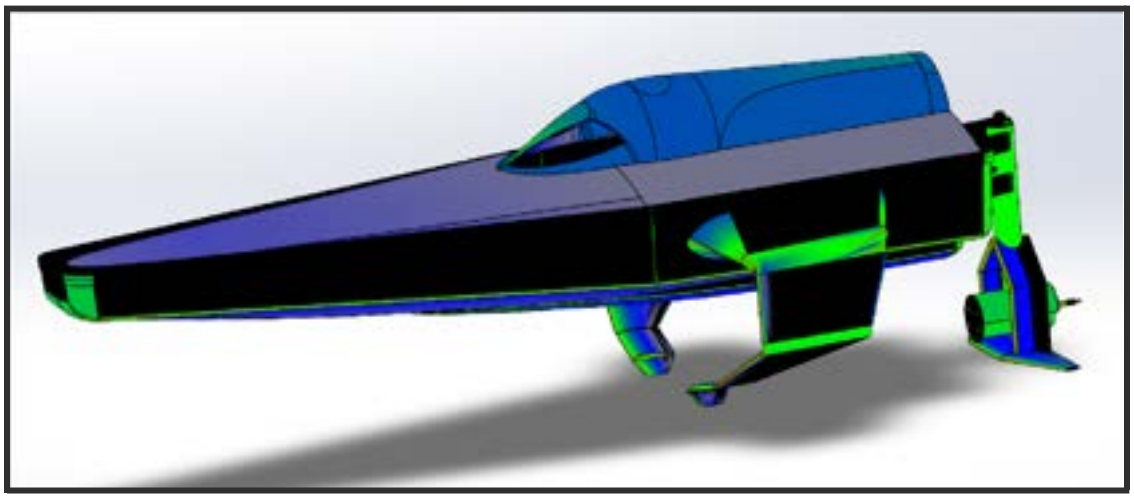

Ben Linzer, Yiru Liu, Dale Rahn, Abbie Danielson, Alex Niva, Stephen Moore

Madison Area Technical College Top Paper PEP26

Abstract

This paper details the design, simulation, and manufacturing of *Daedalus*, a high-performance uncrewed hydrofoiling vessel created by Madison Area Technical College PEP Team for the 2026 ASNE Promoting Electric Propulsion competition. Departing from conventional hull architectures, the team drew inspiration from the E1 Racebird to advance student-driven innovation in marine technology. Central to the project is a sophisticated nonlinear 6-Degree-of-Freedom (6-DoF) dynamic simulation implemented in Python, which was used to analyze craft behavior and make design decisions. The vessel features a custom 6061 aluminum internal skeleton for structural rigidity and a 50.4V peak lithium-polymer electrical system capable of delivering high-discharge power to a 19.5kW motor. This work demonstrates a comprehensive systems-engineering approach to electric marine propulsion, balancing advanced hydrodynamic modeling with robust mechanical fabrication.

Contents

1. Introduction & Mission Overview

The category of uncrewed open for this year's competition proved to be the most advantageous for our design, and given the 2-mile range, 55.5 V power limitation, and 60 lb ballast requirement, our team worked to balance ambition, creativity, and innovation within the parameters of the competition to emulate the E1 Racebird hydrofoil.

While the ASNE Promoting Electric Propulsion (PEP) competition is presented as an annual collegiate race, there is an aspect of the competition that is often overlooked. While electric propulsion itself is not new, many participating teams rely heavily on commercially available designs. Proven hull geometries dominate the competitive landscape. While experience and established knowledge will always play a critical role in engineering, what is often missing is the willingness to explore unconventional solutions—to take risks and move beyond what is already known to work.

The 2026 team from Madison Area Technical College chose a different path. Rather than refining existing concepts, we pursued something new and largely unexplored. We embraced what we believe to be the true spirit of this competition: innovation driven by curiosity and a willingness to challenge convention. Without the constraints of industry experience, student teams are uniquely positioned to explore ideas that might otherwise be dismissed as too ambitious or too risky. Our goal was not simply to achieve the fastest time, but to raise the bar and expand expectations for what is possible within this competition. To that end, we selected a platform so new to the marine industry that no documented full-scale implementation of this design could be found in any setting—academic, commercial, or independent.

At the time this project began, the E1 Series Championship had yet to complete its first full season. With limited publicly available specifications, our only references came from race footage, dry dock imagery, and a 22-inch scale model. From these sources, we reverse-engineered the platform through detailed caliper measurements, radius analysis, and over three hundred collective hours in SolidWorks. The result is a fully developed hydrofoil system, adapted for manufacturability, refined through engineering judgment, and driven by a commitment to push beyond conventional design boundaries. We present this work not only as a competitive entry, but as a contribution to the ongoing evolution of student-led engineering and innovation within the naval community.

2., Background Research

2.1., Hull Selection

The different methods of estimating hull resistance were introduced to us through a comprehensive paper detailing prediction techniques [1]. We initially considered model testing, but due to the difficulty of constructing the necessary hardware, we chose to focus on empirical and simulation techniques instead.

Originally, we considered a twin hull catamaran due to stability concerns from previous years. To predict resistance for the displacement hulls, we implemented the Holtrop & Mennen [2] method in GNU Octave. We quickly realized from this model, along with supporting research, that hull speed limitations would prevent us from reaching the speeds we were targeting, and we moved on to considering a planing hull.

For predicting resistance of planing hulls, we implemented Savitsky's method [3], again in GNU Octave. We performed basic sensitivity analysis to understand how each input parameter affected the model output. Before committing to a specific design, however, we decided to take a more ambitious approach and pursue a hydrofoiling platform instead.

The Racebird is a true hydrofoil platform, utilizing dual inward-curving lifting foils and a twin-rudder T-foil to generate the majority of hydrodynamic lift during operation. The hull is configured as a narrow-beam, low-wetted-area monohull with a shallow-V planing surface and integrated stepped geometry, minimizing drag prior to foil engagement.

The E1 Racebird platform was developed by former NASA and Formula One engineers and refined by Lead Designer Sophie Horne of SeaBird Technologies. This design lineage reflects a high-performance engineering philosophy centered on efficiency, stability, and controlled lift generation at speed. Unlike traditional planing hulls designed for sustained surface operation, this hull is intentionally optimized for efficient acceleration to hydrofoil takeoff. By reducing resistance through both the displacement and planing regimes, the design lowers the power required to reach lift-off velocity and improves overall propulsion efficiency during transition.

Since we were unable to find empirical methods readily available for resistance prediction of a hydrofoiling vessel, we spent a significant amount of time attempting to learn Computational Fluid Dynamics. As students competing in PEP, we did have access to commercial software, but research online cautioned against starting there, as these tools can produce unreliable results when used without a strong understanding of the fundamentals. We started from the ground up—working through fluid mechanics, then aerodynamics, and then doing our best to understand CFD theory. The software we used was OpenFOAM, and we completed multiple unrelated test cases to build familiarity. Figure 1 shows a vortex-induced vibration case used to explore rigid body motion and dynamic meshing. Figure 2 shows a racecar spoiler simulation used to explore RANS modeling with the k-ε turbulence model.

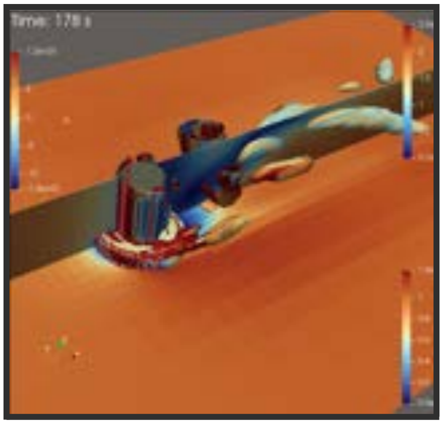

Figure 1 Vortex- vibratio

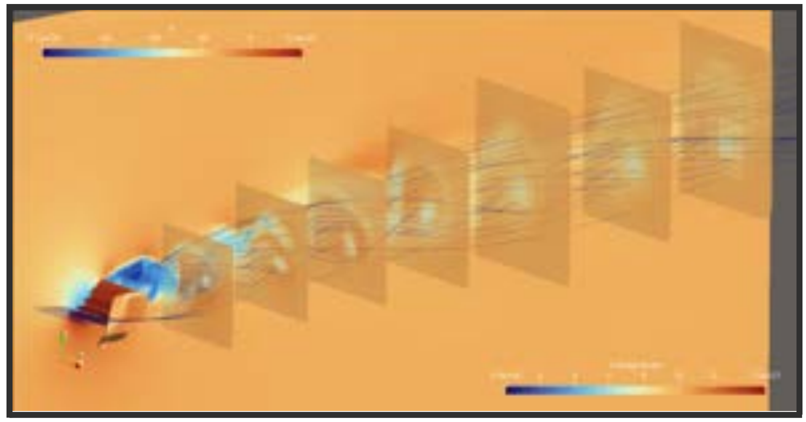

Figure 2 Raceca spoile

We spent approximately two months working through this process before realizing there was still too much left to learn, and it was unlikely we would be able to generate reliable results in time. The main issue we encountered was mesh generation. Our largest wing chord was only 300 mm, with the smallest sections at only 60 mm. At these scales, the Reynolds number remained low enough that laminar-to-turbulent transition needed to be modeled for accurate lift and drag predictions.

This meant we could not rely on the standard k-ω SST model and instead had to use the Langtry-Menter variant, which includes additional transport equations for turbulence intermittency and momentum thickness. To properly resolve this model, a y+ value below 1 was required. Achieving this would have required either an extremely fine mesh beyond our computational capability or a large number of inflation layers that snappyHexMesh struggled to generate.

After reaching this point, we decided to move away from CFD and instead rely on available airfoil data and simplified analysis methods. While this reduced accuracy, it allowed us to continue progressing the design within the time constraints of the project. Figures 3 through 5 show the most refined computational domain we were able to generate before making this transition.

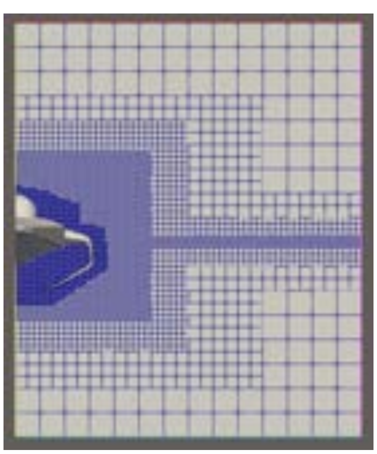

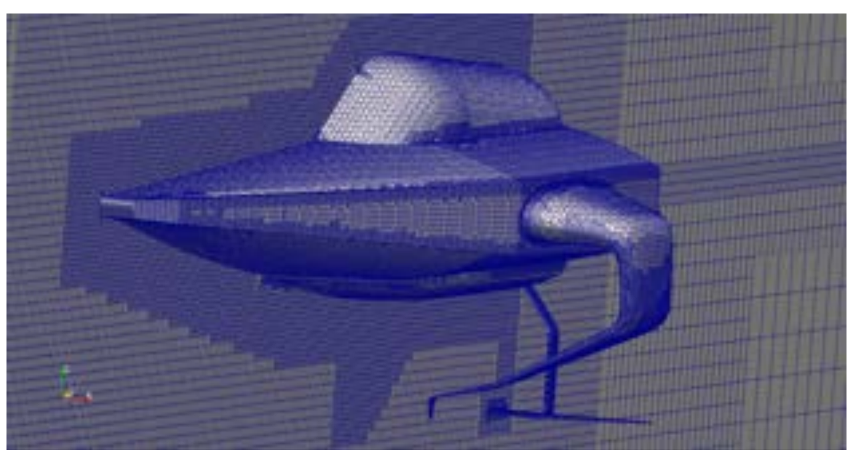

Figure 3. Front of computation domain *Figure 4. Close-up of hull & wing mesh*

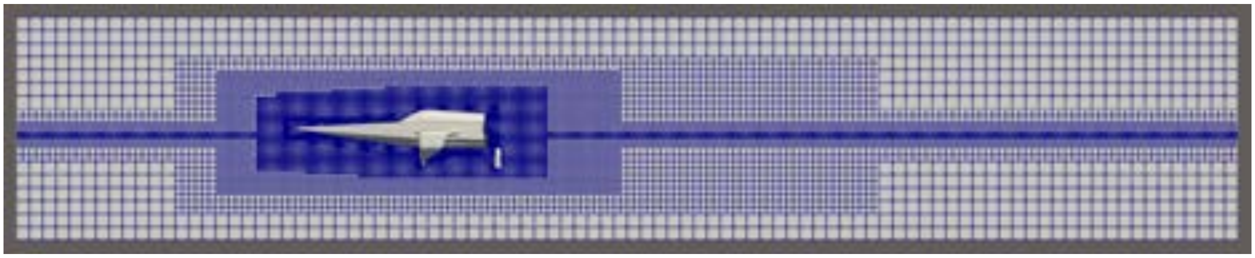

Figure 5. Side of computational domain

3. Hydrodynamic Design & Simulation

3.1. 0-DoF Steady State

We started by creating a zero degrees of freedom steady state model based on force equilibrium. At each velocity, a certain amount of lift must be produced to counteract weight. In this model, the lift coefficient was allowed to vary as a proxy for angle of attack effects. After determining the lift coefficient, the induced drag equation, combined with a fixed baseline drag coefficient, was used to calculate the total drag that needed to be balanced by thrust at each velocity. Propulsion was modeled using Wageningen B-Series polynomial fits for thrust and torque coefficients [4], and the RPM required to counteract drag at each velocity was found through optimization.

With RPM determined, we then calculated the required torque and, using the ideal motor equation, estimated the input voltage and current draw. This, combined with the expected run time, allowed us to generate an initial estimate for required battery capacity.

We quickly realized that this model had too many limitations and unaccounted dynamics to be a good predictor and decided to move on to a one degree of freedom model where height above the free surface, or z, was allowed to vary. Further detail on this model can be found here.

3.2. 1-DoF Steady State

Instead of having a varying bulk lift coefficient for all lift produced, the foils were modeled individually, each with their own lift and drag coefficients based on airfoils of similar shape. We attempted to export our foil shapes and simulate them in Flow5 using boundary element methods, but none of our cases converged, and we lacked the time and experience to troubleshoot further. Using known coefficients was the best option available to us.

Instead of a varying lift coefficient, a fixed amount of lift was generated at each velocity, with any remaining force required to balance weight taken up by buoyancy. To model this, we needed submerged volume at each depth. Using booleans of our hull CAD model—based on the RC E1 Racebird we were replicating—we calculated submerged volume at various depths and fit a quadratic curve through the origin to estimate volume at any given depth. This data, combined with an estimated final mass and a reasonable stationary waterline height, allowed us to determine the required displacement and overall size of the craft. The final scale was approximately 3.6× the RC model, which we multiplied by a safety factor of 1.25 to arrive at the 2.13 m length between perpendiculars mentioned earlier.

With submerged volume defined, we calculated the depth required to generate a given buoyant force and used this to track the vertical position (z) of the craft from stationary conditions through takeoff. After takeoff, sufficient lift was produced by the foils alone to support the craft, causing them to begin surfacing and reducing their effective lifting area. Foil submergence was calculated using the z-position at panel intersections, and remaining lifting area was linearly interpolated since the panels were modeled as trapezoids. Propulsion was again modeled using B-series polynomial fits. Instead of optimization, we identified that K_T behaved as a cubic function of J, allowing us to rearrange for an analytical expression of J at a given thrust, significantly reducing computational cost. We then performed manual optimization by testing propellers with different parameters.

thrust at high advance ratios. A high $A_E P/A/D_0$ ratio was also needed to generate sufficient thrust at low At our target velocity of 15 m/s, a high propeller was required, as only these continued to produce speeds, particularly during takeoff where drag is highest. Because high-speed-optimized propellers are inefficient at low speeds, we briefly considered adding a second motor and propeller under the hull optimized for takeoff.

Modeling showed that, within reasonable diameter and RPM constraints, the secondary propeller could only support approximately 30% of total drag and reduced overall power consumption by about 8% at takeoff. Combined with the added complexity and uncertainty of surface-piercing behavior, this idea was abandoned.

Similar to 0-DoF, power requirements were calculated using torque and the ideal motor equations to determine input voltage and current, and combined with expected run time to estimate battery capacity.

The result was approximately 1050 Wh, leading us to select two 666 Wh batteries wired in series. The motor was also selected to ensure continuous power output exceeded predicted requirements. Although a significant improvement over the previous model, limitations remained. The model was still based on only steady state force equilibrium, not moment equilibrium, meaning angle of attack was assumed constant at 0°. At higher speeds, the model predicted most of the main wing would surface and that nearly all lift would shift to the rear foil, which is clearly unphysical due to the resulting pitching moment.

It became clear that capturing these dynamics required moving to a 2-DoF model. While implementing that, we found many equations aligned with 6-DoF formulations. Although more complex, the additional capability justified the transition. Further detail on the 1-DoF model can be found here.

3.3. 6-DoF Dynamic Simulation

The nonlinear 6-DoF dynamic model was heavily modified from the Research Civil Aircraft Model [5], with the help of another paper dedicated to hydrofoil craft dynamics modeling [6]. The panels were once again modeled individually, this time with a much more robust way of calculating submergence. Instead of comparing z-coordinates at panel intersections, we took the quarter-chord locations at the two ends of each panel, transformed them into world space, and compared the z-coordinates. This took into account pitch and roll effects and allowed accurate submergence even at extreme attitudes.

Foil lift and drag were modeled with coefficients in the stability frame, similar to aerospace models. One problem we encountered was that when the craft was near stationary, the angle of attack and sideslip varied wildly from -90° to 90°. This meant that the lift and drag coefficients no longer stayed in the linear and quadratic regions, respectively. We came up with arbitrary blending functions that we tuned to resemble airfoil data of similar profile shapes. These were sampled and stored in a lookup table and interpolated in 6-DoF.

A similar problem was encountered when trying to model propulsion. Since the model is now dynamic, we needed to model reverse and braking, which caused the advance coefficient J to go out of bounds for the B-series polynomial fits. We switched to a four-quadrant propeller model with Fourier coefficients to represent the four different operating regimes. There were only data for a few select B-series propellers$A_E/A_O = 0.7$ readily available online [7], and from those, the configuration with blade area ratio and pitch diameter ratio *P/D* = 1.4 suited our purpose best.

Unlike the previous steady-state models, where thrust required was known at each velocity, the dynamic model needed to determine thrust produced for a given input voltage. This depended on rotation speed, which depended on required torque, which also depended on rotation speed. This was solved through optimization offline for each propeller configuration at any given input and speed, then stored in a lookup table and interpolated in 6-DoF.

For treatment of the hull, volume center and area centers were needed to determine where buoyant, hydrodynamic lift, and viscous forces acted. The hull volume, area, volume center, and area center were sampled at various booleaned waterline heights, each with sweeps through pitch from -45° to 45° and roll from -60° to 60°. This process was computationally expensive, so values were first sampled on an irregular grid—densely near nominal operating conditions and sparsely at extreme attitudes. The data was then interpolated onto a regular grid for easier access and validated using a custom Plotly visualization. This multidimensional dataset was stored and trilinearly interpolated in 6-DoF. A similar approach was used for the wing roots, where significant displacement occurs at low speeds when buoyant forces dominate. With all forces and moments defined, the equations of motion followed standard 6-DoF rigid body dynamics. Rotation was tracked using Euler angles instead of quaternions, since pitch is limited to ±45°, avoiding gimbal lock concerns.

The model was implemented in Python using an object-oriented structure, with the hull, panels, propulsor, and wing roots each represented as classes. While Python does not strictly enforce OOP, a polymorphic-like structure was used where each class had methods to calculate forces and moments. Performance was improved using Numba JIT, resulting in simulation speeds approximately three times faster than real time. NumPy handled vector and matrix operations, SciPy handled integration, and websockets/asyncio were used to communicate with the front-end visualizer in JavaScript. A separate simulation script handled integration and input/output, while another script broadcast simulation results on a local server. PyGame was used for controller input, and JavaScript with Three.js was used for 3D visualization. Broadcasting results allowed multiple synchronized views, such as telemetry monitoring and real-time visualization of the vessel.

The 6-DoF model was used to guide design decisions. It was found that the wings may not have required aluminum reinforcement to be structurally sound, though fabrication had already progressed too far to make changes. Test runs were completed with telemetry logging, showing that only around one-third of total battery capacity was required to complete the race. Multiple propeller diameters were tested, and current draw was analyzed. To remain within the motor's power output limit while producing sufficient thrust, propeller diameter needed to be approximately 12–14 cm. Enlarged wing geometries were also tested following manufacturability concerns with smaller sections.

All source code from the actual model to parameter generation and interpolation can be found here. Model equations and more screenshots can be found here. Figure 6 shows the craft starting a turn.

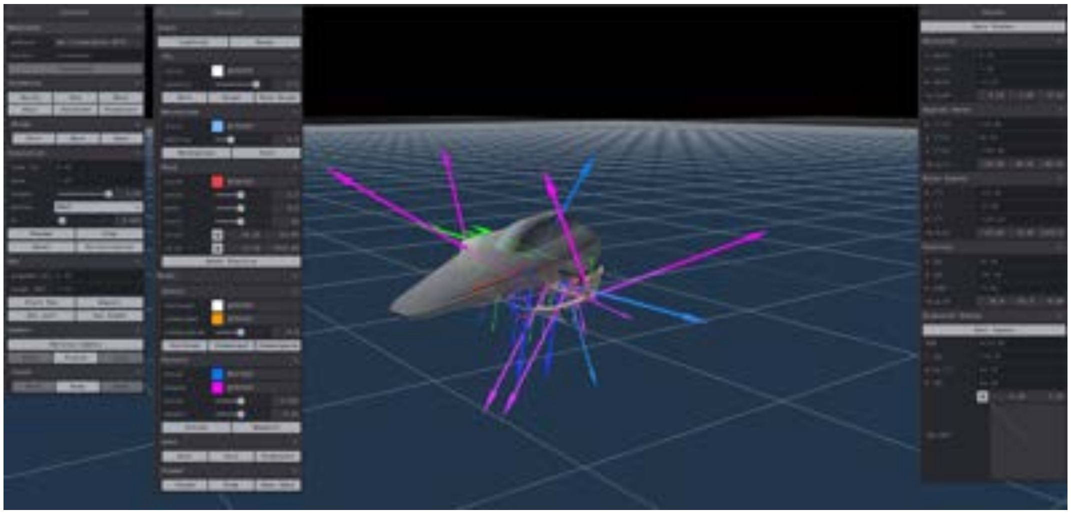

Figure 6. Three.js visualization of 6-DoF simulation

4. Electrical Systems & Control

4.1. Electronics

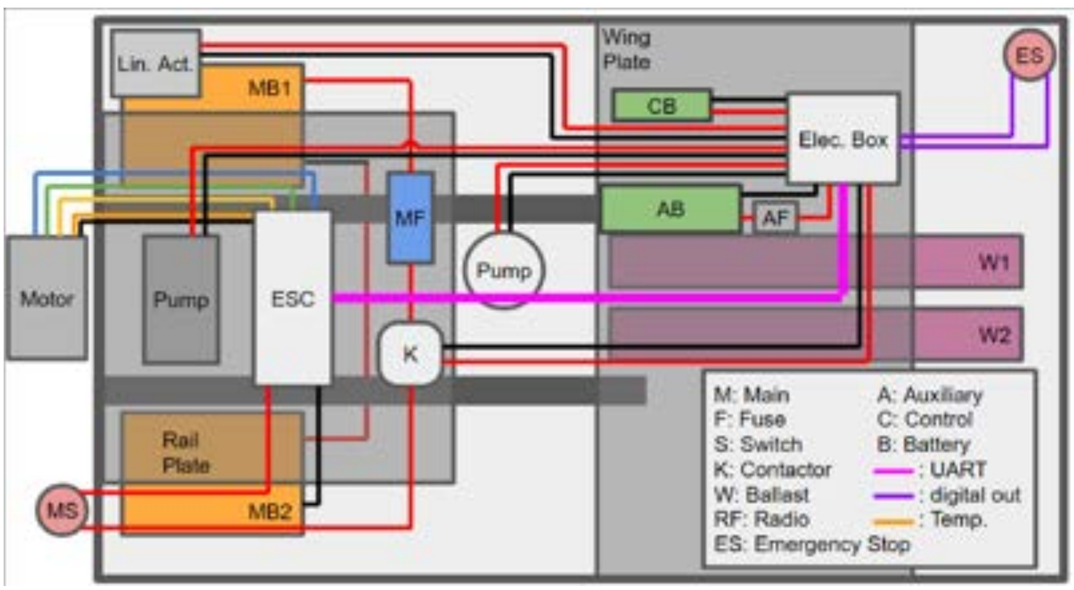

Figure 7. Physical wiring diagram of all components

The electronics consist of a main high power circuit with two 6S 30Ah Tattu Li-Po batteries wired in series for 44.4V nominal and 50.4V peak. This went into a FlipSky 75350 350A ESC then the FlipSky 85165 150KV 19500W motor. This circuit was controlled by a HCZ01-300A contactor which was energized by an auxiliary circuit powered by a 3S battery. This auxiliary circuit also powered cooling pumps for the ESC, bilge pumps in case of significant water ingress, and the linear actuator for rudder actuation and steering.

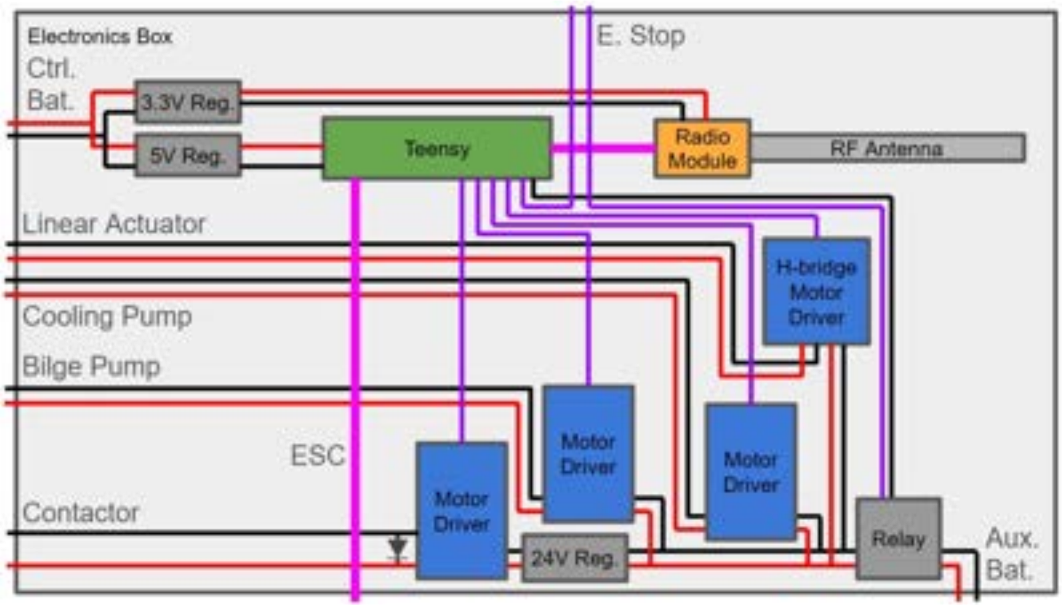

Figure 8. Wiring diagram of components inside waterproof electronics box

The auxiliary circuit was controlled through a relay that was energized by a low power control circuit consisting of the radio module and the microcontroller powered by a 2S battery. We chose the Teensy4.1 as our microcontroller due to its computational power and onboard SD card for data logging capabilities. A simple prototype board was made for mounting these components.

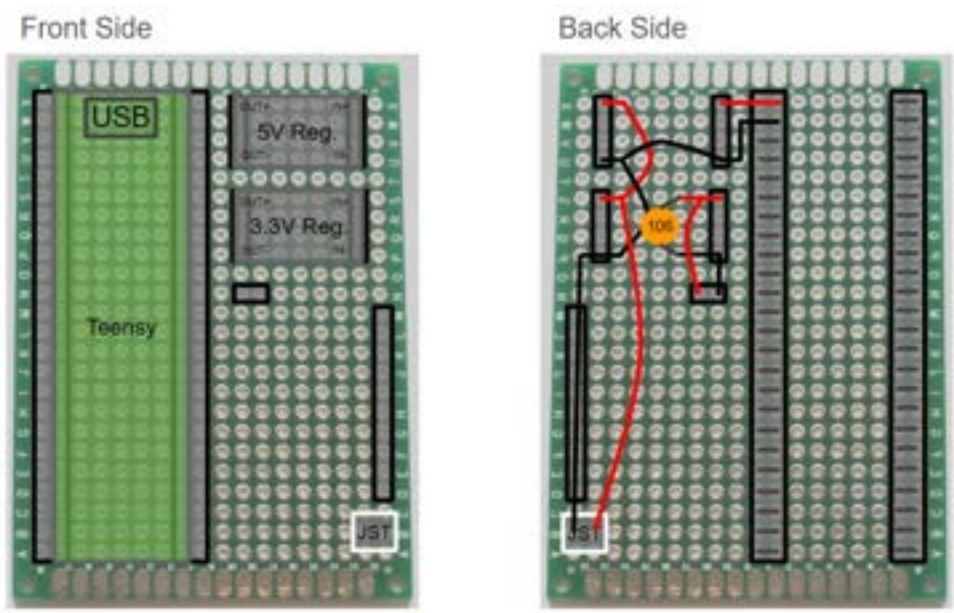

Figure 9. Schematic for control prototype board

For our radio module we considered the RFD900 and the XBee XR 900. After examining our performance requirements, we found the RFD900 to be overkill and that the XBee provided enough capability for our needs at a much lower price which led us to select it as the radio. For the antenna, simple [link budget](#) calculations were conducted. Care was taken to use a two-ray ground reflection path loss model instead of free space path loss due to operating in near proximity to the water surface which reflects and distorts signals. We chose an omnidirectional antenna for the boat since orientation would be changing throughout the run. It was considered to use a directional antenna that could be pointed at the boat on the ground station, but link budget calculations showed that omnidirectional antennas with gains of 2.2dBi could support ranges up to around 1.5-2 miles if one was placed 3m above the water surface which was extremely achievable for the ground station. Omnidirectional antennas for both the ground station and the receiver were decided for simplicity.

4.2. Control Architecture

The control program on the ground station side was done similarly to 6-DoF with python starting a local server and interfacing with the joystick HOTAS controller with PyGame and XBee through the digi-xbee python library. It broadcasted control and telemetry information through websockets. A JavaScript frontend interface was built for monitoring telemetry and keyboard/mouse control if the controller failed. Control signals are received with an XBee on the receiver side and processed on a Teensy 4.1. Safety checks are performed on board as discussed in 6.1. Source code for both ground station and receiver can be found [here](#). Figure 10 shows all electronics laid out and the ground station laptop and controller.

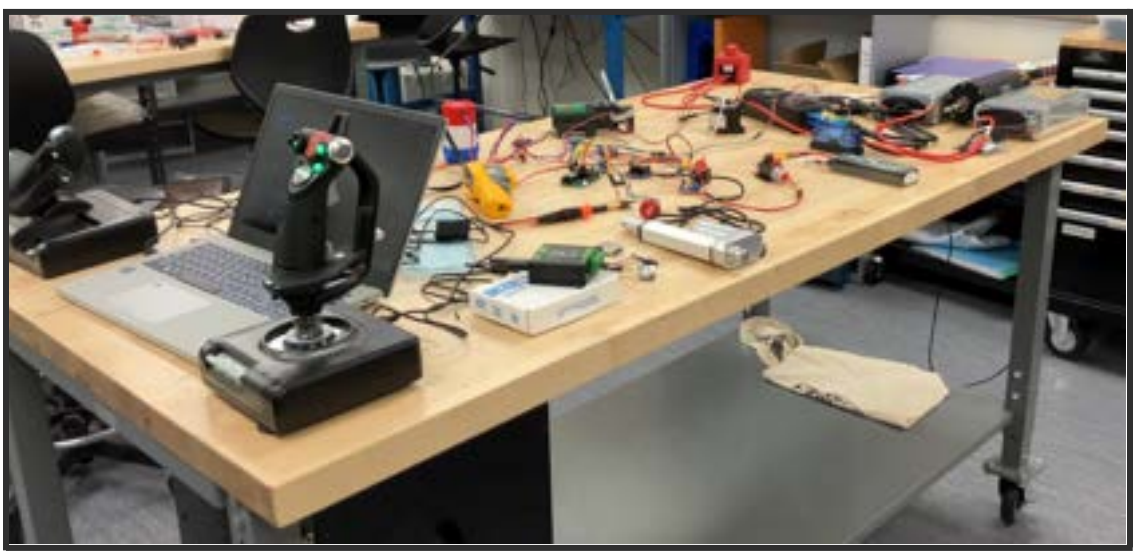

Figure 10 Electronic an groun statio setu

5. Mechanical Design & Manufacturing

5.1. Hull, Hydrofoils and Propellers

The E1 Series Championship had yet to complete its first season of professional racing when we chose this style of build to make our own. With a limited quantity of proprietary specifications available, our sole baseline came from watching races, studying pictures of the boats in dry dock, and a small 22-inch model. Through meticulous caliper and radius measurements, combined with more than three hundred collective hours spent immersed in SolidWorks, our team of mechanical designers replicated the hull of the Racebird. We adapted where necessary based on DFM capabilities, elaborated where creativity felt due, and reverse-engineered a powerful and capable craft.

Production of the hull was achieved through collaboration with industry partners. A CNC-milled solid wood mold was produced by Cascade Mountain Pattern, followed by thermoforming at Krueger Family Industries (KFI) in Portage, WI. Through sponsorship and local support, our team was able to both fund and observe the full production process, providing valuable real-world manufacturing experience. The 80 in LOA hull, with a 25 in beam, was thermoformed from 0.160 in methyl methacrylate (MMA) marine plastic, resulting in a 0.120 in keel and 0.090 in gunwales. Internally, the hull is reinforced with a custom skeletal structure consisting of contoured ribs, a wing connection plate, and a full transom reinforcement plate. These components were laser-cut from 0.185 in 6061-T6 aluminum, fabricated by a fellow mechanical design student, and TIG welded by the team's Lead Designer. Additional gunwale reinforcement is provided by a perimeter of 1 in × 0.125 in 6061-T6 L-channel. This structure provides the required strength to withstand approximately 150 N of load per foil and over 450 N of drag on the rudder and steering assembly.

The wings, rudders, and T-foil assemblies were manufactured using a hybrid construction method. External geometries were 3D printed from PETG-HF and PET-CF17 carbon fiber composite filaments with 0.400 in wall thickness and custom internal infill, surrounding embedded 0.185 in 6061-T6 aluminum core plates. A total of over 218 hrs of print time, along with more than 10 hrs of slicing and preparation, were required using Bambu X1C, X1E, and H2D Pro printers. All propeller testing and production components were printed on Bambu X1E systems using Fiberon PET-CF17 filament.

PET-CF17 was selected based on four primary factors:

Strength:

Tensile strength of approximately 65.9 MPa (XY) and 27.9 MPa (Z), with a bending strength of 109.3 MPa, provided an estimated safety factor between 2.0 and 5.0. A modulus of 5481 MPa and high shear resistance made it suitable for structural components and propeller applications.

Print Speed:

Compared to nylon-based composites, PET-based filaments can be printed at significantly higher speeds, enabling efficient production within tight time constraints.

Moisture Resistance:

PET materials exhibit low hygroscopic behavior, maintaining structural integrity in marine environments where nylon-based materials can degrade without extensive post-processing.

Safety:

PET-CF17 avoids the emission of hazardous volatile organic compounds associated with nylon printing, making it more suitable for use in academic lab environments without specialized ventilation systems.

The hull cap and additional prototype components were printed in three sections on a modified Elegoo OrangeStorm Giga printer, featuring an 800 × 800 × 1000 mm build volume. The final cap and access panels required more than 15 consecutive days of printing to complete.

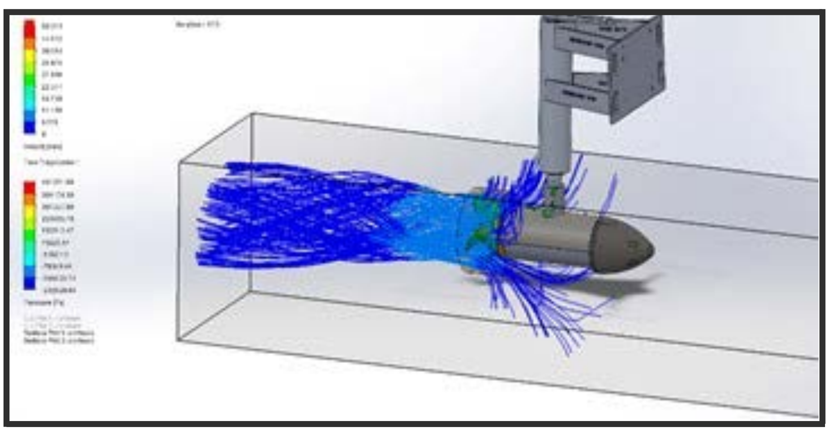

Figure 11 Solidworks flow simulatio

Figure 12 B4-70- propelle

Producing a propeller capable of withstanding the output of the Flipsky 85165 19.5 kW motor, while accommodating the 85 mm diameter motor housing, proved to be one of the most challenging aspects of this build. With no prior experience in marine propulsion within the team, development began from first principles and expanded across multiple technical sources and fluid simulation tools.

Two propeller designs were pursued. A Wageningen B-series 4-blade propeller was selected as the primary candidate, generated using Wageningen's design method and adapted with a conical hub to match the motor housing. Blade roots and tips were reinforced to meet DFM requirements for additive manufacturing.

In parallel, a custom 3-blade toroidal propeller was developed as an experimental design. While this concept aligned with the team's focus on innovation, the geometry introduced significant manufacturing challenges, particularly in support removal and post-processing due to the continuous blade structure. An outer diameter of 140 mm was selected based on electrical loading constraints. Pitch angles of 27°, 29°, 31°, and 33° were evaluated, with 33° chosen for final implementation.

With a peak motor output of 19.5 kW, power-based analysis and SolidWorks Flow Simulation indicate thrust values on the order of 1300 N are achievable for the B-series 4-blade propeller within the expected operating speed range. This aligns with simulation results and suggests the propeller is appropriately matched to the system's performance targets, while accounting for expected real-world efficiency losses.

5.2. Internal Skeleton

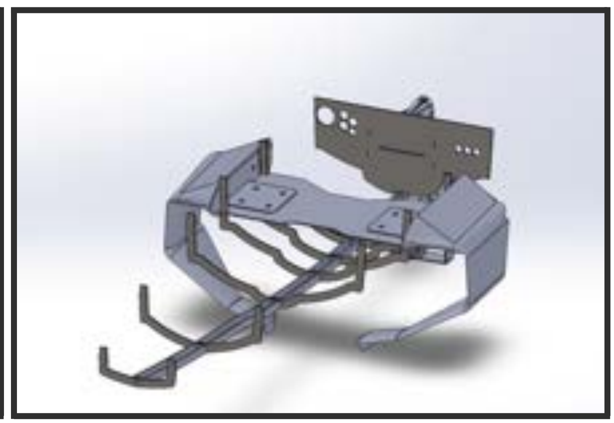

Figure 13 Rib an Win plat

Figure 14 Skeleto CAD detaile

The internal skeleton of the hull was designed to distribute compression, tension, and torsional loads generated by the wings and rear T-foil assembly. The primary components consist of gunwales, ribs, spine, wing plates, and transom plate.

The gunwales were constructed from 1 in × 1 in × 1/8 in 6061 aluminum L-channel. Their fitment interfaces along the upper edges of the hull and were welded to the ribs. The gunwales terminate at both the bow and the transom plate. Their primary function is to distribute loads acting on the hull across the length of the boat, improving overall structural rigidity.

The ribs were also fabricated from 6061 aluminum and were welded to the L-channel gunwales. Each rib was contoured to match the hull profile to minimize warping and deformation. In addition to supporting the hull structure, the ribs connect the wing mounts to the gunwales, allowing loads from the wings to be distributed throughout the hull.

The spine was 3D printed from PETG laid longitudinally along the centerline of the boat between the ribs.

The spine served two primary functions: maintaining consistent spacing between the ribs and reducing vibration within the structure. It connects all six ribs and extends to the transom plate, providing an additional attachment point that prevents the ribs from flexing in the bow-to-stern direction. This configuration creates a third structural constraint that assists in maintaining rib alignment and stability. The wing mounting system consisted of three primary components: the external wing plate, internal wing plate, and central wing plate. The external wing plate is a 3D printed PET-CF12 component designed to prevent the 5/8 in threaded heated insert from pulling through the wing and into the hull. The internal wing cores were fabricated from 6061-T6 aluminum and TIG welded to both the ribs and the central wing plate. This plate transfers loads from the wings into the internal structural framework and forms the slot through which the wings pass into the hull. The wings slide through this slot and are bolted to the central wing plate. The bolts connected to the 5/8 in heated insert are tightened against this plate to ensure that the wings remain securely positioned. The central wing plate connects the left and right wings and was designed to resist torsional loads. These loads may result from wave interaction with the wings or from uneven loading conditions during turning maneuvers. The transom plate serves as the primary structural interface at the rear of the hull. The spine is attached to the transom plate, and the rudder and T-foil assembly are also mounted to this component. The transom plate ensures that the rudder assembly remains securely attached while also maintaining alignment between the T-foil and the wings. Proper alignment of these components is critical for maintaining stability when the vessel is operating on hydrofoils.

5.3. Rudder Assembly

The material used in the assembly of the rudder is 6061-T6 aluminum, as this provides the strength required to resist the forces and moments acting upon the rudder while being lighter than steel. The aluminum was used for the steering shaft, shaft housing, hydrodynamic profile supports, and motor housing. The hydrodynamic profiles were designed with the intent to have a sheet of aluminum inside to provide structural support and connection points for the 3D printed PET-G. The steering shaft was sized to withstand the lift, drag, and thrust forces/moments acting upon it from the T-Foil, forward velocity and the motor. The vertical sections of the rudder were designed to have a low drag profile, while the bottom horizontal sections were designed to provide about 20% of the lift for the boat. The design includes a single vertical steering shaft with the motor housing directly in the bottom. The T-Foil was attached by two vertical sections that then angle into the steering assembly; these have aluminum cores and were welded to the steering shaft.

6. Risk Management & Safety

6.1. Control Failure

An intelligent receiver that performs onboard safety checks (see 4.2 for source code) was used in case of communication loss and/or onboard hardware malfunction. If the link to the ground station is lost for one second, throttle and steering are cut to zero.

The ESC provides active data feedback, and if the link to the ESC is lost for one second, main power through the contactor is cut. The contactor also has an auxiliary circuit that provides feedback on whether the coils are energized. If it is commanded to release but fails to do so after one second, the auxiliary power relay is cut.

If at any point off-nominal performance is observed, the ground station has the ability to cut both main and auxiliary circuits. If all of the above measures fail, there is a physical E-Stop that cuts power to the auxiliary circuit. If this also fails, a physical 300 A turn switch is wired in series with the main circuit. This setup provides strong safety guarantees, as it is extremely unlikely that all of these measures would fail simultaneously.

6.2. Thermal Management

Basic thermodynamic calculations were done for the ESC. Assuming operation at max power and maintaining temperatures below 60 °C, we found a required volumetric flow rate of approximately 1 L/min. A 3 L/min cooling pump was selected to provide a comfortable safety margin. The pump is controlled through PWM and can be operated below maximum output if testing shows sufficient cooling is achieved.

6.3. Adequate Steering

To avoid an inadequate steering system that was too sluggish or not powerful enough to overcome hydrodynamic forces, expected forces and torques were determined using 6-DoF. We initially considered using a servo, but found that it provided insufficient torque, and a gear reduction system would have been too complex to manufacture. We ultimately selected a linear actuator. 6-DoF was again used to determine reasonable actuation speeds and travel ranges required for effective maneuverability. Calculations were done to ensure the selected linear actuator met the required specifications and provided the desired performance.

6.4. Positive Buoyancy

The final minor risk identified was flooding. Significant care was taken to watertight seal the entire hull. If any amount of water would enter the hull, a bilge pump is in place to ensure the craft remains afloat. In addition, air bladders required by the rules ensure the craft maintains positive buoyancy even in the case of complete flooding.

7. Project Management

Each team member's skillset and schedule were assessed at the beginning of the project. This allowed us to identify each team member's strengths and gave them the space to work creatively and effectively within their functional area. At the same time, understanding weaknesses helped us support one another and minimize friction points, promoting efficient workflow. Team dynamics, management, and communication are essential components of any successful team. Our team achieved both by setting realistic and measurable goals throughout our condensed timeline. These goals were continuously evaluated and adjusted as the project progressed, allowing us to stay on track while adapting to challenges as they arose.

8. Conclusions & Future Work

Although significant modeling and simulation were done, model validation was very limited due to time constraints and lack of access to adequate testing facilities. The added mass effect and cavitation, both extremely important to hydrofoiling crafts, were not modeled in 6-DoF. Future teams are encouraged to start physical prototyping early for real world testing.

We initially wanted to do autonomous control with onboard IMU, GPS, and ultrasonic distance sensors for waterline height. We then would have used sensor fusion with state estimation, PID/LQR/FSF control combined with GPS waypoint navigation for a robust automated system. A Real-Time Operating System could then be used on the USV receiver for timely sensor handling.

The current 6-DoF model can easily be augmented with equations for geodetic positions through the WGS84 model. Trimming and linearization can then be done for additional stability analysis and control system design. This setup was ultimately abandoned due to time constraints for direct control from a chase boat, and the receiver running a superloop. The required hardware and sensors were already purchased, and futures teams are encouraged to utilize these resources. The ground station interface being in JavaScript allowed flexibility for future expansion leveraging Three.js for 3D visualization and more advanced data feedback.

References

E. Lindbergh and F. Ahlstrand, "Methods to Predict Hull Resistance in the Process of Designing Electric Boats," Master's thesis, Dept. Mechanical Engineering, KTH Royal Institute of Technology, Stockholm, Sweden, 2020. Source

J. Holtrop and G. G. J. Mennen, "An approximate power prediction method," *Int. Shipbuilding Progress*, vol. 29, no. 335, pp. 166-170, Jul. 1982. Source

D. Savitsky, "Hydrodynamic design of planing hulls," *Mar. Technol. SNAME News*, vol. 1, no. 4, pp. 71–95, Oct. 1964. Source

M. M. Bernitsas, D. Ray, and P. Kinley, "K_T, K_Q and efficiency curves for the Wageningen B-series propellers," Dept. Naval Archit. and Mar. Eng., Univ. Michigan, Ann Arbor, MI, USA, Rep. 237, May 1981. Source

FM(AG08), "Robust flight control design challenge problem formulation and manual:\ The Research Civil Aircraft Model (RCAM)," GARTEUR, Tech. Rep. GARTEUR/TP-088-3, Jun. 1995. Source

M. Martin, "Hydrofoil craft dynamics in a realistic sea including automatic control," Hydronautics, Inc., Laurel, MD, USA, Tech. Rep. 463-10, Nov. 1967. Source

R. F. Roddy, D. E. Hess, and W. Faller, "Neural network predictions of the 4-quadrant Wageningen propeller series," Naval Surface Warfare Center Carderock Division, West Bethesda, MD, USA, Tech. Rep. NSWCCD-50-TR-2006/004, Apr. 2006. Source

Massachusetts Maritime Academy

Team Name: Birddoggers

Division:

Crewed – Planing Crewed - Displacement

Uncrewed – Autonomy Uncrewed – Over-the-Horizon

☑ Uncrewed – Open Uncrewed – Budget Warrior

Photo of Team with Boat:

List of Members on Team: Knox Ackerman, Dhillan Maxwell-Coimbra, Michael Voci

Table of Contents

Background

Marine propulsion systems have historically been dominated by internal combustion systems that are inherently constrained by thermodynamic inefficiencies, mechanical complexity, and fuel-dependent operation. These limitations become more pronounced in unmanned platforms, where reliability, controllability, and system simplicity are critical design drivers.

As the global demand for efficient, sustainable, and resilient engineering solutions continues, efforts put forth in the maritime industry have further intensified while facing the challenges of reducing environmental impact while maintaining robust operational performance. Electric propulsion introduces an opportunity to address industry challenges under fundamentally different standards based on direct electromechanical energy conversion, enabling tighter system integration and improved controllability.

Within the PEP competition framework, this shift allows for a design approach centered on efficiency, modularity, and repeatable performance under constrained operational conditions. Team Birddoggers has worked to develop our vessel with these principles as the foundation for system-level optimization.

Technological Advancements
Advances in electric propulsion have been driven by increased battery power density, improved motor efficiency, and more capable embedded control systems. High-discharge energy storage supports dynamic loading, while modern motor controllers enable precise regulation of torque and speed through closed-loop control. Embedded computing platforms further allow real-time sensor integration and adaptive response. Together, these technologies enable highly responsive and tightly integrated propulsion systems.

Environmental Impact
From an environmental perspective, electric propulsion removes the need for onboard combustion, eliminating localized emissions and reducing environmental contamination. These systems also produce lower acoustic and vibrational signatures due to smoother operation and fewer moving components. This reduction in disturbance is especially important in marine environments, where noise and emissions can impact ecosystems. As a result, electric propulsion supports lower-impact marine operation.

Economic Considerations
Electric propulsion systems shift the cost from ongoing fuel consumption to initial system investment. Although upfront costs are higher, operational expenses are reduced through improved efficiency, lower maintenance requirements, and fewer failure points. The absence of fuel dependence also stabilizes long-term costs. For frequently operated systems, this results in a more favorable total cost of ownership.

Industry Challenges and Future Development
Key limitations of electric propulsion remain tied to energy storage capacity and system endurance. Battery constraints require careful power management, while additional challenges include thermal control, environmental sealing, and system reliability. Future work will focus on improving energy density, refining control strategies, and enhancing system robustness. Continued advancements will expand the performance and applicability of electric marine systems.

Design and Analysis

The initial design began with determining the vessel's design speed and duration to be competitive in the race. The design speed of 22 miles per hour was calculated from the average speed of the PEP25 Uncrewed-Open champion, 5 minutes and 58 seconds.

Electronics were given a team requirement to maintain an IP65 rating across all components across the system. This rating was determined based on the design goal of mitigating issues caused by water and weather entering a deck covering without sacrificing velocity.

Key Performance Parameters

The chart below outlines the most critical system-level performance parameters of the unmanned electric propulsion watercraft, beginning with the most important to the least important, that will yield effective results for a full-scale system:

Table 1: Key Performance Parameters

Importance	Parameter	Description
1	Payload	The watercraft shall carry an effective payload of 60 lbs without issue.
2	Battery Life	The watercraft shall have a full-load minimum runtime of 40 minutes.
3	Cost Effectiveness	The watercraft's operational costs shall be at least 25% less than the operational costs of a similar-use manned internal combustion engine watercraft.
4	Reliability	The watercraft shall complete at least 90% of missions with
		minimal issues.
5	Speed	The watercraft shall operate at a speed of at least 22mph with a full payload.
6	Scalability	The watercraft shall consist of a robust design where scalability and manufacturability are easily achieved.
7	Ease of Use	The watercraft shall be simple to operate and control, with full training requiring less than 30 minutes.

Hull

Initial hull design and selection began with estimating the total displacement of the vessel with full competition load. The initial weight estimate was 220 pounds. This estimate was based on selections made for a battery and propulsion motor, as well as other component weight estimates. The estimate of arrangeable ballast accounting for ~25% of the total weight allows for less concern to be given to the weight distribution of fixed components and the use of competition ballast to optimize weight distribution.

Using this estimate, the required area for planing was calculated, with the equation from Performance by Design, to be 14.8 square feet. The unitless hull loading coefficient used was 6, based on the recommendation from *Performance by Design*.

$$\textit{Planing Area}\ (ft^2) = \textit{Hull Loading Coefficient} \times \textit{Displacement}(ft^3)^{2/3}$$

This estimate was used to help inform initial design requirements for the boat. However, after analysis of available boat kits, it was determined that all available models would have sufficient planing area.

The model selected for construction was the Cocktail Class Racer from Chesapeake Light Craft. This model was selected because of the lightweight design was the smallest size kit that was readily available for construction, while having sufficient freeboard to satisfy reliability concerns relating to sea state during the competition. It also has approximately 16 square feet of planing area, meeting the calculated requirement.

Propulsion System

Initial considerations of the drivetrain and propulsion system included a jet drive, an inboard motor, and an outboard motor. The outboard motor was dismissed due to the number of moving parts and potential for failure introduced with such a system. A jet drive was strongly considered, particularly due to the ease of implementing an effective low drag steering system, but was rejected due to concerns over fitting it into hull geometry and finding or designing a jet drive suitable for the application. The inboard powered propeller system was selected for its reliability and the greater commercial availability of components, providing a greater opportunity to select and modify components to optimize performance.

Drivetrain design began with an analysis of options for electric motors utilizing 48-volt power while maximizing power within our budget. Motor selection was also based on adherence to IP65 or better standard. The MotEnergy ME1718 motor was selected to drive our vessel, as this specific motor met our requirements to achieve the design speed of 22 mph when paired with our propeller. This 48V motor generates 6kW and 14.3 Newton-meters of torque at its maximum motor speed of 4,000 rpm. The Sevcon

G4845 motor controller is paired with the ME1718 6kW motor, intended to operate with high efficiency, and is designed with IP66 protection, appropriate for marine applications. This motor controller was additionally selected due to its compact form factor, with dimensions of 8.9” x 6.7” x 3” that would allow for this motor controller to adequately fit within our designated control box.

To power this motor, our team researched highly capable 48V batteries that were widely available and suited our needs for high power and low weight. The battery selected was VEVOR’s 55.5V 105 Ah battery that provides ample energy storage to last the duration of the competition based on past PEP Competition course completion times. The following figure describes the general high voltage one-line diagram.

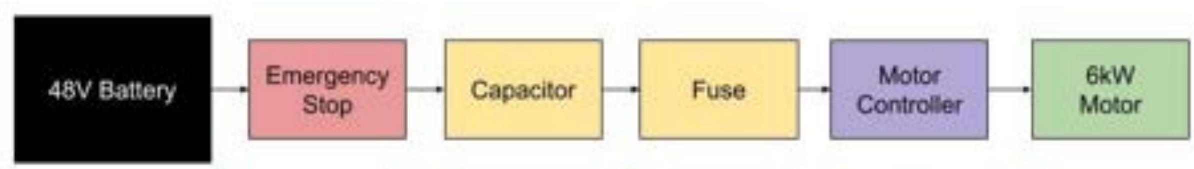

Figure 1: High voltage one-line diagram

In addition to its technical capabilities, the VEVOR 48V 105Ah battery features built-in overcharge control and management during charging and discharging, capable of handling short circuits as well as integrated safeguards for both high and low temperatures during charging and discharging.

$$Battery\ Depletion\ (mins) = \frac{80\% \times Capacity\ (Ah) \times Voltage\ (V) \times Battery\ Efficiency\ (\%)}{Load\ Power\ (W) \times Motor\ Efficiency\ (\%)} \left[\frac{60\ mins}{1\ hr}\right]$$

Using the table and above battery depletion estimate, the estimated time until the battery is depleted from a full charge is 41.6 minutes. Based on the previous PEP competition course completion times being in the 5-10 minute range, this no-load battery depletion estimate seemed adequate for competitive runtimes.

Table 2: Energy Consumption Metrics

Input	Value
Capacity	105 Ah
Voltage	48 V
Battery Efficiency	95.00%
No-Load Power Output	6,000 W (continuous)

Motor Efficiency	92.00%

Propeller diameter and pitch were determined by estimating slip using Gerr's slip chart from *The Nature of Boats*. At a design speed of 22 mph, slip was estimated at 0.26. From *Performance by Design,* a thrust reduction factor due to our shaft angle was taken as 0.1. The required pitch was calculated to be 8.6 inches for design speed.

From The Nature of Boats:

$$Required\ Blade\ Area\ (sq.in) = \frac{100 * horsepower}{knots * \sqrt{knots}}$$

At our design speed, the calculated required blade area was 9.7 square inches.

The propeller diameter will be machined down from the purchased propeller options to optimize the drivetrain performance. Several propellers have been purchased for final selection, dependent on trials.

Steering

The design for our steering system was based on the desire to minimize drag in the water and the analysis of the course, indicating a lack of need for rapid maneuverability. To accomplish steering, motor-actuated trim tabs that can be lowered during steering and raised on straightaways were selected. The trim tabs selected for this purpose were the Bennet Marine SLT6 with the Fuserish electric conversion kit. The electric conversion kit uses 12V inputs to extend or retract the struts, controlled by the Raspberry Pi 3/Navio2 controller.

Controls

The control system was designed to maximize the versatility of the vessel and the reliability of the electronic systems. The main controller selected was a combination of a Raspberry Pi 3B+ and a Navio2 autopilot hat. This combination was selected as it includes extensive documentation and open-source software, as well as a suite of sensors that could be used to implement autopilot and additional features. The Navio2 system includes a GPS, compass, accelerometer, gyroscope, and 14 pulse width modulation (PWM) outputs.

The on-board receiver communicates with the operator's handheld radio transmitter. The radio receiver communicates with the Raspberry Pi/Navio2 flight controller. This controller manages the two trim tab actuators through reversing relay packs, controls motor direction forward or reverse via a built-in relay contactor and regulates motor speed using a servo motor that manipulates the throttle control's three-pin potentiometer.

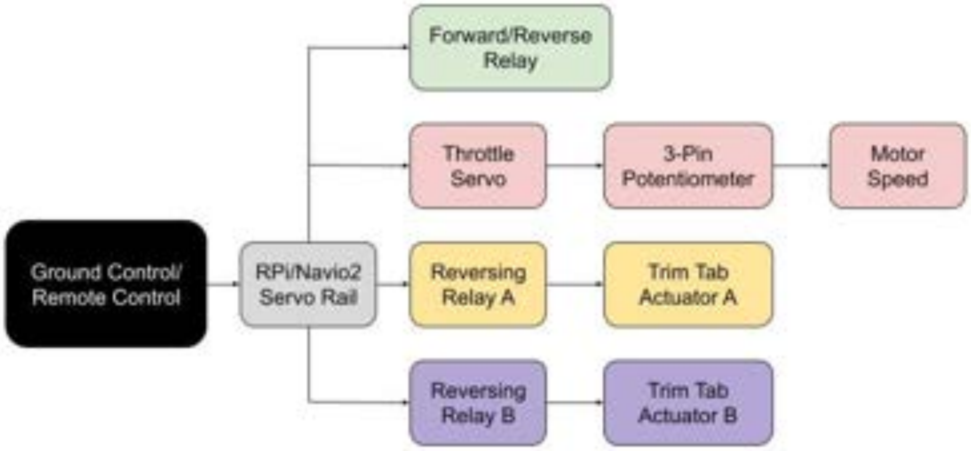

Figure 2: Control System Diagram

The control system was engineered to draw power from an independent 12V Lithium Polymer (LiPo) battery. This dedicated battery supplies power to the controller, the servo rail, the trim tab actuators, and the bilge pumps. This separate battery system was chosen to ensure a power source distinct from the propulsion system's supply, thereby mitigating the complications associated with utilizing a 48V battery to power a 12V system.

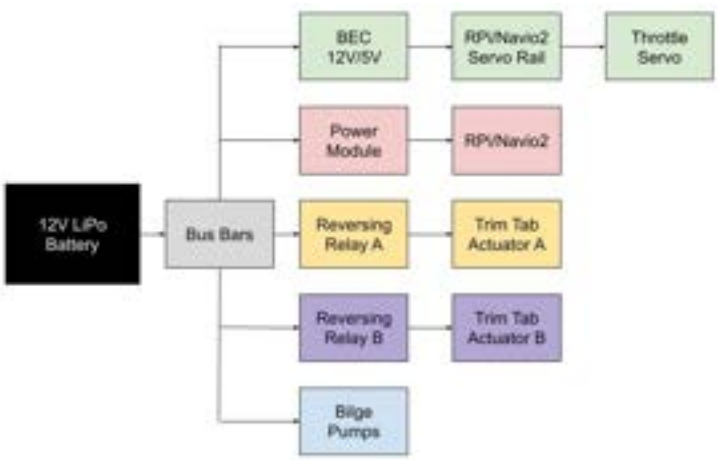

Figure 3: Low voltage power distribution

Overview of Build and Fabrication Processes

Hull

Hull construction was conducted according to the instructions provided by Chesapeake Light Craft for the Cocktail Class Racer. Minor modifications were made to reduce weight by only placing fiberglass along interior seams rather than full panels in each interior compartment.

The precut plywood boards were drilled to provide spots for the temporary wire ties. Sections of plywood were glued together for the transom and the midship bulkhead. These pieces were placed, and the plywood sections were tied together using copper wire ties to form the hull. The interior compartments were epoxied along the seams with a wood-thickened epoxy, then fiberglassed over top. The interior was finished by coating all bare wood surfaces with two coats of epoxy resin. The boat was then flipped over, where the harsh angles were rounded to enable the fiberglass wrap to remain strong. The entire exterior of the boat was fiberglassed with an overlap along the keel and the edges of the transom. This fiberglass, once cured, received a second layer of semi-thickened epoxy to fill in low spots. This layer was then sanded smooth.

Closed-cell foam was cut out from sheets and installed in empty compartments to satisfy the positive buoyancy requirement.

$$Floatation\ per\ Pound\left(\frac{lbm\ water}{lbm\ foam}\right) = \frac{Density\ of\ Water\left(\frac{lbm}{cu.ft.}\right) - Density\ of\ Foam\left(\frac{lbm}{cu.ft.}\right)}{Density\ of\ Foam\left(\frac{lbm}{cu.ft.}\right)}$$

The equation provides the required mass of foam to be installed. This enables the foam installed to be measured by mass rather than volume.

Table 3:Buoyancy of components

Item	Weight (lbs)	Volume (cu.in.)	Buoyancy (lbs)	Submerged Wt.(lbs)	Notes
Hull	NA	NA	NA	0	Wood/epoxy construction has positive buoyancy
Battery	87.0	1440	52.0	35.0	Lithium Chemistry
Motor	20.5	170	6.1	14.4	IP-65 rated for submersion
Cables	14.0	0	0.0	14.0	Negligible volume
Controls	14.0	1638	59.2	-45.2	Controls inside a sealed carry case (buoyant)
Steering	8.0	0	0	8.0	Negligible volume
Shaft	6.2	14.7	0.5	5.7	Steel 5/8" diameter x 48" long
Shaft Coupling/Seals	4	0	0	4.0	Negligible volume
Propeller	0.64	0	0	0.6	Negligible volume
Payload	60	0	0	60.0	Negligible volume
Miscellaneous/Margin	20	0	0	20.0	Negligible volume
Foam Buoyancy	3.37	3859	139.4	-136.0	EPS foam at 1.509 lbs/ft3
TOTAL	**238**		**257**	**-19**	**NET Buoyancy (-) with foam**

Drivetrain

Drivetrain construction began with routing a slot in the bottom of the vessel for the shaft to pass through. This slot was located by placing a disk the size of the propeller on the end of the shaft tube and locating the spot where penetration through the hull was necessary.

The shaft tube then had the shaft and motor installed to ensure proper clearances were met as components were aligned. The shaft was installed into the tube with two radial bearings on each end to support the shaft inside the tube. With all the components aligned, the motor mount was epoxied into place along with the shaft tube. Minor misalignment between the motor and shaft tube was handled by adjusting the motor with shims on the mount and the flexible coupling on the motor shaft.

The propeller was installed by machining the hub of the propeller down to the size of the shaft and drilling a cross-hole through the shaft for a pin to prevent rotation of the propeller on the shaft. The main thrust bearing was installed between the propeller hub and the end of the shaft tube.

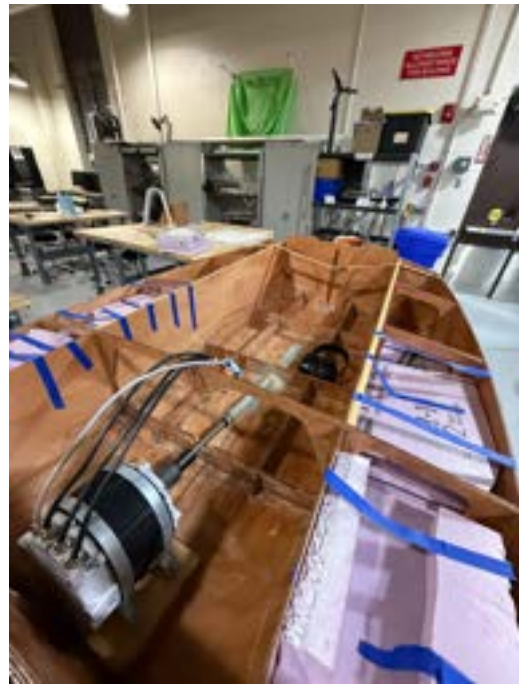

Figure 4: Shaft and motor installation

Our team chose a standard pool pump motor seal for the propeller shaft due to its proven suitability for water-heavy environments, offering superior waterproofing and reliability compared to traditional seals like stuffing boxes. This choice was also driven by performance considerations, as the mechanical seal design produces significantly less friction, contributing to higher efficiency and helping the boat achieve its target speed of 22 mph. Furthermore, the selection was highly practical from a logistics and budget standpoint, as these commercial components are readily available, cost-effective, and feature a cartridge-style design that simplifies both installation and quick maintenance or repair. Relying on a robust, mass-produced component to ensure a reliable, low-drag interface between the drivetrain and the water supports our mission to maximize competitive runtime while minimizing complexity and cost.

Steering

The trim tabs were placed as far apart as possible on the transom to maximize the total turning moment. The default height of the trim tab actuators was defined by setting the most retracted spot of the trim tabs to be ¾ of an inch above the bottom of the vessel when fully retracted. This positioning was selected to maximize the speed of the vessel when going straight ahead, while allowing sufficient actuation of the trim tabs into the water to provide the turning moment from the trim tabs.

Figure 5: Trim tab for steering

Controls

A Raspberry Pi 3+ (RPi) was selected as the main computer module; when paired with the Navio2 Autopilot hat, controls integration was a seamless process. The Navio2 component served as the interface between our Ground Control and the RPi. The Navio2 was specifically selected for its expandability and ease of use, allowing for the addition of a camera as well as fully autonomous capabilities for drone control. The Navio2 allowed for individual control of each trim tab, motor speed & rotation, and bilge pump control through its servo rail that utilized pulse-width modulation (PWM) to send control signals to these components.

In addition to its ease of implementation, the Navio2 was selected due to its robust and redundant systems. If wireless telemetry fails, the Navio2 has the option to utilize remote control transmission as a backup failsafe. In the event that the voltage regulator that directly powers the Navio2 via its power module fails, the Navio2 will reroute and receive power from the servo rail.

After identification of the vessel's functional requirements, a control system specification was performed to identify our system's operational modes and transitions between these modes while referencing our functional requirements. The following table describes the vessel's control components and their associated role in our system:

Table 4: Control system elements

Control Component	Description
Remote Controller	User input interface for propulsion and directional commands to the system.
Remote Controller Antenna	Communicates user interface input commands to the on-board receiver.
On-Board Receiver Antenna	Receives user interface input and transfers information to the On-Board Receiver.
On-Board Receiver	Communicates user input to our on-board controller module (Raspberry Pi).

On-Board Controller	Outputs signal (reflective of user input commands) to the Electric Propulsion Control component (Motor Controller) and directional component (Servo Motor). The controller also integrates the entirety of the on-board systems for effective communication and operation.
Electric Propulsion Control (Motor Controller)	Acts as an intermediary between the battery + controller/transmitter and the motor to control its speed and direction. It takes signals from
	the transmitter and translates them into timed electric signals for the motor. This allows the user to start, stop, and run the motor at various speeds and to reverse its direction.
Directional Control (Trim Tab Actuation)	Translates user input signals from the remote controller into specific trim tab actuation, allowing for steering and maneuvering of the vessel.

The following table describes the system's operational modes, inputs, and processes:

Table 5:Control processes

Operational Mode	Input	Process
Power Off	The vessel should receive no power when the Main Disconnect is in the (OFF) position.	Main Disconnect position turned to OFF will stop the flow of power to the vessel from the battery system.
Power On	The vessel should be receiving operational power when the Main	Main Disconnect position turned to ON will allow the flow of power to the vessel from the battery system.

	Disconnect is in the (ON) position.	
Propulsion Forward Direction	The vessel should move in the forward direction when the user interface input moves the propulsion control to the upward (forward) position.	User interface input should be communicated to the on-board receiver, then to the controller module (Raspberry Pi), which will communicate with the motor controller. The motor controller will signal this request to the motor, which should then turn in the clockwise direction at a relative speed based on the user input.
Propulsion Reverse Direction	The vessel should move in the forward direction when the user interface input moves the propulsion control to the downward (reverse) position.	User interface input should be communicated to the on-board receiver, then to the controller module (Raspberry Pi), which will communicate with the motor controller. The motor controller will signal this request to the motor, which should then turn in the counterclockwise direction at a relative speed based on the user input.
Turn Vessel Left	The vessel should turn to the left when the user	User interface input should be communicated to the on-board receiver, then to the controller
	interface input moves the directional control to the left position.	module (Raspberry Pi), which will communicate with the servo motor. The servo motor, along with the attached rudder, will then turn to the left at an angle relative to the user input.

Turn Vessel Right	The vessel should turn to the right when the user interface input moves the directional control to the right position.	User interface input should be communicated to the on-board receiver, then to the controller module (Raspberry Pi), which will communicate with the servo motor. The servo motor, along with the attached rudder, will then turn to the right at an angle relative to the user input.

Risk

Initial design and manufacturing required understanding the risks and issues associated with the fabrication and execution of a remote-controlled payload-capable high-speed vessel. Risks such as propeller design, battery life, time management, and cost of materials were factored into our component decisions and largely impacted our final design result.

Table 6: Risk Matrix

Risk Matrix	Birddoggers - Unmanned Electric Watercraft	Date:	3/24/2026		
Title	Description	Impact	Type	Mitigation Plan	Status
Propeller Design	**IF** our initial propeller design does not meet desired outcome, **THEN** additional scheduling is needed to redesign the propeller/drivetrain system	High	TECHNICAL	Order a critical spare as a back-up propeller that will satisfy criteria/investigate cost of procuring gearing system to serve as backup.	IN-PRG: Several propellers have been ordered and are stored in the laboratory. Field testing will need to be performed after machining of the shaft to select the propeller that best-fits our needs.
Parts Lead Time	**IF** there is a long lead time for specialty parts, **THEN** the parts will not arrive on-time.	MED	SCHEDULE	Research other parts suppliers or manufacturers as back-up and avoid relying in a single source for parts, materials, and labor.	CLOSED: Propellers have been purchased and alternatives are readily available to ship in <1 week.
Cost of Parts	**IF** all components and travel costs exceed $12,000, **THEN** we will not have enough money to complete the project.	MED	TECHNICAL	Proper planning, budgeting, and corporate sponsorships through the PEP 2026 Competition can be reached out to if needed.	CLOSED: Bill of Materials reflects all quoted amounts and budgets for individuals systems have been established, as well as a budget for miscellaneous and unexpected purchases. $12,000 is the total amount granted to our team, $4,000 has been alloted for travel to the competition, and the remaining $6,000 has been budgeted for each system.
Battery Life	**IF** battery capacity is insufficient for a 2-mile course, **THEN** a new battery will need to be reassessed.	LOW	TECHNICAL	Perform calculations to ensure that this battery will be sufficient for a 2-mile course at maximum output.	CLOSED: Battery has arrived (48V, 105Ah), and the battery battery deplection time with no load has been calculated at 41.6 minutes. With all major components accounted for, it can be assumed that the final weight of the vessel, including the 60 lb payload it is designed for, will be within 10% of 220 lbs.
Weather Conditions	**IF** the weather at the competition is unwelcoming, **THEN** the vessel needs to account for this in its design.	MED	TECHNICAL	Research weather conditions at the meet location as well as weather-resistant equipment.	CLOSED: The weather mid-April in Portsmouth, Virginia is typically mild with temperatures around the 53-69°F range. Historically, there is about a 30% probability of precipitation mid-April, and an average monthly rainfall of 3.15". IP rated equipment shall be used where possible.
Hull design	**IF** the watercraft proves unseaworthy, **THEN** a full vessel redesign will need to be assessed.	HIGH	TECHNICAL	Thoroughly research past competition and naval architecture to ensure seaworthiness is maximized.	CLOSED: Team has purchased a naval architecture book and is researching similar use-cases. The hull is currently in its production stages.

These risks were identified in order of highest impact to lowest impact and were sub-categorized by the type of risk, with the technical type defined as a risk that affects design and schedule, and a schedule type defined as a risk that mainly affects our design and fabrication schedule.

Mitigation plans were established to be prepared for these risks.

Understanding that this vessel is intended to be remotely controlled in all-conditions meant the procurement of weather-resistant and marine-grade components. When waterproof components were unavailable, our team's solution was to select the Apache 3800 case to contain and protect sensitive hardware. The Apache 3800 water-tight carrying case was specifically selected for its size and waterproof capabilities, allowing all critical components to reside within the case and prevent water ingress. Watertight grommets were installed on the case to allow for connection between our trim tab actuators, motor, and battery.

The most critical risk identified was the selection of the propeller. Intensive research was conducted, utilizing *The Nature of Boats* by Dave Gerr as well as consulting local industry experts. To combat this risk, multiple types of propellers were purchased according to design criteria. These propellers are then to be tested, and a final selection made based on performance.

In addition to these risks, our team has integrated two 12V submersible aquarium pumps as bilge pumps into the vessel's design; minimal, unpreventable water ingress into the hull is an expected risk. These pumps act as a critical safeguard against minor leaks and ingress from our propeller's shaft, preventing water accumulation that could damage non-IP-rated components. Active dewatering is essential for maintaining the designed light displacement and weight distribution, which directly supports our team's ability to achieve the target speed of 22 mph by preventing increased drag from water weight. Managing water ingress ensures the long-term reliability of all electronic and control systems, enhancing the vessel's endurance to complete the entire competition course, even in challenging sea conditions. The 12V pumps are powered by the dedicated low-voltage control battery, ensuring their operation is independent of the main 48V propulsion system. These pumps were selected for their minimal power consumption and are to be controlled via our main RPi controller.

Appendix A: Bill of Materials

Our team's Bill of Materials

Unmanned Electric Propulsion Watercraft Bill of Materials				*Total Cost:*		$8,097.31		*NOTE: Line items marked YELLOW have been ordered*	
				Remaining Budget:		$1,902.68			
ID#	**Item Description**	**Make Buy**	**Lead Time**	**Unit Cost ($)**	**Qty**	**Extended Cost**	**Cost Basis**	**BOM Notes**	**Product Online Link**
	Hull Assembly ($2000 Budgeted)					**$1,808.38**			
6	Cocktail Class Racer Hull Plywood Kit	B	2 wk	$1,269.00	1	$1,269.00	Q	delivered	CLCboats.com
4	Clear HP Epoxy Kit	B	1 wk	$192.99	1	$231.59	Q	delivered	TotalBoat.com
7	Fiberglass sheet	B	2 wk	$70.56	1	$84.67	Q	delivered	TotalBoat.com
11	1-1/4" OD, 1" ID Fiberglass Round Tube	B	1 wk	$17.97	1	$17.97	Q	delivered	MGS,Inc.
	Control System ($1500 Budgeted)					**$1,335.38**			
14	Transceiver (Navio2)	B	1 wk	$268.18	1	$268.18	Q	delivered	HiPi.io
21	Trim tab electric conversion kit	B	<1 wk	$219.99	1	$219.99	Q	delivered	Amazon
20	Trim tab	B	<1 wk	$124.22	1	$124.22	Q	delivered	Amazon
12	Raspberry Pi 3	B	1 wk	$40.00	1	$40.00	Q	delivered	PiShop.us
35	Remote Controller with Transceiver	B	1 wk	$59.99	1	$59.99	Q	delivered	Amazon
40	SiK Telemetry Radio (100mW 915MHz)	B	1 wk	$58.99	1	$58.99	Q	ordered	Holybro
13	12V Battery	B	1 wk	$56.10	1	$56.10	Q	delivered	Newark.com
32	Reversing Relay Modules	B	1 wk	$46.99	1	$46.99	Q	delivered	Amazon
17	Steering Servo Motor	B	1 wk	$37.97	1	$37.97	Q	delivered	Amazon
34	Battery Eliminator Circuit (BEC)	B	1 wk	$16.99	1	$16.99	Q	delivered	Amazon
33	Reversing Relay Module	B	1 wk	$13.99	1	$13.99	Q	delivered	Amazon
	Propulsion System ($4000 Budgeted)					**$3,426.36**			
41	Motor & Motor Controller	B	3-4 wks	$2,690.00	1	$2,690.00	Q	delivered	ElectricMotorsport.com
43	7/8" x 5/8" Stepdown Coupling	B	<1 wk	$179.38	1	$179.38	Q	delivered	Stafford
46	Solas Amita Three Blade propeller (7.25 X 5P)	B	1 wk	$68.99	1	$68.99	Q	delivered	WholesaleMarine
47	Vibration-Damping Flex Shaft Coupling	B	1 wk	$33.93	2	$67.86	Q	delivered	McMaster-Carr
49	Clamping Shaft Collar	B	1 wk	$46.77	1	$46.77	Q	delivered	McMaster-Carr
42	Driveshaft	B	<1 wk	$27.22	1	$27.22	Q	delivered	McMaster-Carr
47	Shaft Seal	B	1 wk	$8.74	1	$8.74	Q	delivered	Amazon
	Electrical ($1200 Budgeted)				**1**	**$1,151.20**			
57	48V Battery w/ Charger	B	4 days	$770.99	1	$770.99	Q	delivered	Vevor
60	2/0 Red Wire	B	1 wk	$7.68	8	$61.44	Q	delivered	West Marine
61	2/0 Black Wire	B	1 wk	$7.68	8	$61.44	Q	delivered	West Marine
58	Disconnect	B	1 wk	$40.99	1	$40.99	Q	delivered	WestMarine.com
67	2/0 Gauge Power Connector	B	1 wk	$35.95	1	$35.95	Q	delivered	Grainger
65	Connector terminals	B	<1 wk	$33.45	1	$33.45	Q	delivered	Grainger
64	12V Terminal Bus Bar	B	1 wk	$16.99	1	$16.99	Q	delivered	Amazon
62	Fuse holder	B	1 wk	$15.30	1	$15.30	Q	delivered	West Marine
59	Wiring Harness	B	1 wk	$0.00	1	$0.00	Q	Purchase if lab doesn't have	N/A
	Miscellaneous ($1000 Budgeted)					**$375.99**			
70	Ballast for competition	M	1 wk	$69.41	3	$208.23	Q	delivered	McMaster-Carr
72	Weight Bags	B	1 wk	$48.10	2	$96.20	Q	delivered	McMaster-Carr
69	Bilge Pumps	B	1 wk	$24.99	1	$24.99	Q	delivered	Ebay.com